# ULTRASONICALLY INDUCED SODIUM SUPERHEAT

by
Robert Eric Nystrom

A dissertation submitted in partial fulfillment
of the requirements for the degree of
Doctor of Philosophy in the
University of Michigan
1969

Doctoral Committee:

Professor Frederick G. Hammitt, Chairman
Associate Professor John M. Carpenter
Professor William Kerr
Professor Clarence A. Siebert
Assistant Professor Louis P. Solomon
Associate Professor Wen-Jei Yang

# A B S T R A C T

## ULTRASONICALLY INDUCED SODIUM SUPERHEAT

by

Robert Eric Nystrom

Chairman: Frederick G. Hammitt

The objective of this study is to determine the superheat requirements necessary to produce nucleate boiling in liquid sodium as a function of the temperature rise rate for very rapid rise rates as well as a function of the temperature itself. Superheat is defined as the amount that the temperature of the liquid has to be increased above the saturation temperature before nucleate boiling occurs in the liquid. By determining the onset of cavitation in liquid sodium which actually measures the effective vapor bubble radius in the sodium, and then converting this data to superheat requirements using the thermodynamic properties of sodium, the objective was obtained. Cavitation was produced in the liquid sodium by utilizing a high temperature ultrasonic vibratory cavitation facility. This facility incorporates a transducer horn assembly which transmits sinusoidal pressure waves at the transducer horn resonant frequency through the liquid sodium. The liquid sodium is contained in a stainless steel cylindrical container which is surrounded by heating coils.

Using four transducer horn assemblies of different resonant frequencies, the onset of cavitation in liquid sodium was observed over a frequency range of 14 to 25 kHz. For each frequency the temperature of the liquid sodium was varied

from 500 to 1500°F. The onset of cavitation was detected using a stainless steel acoustic probe which detected the noise signal produced by the collapse of the cavitation bubbles.

A theoretical expression for the pressure field, which was experimentally verified, was evaluated using the data obtained at the onset of cavitation. It was observed that at the onset of cavitation the peak pressures of the applied sinusoidal pressure field ranged from 73 psi for a sodium temperature of 500°F and a frequency of 25 kHz to 7 psi at 1500°F and at a frequency of 14 kHz. For a constant frequency the required change in liquid pressure at the onset of cavitation decreased approximately linearly for increasing liquid temperature. By maintaining the temperature of the sodium constant it was determined that the cavitation threshold is essentially independent of frequency for frequencies up to approximately 20 kHz. For frequencies above 20 kHz the change in liquid pressure required at the onset of cavitation begins to increase sharply.

It was assumed that spherical vapor bubbles served as nucleation sites for the onset of cavitation. By knowing the change in liquid pressure required at the onset of cavitation, the effective radii of these bubbles were determined. By assuming that these bubbles would also serve as nucleation sites for nucleate boiling in the heat transfer case the superheat required to initiate this nucleate boiling was then calculated using the thermodynamic properties of sodium. It was found that the required superheat decreased for increasing

saturation temperature. The superheat requirements ranged from approximately 1250°F at a saturation temperature of 500°F and a frequency of 24.5 kHz to approximately 20°F at a saturation temperature of 1500°F and a frequency of 14.0 kHz.

Using the frequency dependence an equivalent heating rate for the applied superheat was determined. The heating rate as here used is defined as the increase in temperature above the saturation temperature per unit time which is required to produce nucleate boiling in the liquid. For heating rates below approximately $10^6$ °F/sec the superheat requirements are essentially independent of heating rate. For heating rates above $10^6$ °F/sec the required superheat begins to increase rapidly.

Since the conditions used in this experiment were similar to conditions found in sodium cooled nuclear reactors it is felt that the data developed in this study on the behavior of liquid sodium can be used in reactor analysis for conditions which may produce rapid changes in the liquid sodium pressure or temperature.

## ACKNOWLEDGMENTS

The guidance and assistance given the author by Professor Frederick G. Hammitt, Assistant Professor Louis P. Solomon and the other members of the doctoral committee are gratefully appreciated. The author wishes to thank Dr. Robert Cheesewright* of Queen Mary College, University of London, London, England for his many helpful suggestions.

The financial support of this research project by the National Science Foundation is gratefully acknowledged.

The author is also grateful to Mr. Alton E. Klickman of the Atomic Power Development Associates, Inc. of Detroit, Michigan for the sodium analysis and for his interest in the study. Thanks are due also to Mr. Edward Rupke, Instrument Shop Supervisor, and Mr. William Rekewitz, Instrument Shop Foreman for many helpful suggestions and fabrication of the necessary hardware.

A special thanks to my wife Marsha and my two sons James and Jeffrey whose patience and understanding are especially appreciated.

---

* On leave to the Nuclear Engineering Department, The University of Michigan during this period.

TABLE OF CONTENTS


Page

ACKNOWLEDGMENTS . . . . . ii

LIST OF TABLES . . . . . vi

LIST OF FIGURES . . . . . vii

Chapter

I. INTRODUCTION AND LITERATURE SURVEY . . . . . 1

A. Objective of Investigation . . . . . 1
B. Introduction . . . . . 1
1. Selection of Sodium as a Reactor Coolant
2. Sodium Behavior as Related to Reactor Safety
C. Historical Background . . . . . 8
D. Problem Statement . . . . . 23

II. EXPERIMENTAL EQUIPMENT . . . . . 29

A. Description of Overall System . . . . . 29
B. Ultrasonic Transducer Horn Assembly . . 31
C. High Temperature Cavitation Vessel . . 41
D. Furnace Arrangement . . . . . 44
E. Baffle Plate . . . . . 46

III. DETERMINATION OF THE PRESSURE FIELD PRODUCED BY THE ULTRASONIC TRANSDUCER . . . . . 51

A. Introduction . . . . . 51
B. Theoretical Expression for the Pressure Field . . . . . 53
C. Measurement of the Vibrational Displacement of the Horn Tip . . . . . 62
D. Development of a Pressure Probe for Pressure Field Measurements . . . . . 74
1. Construction of the Pressure Probe
2. Calibration of the Pressure Probe
E. Experimental Measurement of the Pressure Field . . . . . 88

Chapter Page

F. Comparison of Experimental Results with Theoretical Results . . . . . 94
G. Conclusion to Chapter III . . . . . 106

IV. DETERMINATION OF THE ONSET OF CAVITATION . . 108

A. Introduction . . . . . 108
B. Selection of Method for Determining Onset of Cavitation . . . . . 108
1. Effects Produced by Cavitation
2. Methods Used to Determine the Onset of Cavitation
3. Selection of a System for Determining the Onset of Cavitation
C. Development of the Acoustic Probe . . . 112
1. Construction of the Acoustic Probe
2. Experimental Evaluation of the Acoustic Probe
D. Conclusions on Chapter IV . . . . . 125

V. EXPERIMENTAL INVESTIGATIONS IN LIQUID SODIUM . . . . . 126

A. Introduction . . . . . 126
B. Experimental Equipment . . . . . 126
C. Description of Test Specimens Used in Liquid Sodium . . . . . 129
D. Sodium Handling Technique . . . . . 130
E. Experimental Procedure . . . . . 134
1. Calibration of Counterweight Crystal
2. Determination of the Onset and Cessation of Cavitation
F. Sodium Analysis . . . . . 138
G. Discussion of Experimental Results . . 141
1. Experimental Results
2. Data Scatter
3. Fluid Nonlinearity (Hysteresis)
4. Frequency Dependence
5. Temperature Dependence
H. Conclusion to Chapter V . . . . . 162

VI. CONVERSION OF THE ONSET OF CAVITATION DATA TO SODIUM SUPERHEAT REQUIREMENTS . . . . . 164

A. Introduction . . . . . 164
B. Calculation of Changes in Pressure Required at the Onset of Cavitation . . 165
C. Review of the Cavitation Process . . . 170

Chapter Page

D. Conversion to Superheat Requirements . 176
E. Discussion of Superheat Results. . . . 185
F. Calculation of Heating Rate . . . . . 191
G. Summary to Chapter VI . . . . . 194

VII. SUMMARY, CONCLUSIONS, AND SUGGESTIONS FOR FURTHER STUDY . . . . . 197

A. Summary . . . . . 197
B. Conclusions . . . . . 200
C. Suggestions for Further Study . . . . 201

APPENDIX . . . . . 203

A. Derivation of the Superheat Equation, Eq (1.3) . . . . . 203

REFERENCES . . . . . 206

## LIST OF TABLES


Table | Page

1. Comparison of Properties of Sodium and Potassium with Water . . . . . 4
2. Estimated Liquid Superheats Required to Sustain Boiling with the Alkali Liquid Metals at 1 Atm Pressure . . . . . 21
3. Length of Stainless Steel Exponential Horn Section and Corresponding Resonant Frequency . 39
4. Counterweight Crystal Voltage at the Onset and Cessation of Cavitation in Partially Degassed Distilled Water . . . . . 123
5. Counterweight Crystal Voltage at the Onset and Cessation of Cavitation in Liquid Sodium at 18534 Hz and 1465°F . . . . . 139
6. Analysis of Sodium Used in This Experiment and Analysis of Sodium Used in the Enrico Fermi Nuclear Reactor . . . . . 142
7. Numerical Values Used in the Calculation of Sodium Superheat . . . . . 181
8. Numerical Values Used in the Comparison of Superheat Results Using Eq (1.3) with Results Shown in Fig 45 . . . . . 186

## LIST OF FIGURES


| Figure | | Page |
|---|---|---|
| 1. | Typical Boiling Curve for Water at One Atmosphere | 10 |
| 2. | Liquid Superheat with Potassium, 0.006-in.-diam Holes in Surface | 18 |
| 3. | Liquid Superheat with Sodium, 0.006-in.-diam Holes in Surface | 19 |
| 4. | Block Diagram of the High-Temperature Ultrasonic Vibratory Facility | 30 |
| 5. | Photograph of the High-Temperature Ultrasonic Cavitation Facility | 32 |
| 6. | Exponential Horn and Ultrasonic Transducer Assembly | 33 |
| 7. | Typical Waveform Showing Position of Nodes and Antinodes on Transducer Assembly | 36 |
| 8. | Cavitation Test Specimen | 40 |
| 9. | High-Temperature Cavitation Vessel and Ultrasonic Transducer | 42 |
| 10. | High-Temperature Cavitation Vessel and Ultrasonic Transducer Assembly Mounted in Furnace | 45 |
| 11. | Schematic of Variac, Furnace, and Temperature Controller | 47 |
| 12. | Photograph of the Baffle Plate Mounted to the Vessel Top Plate | 49 |
| 13. | Cavitation Vessel, Baffle Plate, and Transducer Horn Assembly | 54 |
| 14. | Curves of Resonant Frequency for Various Modes of Vibration | 61 |

Figure Page

15. Calibration Curve for KD-38 Fotonic Sensor . . . . . 68

16. Experimental Arrangement for Calibrating Counterweight Crystal . . . . . 69

17. Counterweight Calibration Curves for the 14.4 kHz and 18.5 kHz Transducer Horn Assemblies . . . . . 71

18. Typical Waveforms Observed During Counterweight Crystal Calibration . . . . . 72

19. Experimental Arrangement Used to Determine Test Fluid Loading Effect . . . . . 73

20. Cross Sectional View of Tip of Pressure Probe . . . . . 77

21. Pressure Probe with Attached Coaxial Cable . . 78

22. Experimental Arrangement for Pressure Probe Calibration . . . . . 79

23. Photographs of Pressure Probe Calibration System . . . . . 82

24. Top View of Aluminum End Section . . . . . 83

25. Calibration Curve for Pressure Probe . . . . . 86

26. Photograph of Typical Voltage Waveforms Observed During Pressure Probe Calibration . . . . . 87

27. Experimental Arrangement for Mapping Pressure Field . . . . . 89

28. Photographs of Cavitation Vessel, Positioner, Pressure Probe, and Dial Indicator . . . . . 91

29. Photographs of Voltage Waveforms Observed During Pressure Field Mapping . . . . . 93

30. Pressure Distribution in Z Direction for $\ell$ = 2.22 inches, Frequency = 18560 Hz, and A = $1.50 \times 10^{-5}$ inches . . . . . 96

31. Pressure Distribution in Z Direction for $\ell$ = 0.75 inches, Frequency = 14498 Hz, and A = $4.43 \times 10^{-5}$ inches . . . . . 101

Figure Page

32. Schematic Cross Sectional View of the Crystal Assembly for the Acoustic Probe . . . . . 115

33. Experimental Arrangement to Determine Performance of Acoustic Probe . . . . . 117

34. Photographs of Typical Waveforms Observed Prior to and at the Onset of Cavitation . . 119

35. Curves of Resonant Frequency for Various Modes of Vibration Using Liquid Sodium as the Test Fluid . . . . . 128

36. Counterweight Crystal Calibration Curves for the 14, 20, 22, and 25 kHz Transducer Horn Assemblies . . . . . 135

37. Photographs of Typical Waveforms Observed Prior to and at the Onset of Cavitation in Liquid Sodium . . . . . 140

38. Counterweight Crystal Voltage at Onset of Cavitation in Liquid Sodium Using the 14, 20, 22, and 25 kHz Transducer Horn Assemblies . . . . . 143

39. Counterweight Crystal Voltage at Cessation of Cavitation in Liquid Sodium Using the 14, 20, 22, and 25 kHz Transducer Horn Assemblies . . . . . 147

40. Counterweight Crystal Voltage at Onset of Cavitation Versus Frequency for Liquid Sodium Temperatures of 500, 1000, and 1500°F . . . . . 154

41. Peak Pressure of Sinusoidal Pressure Wave at Onset of Cavitation Versus Liquid Sodium Temperature Using the 14, 20, 22, and 25 kHz Transducer Horn Assemblies . . . 168

42. Peak Value of Sinusoidal Pressure Wave at Onset of Cavitation Versus Frequency for Liquid Sodium Temperatures 500, 750, 1000, 1250, and 1500°F . . . . . 169

43. Relationships Among Atmospheric Pressure, $P_a$, Vapor Pressure, $P_v$, and Applied Sinusoidal Pressure Field, $P_o \sin \omega t$ . . . . 172

Figure Page

44. $2\sigma/R'$ Versus Temperature of Liquid Sodium at the Onset of Cavitation for 14, 17.5, 21, and 24.5 kHz . . . . . 180

45. Liquid Sodium Superheat Versus Saturation Temperature for 14, 17.5, 21, and 24.5 kHz . . 183

46. Liquid Sodium Superheat Versus Frequency for Saturation Temperatures 500, 750, 1000, 1250, and 1500°F . . . . . 184

47. Application of a Sinusoidal Temperature Change of Frequency f to Liquid Sodium Initially at its Saturation Temperature $T_{sat}$ . . . . . 193

48. Heating Rate Versus Liquid Sodium Superheat for Saturation Temperatures 500, 750, 1000, 1250, and 1500°F . . . . . 195

# CHAPTER I

# INTRODUCTION AND LITERATURE SURVEY

## A. Objective of Investigation

The objective of this investigation is to obtain data on the behavior of liquid sodium under conditions which may be encountered when sodium is used as a coolant in a fast breeder nuclear reactor. An experiment was designed to determine the amount of superheat required to produce nucleate boiling in liquid sodium both as a function of the heating rate and as a function of the temperature of the liquid sodium.

## B. Introduction

### 1. Selection of Sodium as a Reactor Coolant

In choosing a coolant for a fast breeder nuclear reactor several requirements for the coolant must be considered.[1] The major requirements are

1) the moderation of the neutrons by the coolant must be low. This requires that the coolant have a high mass number so that a minimum amount of energy is transferred from the neutron to the coolant nuclei during a collision.

2) the coolant should possess high heat transfer capability and a high heat capacity. Because the effective fission cross sections in fast reactors are relatively small compared to those for thermal reactors, a high concentration

of fissile fuel is required. This results in a relatively high power density and thus requires that the coolant possess high heat transfer characteristics.

3) the coolant should possess a high boiling point. The boiling point of the coolant should be above the normal operating temperature of the core so that high pressurization which would demand greater wall thicknesses is not necessary.

The above requirements are perhaps most important in choosing a coolant for a fast reactor. However, other factors must also be considered. The coolant should have little corrosive effects on container walls. It should not become radioactive or, if radioactive, the half-life should be short. The coolant should possess a low neutron absorption cross section. The cost of the coolant should be low.

No one particular coolant satisfies all the above requirements. The coolants which most nearly satisfy the above requirements are the liquid metals, namely bismuth, gallium, lead, lithium, mercury, potassium, rubidium, sodium, tin, zinc, sulfur, and phosphorus. However, most of the liquid metals possess one or more major disadvantages.[2] Bismuth has a high melting point, approximately 520°F, and would require excessive pumping power due to its high density. Bismuth also presents, as does lead, a high temperature containment problem. Gallium is expensive, approximately $675/lb. Lead has a high melting point, 620°F, and would require excessive pumping power. Lithium is expensive, approximately $54/lb. Mercury has a low boiling point, a high absorption cross-section,

requires high pumping power, and is expensive. Rubidium is expensive, $390/lb. Tin possesses relatively poor thermal properties. Zinc has too high a melting point, 787°F. Sulfur has too low a boiling point. Phosphorus is highly corrosive. Sodium and potassium possess many of the necessary characteristics without having a major disadvantage and are compatible with the common stainless steels up to the necessary operating temperatures. A comparison of the characteristics of sodium and potassium with water is shown in Table 1.

Because sodium has better thermal properties and a lower cost, sodium is preferred over potassium. A mixture of sodium and potassium, referred to as NaK, is also considered as a fast reactor coolant.

## 2. Sodium Behavior as Related to Reactor Safety

Before proceeding further with any discussion on the investigation of the properties of sodium, it is felt that it is necessary to briefly review the safety considerations in fast reactor design. A review of the safety considerations indicates the need for obtaining additional information on liquid sodium properties.

In reviewing the safety design of fast reactors one must consider two basic features by which fast reactors differ from thermal reactors. First, the prompt neutron lifetime in a fast reactor is approximately $10^{-7}$ sec as compared to $10^{-4}$ sec for a thermal reactor.[3] The prompt neutron lifetime is the average time from the emission of a neutron during fission to the absorption of the neutron somewhere in the

TABLE 1

COMPARISON OF PROPERTIES OF SODIUM AND POTASSIUM WITH WATER

| Property | Water | Sodium | Potassium |
|---|---|---|---|
| M. P., $^{o}F$ | 32 | 208 | 146 |
| B. P., $^{o}F$ | 212 | 1618 | 1402 |
| Thermal Cond BTU/ft hr $^{o}F$ | 0.248 | 37[a] | 21.2[a] |
| Specific Heat BTU/lb $^{o}F$ | 1 | 0.301[a] | 0.182[a] |
| Cost/lb | - | $0.17[b] | $3.66[b] |

[a] Measured at 1000$^{o}F$.

[b] Estimated as of 1960.

reactor. Therefore, for large changes in the reactivity where the excess reactivity exceeds the effect of delayed neutrons (neutrons produced by decay of fission fragments) the power level of a fast reactor will rise with a shorter period than that of a thermal reactor. Second, because the fission cross sections are small for high neutron energy the fast reactor must possess a high concentration of fissile fuel in order to become critical. This high fuel concentration results in the reactor being very sensitive to small changes in the loading of the fuel. These differences require the ability to predict the behavior of the coolant of a fast reactor under any adverse condition which may result in a rapid change in the temperature of the reactor.

The behavior of the liquid sodium and how it affects the operation of a fast reactor can generally be determined by considering the effect of changes in the density of the sodium on the temperature coefficient of the reactor. A positive temperature coefficient is defined as an increase in reactivity of the reactor for an increase in the temperature of the reactor. A negative temperature coefficient is defined as a decrease in the reactivity for an increase in temperature. For safe operation of a reactor a negative temperature coefficient is desired since an increase in temperature would decrease the reactivity which in turn would then lower the temperature.

The sodium temperature coefficient consists of two main parts.[4] First, as the temperature of the reactor increases, the sodium becomes less dense so that more neutrons are allowed

to escape from the core and thus the reactivity of the reactor is decreased. Second, as the sodium density decreases with increasing temperature the moderating effect of the sodium is reduced which results in a hardening of the neutron energy spectrum, i. e., the average energy of the neutrons is increased. This results in more U-238 fissions and less non-fission captures by U-238, and also results in a greater number of fission neutrons emitted during the fission of Pu-239. Therefore, the result of the hardening of the energy spectrum of the neutrons is an increase in the reactivity of the reactor and thus a positive temperature coefficient. The negative temperature coefficient is generally controlling for small core sizes with large leakage. However, for large cores the positive coefficient can cancel the negative coefficient since the relative importance of leakage becomes small for such cores, with the result that the overall sodium temperature coefficient may be positive.[5]

There are other temperature coefficients in a fast reactor such as axial fuel expansion, Doppler broadening, fuel element bowing, and radial core expansion. However for the present discussion we are primarily interested in the changes in the reactivity due to changes in the density of the sodium.

From the above discussion we have seen that the sodium temperature coefficient may be positive or negative depending upon the geometry of the reactor core. Independent of whether this coefficient is negative or positive, its magnitude and the reaction time of the sodium to a change in temperature must be determined so that an accurate analysis of

the response of the reactor to a change in temperature can be made. For example, let us assume that the sodium coefficient reduces the reactivity for a temperature increase. Now, let us assume that the reactor experiences a large increase in temperature in a very short period of time. Two questions arise:

1) is this increase in temperature sufficient to produce a significant change in the density of the sodium, i. e., will boiling occur in the sodium?

2) if boiling occurs in the sodium, how soon after the temperature is increased, will this boiling occur?

The answers to both of these questions must be known; then, it can be determined if and when the negative sodium coefficient arises in order to reduce this increase in temperature.

The increase in the temperature of the reactor which may result in boiling of the sodium may be brought about by several causes. A coolant pump which circulates the sodium through the reactor may fail which would result in a rapid buildup of temperature in the core. A coolant channel in the core may become plugged by a foreign object, and this would result in a local temperature increase in the region of the plugged channel. An inadvertent withdrawal of a control rod would result in a temperature increase in the core. It is conceivable that this temperature increase (which may be produced by any of the above mechanisms) may occur in a very short period of time, possibly on the order of seconds or less.[6]

A question which may arise at this time is the following. If the temperature of the reactor increases, then will boiling occur when the temperature of the sodium reaches its "boiling point?" It is pointed out in the next section that for boiling to occur within the bulk of the sodium and not at a free surface the temperature of the sodium must be increased above its "boiling point." It is pointed out that this increase in the temperature above the "boiling point" may vary from a few degrees to several hundred degrees. It is indeed this uncertainty in the amount that the temperature has to be increased above the "boiling point" which produces the difficulty in predicting the behavior of sodium and thus the behavior of the reactor under large and rapid changes in its temperature. This increase in temperature above the "boiling point" is not a constant quantity but depends on such factors as gas content in the sodium, impurities in the sodium, conditions of the heat transfer surfaces, the temperature of the sodium, and also on the time of application of the increase in temperature, which is necessary to produce boiling.

## C. Historical Background

Man has probably observed the phenomenon of boiling of liquids since the discovery of fire; however, until recent years little understanding has been gained concerning this phenomenon.

One of the first experiments conducted which resulted in a great advance in the understanding of boiling was conducted by Nukiyama[7] in 1934. He submerged a thin platinum wire in

water at 212°F and heated the wire electrically to produce boiling. He observed that as he increased the temperature of the wire the heat transferred from the wire increased smoothly until the wire temperature reached about 300°F. At this point the temperature of the wire jumped to about 1800°F. A further increase in the wire temperature resulted in a smooth increase in the heat transferred from the wire. By decreasing the temperature of the wire down from 1800°F Nukiyama found that the heat transfer rate decreased smoothly until the temperature reached approximately 570°F. At this point the temperature jumped to below 300°F. Below this point the system followed the same curve that was obtained for an increase in temperature. A boiling curve similar to Nukiyama's results is shown in Fig 1.

Nukiyama concluded that three types of boiling are represented by the boiling curve. The first type of boiling encountered by Nukiyama is now known as nucleate boiling. As the temperature is increased above 212°F bubbles form and grow at discrete points on the wire. As the temperature is increased bubbles form and grow at additional points or sites until the entire wire is covered by bubbles which is represented by point B on the curve. At this point the boiling becomes film boiling and the temperature jumps to point D. The name film boiling applies since the wire is now surrounded by a film of vapor and the heat transfer from the wire to the water must pass through this film of vapor and to produce the same heat transfer rate through this film as with nucleate boiling requires

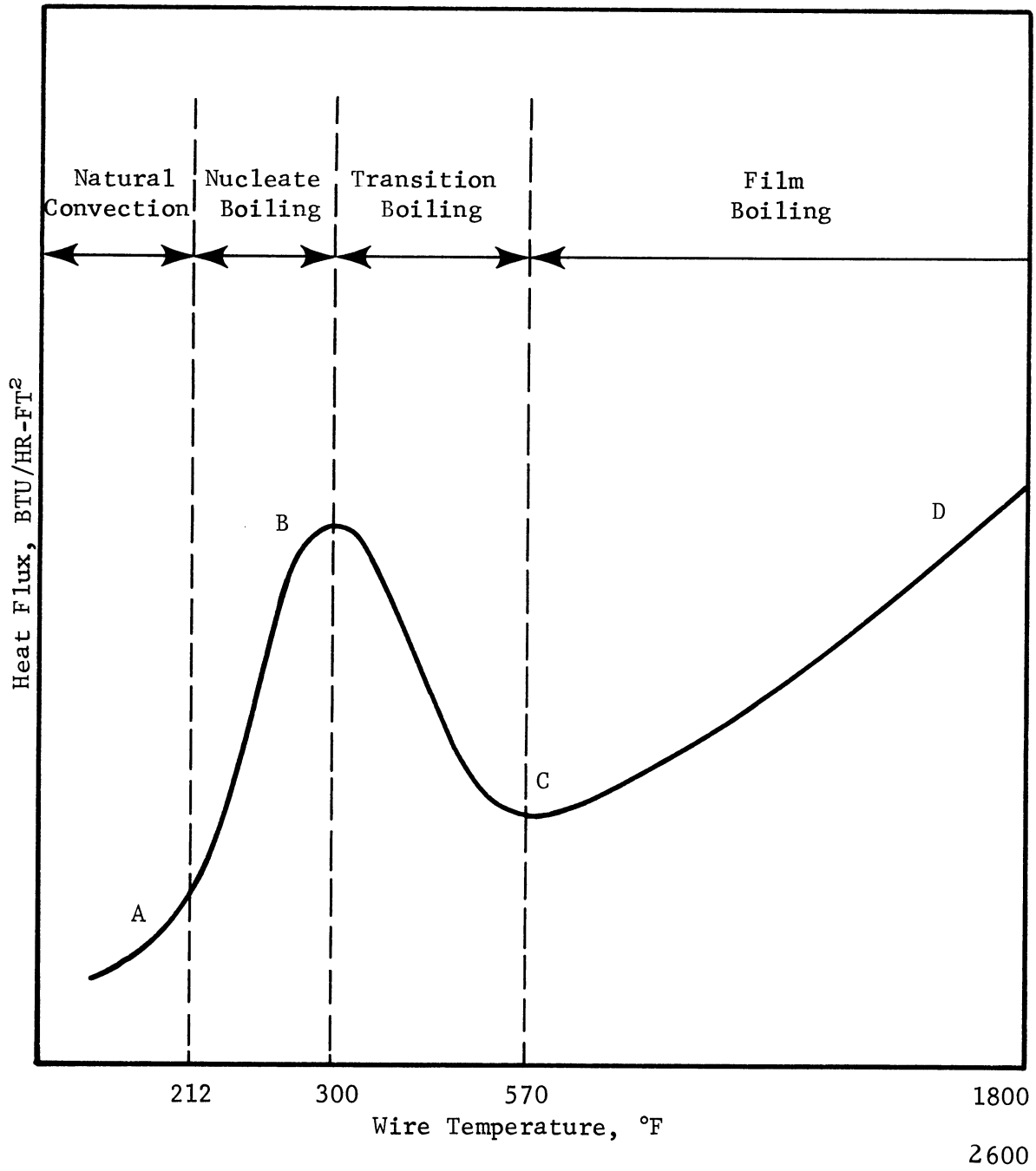


FIGURE 1. TYPICAL BOILING CURVE FOR WATER AT ONE ATMOSPHERE

much higher temperature differentials. At these higher temperatures a larger portion of the heat is being transferred by radiation, and the remainder by conduction across the vapor film. The portion of the curve BC is referred to as metastable or transition boiling. The heat flux in this region decreases as the temperature increases. In this region of the curve there are no active sites for nucleation. The portion of the curve up to point A does not represent boiling but rather heating by natural convection. For the remainder of this study we are primarily concerned with the nucleate boiling process.

Nucleate boiling is characterized by two separate processes, the formation of bubbles (nucleation) and the subsequent growth of these bubbles.[8] In order for the first process to occur there must exist in the liquid sites or locations from which the bubbles can originate. The exact nature of these sites has not been established; however, there are several theories as to possible descriptions of these sites. Blake[9] suggests that nucleation originates from extremely small bubbles (radii of approximately $10^{-7}$ cm) which are stabilized in ordinary liquids, although the method of stabilization is not known. Harvey et al[10] propose that small gas or vapor bubbles could become stabilized in cracks in the nonwettable surface of minute solid particles in the liquid or in the surface of the liquid container. Ibelle[11] provides descriptions of other possible sites for bubble nucleation; however, most investigators feel that nucleation originates

from cracks in either nonwettable surfaces of minute particles which are suspended in the liquid or from cracks in nonwettable surfaces of the liquid container.

If we assume that we have a small spherical vapor bubble of radius R in unstable equilibrium in a liquid, then writing a force balance equation for the bubble, we obtain

$$P_V - P_L = \frac{2\sigma}{R} \tag{1.1}$$

where

$P_V$ = vapor pressure inside bubble

$P_L$ = liquid pressure

$\sigma$ = surface tension

$R$ = radius of bubble.

Unstable equilibrium exists in that for a bubble of radius greater than R, Eq (1.1) is no longer satisfied and the bubble will grow. For a bubble of radius less than R, Eq (1.1) is again no longer satisfied and the bubble will collapse. Therefore, if we have a vapor bubble of radius R stabilized in the liquid, or if we have a crack in a nonwettable surface where the radius of curvature of the liquid-vapor interface is R, then in order to initiate bubble growth in the liquid, conditions must be such that Eq (1.1) is satisfied before bubble growth can occur.

From Eq (1.1) we see that the pressure inside the bubble must exceed the pressure of the liquid because of the surface tension effect. This difference in pressure between the vapor and the liquid is generally satisfied in most boiling

applications by maintaining the pressure of the liquid constant, and by increasing the temperature of the liquid until the increase in vapor pressure produced by this increase in temperature satisfies Eq (1.1). It should be noted that the saturation temperature corresponding to the pressure of the liquid is generally referred to as the "boiling point" of the liquid. The saturation temperature is defined as the temperature of the vapor at the interface betweeen a liquid and its vapor.[12, 13] The pressure of the vapor at the saturation temperature is referred to as the saturation pressure and may not be the same as the liquid pressure. For example, if a beaker of water open to the atmosphere is held at a constant uniform temperature of 70°F, the temperature of the vapor at the surface is 70°F and the vapor pressure is 0.36 psia.[14] Since the vapor pressure is not equal to the liquid pressure the 70°F temperature is not referred to as the "boiling point" of the liquid. If the water is now maintained at a constant temperature of 212°F the temperature of the vapor at the surface is 212°F and the vapor pressure is 14.7 psia.[14] Since the vapor pressure is now equal to the liquid pressure the 212°F temperature is referred to as the "boiling point" of the liquid. For nucleate boiling to occur within the liquid the temperature of the liquid must be increased above the "boiling point" since the vapor pressure associated with this increase in temperature must exceed the liquid pressure in order to overcome the surface tension effect. If the temperature of the liquid is increased above the "boiling point" such that Eq (1.1) is satisfied, then a further increase

in temperature would produce further evaporation at the bubble wall and would cause the radius R to become larger, so that Eq (1.1) would no longer be satisfied and the bubble would grow without limit.

If we consider the case of a spherical bubble which contains a small amount of undissolved gas, then Eq (1.1) takes the form

$$P_v + P_g - P_L = \frac{2\sigma}{R} \qquad (1.2)$$

where

$P_g$ = partial pressure of the undissolved gas.

From Eq (1.2) we note that the change in temperature necessary to satisfy this equation is less than for Eq (1.1) for the same bubble radius R since the required vapor pressure is now reduced by the amount $P_g$. In fact, the liquid may boil at temperatures below its "boiling point" if $P_g$ is large enough.

The amount that the temperature of a liquid has to be increased above its "boiling point" in order to produce nucleate boiling in the liquid is referred to as superheat.[11, 13] To obtain an explicit expression for this superheat requirement Ellion[15] in 1954 combined the Clausius-Clapeyron equation which relates changes in pressure to changes in temperature along the saturation curve with Eq (1.1) and by using the ideal gas law approximation he obtained

$$T_v - T_{SAT} = \frac{G\, T_v\, T_{SAT}}{h} \ln\left(1 + \frac{2\sigma}{R\, P_L}\right) \qquad (1.3)$$

where

$T_v$ = temperature of vapor in bubble

$T_{SAT}$ = saturation temperature of liquid corresponding to the pressure of the liquid

$G$ = ideal gas constant

$h$ = latent heat of vaporization.

Eq (1.3) which is derived in Appendix A predicts the amount of superheat, i. e., the amount that the temperature of the liquid has to be increased above its "boiling point" in order to produce nucleate boiling in a liquid with initial vapor bubbles of radius R. From Eq (1.3) it can be seen that as R is increased the superheat requirement is decreased and as R becomes infinite (plane interface between liquid and vapor) the superheat requirements become zero. At this point we have surface evaporation and the temperature of the vapor at this surface is at the "boiling point" or the saturation temperature corresponding to the pressure of the liquid. As R is reduced the superheat requirement becomes larger and as R approaches zero the superheat requirement becomes infinite. However, the conditions of perfect purity and surface smoothness are unobtainable so that superheat requirements remain finite.

To verify Eq (1.3), Wallis and Griffith[16] in 1959 carried out nucleation experiments by immersing in water a copper sheet containing a conical cavity made by pressing into the surface of the copper a phonograph needle having an apex angle of 18°. Using the cavity radius at its mouth as R, their data of superheat required to produce nucleation and bubble

growth agreed quite well with Eq (1.3).

Berenson[17] using a heated copper surface showed that higher wall superheats were required to boil pentane from smoother surfaces. The smoother surface has smaller cavities and hence the radius of curvature of the vapor bubble is smaller than for the rough surface and from Eq (1.3) requires a greater wall superheat for bubble growth.

Farber and Scorah[18] using chromel-c wire submerged in water showed that a smaller wall superheat is required for boiling as the pressure of the liquid is increased and this result is consistant with Eq (1.3).

Eqs (1.1) and (1.3) appear to reasonably explain the behavior of water and other organic fluids when subjected to conditions which lead to nucleate boiling in the fluid. Since the surface tensions of the alkali metals do not differ greatly from the surface tension of water, it appeared reasonable that Eqs (1.1) and (1.3) could be used to predict the behavior of the liquid metals under nucleate boiling conditions.

Edwards and Hoffman[19] used a natural circulation loop to study nucleate boiling in liquid sodium and liquid potassium. Using a surface containing 0.006 inches diameter holes they found reasonably good agreement between the experimental superheat required to initiate boiling and the superheat predicted by Eq (1.3). The comparison between experimental results and the theoretical curve for a bubble radius of 0.003 inches obtained by Edwards and Hoffman is

shown in Fig 2 for potassium and in Fig 3 for sodium. Also shown in Figs 2 and 3 are theoretical curves for various values of R to indicate the effect of a change in R. The agreement for sodium is not as good as that for potassium. However, this may be due to the uncertainty in the surface tension values used for sodium.

Marto and Rohnsenow[20] investigated the effects of surface conditions on nucleate boiling and found that the smoother the surface the greater the superheat requirement for nucleate boiling in liquid sodium. They also determined that as the pressure of the system was reduced the superheat requirement was increased. Both of these effects are in agreement with the behavior predicted by Eq (1.3).

At high pressures where $T_V - T_{sat}$ is small, Krakoviak[21] assumed that

$$\ln\left(1 + \frac{2\sigma}{R P_L}\right) \approx \frac{2\sigma}{R P_L}$$

so that Eq (1.3) becomes

$$T_V - T_{SAT} = \frac{2\sigma G T_V T_{SAT}}{R P_L h} \qquad (1.4)$$

Eq (1.4) was then applied to water and to the liquid metals and the two cases were combined to obtain

$$\frac{(T_V - T_{SAT})_W}{(T_V - T_{SAT})_X} = \frac{(\sigma T_V V_{fg})_W (hR)_X}{(\sigma T_V V_{fg})_X (hR)_W} \qquad (1.5)$$

where

$V_{fg}$ = specific volume change between liquid and vapor

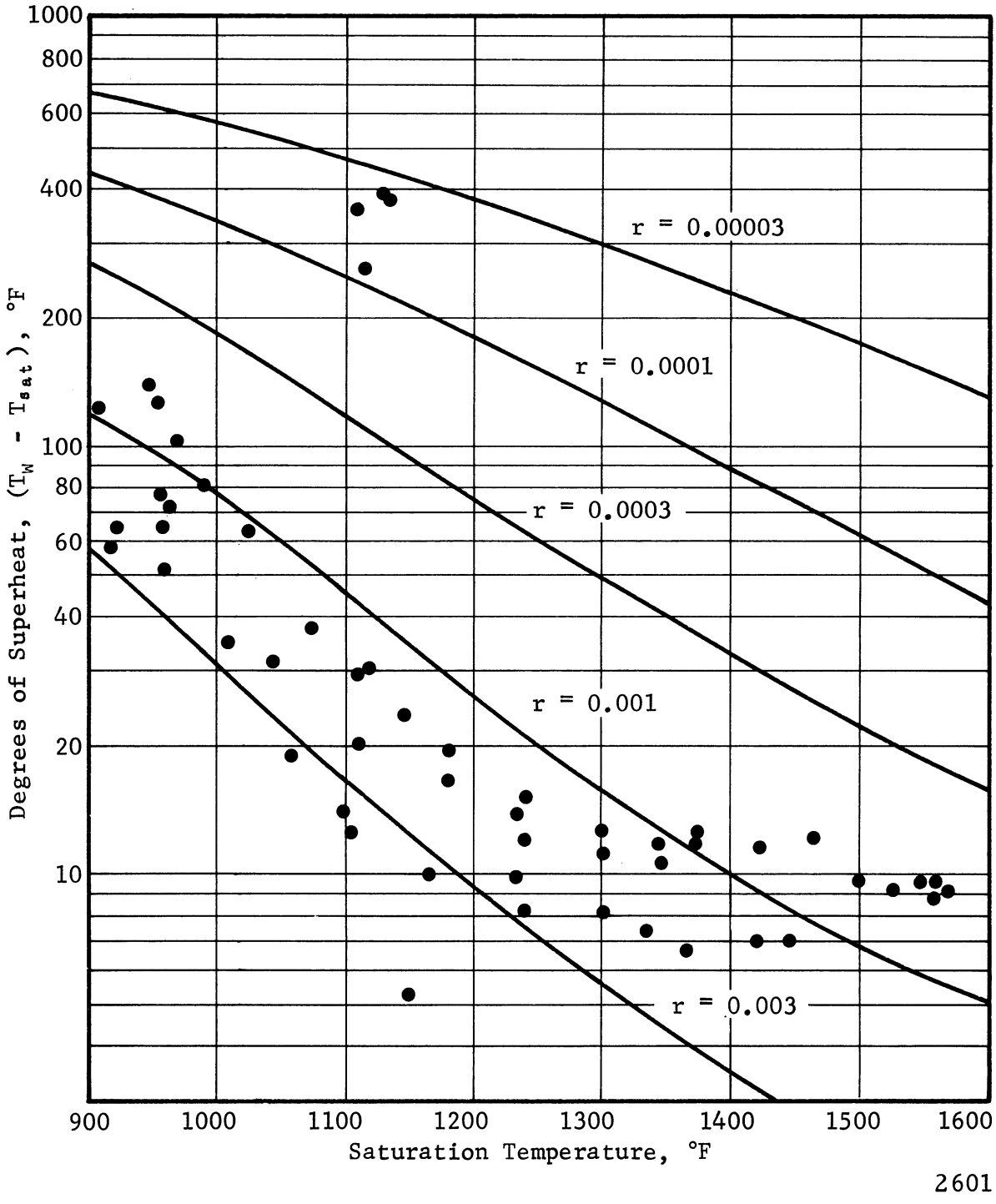


FIGURE 2. LIQUID SUPERHEAT WITH POTASSIUM, 0.006-INCH-DIAMETER HOLES IN SURFACE

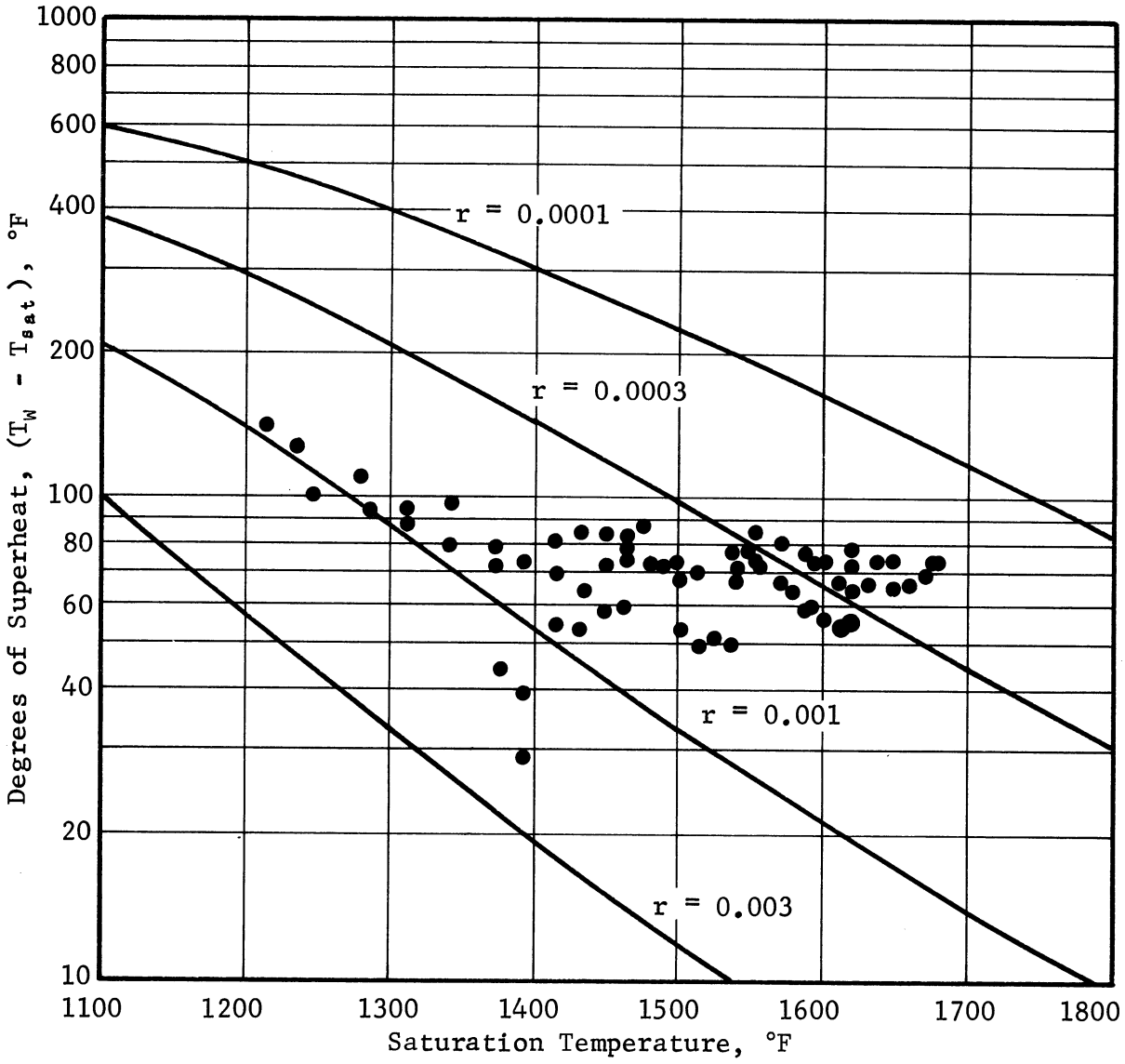


FIGURE 3. LIQUID SUPERHEAT WITH SODIUM, 0.006-INCH-DIAMETER HOLES IN SURFACE

and the subscripts w and x refer to the water and the liquid metal, respectively. For purposes of specifying the surface conditions Krakoviak chose two values of superheat for water. The first superheat value was 30°F which was obtained for water at 1 atm which produced boiling from a smooth surface. The second superheat value for water was 90°F which was obtained at 1 atm for boiling from a much smoother surface and with a much cleaner sample of water. Using these values of superheat Krakoviak then was able to calculate superheat requirements for any of the liquid metals under the same conditions, i. e., with the same surface conditions and same liquid pressure. Krakoviak's calculations and comparisons are summarized in Table 2. From Table 2 it can be seen that the measured values of superheat for the liquid metals are between the calculated values of superheat using the two temperatures as a basis for the calculations. It would be expected that the measured values should correspond more closely to the case when the 90°F superheat was used for water since liquid metals wet most metals easily, and this would therefore reduce the number of nucleation sites. Also, the liquid metals used are generally of very high purity and are in contact with clean surfaces in the absence of inert gases. These conditions correspond more closely to the conditions describing the water case when 90°F of superheat was required for nucleation and bubble growth.

Considerable work has been done in recent years investigating heat transfer for liquid metals which has not been mentioned above. A more complete review is given by

TABLE 2

ESTIMATED LIQUID SUPERHEATS REQUIRED TO SUSTAIN BOILING WITH THE ALKALI LIQUID METALS AT 1 ATM PRESSURE

| Fluid | Calculated Superheat Based on 30°F for Water, °F | Measured Superheat, °F | Calculated Superheat Based on 90°F for Water, °F |
|---|---|---|---|
| Na | 258 | - | 774 |
| K | 125 | 342 | 375 |
| Rb | 101 | 135 | 303 |
| Cs | 67 | - | 201 |

Dwyer[22] who summarizes recent developments in liquid metal heat transfer and cites 100 references. However, the liquid metal investigations discussed above which investigate superheat requirements are representative of the advances made in heat transfer through nucleate boiling in the liquid metals.

In reviewing the nucleate boiling experiments it was noted that surface conditions and impurity content were considered as controlling parameters in determining superheat requirements. However, there are relatively few experiments in which the application time of the superheat was treated as a variable. In the experiments which have been reviewed above, the heating rate which is defined as the rate of increase in temperature above the saturation temperature per unit time, was of such duration that these experiments could be considered steady state experiments.

Hall and Harrison[23] conducted transient boiling experiments in water using an electrically heated ribbon immersed in water. The heating rate was exponential with periods ranging from 0.7 millisec to 5 millisec. They found that as the period was increased the superheat requirements were reduced. For example, with water at 20°C the superheat required to produce boiling with a 0.7 millisec period was 82°C; whereas, the superheat required with a 5 millisec period was only 53°C. Also, they indicated that as the temperature of the system was increased the superheat requirements were reduced.

Johnson[24] conducted similar transient boiling experiments in water with exponential heating rates. His shortest period was 5 millisec and the trends reported were in agreement with Hall and Harrison.

There appears to be essentially no experimental data available on the transient boiling of liquid metals, although some theoretical work in this area has begun.[25] Although their experiment was not designed to determine the time dependence on superheat requirements, Holtz and Singer[26] did report that incipient boiling superheat requirements for sodium increased slightly with an increase in heat flux. Their heating rates were relatively slow, however. The trend does indicate that as the heating rate is increased the superheat requirement is increased. As mentioned above this trend is in agreement with transient boiling data obtained for water.

## D. Problem Statement

It was pointed out earlier that large changes in temperature of a sodium cooled fast reactor may occur in a very short period of time. It therefore becomes necessary to determine superheat requirements as a function of the heating rate for the liquid sodium. As pointed out in the previous section the heating rate is defined as the rate of increase in temperature above the saturation temperature per unit time. For example, if it were determined that in a steady state (slow heating rate) experiment 100 degrees of superheat were necessary to produce boiling in a liquid for a specific

set of conditions, would this 100 degrees of superheat produce boiling in the same liquid under the same set of conditions but with an increase in the heating rate? If there is a change in the superheat requirements as the heating rate is increased, then it becomes necessary to determine this dependence in order to be able to predict the behavior of the sodium coolant as rapid changes in the reactor temperature occur. Knowing the time dependence the response of the reactor to rapid changes in temperature can be more accurately predicted.

The question now arises as to how one may determine the time dependence of superheat requirements experimentally? One method is to use heat transfer techniques in which the pressure of the system is held constant and the temperature of the system is increased above the "boiling point" of the liquid until nucleate boiling occurs. However, another approach to producing boiling in a liquid can be taken. It has been pointed out earlier that in order to produce nucleate boiling in the liquid Eq (1.1) must first be satisfied. Instead of maintaining the pressure of the liquid constant and then increase the temperature of the system until the saturation pressure corresponding to this increase in temperature satisfies Eq (1.1), the temperature of the system can be held constant and then the pressure of the liquid lowered until Eq (1.1) is satisfied. This is the technique used in cavitation studies to produce cavitation bubbles in a liquid. The essential difference between nucleate boiling studies and cavitation studies is only that in cavitation studies once nucleation and

bubble growth is established, the pressure field is again altered such that these bubbles are then forced to collapse. Therefore, it seems reasonable that cavitation techniques could be used to investigate the concept of nucleate boiling. In using cavitation techniques to produce boiling in the liquid the interest would be focused on the conditions leading to nucleation and bubble growth and not on the effects produced by the collapse of these bubbles. It should be emphasized that the common feature between the heat transfer technique and the cavitation technique in producing nucleation and bubble growth is that Eq (1.1) must be satisfied. Since Eq (1.1) has been substantiated both in water and in liquid metals it is clear that data obtained by cavitation techniques can be related to nucleate boiling requirements.

Experiments have been performed in which nucleate boiling was produced by maintaining the temperature of the liquid constant and by lowering the pressure of the liquid below the vapor pressure in order to produce boiling. For example, Hooper et al[27] produced boiling by heating a sample of pressurized water above the saturation temperature corresponding to atmospheric pressure. The pressure was then suddenly lowered to atmospheric pressure leaving the water in a superheated condition which then produced nucleate boiling in the liquid. They obtained superheats between $10^{\circ}F$ and $50^{\circ}F$ with time delays between the release of pressure and the occurrence of nucleation on the order of 4 to 8 millisec.

There are several advantages in using cavitation

techniques to produce nucleate boiling in a liquid. The primary advantage is that cavitation, or boiling, can be produced in this manner in very short periods of time which are inaccessible using standard heat transfer techniques. In ultrasonic cavitation studies the liquid is subjected to a sound wave whose negative pressure pulses are sufficient to lower the local pressure in the liquid below the vapor pressure corresponding to the temperature of the liquid so that nucleation and bubble growth occur. For a frequency of 20 kHz the duration of this negative pressure which produces boiling in the liquid is 25 microsec. The duration of this pulse can be changed by merely changing the frequency of the sound wave. A second advantage in using cavitation techniques to study nucleate boiling is that these techniques have been used for a number of years at the University of Michigan to investigate cavitation phenomena. A minimum amount of additional instrumentation is necessary to apply these techniques to the study of nucleate boiling in liquid sodium. A third advantage is the relative economy and simplicity with which the experiment can be accomplished using this approach, even with high temperature sodium.

In view of the above discussion it was decided to use the University of Michigan high-temperature ultrasonic vibratory facility to determine superheat requirements for liquid sodium both as a function of temperature and as a function of heating rate. The amplitude of the sound wave is gradually increased until the onset of cavitation is established.

The onset of cavitation is identified with nucleation and bubble growth, i. e., the onset of nucleate boiling in the liquid. Knowing the changes in pressure necessary to produce this boiling, and knowing the frequency of the sound wave, this data is then converted to superheat requirements. This process is repeated for several frequencies so that a curve of superheat requirements versus heating rate can be determined. Since the ultrasonic facility has the capability of controlling the temperature, superheat requirements are determined as a function of temperature for a temperature range of 500°F to 1500°F.

To obtain the above data the following substantial steps were accomplished.

1) Develop and experimentally verify a theoretical expression for the pressure field produced by the ultrasonic cavitation facility.

2) Develop a system to determine the onset of cavitation in liquid sodium.

3) Develop the capability of measuring all necessary parameters at the onset of cavitation so that the pressure field can be evaluated.

4) Experimentally determine the onset of cavitation in liquid sodium both as a function of frequency and as a function of the sodium temperature.

5) Calculate the changes in pressure necessary to produce cavitation in the liquid sodium using the experimentally determined parameters obtained at the onset of cavitation

6) Convert pressure data to superheat requirements to obtain curves of superheat requirements both as a function of heating rate and as a function of saturation temperature of the liquid sodium.

# CHAPTER II

## EXPERIMENTAL EQUIPMENT

### A. Description of Overall System

The University of Michigan high-temperature ultrasonic vibratory cavitation facility is described in detail elsewhere.[28] However, in connection with its use for the present investigation, certain modifications have been incorporated. Hence, a description of the modified facility will be given here.

Fig 4 is a schematic diagram of the modified facility indicating the audio oscillator, power amplifier, transducer assembly, exponential horn, containment vessel, baffle plate, furnace, counterweight crystal, oscilloscope, frequency counter, and the vacuum tube voltmeter (VTVM). A sinusoidal voltage signal, supplied by the variable frequency audio oscillator, is amplified and applied to a lead zirconate titanate electrostrictive piezoelectric crystal. The application of an electric field to an electrostrictive crystal produces a mechanical strain, the magnitude of which is proportional to the square of the applied field strength. The crystals are polarized so that the application of the sinusoidal voltage causes a sinusoidal strain at the same frequency.[29] The crystal displacements are transmitted through the transducer assembly and are amplified by the exponential portion of the assembly. The

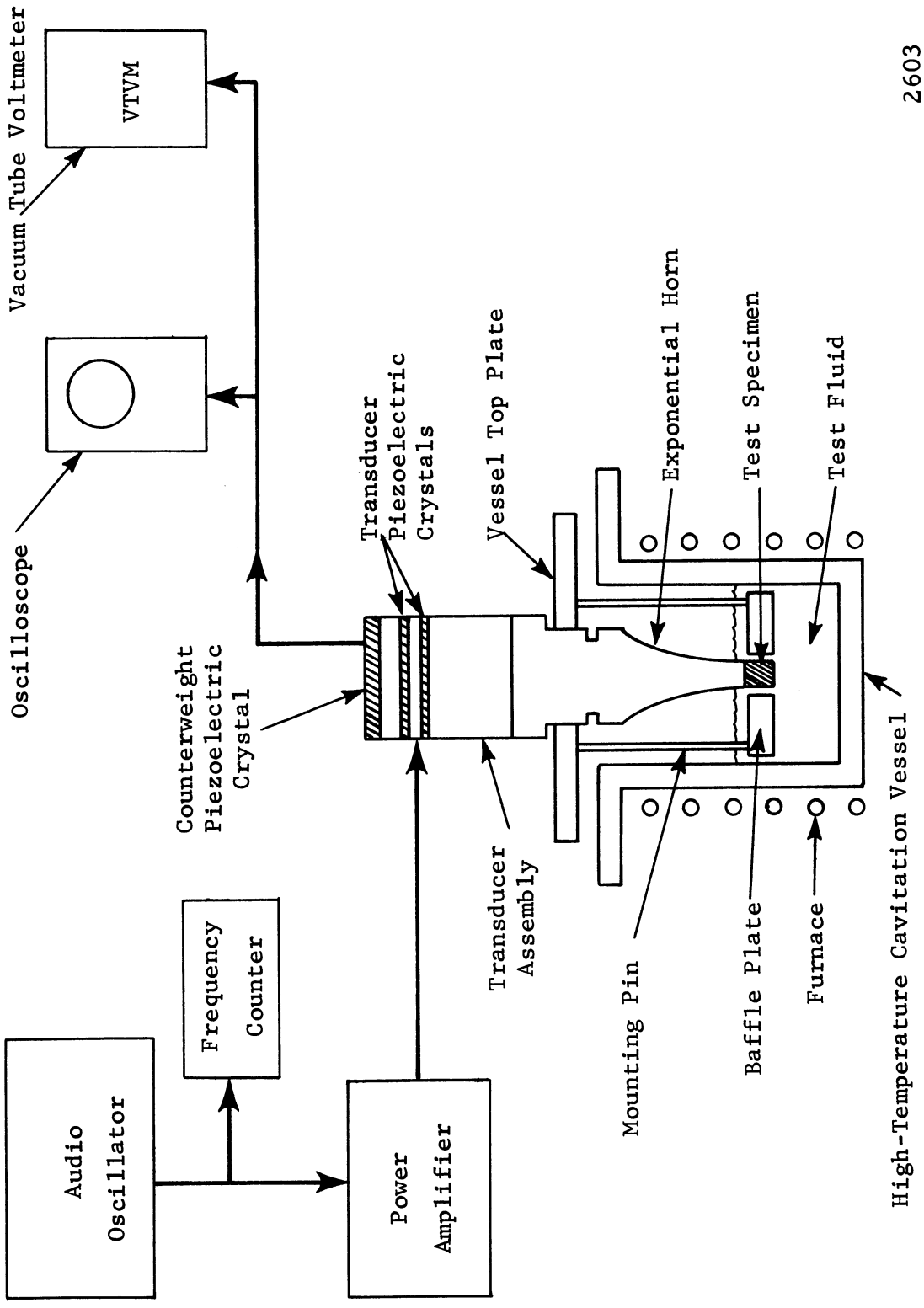


FIGURE 4. BLOCK DIAGRAM OF THE HIGH-TEMPERATURE ULTRASONIC VIBRATORY FACILITY

amplification factor is a ratio of the diameter of the upper portion of the transducer assembly to the diameter of the tip of the exponential portion of the assembly.[30] A test specimen attached to the bottom of the transducer will then mechanically vibrate at the frequency of the applied voltage with a sinusoidal varying amplitude, the magnitude of which is greater than the vibrational amplitude of the crystals because of the amplification effect of the exponential portion of the transducer assembly. This motion of the tip of the test specimen produces pressure waves which are propagated in the test fluid. If the negative portion of these waves are such that the local pressure within the test fluid is reduced below a certain level, cavitation or boiling may occur in the test fluid. Different materials can be used for the test specimen, and various test fluids have been introduced into the cavitation vessel for cavitation experiments at temperatures ranging from ambient to 1500°F. A cover gas system is employed to control the atmosphere above the test fluid in the cavitation vessel. Fig 5 is a photograph of the ultrasonic facility showing the audio oscillator, amplifier, frequency counter, voltmeter, oscilloscope, temperature controllers, temperature indicator, furnace, cover gas system, cooling lines, and the transducer horn assembly installed in the cavitation vessel.

## B. Ultrasonic Transducer Horn Assembly

The general features of an ultrasonic transducer horn assembly of the type used in this investigation are shown in Fig 6. Two lead zirconate-titanate crystals,

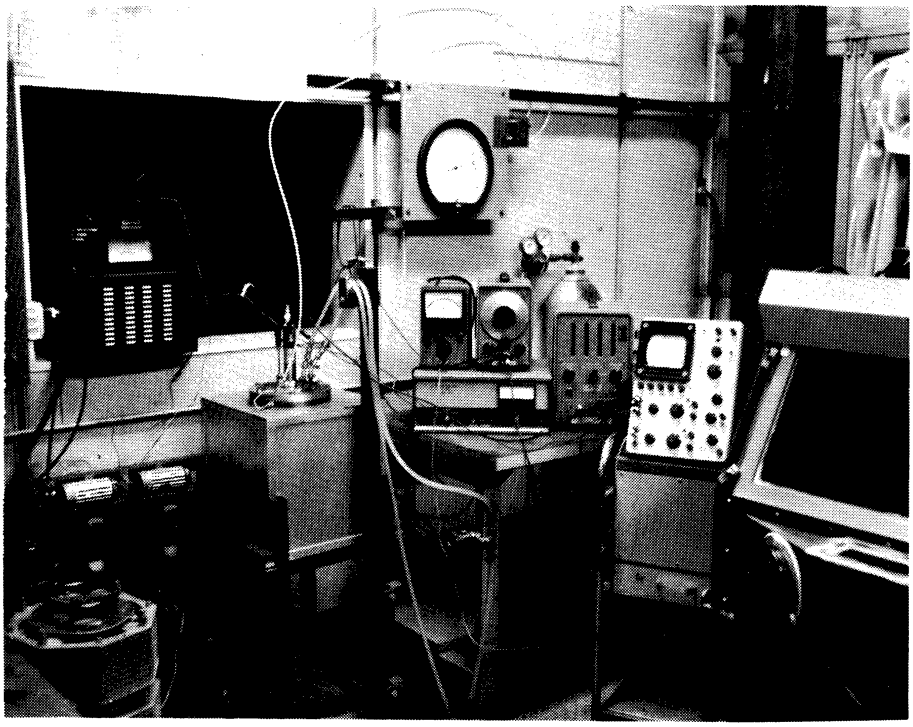

2604

FIGURE 5. PHOTOGRAPH OF THE HIGH-TEMPERATURE ULTRASONIC CAVITATION FACILITY

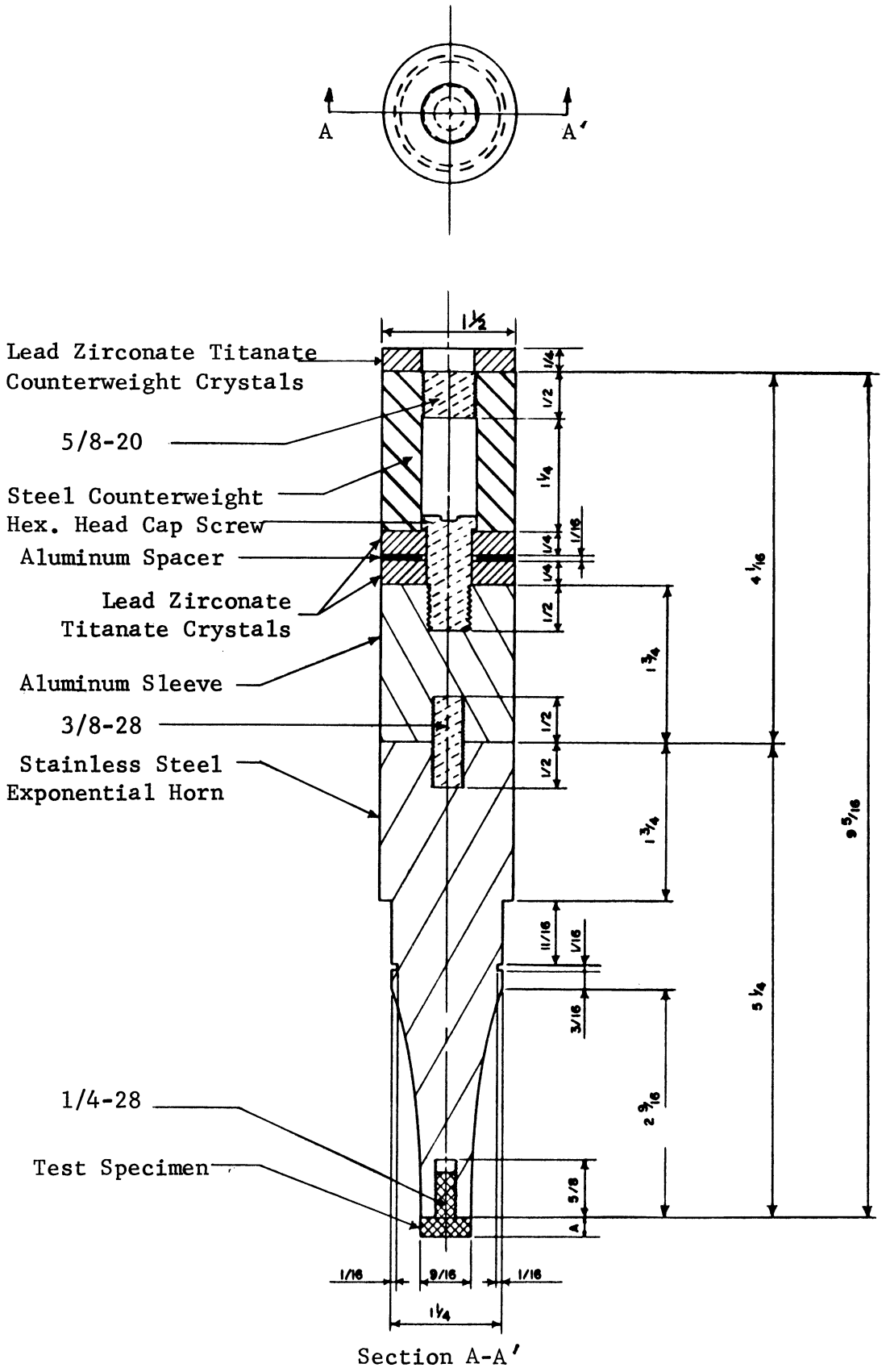


Section A-A'

2605

FIGURE 6. EXPONENTIAL HORN AND ULTRASONIC TRANSDUCER ASSEMBLY

separated by an aluminum spacer which serves as an electrode, are connected to the aluminum sleeve by an internal bolt which passes through the steel counterweight, crystals, and the spacer, and terminates in the aluminum section. The internal bolt is electrically insulated from the crystals and aluminum spacer so that the steel counterweight, the upper surface of the top crystal, and the lower surface of the lower crystal are electrically the same point (ground). The second electrode is attached to the upper steel counterweight. The surfaces of the crystals are silver plated to provide electrical contact between the crystal surfaces and the metal surfaces of the aluminum electrode and the transducer assembly. The exponential horn is attached to the aluminum section by means of an internal threaded rod. This allows for easy removal of the exponential horn from the transducer assembly without disturbing the crystal assembly.

An important consideration in designing a transducer horn assembly is the transfer of the acoustic energy from the crystals to the tip of the exponential horn. To realize an efficient transfer of energy it is necessary to achieve a proper acoustic match between the various materials making up the assembly. For example, if one considers the reflection and transmission of plane waves at the plane interface of two materials, the reflection coefficient approaches zero and the transmission coefficient approaches unity as the acoustic impedances of the two media approach one another.[31] The acoustic impedance of a medium is the product of its density

and the velocity of sound in the medium. Since there is a large difference between the acoustic impedance of the crystals and the acoustic impedance of the stainless steel exponential horn, it was necessary to use a material (such as aluminum) for the center section of the assembly, so that a reasonably close match could be obtained between the impedances of the crystal and the exponential horn. In assembling the transducer assembly care must be taken to insure that no air gaps exist at the interfaces between different components of the assembly since these air gaps greatly reduce the transfer of acoustic energy. In addition to having smoothly ground surfaces for each component, a thin layer of a compound such as silicon should be applied to each surface prior to assembly to prevent air gaps from remaining at the interfaces.

A second important consideration in the design of such a transducer is the dimensions of the various sections of the assembly. Typically, the length of the upper section and the length of the exponential section each correspond to half the wavelength of the acoustic wave propagated in it. Fig 7 is a schematic of a typical waveform showing the position of the nodes and antinodes along the length of the assembly. The amplitude of this waveform represents the vibrational displacements produced by the motion of the crystals. Therefore, the tip of the horn should correspond to an antinode so that maximum tip displacements can be produced. Since the horn must be supported, the support attachment should be at a node in order to minimize any damping which may be produced by the

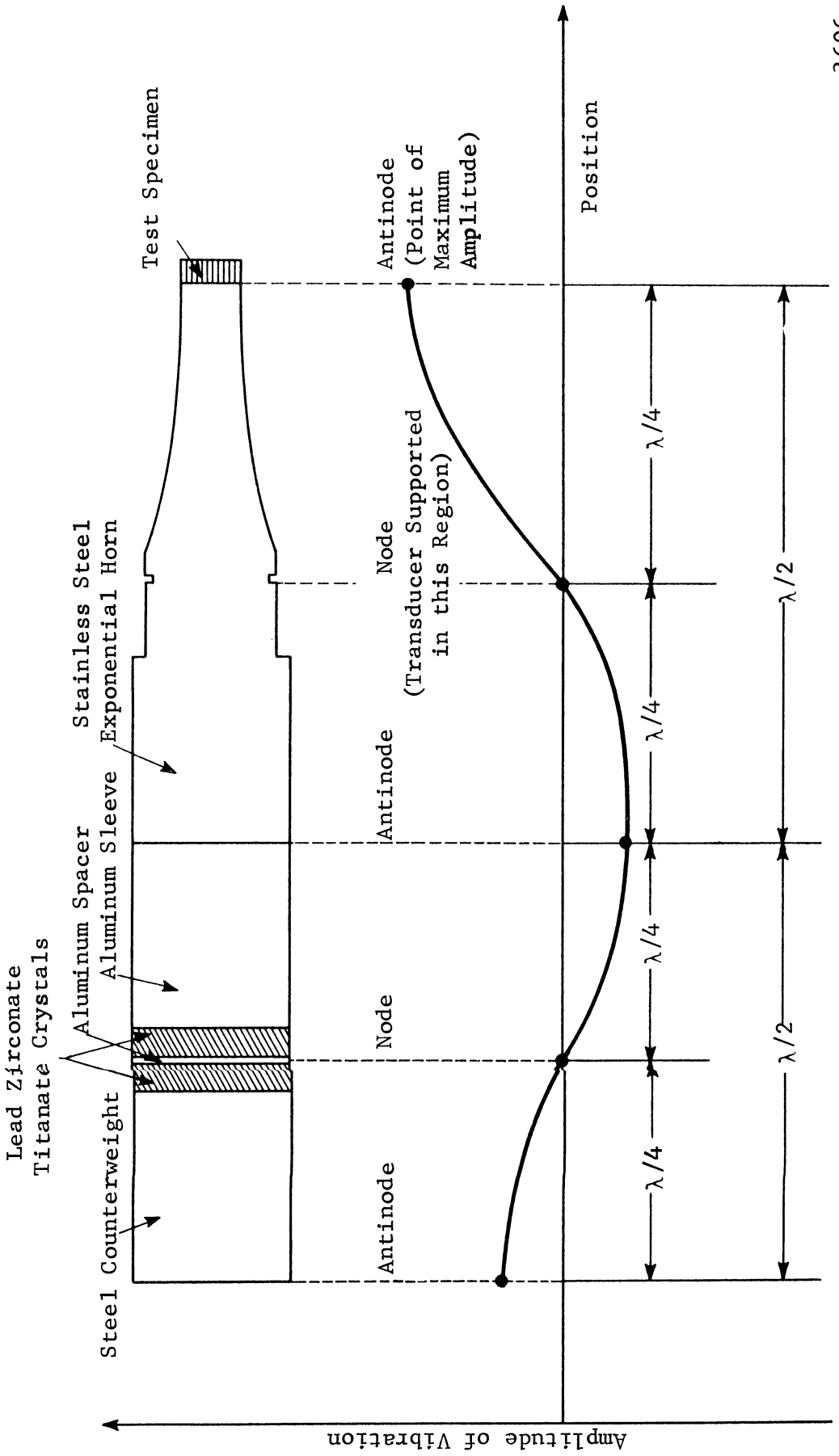


FIGURE 7. TYPICAL WAVEFORM SHOWING POSITION OF NODES AND ANTINODES ON TRANSDUCER ASSEMBLY

support structure. Due to symmetry the aluminum spacer electrode located between the two crystals must be a nodal point. From Fig 7 it is seen that an antinode will exist at the tip of the horn and a node will exist at the aluminum spacer between the crystals if the length of the entire section is made equal to one wavelength. The velocity of sound in aluminum and stainless steel is approximately 16,000 ft/sec. Therefore, it is possible to compute the length of assembly, given the applied frequency, or to compute the frequency, given the length. The original transducer assembly used in this laboratory, as described by Garcia[28], was designed using a length of approximately 10 inches. The resonant frequency for this assembly can be approximately determined by using the expression

$$c = f\lambda \tag{2.1}$$

where

$c$ = velocity of sound
$f$ = frequency
$\lambda$ = wavelength.

Using 10 inches as the wavelenth, the resonant frequency from Eq (2.1) is approximately 21 kHz.

For the present investigation it was necessary to operate at several different frequencies. Generally, to operate at a different frequency at maximum efficiency the dimensions of the entire transducer assembly must be changed to a length which corresponds to the desired wavelength.

However, it was experimentally determined that the resonant frequency of the transducer horn assembly could be satisfactorily altered by merely changing the length of the exponential horn section. For this investigation a frequency range of approximately 14 to 25 kHz was chosen with four transducer horn assemblies possessing resonant frequencies at approximately 14, 20, 23, and 25 kHz. The choice of frequencies was partly governed by the desire that the resulting lengths of the exponential portion of the assemblies would not require extensive modification of the cavitation vessel. Table 3 lists the dimensions of the exponential horn sections used, with the resulting resonant frequencies. The same transducer assembly (consisting of the steel counterweight, the two crystals and aluminum spacer, counterweight crystal, and the aluminum section) was used for all exponential horn sections. The dimensions of this transducer assembly are indicated in Fig 6. It should be emphasized that by merely changing the length of the exponential portion of the assembly to achieve a different resonant frequency, a maximum efficiency of the input power to the transducer assembly is not realized. This approach was taken due to the convenience of merely changing exponential horns in order to change the resonant frequency, and because the resulting vibrational displacements at the various frequencies were sufficient for this investigation.

The details of the test specimen which is screwed into the end of the exponential horn are shown in Fig 8. For stainless steel, dimension A is 0.250 inches and dimension

TABLE 3

LENGTH OF STAINLESS STEEL EXPONENTIAL HORN SECTION AND CORRESPONDING RESONANT FREQUENCY

| Distance from Top Surface to Point of Support | Distance from Support to Tip of Specimen | Total Length Including Spec | Resonant Freq[a] |
|---|---|---|---|
| 3.69 inches | 4.50 inches | 8.19 inches | 14554 Hz |
| 2.44 | 3.03 | 5.47 | 20264 |
| 2.25 | 2.63 | 4.88 | 23082 |
| 1.94 | 2.31 | 4.25 | 25471 |

[a] Measured in water at 70°F

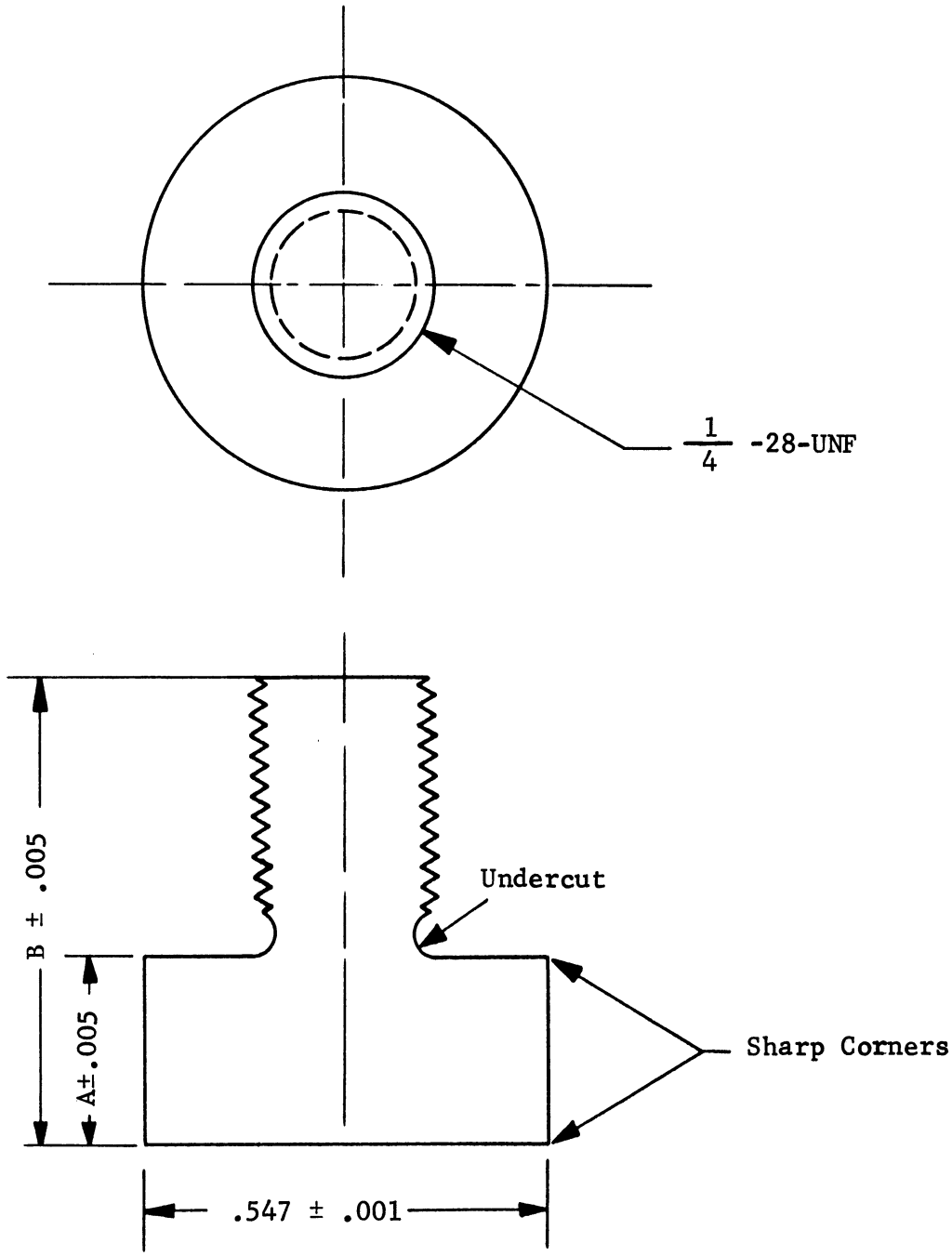


NOTE: Dimensions "A" and "B"
Vary with Specimen Material

2607

FIGURE 8. CAVITATION TEST SPECIMEN

B is 0.625 inches. A special wrench which grips the cylindrical surfaces of the specimen is used, so that during installation and removal no material is removed from the test specimen by the wrench, and the bottom surface is not scratched or damaged.

The counterweight crystal (Fig 6) consists of a lead zirconate-titanate piezoelectric crystal cemented to the top surface of the steel counterweight section of the transducer assembly. This crystal is used to indirectly monitor the vibrational displacement of the test specimen which is connected to the tip of the exponential horn. The developemnt of this displacement measuring system is discussed in Chapter III.

C. High Temperature Cavitation Vessel

The high temperature cavitation vessel designed by Garcia[28] has been used for several liquid metals, viz., lead-bismuth, mercury, and lithium at temperatures up to 1500°F in some cases for extended periods of time. This facility therefore appears suitable for investigations using liquid sodium at temperatures up to 1500°F.

Fig 9 is a schematic diagram of the high temperature cavitation vessel with the transducer assembly installed. The cavitation vessel itself is 316 stainless steel, cylindrical in shape with an inside diameter of 3.42 inches, a wall thickness of 0.125 inches, a bottom thickness of 0.500 inches, with an overall length of 5.750 inches. The upper portion of this cylindrical section was designed to minimize heat transfer to the vessel top plate. The stainless steel vessel top

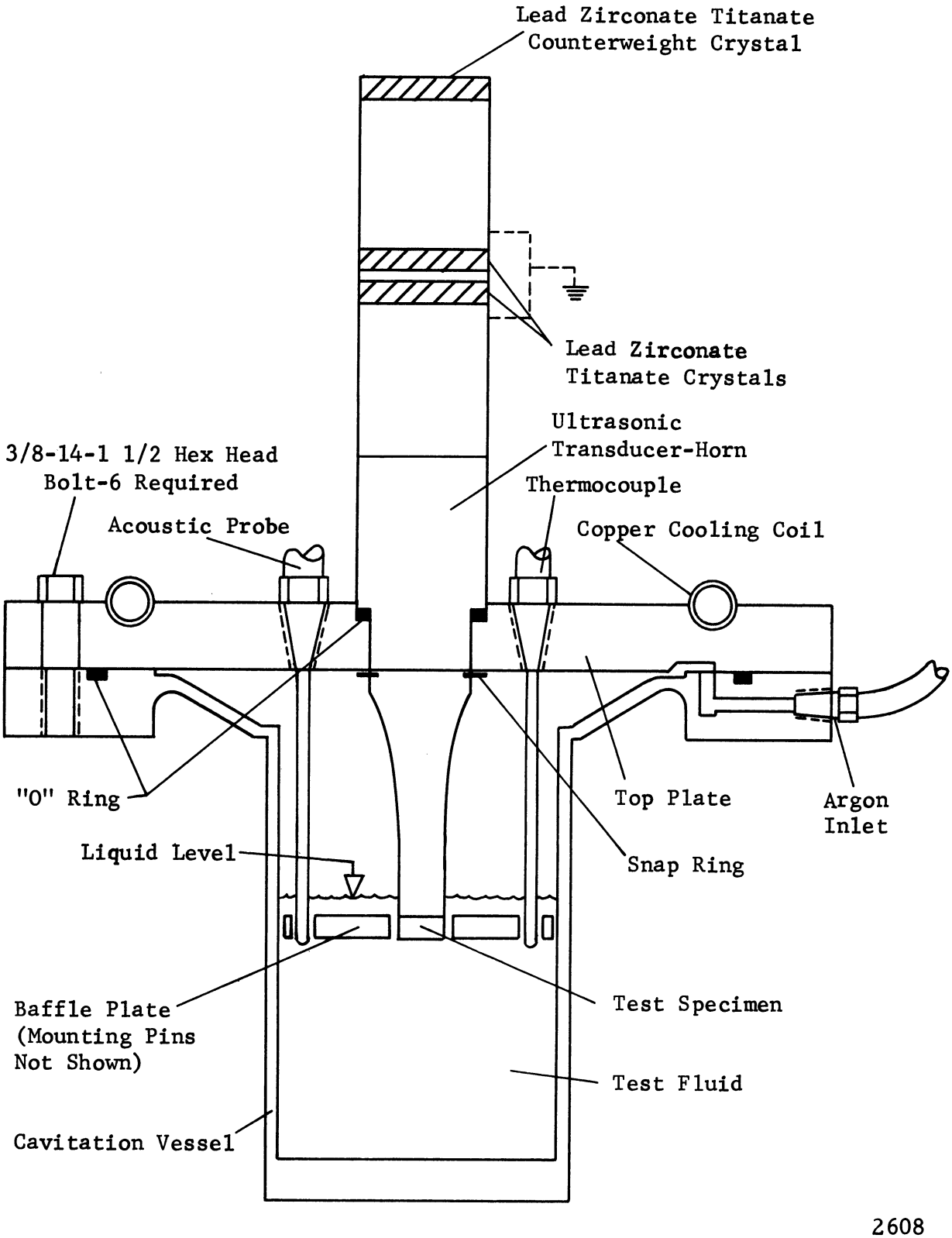


FIGURE 9. HIGH-TEMPERATURE CAVITATION VESSEL AND ULTRASONIC TRANSDUCER

plate is secured to the vessel flange by means of six bolts as indicated in Fig 9. Sealing at this point is achieved by means of an "O" ring which is fitted into a suitable groove in the vessel flange. The vessel flange is tapped and fitted with a valve to allow for passage of a cover gas into the vessel. The top plate is tapped and fitted for a Conax packing gland which provides for a thermocouple to be inserted into the vessel and down into the test fluid. A second packing gland is provided in the vessel top plate to allow for insertion of an acoustic probe which is discussed in greater detail in Chapter IV. Cooling of the vessel top plate is achieved by circulating water through the copper coil soldered into a groove in the top plate. When operating at high temperatures care must be taken to insure that the temperature in the vicinity of the "O" ring horn seal and flange gasket does not become excessive. Also, it is necessary that the temperature of the crystals does not exceed the Curie Point, the temperature at which the crystals lose their polarization. For lead zirconate-titanate this temperature is approximately 660°F.[32] Past operating experience with this facility has indicated that for extended operations at 1500°F the temperature of the upper section of the transducer assembly is maintained at a suitable level if in addition to the cooling water a small air fan is directed at the horn.

In securing the transducer assembly to the vessel top plate, two requirements had to be considered. First, the transducer must be clamped in such a manner that the acoustic

waves transmitted through the assembly are not damped by the clamping mechanism. Second, the clamping arrangement must provide a seal so that there is no loss of cover gas or in-leakage of air. To secure the transducer a rubber "O" ring with dimensions 1 1/4 inches x 1 1/2 inches x 1/8 inches is provided to slip around the transducer horn and to seat in a groove provided in the top plate. The horn is held in proper axial position to suitably squeeze the "O" ring, by fastening a snap ring around the horn directly below the top plate. The arrangement provides a positive seal and does not result in a decrease in horn amplitude because the "O" ring is soft enough not to restrain the low amplitude, high frequency vibration at this point. A patent has been granted for this arrangement under the title, "Seal Holder Device for Ultrasonic Vibratory Unit."

D. Furnace Arrangement

The furnace used to heat the cavitation vessel is shown in Fig 10 (with the vessel installed). The furnace is fitted with an opening of suitable dimensions so that the vessel can be easily inserted and removed. It is in the shape of a cube, 16 inches on a side. The outer covering consists of 1/16 inch sheet metal. Located in the center of the furnace is an alundum crucible, cylindrical in shape with a 6 inch diameter and a 12 inch length. Heating coils are wound around this crucible. The remaining volume of the furnace is filled with insulating material. The power rating of the furnace is

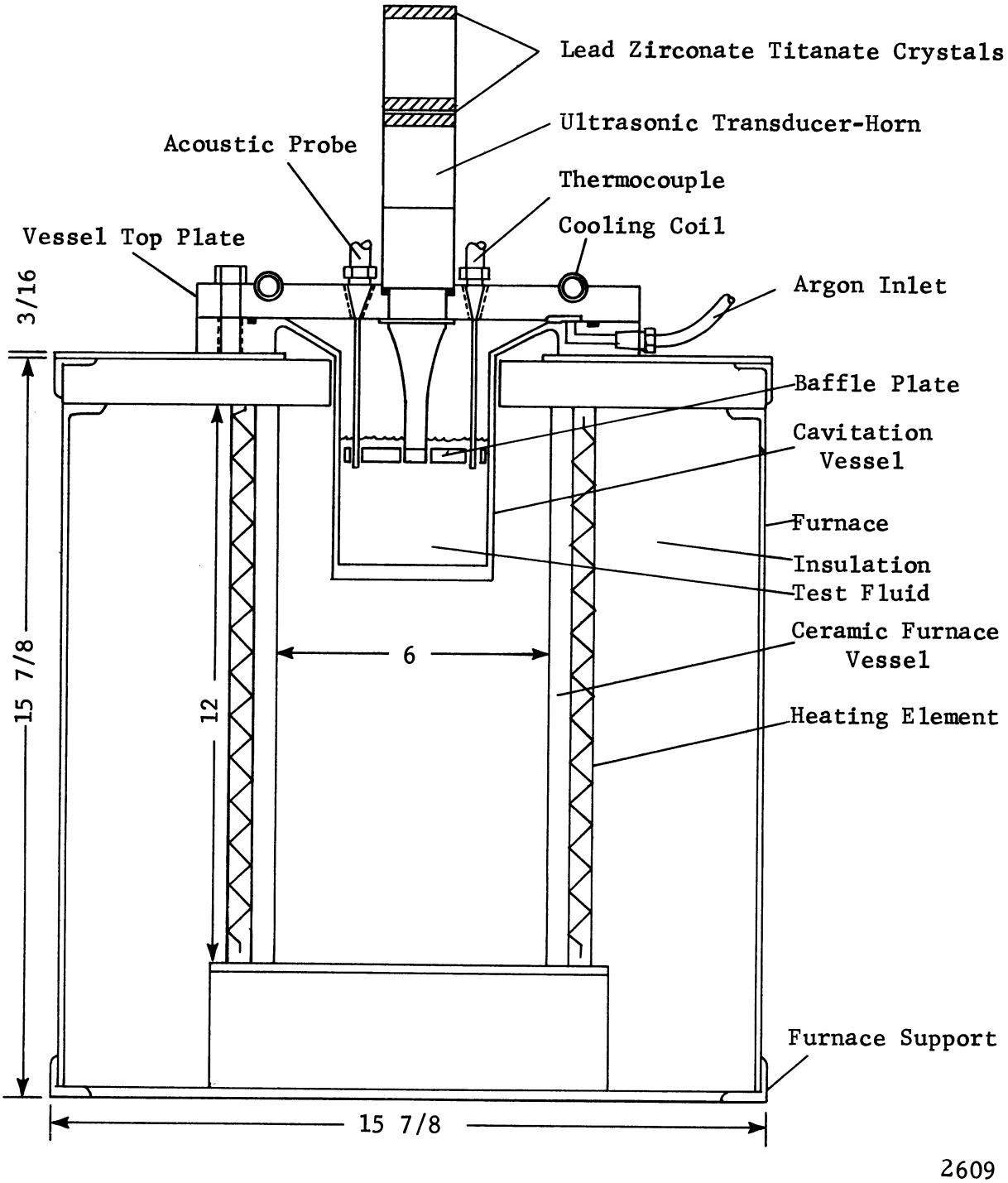


FIGURE 10. HIGH-TEMPERATURE CAVITATION VESSEL AND ULTRASONIC TRANSDUCER ASSEMBLY MOUNTED IN FURNACE

3000 watts at 220 volts. It is capable of raising the temperature of the test fluid within the cavitation vessel from room temperature to 1500°F in approximately three hours.

A Foxboro automatic temperature controller was used for control of the furnace temperature. A thermocouple was embedded in the alundum cement surrounding the heating element. This thermocouple was then connected to the controller. The controller is an ON-OFF type equipped with a standard mercury switch. When the process temperature is below the set point, the full 220 volts is applied to the windings of the furnace. When the process temperature exceeds the set point, the mercury switch opens, reducing the voltage to zero. Once the desired temperature is reached, it is possible to achieve finer control by reducing the voltage applied to the windings by means of a variac. Fig 11 is a schematic indicating the relationship and connections necessary to achieve this control. The thermocouple used for temperature control in this application is of chromel-alumel. The automatic temperature controller is driven by a small motor requiring a 220 volt supply. The heating coil thermocouple and the thermocouple used to measure the test fluid temperature inside the cavitation vessel were connected to a Brown potentiometer pyrometer for visual monitoring of the facility temperatures.

E. Baffle Plate

As indicated in Fig 4 a circular stainless steel plate is installed in the cavitation vessel and serves as a baffle plate. It is pointed out in the next chapter that

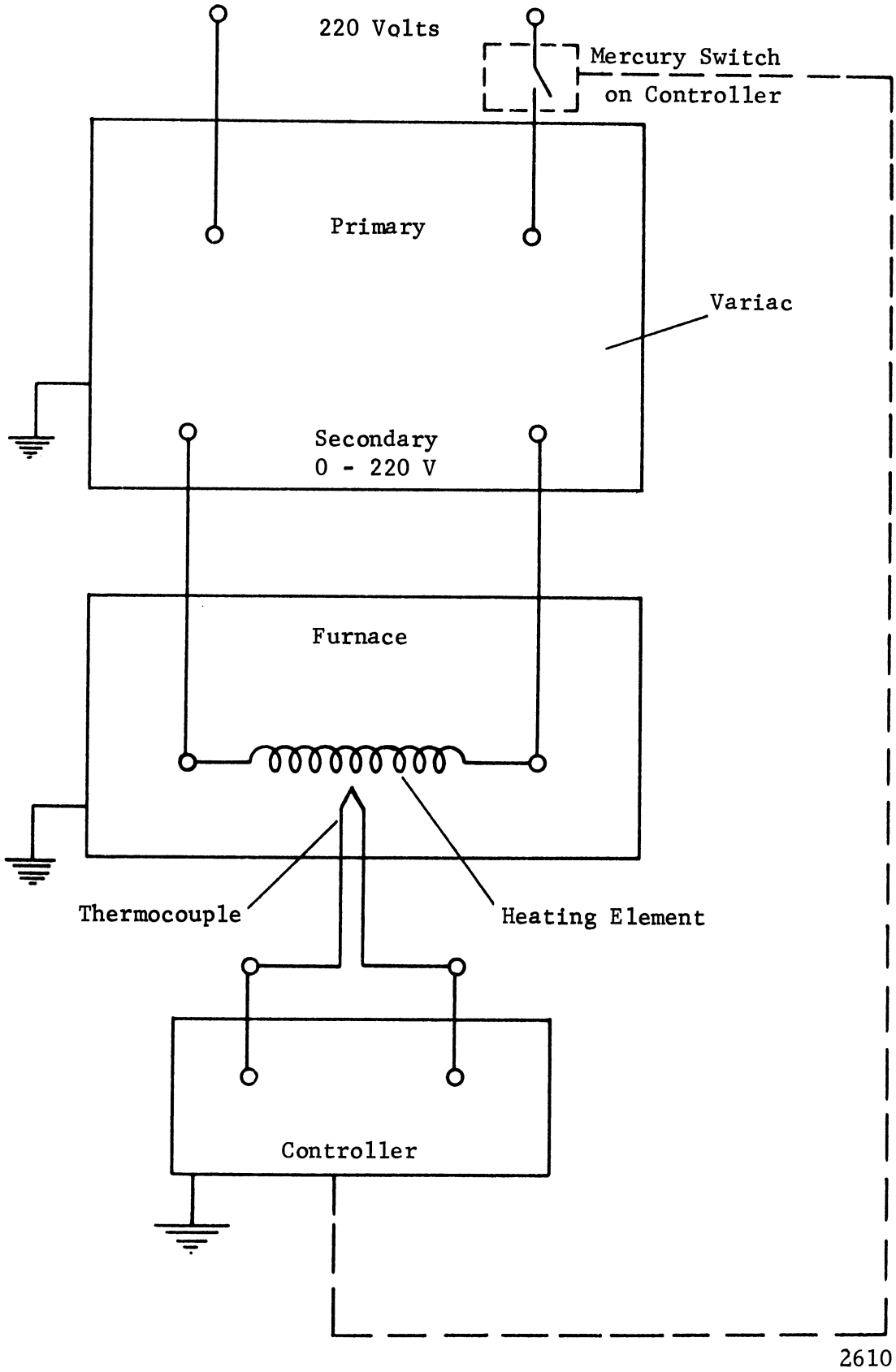


FIGURE 11. SCHEMATIC OF VARIAC, FURNACE, AND TEMPERATURE CONTROLLER

in order to readily solve the differential equation describing the pressure field inside the cylindrical cavitation vessel, certain boundary conditions must be imposed. To impose these boundary conditions experimentally, a 1/4 inch circular plate of 3 3/16 inches diameter is rigidly mounted to the vessel top plate by means of three 3/8 inch diameter stainless steel mounting pins. The baffle plate is positioned so that its bottom surface is flush with the bottom surface of the test specimen in the at-rest condition. This plate prevents fluid motion in the plane defined by the bottom surface of the plate, and thus presents a rigid boundary to the test fluid. The diameter of the center hole in the baffle plate is approximately 0.080 inches greater than the diameter of the test specimen. This experimentally determined clearance allows for proper axial movement of the test specimen within the hole of the baffle plate even during operation at high temperatures when uneven heating or cooling of the baffle plate arrangement may cause the baffle plate to shift, causing the test specimen to "rub" against the baffle plate. This effect was also minimized by fabricating the mounting pins, baffle plate, test specimen, and exponential horn from stainless steel so that the coefficient of thermal expansion would be identical for all components. In operating with exponential horns of different lengths, the length of each mounting pin is adjusted so that the bottom surface of the baffle plate is flush with the bottom surface of the test specimen. Fig 12 is a photograph showing the baffle plate mounted to the vessel top plate.

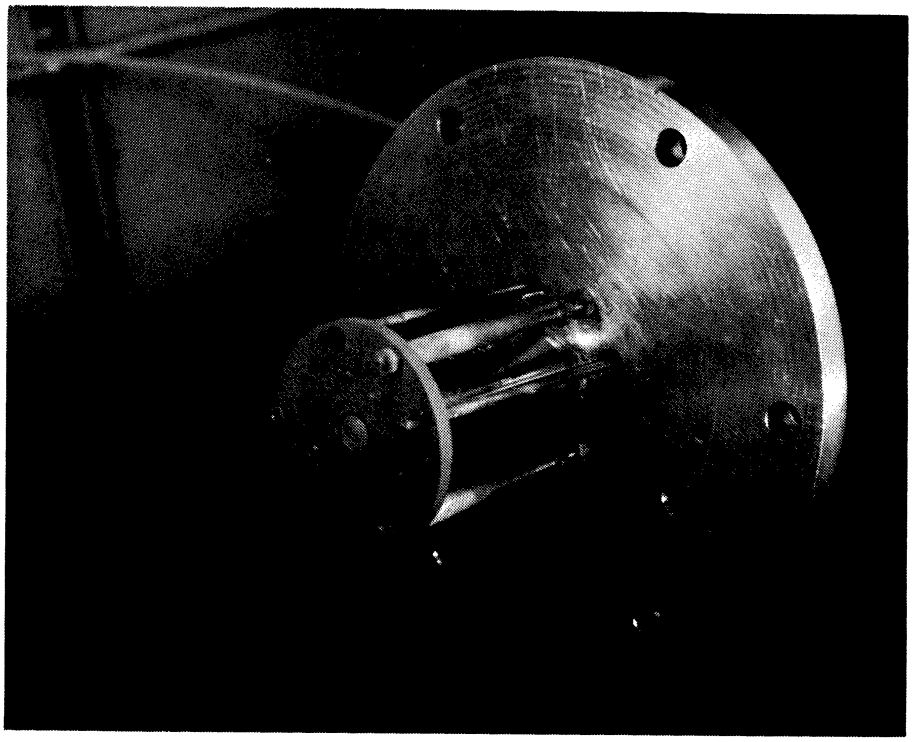

2611

FIGURE 12. PHOTOGRAPH OF THE BAFFLE PLATE MOUNTED TO THE VESSEL TOP PLATE

The exponential horn, mounting pins, thermocouple probe, and the acoustic probe can also be seen in Fig 12.

It was interesting to note that in using the ultrasonic facility for cavitation damage studies the use of the baffle plate greatly increased the uniformity of the damage pattern. In conducting cavitation studies in test fluids of low density such as water, without the baffle plate, the damage is not spread uniformly over the surface of the test specimen exposed to cavitation bubbles. Irregular pitting takes place, and much of the area exposed to cavitation bubbles is relatively free of cavitation damage. With the baffle plate installed, the cavitation damage sustained by the test specimen becomes much more uniform across the face of the test specimen, and the amount of damage is increased. In a comparison test using a 303 stainless steel specimen there was an increase in cavitation damage rate of approximately 50 per cent with the baffle plate for a 12 hour test period as compared with a similar test without the baffle plate. Using the baffle plate increased the damaged area on the test specimen by approximately 30 per cent. In view of the above results, a patent application has been filed under the title "Baffle Plate for Ultrasonic Vibratory Facility."

# CHAPTER III

## DETERMINATION OF THE PRESSURE FIELD PRODUCED BY THE ULTRASONIC TRANSDUCER

### A. Introduction

In order to determine superheat requirements using cavitation techniques the pressure field produced by the ultrasonic transducer must be known. It is pointed out in Chapter I that the vibrational motion of the tip of the test specimen immersed in the test fluid produces sound waves which are transmitted through the test fluid. As the power to the ultrasonic transducer is increased the amplitude of these pressure waves is increased. If the negative pulse of these sound waves reduces the pressure of the test fluid below a certain value cavitation may occur in the test fluid. For example, if it is assumed that spherical vapor bubbles serve as nucleation sites for the cavitation process, the liquid pressure must be reduced below the vapor pressure in order to overcome the surface tension effect as indicated in Eq (1.1). The vapor pressure can be determined from the temperature of the liquid. Therefore, if the magnitude of the pressure waves being produced by the transducer is known at the onset of cavitation in the liquid, then the change in pressure necessary to produce cavitation can be established. From this

data the superheat requirements for the liquid can then be calculated.

One method of determining the pressure field produced by the transducer would be direct measurement. However, this method has several disadvantages for use in high temperature sodium as here required. Most pressure probes utilize piezoelectric crystals which are temperature limited. The Curie temperature of piezoelectric crystals is well below 1500°F which is the upper limit of the temperature range for this experiment. A second disadvantage is that sodium at high temperatures is highly corrosive and would greatly limit the materials used in the construction of the probe. These disadvantages render this system inappropriate for the present investigation.

The method selected for this investigation of determining the pressure field produced by the ultrasonic transducer in sodium is to develop a theoretical expression describing the pressure field, and then experimentally verify this theoretical expression using a test fluid other than liquid sodium (such as water). This approach involves the development of a theoretical expression which would be a function of geometry, various fluid parameters, and parameters describing the motion of the tip of the test specimen. By monitoring the necessary parameters, this expression describing the pressure field can be experimentally checked. It can be verified by using a suitable pressure probe to directly measure the pressure field. These results can then be compared with the predicted

pressure values to insure that the theoretical expression is a reasonable representation of the pressure field produced in the test fluid

The following sections of this chapter describe the theoretical expression for the pressure field, methods of measuring the necessary parameters, development of a pressure probe, and the correlation between predicted and experimental values for the pressure field.

## B. Theoretical Expression for the Pressure Field

As discussed in Chapter II, the cavitation vessel consists of a stainless steel right circular cylinder. A circular baffle plate is mounted to the vessel top plate so that the bottom surface of the test specimen is flush with the bottom surface of the baffle plate. This arrangement is shown in Fig 13. From Fig 13 it can be seen that the sound waves produced by the motion of the tip of the test specimen are effectively transmitted into a closed container. There are small clearances between the test specimen and the baffle plate and between the baffle plate and the vessel wall. However, it is felt that these clearances do not significantly invalidate the approximation that the combination of the baffle plate and cavitation vessel can be represented by a closed containter. It is assumed that this closed container is rigid, i. e., there is no motion of the container walls due to the pressure waves. For example, if we consider a plane wave incident normally to a plane boundary separating two media, 1 and 2, then the

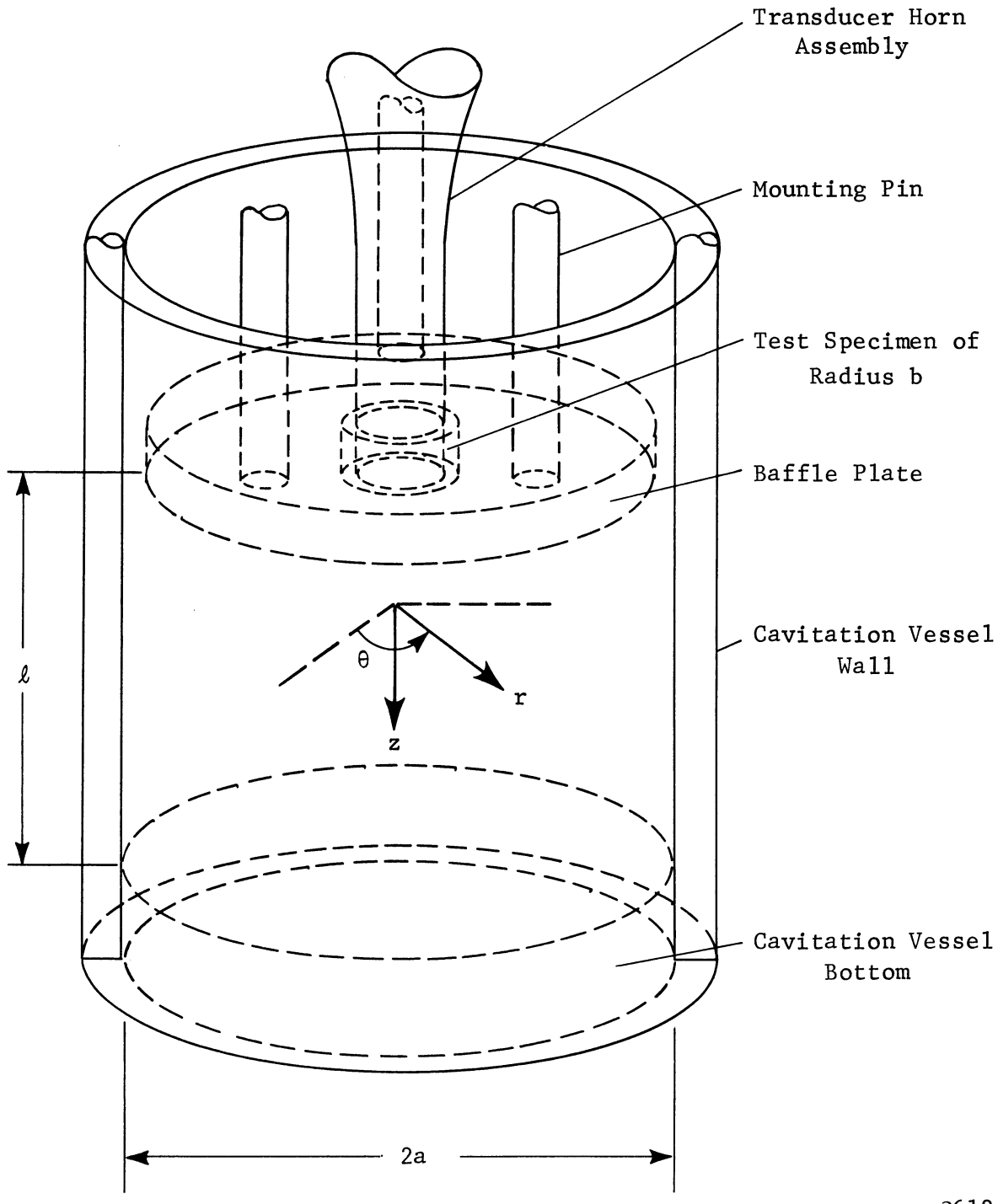


FIGURE 13. CAVITATION VESSEL, BAFFLE PLATE, AND TRANSDUCER HORN ASSEMBLY

particle velocities of medium 2 is given by[33]

$$\xi_2 = \frac{2\rho_1 C_1}{\rho_1 C_1 + \rho_2 C_2}\,\xi_1 \qquad (3.1)$$

where

$\xi_1$ = particle velocities of medium 1

$\xi_2$ = particle velocities of medium 2

$\rho$ = density of medium

$C$ = velocity of sound in medium.

The density of steel is approximately 7.8 times the density of water, and the velocity of sound in steel is approximately 4 times the velocity of sound in water.[33] Using Eq (3.1), the velocity of the steel at the plane boundary is approximately 6 per cent of the incident pressure wave velocity. Thus a water steel boundary is essentially a rigid boundary.

As indicated in Fig 13, the length of the closed container is represented by $\ell$, the radius of the container is represented by $a$, and the radius of the test specimen is represented by $b$. A cylindrical coordinate system was chosen such that the z axis coincides with the vertical axis of the transducer assembly, and the point z=0 and r=0 represents the center of the bottom surface of the test specimen. The test specimen is driven sinusoidally at small amplitudes perpendicular to the plane of the baffle plate by the piezoelectric driving crystals. Let A be the maximum amplitude of displacement of the test specimen. The displacement of the test specimen is then $A\sin\omega t$ and the velocity is $U_0\cos\omega t$, where $\omega$ is the angular frequency of vibration and $U_0 = \omega A$ is the maximum

velocity of the test specimen.

It is desired to determine the amplitude of the oscillating pressure at any point within the closed cavitation vessel. Since the component of the fluid velocity normal to all walls is known (The fluid velocity normal to all walls is zero since we have assumed the walls are rigid.) this problem may be solved by using the velocity potential approach. The following analysis was developed by Lansing et al.[34]

Neglecting viscosity and other dissipative forces, the perturbation velocity potential within the vessel must satisfy the wave equation[35]

$$\frac{\partial^2\Phi}{\partial r^2} + \frac{1}{r}\frac{\partial\Phi}{\partial r} + \frac{1}{r^2}\frac{\partial^2\Phi}{\partial\theta^2} + \frac{\partial^2\Phi}{\partial z^2} = \frac{1}{c^2}\frac{\partial^2\Phi}{\partial t^2} \qquad (3.2)$$

where

$\Phi$ = velocity potential

$c$ = velocity of sound in the test fluid.

The following boundary conditions must be satisfied.

1) The fluid in contact with the test specimen must follow the test specimen motion.

$$\left.\frac{\partial\Phi}{\partial z}\right|_{z=0} = U_0 \cos\omega t \qquad 0 \le r \le b$$

2) The component of fluid velocity normal to the baffle plate must vanish.

$$\left.\frac{\partial\Phi}{\partial z}\right|_{z=0} = 0 \qquad b \le r \le a$$

3) The component of fluid velocity normal to the bottom surface of the vessel must vanish.

$$\left.\frac{\partial \Phi}{\partial z}\right|_{z=\ell} = 0 \qquad 0 \le r \le a$$

4) The component of fluid velocity normal to the cylindrical wall must vanish.

$$\left.\frac{\partial \Phi}{\partial r}\right|_{r=a} = 0 \qquad 0 \le z \le \ell$$

When the potential satisfying the above boundary conditions is determined, the perturbation pressure, $P'$, at any point in the vessel is given by[35]

$$P' = -\rho_0 \frac{\partial \Phi}{\partial t} \tag{3.3}$$

where

$\rho_0$ = mean density of the test fluid.

Using the technique of separation of variables, and applying the above boundary conditions, the solution to Eq (3.2) can be obtained. Inserting this solution into Eq (3.3) the perturbation pressure can then be established. The details of this analysis are omitted here, but can be found in reference 34.

The perturbation pressure as determined by the above analysis can be written as

$$P' = P(\bar{z}, \bar{r}) \sin \omega t \tag{3.4}$$

in which the amplitude $P(\bar{z}, \bar{r})$ is given in nondimensional form by

$$P(\bar{z}, \bar{r}) = \bar{\ell}\bar{k}\rho_0 U_0 c \left\{ \frac{\lambda^2 \cos[\bar{\ell}\bar{k}(1-\bar{z})]}{\bar{\ell}\bar{k}\sin[\bar{\ell}\bar{k}]} \right. \tag{3.5}$$

$$\left. + 2\lambda \sum_{j=1}^{\infty} \frac{\cos[\bar{K}_j(1-\bar{z})]\, J_0(\alpha_j \bar{r})\, J_1(\alpha_j \lambda)}{\alpha_j \bar{H}_j J_0^2(\alpha_j)} \right\}$$

where

$$\bar{\ell} = \ell/a$$
$$\bar{z} = z/\ell$$
$$\bar{r} = r/a$$
$$\bar{k} = a\bar{\omega}$$
$$\bar{\omega} = \omega/c$$
$$\lambda = b/a$$
$$\bar{K}_j = \bar{\ell}(\bar{k}^2 - \alpha_j^2)^{1/2}$$
$$\alpha_j = j \text{ th zero of } J_1$$
$$J_1 = \text{Bessel function of the first kind of order 1}$$
$$J_0 = \text{Bessel function of the first kind of order zero}$$
$$\bar{H}_j = \bar{K}_j \sin \bar{K}_j .$$

Examination of Eq (3.5) shows that resonant conditions within the cavitation vessel may be associated with longitudinal modes, transverse modes, or a combination of longitudinal and transverse modes. Resonance involving purely longitudinal modes occur when

$$\sin(\bar{\ell}\bar{k}) = 0$$

or when

$$\bar{\ell}\bar{k} = n_z \pi$$

where

$$n_z = 0, 1, 2, 3, \ldots$$

Resonance due to purely transverse modes occurs whenever

$$\bar{K}_j = 0$$

or when

$$\bar{k} = \alpha_j$$

Resonance involving both the longitudinal and transverse modes occurs when

$$\sin \bar{K}_j = 0$$

or when

$$\bar{\ell}\left(\bar{k}^2 - \alpha_j^2\right)^{\frac{1}{2}} = n_z \pi$$

Rearranging the above expression we obtain

$$f_{jz} = \frac{c}{2a}\left[\left(\frac{\alpha_j}{\pi}\right)^2 + n_z^2\left(\frac{a}{\ell}\right)^2\right]^{\frac{1}{2}} \qquad (3.6)$$

where $f_{jz}$ represents the resonant frequency of the $jz$ mode. For $j = 0$, Eq (3.6) represents the resonant frequencies of the pure longitudinal modes. For the subscript $z = 0$, Eq (3.6) represents the resonant frequencies for pure transverse modes. For $j \neq 0$ and $z \neq 0$, Eq (3.6) represents resonant frequencies for a combination of longitudinal and transverse modes. Therefore, for $j = 0, 1, 2, 3, \ldots$ and $z = 0, 1, 2, 3, \ldots$, Eq (3.6) represents the resonant frequencies for all possible modes in the cavitation vessel.[36] Under any of these modes Eq (3.5) predicts infinite pressure. This is because damping, and other nonlinear effects in the formulation and solution of the problem were neglected. In practice one should expect high but not infinite pressure amplitudes at the resonant conditions.

From the above discussion it is felt that Eq (3.5) would more accurately predict the pressure field inside the cavitation vessel at conditions far removed from any resonant condition or mode since at resonant conditions Eq (3.5) predicts infinite pressures which are not realistic. To determine these

conditions, Eq (3.6) was plotted as a function of the length of the cavitation vessel, $\ell$, using water as the test fluid. For distilled water at 70°F, c = 4862 ft/sec.[37] For the cavitation vessel, $2a$ = 3.44 inches. These curves are shown in Fig 14. It is pointed out in Chapter II that the frequency range for this investigation is from approximately 14 to 26 kHz. Within this frequency range it can be seen from Fig 14 that as the length of the cavitation vessel is increased no resonant conditions are achieved until the length reaches about 1.2 inches. At this point the first longitudinal mode is encountered. The first combination mode occurs at a length of 2.2 inches. Additional longitudinal resonant modes are encountered as the length of the vessel is further increased. For a length of 4.3 inches four different resonant modes are represented in the frequency range of interest. It can be seen that as the length of the cavitation vessel is increased, the number of resonant modes which must be considered also increases. Therefore, in choosing a length for the cavitation vessel such that no resonant conditions are encountered over the desired frequency range, the length of the cavitation vessel must be relatively short.

In order to evaluate Eq (3.5) the various parameters included therein must be determined. The fluid parameters are the density, $\rho_o$, and the velocity of sound, $C$, in the fluid. For the test fluids of interest, these quantities, which are a significant function of temperature only, are known. The geometry parameters are the length of the vessel,

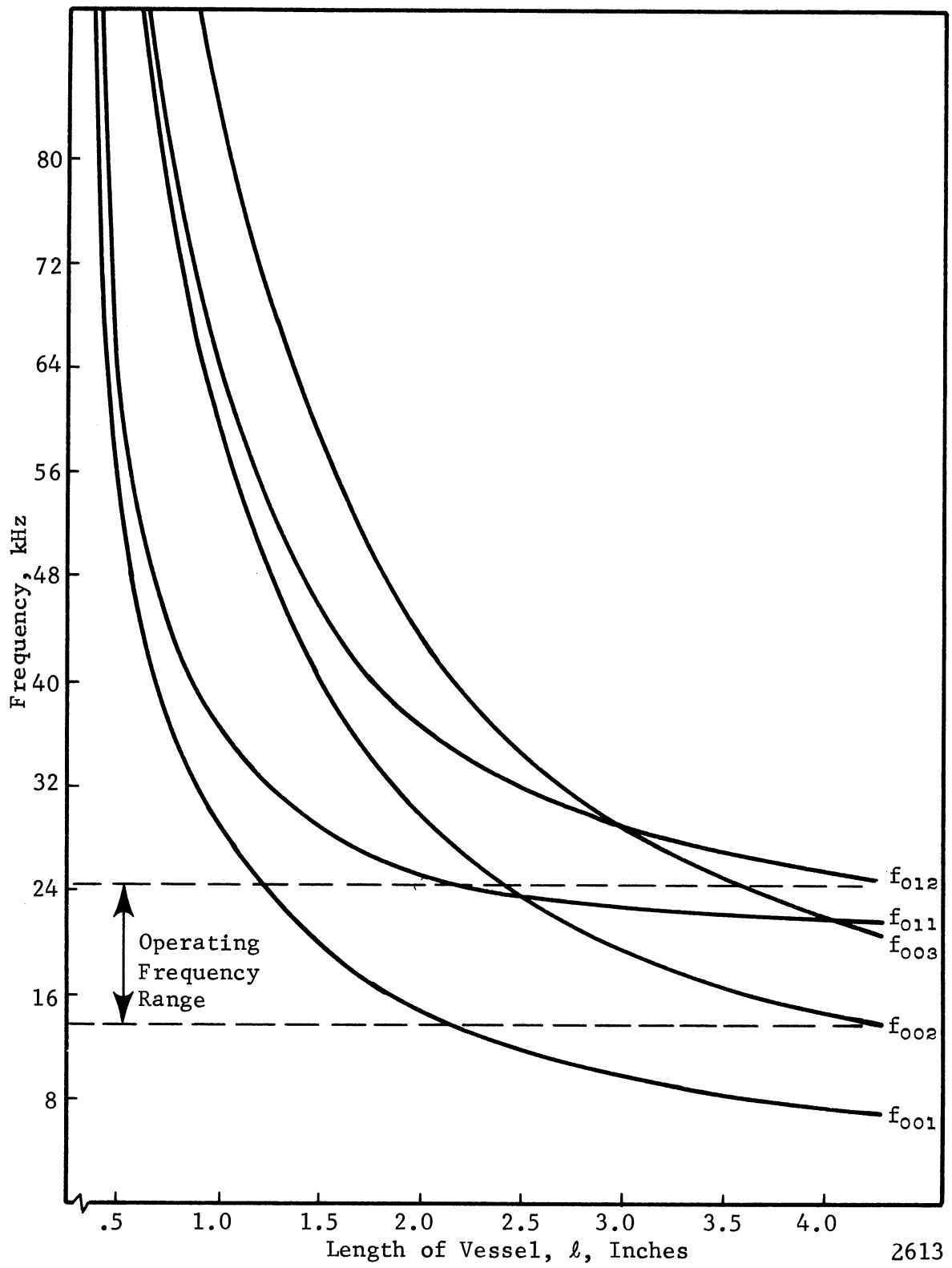


FIGURE 14. CURVES OF RESONANT FREQUENCY FOR VARIOUS MODES OF VIBRATION

$\ell$, the radius of the vessel, $a$, and the radius of the test specimen, $b$ ; obviously these are known quantities. The transducer parameters are the frequency, $f$, and the tip displacement, A. The frequency of the input voltage signal, which is the frequency of the vibrational motion of the tip of the test specimen, can be determined by using an electronic frequency counter. The only remaining parameter which must be determined in order to establish the pressure field within the cavitation vessel is the tip displacement, A. Once the tip displacement is determined, Eq (3.5) can be evaluated which gives the pressure at any point within the cavitation vessel.

## C. Measurement of the Vibrational Displacement of the Horn Tip

It is pointed out in the previous section of this chapter that in order to evaluate Eq (3.5) which describes the pressure field inside the cavitation vessel, it is necessary to determine the vibrational displacement of the tip of the exponential horn. Generally this can be accomplished by two different methods. The first method consists of measuring the motion of the tip itself. This involves positioning some sort of device in the proximity of the horn tip which can sense its motion. The output signal of this device is connected to an appropriate readout meter located outside the cavitation vessel. The second method is to indirectly measure the motion of the test specimen. For example, the vibrational displacement of the top surface of the steel counterweight section of the

transducer section could be measured, and this measurement could then be related to the vibrational motion of the horn tip. The first method is not appropriate for the present investigation because of the limitations imposed by the high operating temperatures and by the corrosive action of liquid sodium. Therefore, the second method was selected.

As pointed out in Chapter II, if a sinusoidal voltage signal is applied to the lead zirconate-titanate piezoelectric crystals of the transducer assembly, the resulting displacements transmitted through the transducer assembly will vary sinusoidally. If we select an arbitrary reference at any point in the transducer assembly, and if we let $y$ be the vibrational displacement about the reference point, then

$$y = y_0 \sin \omega t \tag{3.7}$$

where

$y_0$ = maximum displacement about reference point

$\omega$ = angular frequency of vibration.

The acceleration, $a$, at the reference point can be obtained by differentiating Eq (3.7) twice:

$$a = \frac{d^2y}{dt^2} = -\omega^2 y_0 \sin \omega t$$

or

$$a = -\omega^2 y \tag{3.8}$$

From Eq (3.8) it can be seen that the acceleration at any point in the transducer assembly is proportional to the particle displacement at that point. Therefore, by utilizing a system which responds to acceleration a measurement can be obtained which is proportional to displacement.

Commercially available piezoelectric accelerometers produce a voltage which is proportional to the applied acceleration. Because of mechanical limitations the upper limit of the applied acceleration for continuous monitoring is approximately $2 \times 10^6$ cm/sec$^2$ for the majority of available accelerometers. For measurements at 25 kHz the maximum displacement which can be measured by an accelerometer as determined by Eq (3.8) is approximately 0.03 mils ( 1 mil = 0.001 inch). If the accelerometer is attached to the top surface of the transducer counterweight and if the maximum displacement experienced by the accelerometer is 0.03 mils then the maximum displacement at the tip of the exponential horn is 0.03M mils where M is the mechanical amplification factor of the horn. It is pointed out in Chapter II that the amplification factor for an exponential horn is the ratio of end diameters of the horn and for the exponential horns used in this investigation M is approximately 3. Therefore the maximum tip displacement which could be measured with such a system would be approximately 0.09 mils. The transducer horn assemblies used in this investigation possess the capability of producing tip displacements up to 1 mil. The use of an accelerometer mounted on the top surface of the counterweight would greatly reduce the displacement producing capabilities of the transducer horn assemblies, and thus this method was not used for the present study.

The piezoelectric effect which is described in Chapter II is reversible.[38] If a piezoelectric crystal which is attached

to the transducer assembly is subjected to a mechanical strain which is produced by accelerating the crystal, an electric field will be set up in the crystal. The resulting voltage signal produced by the strained piezoelectric crystal is proportional to the applied acceleration. Since the acceleration is proportional to displacement, the output voltage signal of the piezoelectric crystal will be proportional to the particle displacement of the transducer assembly. Therefore, it was decided to attach a piezoelectric crystal to the transducer assembly as a means of indirectly monitoring the vibrational displacement of the test specimen.

A lead zirconate-titanate piezoelectric crystal, identical to the crystals used to drive the transducer assembly, was attached to the top surface of the counterweight section of the assembly (Fig 6). This point of attachment was selected since it is readily accessible for electrical connections. Also, the temperature of the counterweight section is maintained at low level during tests with fluid temperatures up to 1500°F because of the necessity of maintaining the driving crystals at low temperature, and thus the crystal output will not be affected by temperature change. A conducting epoxy known as Eccobond Solder 57C* was used to attach the crystal to the counterweight. An electrical connector was also cemented to the top surface of the crystal using the conducting epoxy. By connecting wires to the steel counterweight and to the

---

* Obtained from Emerson & Cuming, Inc., Canton, Mass.

connector on the top surface of the crystal the voltage produced by the counterweight crystal can be monitored using a VTVM or an oscilloscope. In order to relate the counterweight crystal output voltage to test specimen displacement, a calibration curve of tip displacement versus counterweight crystal voltage must be established.

To establish the calibration curve for the counterweight crystal, a KD-38 fotonic sensor* was used to measure the vibrational displacements of the test specimen. This is a non-contact optical proximity detector measuring displacements or vibrational motion from DC to 40 kHz. The 0.109 inch diameter sensing probe contains 600 randomly distributed strands of glass fiber optics encased in a plastic covered flexible steel monocoil jacket. Half of the fibers transmit light which, after being reflected from the observed object, is captured by the remaining 300 fibers and translated into an analog output voltage signal. Static signals can be read directly from the integral meter which is calibrated from zero to one volt, or applied to external equipment via the output jack. Dynamic signals (vibration) can be read by using the KD-38 output with an oscilloscope or a VTVM.

The fotonic sensor senses movement of the target surface by detecting changes in the intensity of the light being reflected by the target surface. When the probe is placed against the target surface, the output voltage is zero.

---

* Obtained from MTI Instruments Division, Latham, New, York.

As the distance between the probe and the target surface is increased the output voltage increases until it reaches a maximum value of one volt for a gap distance of 20 mils. If the distance between the probe and the target surface is increased beyond 20 mils the output voltage will begin to decrease. The fotonic sensor calibration curve (supplied by the manufacturer) of output voltage versus gap distance is shown in Fig 15. From Fig 15 it can be seen that this calibration curve is linear from approximately 3 to 5 mils. For dynamic measurements if the distance between the probe and the target surface is set at 4 mils, then vibrational displacements of the target surface of magnitudes up to 2 mils peak-to-peak will produce a linear output voltage. The slope of the linear portion of the calibration curve is 0.0071 mils/millivolt. Since the peak-to-peak displacements produced by the ultrasonic transducer assembly do not exceed 2 mils and since the frequencies used for the present investigation are less than 40 kHz, the KD-38 fotonic sensor is suitable for calibrating the counterweight crystal.

Fig 16 is a schematic diagram showing the experimental arrangement used to calibrate the counterweight crystal. The transducer horn assembly was mounted in the vessel top plate. An aluminum sensor probe adaptor plate was rigidly mounted to the vessel top plate with three mounting pins. A hole with a diameter slightly larger than the diameter of the probe is located in the center of the adaptor plate. The probe was inserted into this hole, and the distance between the probe and

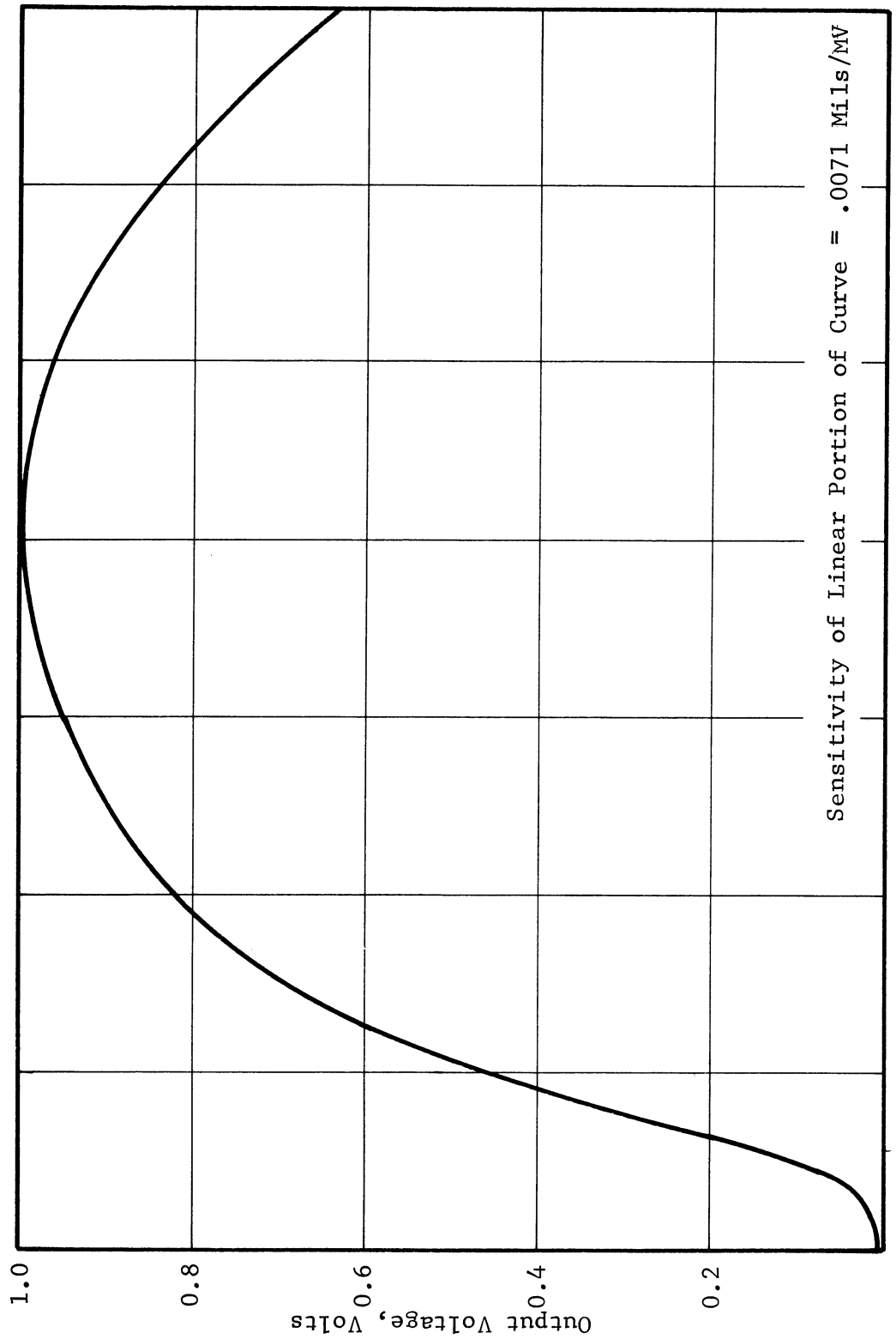


FIGURE 15. CALIBRATION CURVE FOR KD-38 FOTONIC SENSOR

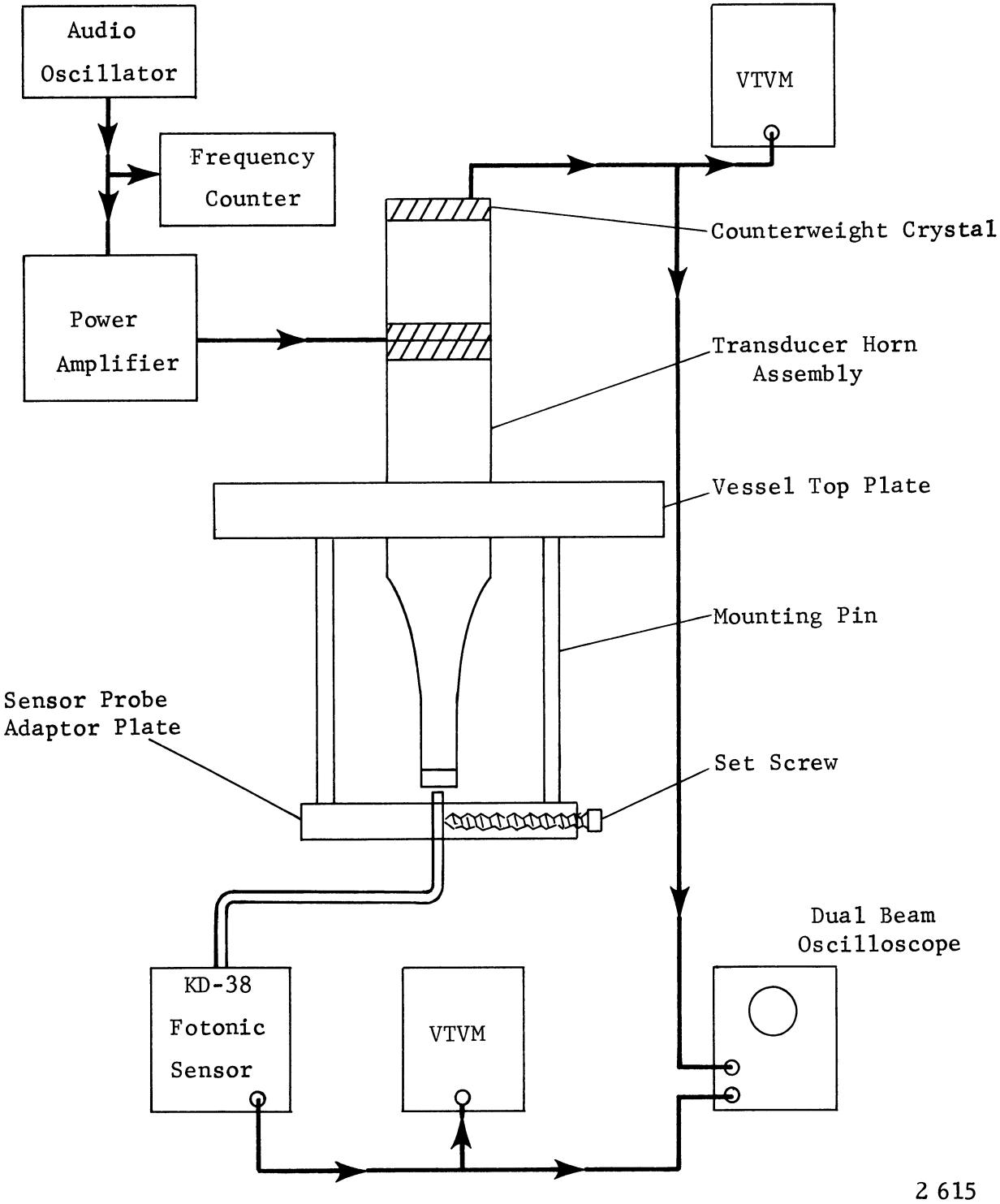


FIGURE 16. EXPERIMENTAL ARRANGEMENT FOR CALIBRATING COUNTERWEIGHT CRYSTAL

the bottom surface of the test specimen was adjusted to 4 mils by noting the fotonic sensor output voltage. The probe was secured in this position by means of a set screw. To obtain the counterweight calibration curve the voltage signal applied to the transducer assembly was held constant at a relatively low level. The output voltages from the fotonic sensor and counterweight crystal were then recorded. The voltage to the transducer assembly was increased to a higher level and the procedure was repeated. This process was repeated several times so that a calibration curve for the counterweight crystal could be established. The above procedure was repeated for the two exponential horns used in the pressure field measurements, since for each horn used, the counterweight crystal calibration curve will be different. Shown in Fig 17 are the counterweight crystal calibration curves of counterweight crystal output voltage (RMS volts) versus test specimen displacement (zero to peak) in inches for a 18.5 kHz exponential horn and a 14.4 kHz exponential horn. During the calibration procedure the waveforms of the output voltages of the fotonic sensor and the counterweight crystal were observed by using a dual beam oscilloscope. Fig 18 are photographs of two sets of typical waveforms observed during the counterweight crystal calibration.

A question now arises as to the effect of the test fluid on the motion of the test specimen. In other words, will the calibration curves for the counterweight crystal measured in air be valid when the horn tip is immersed in the test fluid? The experimental arrangement shown in Fig 19 was

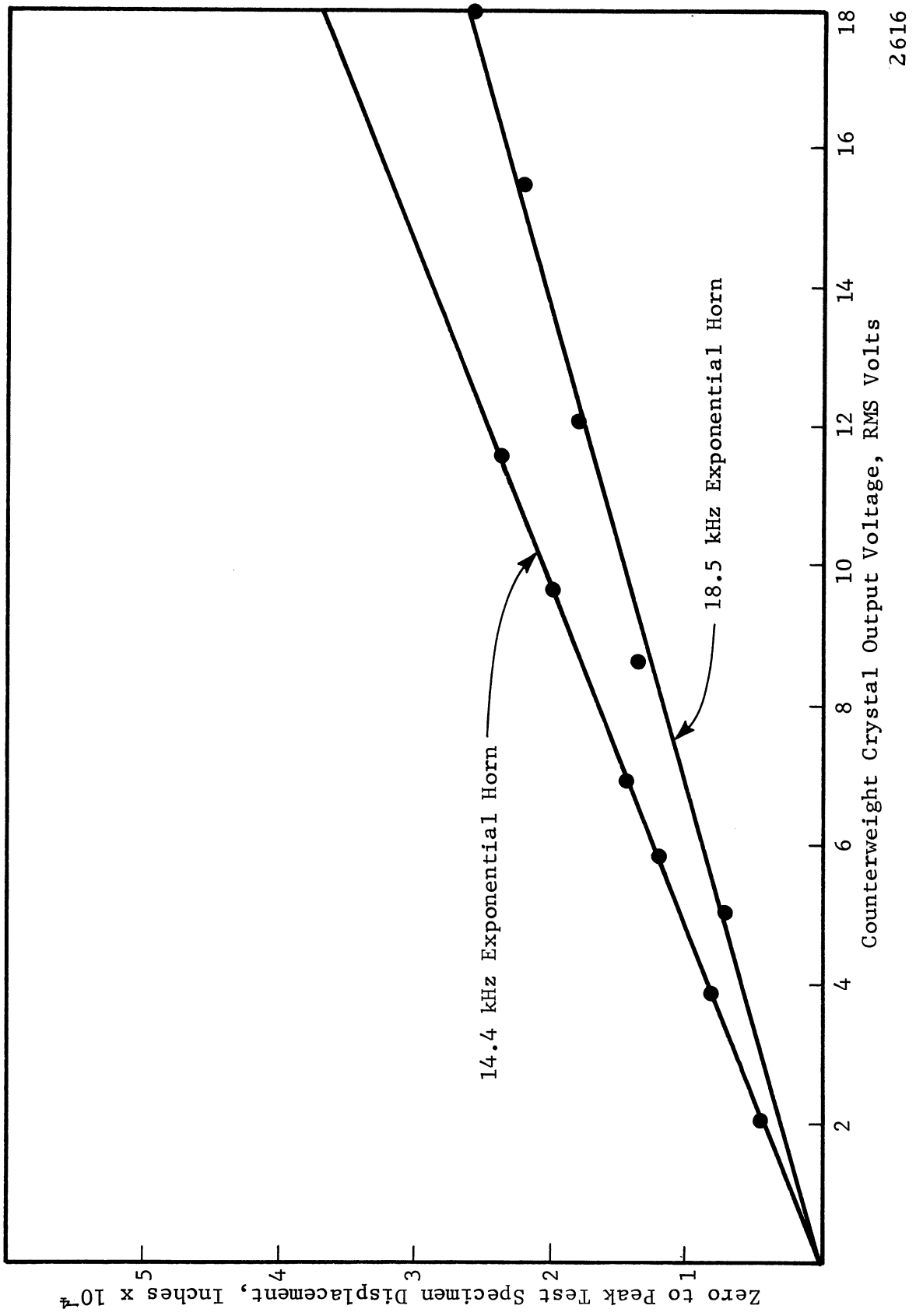


FIGURE 17. COUNTERWEIGHT CALIBRATION CURVES FOR THE 14.4 KHZ AND 18.5 KHZ TRANSDUCER-HORN ASSEMBLIES

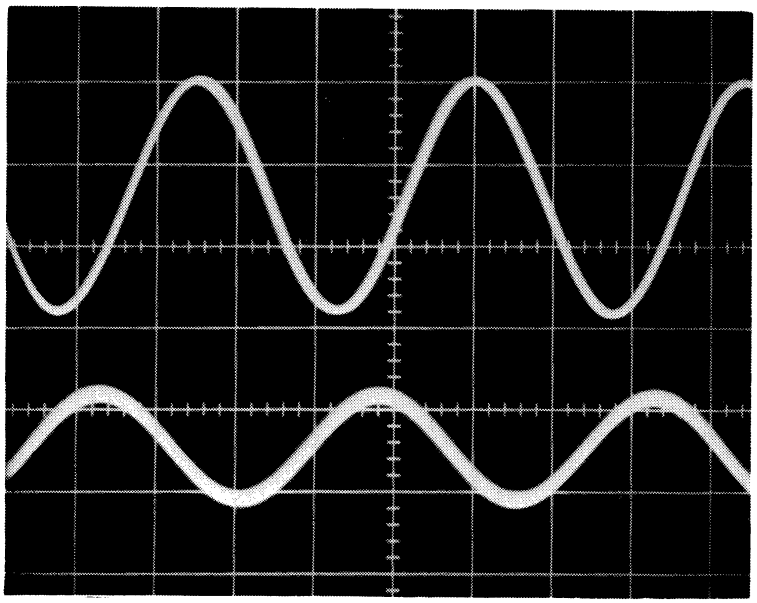

COUNTERWEIGHT
CRYSTAL VOLTAGE

5 Volts/CM
20 Microsec/CM

FOTONIC SENSOR
VOLTAGE

20 Millivolt/CM
20 Microsec/CM

WAVEFORMS FOR 14.4 EXPONENTIAL HORN

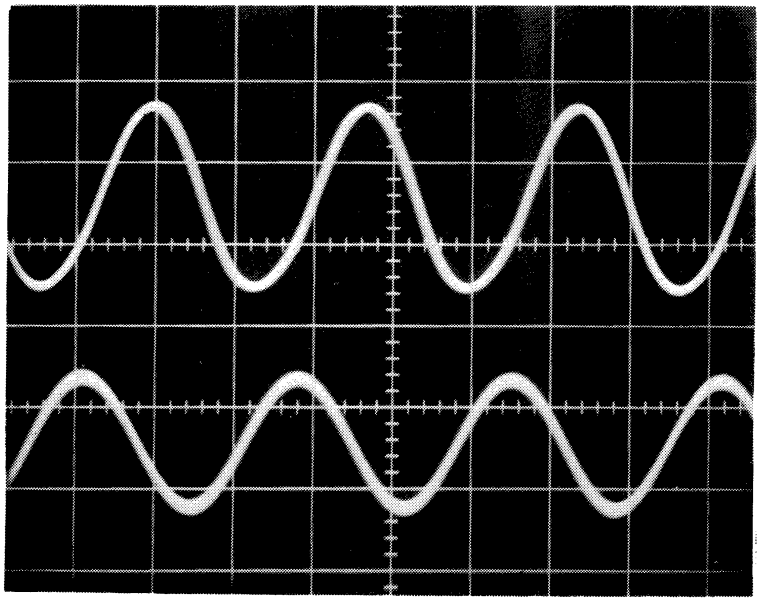

COUNTERWEIGHT
CRYSTAL VOLTAGE

10 Volts/CM
20 Microsec/CM

FOTONIC SENSOR
VOLTAGE

20 Millivolts/CM
20 Microsec/CM

WAVEFORMS FOR 18.5 KHZ EXPONENTIAL HORN

2617

FIGURE 18. TYPICAL WAVEFORMS OBSERVED DURING COUNTERWEIGHT CRYSTAL CALIBRATION

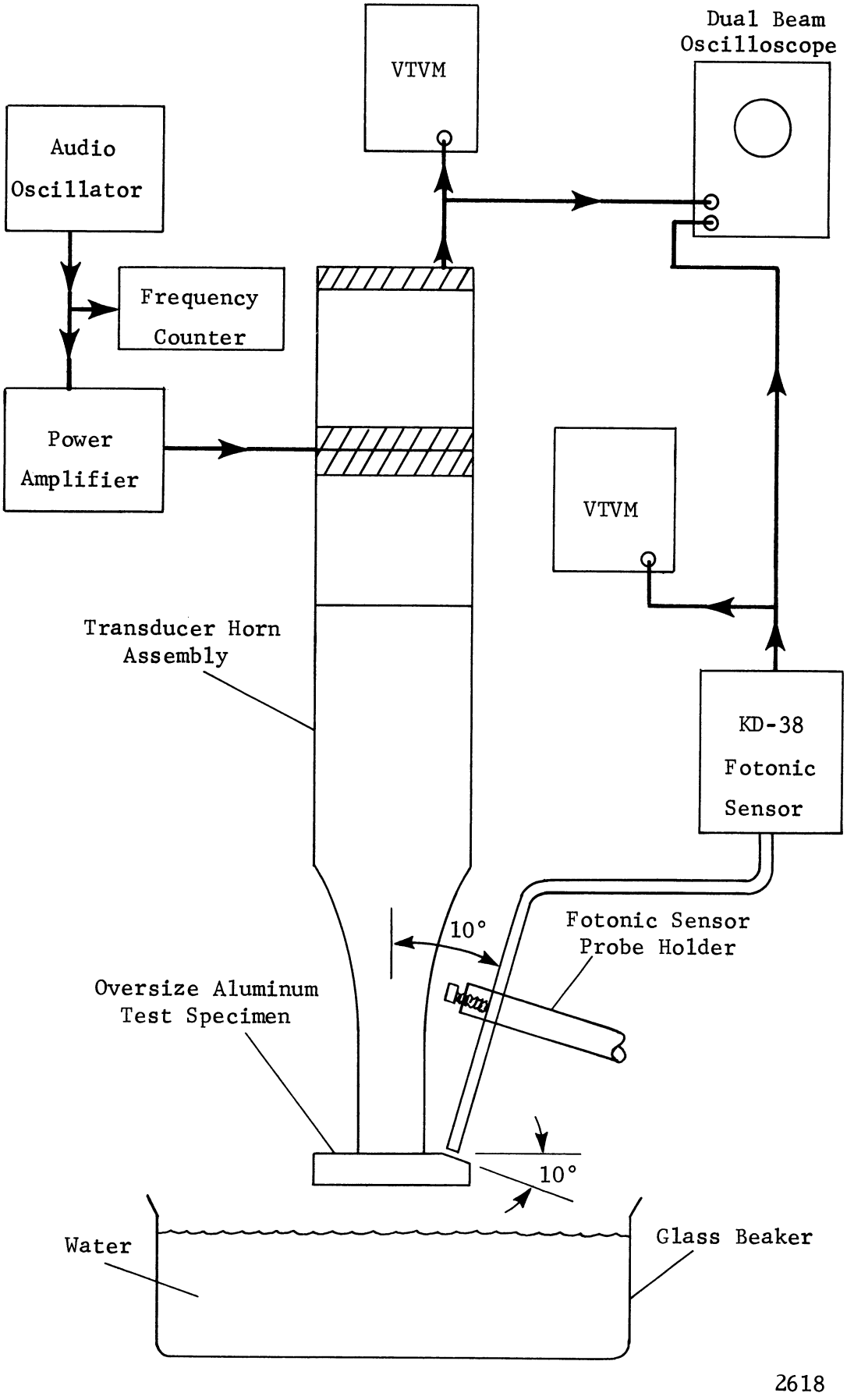


FIGURE 19. EXPERIMENTAL ARRANGEMENT USED TO DETERMINE TEST FLUID LOADING EFFECT

used to determine the loading effect of the test fluid upon the motion of the test specimen. An oversize aluminum piston was fabricated with a diameter of 7/8 inches and a thickness of 19/64 inches. With these dimensions the weight of the aluminum specimen is approximately the same as that of the stainless steel specimens attached to the horn used in this experiment. A $10^{o}$ beveled surface was ground on one side of the top surface of the aluminum specimen. The fotonic sensor probe which was positioned above the test specimen was inclined at an angle of $10^{o}$ with respect to the transducer assembly to avoid interference with the horn and to match the angle of the beveled surface. With this arrangement the beveled surface of the test specimen, and the surface of the sensor probe were parallel. A calibration curve was then obtained for the counterweight crystal with the aluminum specimen in air. The specimen was then submerged to a depth of approximately 1/8 inches in water and the calibration procedure was then repeated. The two calibration curves obtained with no loading and with loading were identical. It may be concluded that the effect of immersing the test specimen into water has no effect on the test specimen displacements produced by the transducer assembly within the range of displacements tested (approximately 0.5 mils peak-to-peak).

## D. Development of a Pressure Probe for Pressure Field Measurements

### 1. Construction of the Pressure Probe

As pointed out earlier in this chapter it is necessary

to verify experimentally Eq (3.5), which describes the pressure field produced inside the cavitation vessel. To obtain this verification a small pressure probe was required which could be used to map the pressure field inside the cavitation vessel. The diameter of this probe must be small compared to the diameter of the test specimen so that its presence will not appreciably perturb the pressure field to be measured. The probe must be sufficiently sensitive and of high enough response rate that it will respond to the small changes in pressure being produced in the vessel. Since no suitable commercial probe was available, the author developed the unit described below.

A barium titanate piezoelectric crystal was selected as the sensitive element for the pressure probe, since its efficiency of transforming applied loads to voltage is relatively high compared to other piezoelectric crystals.[39] The crystal is cylindrical in shape with an outside diameter of 0.063 inches, a length of 0.061 inches, and a wall thickness of 0.012 inches. It has a resonant frequency of 1600 kHz, well above the frequency range of this experiment. The crystal was polarized in the axial direction and its end surfaces coated with silver to provide electrical contact. An aluminum plate 0.063 inches in diameter and 0.010 inches thick was cemented with conducting epoxy to the top surface of the crystal cylinder. A small electrical wire was attached at this cemented surface. A nylon insulator together with a second electrical wire were cemented with conducting epoxy to the bottom surface of the

cylinder. The insulator has a 0.075 inch diameter and a thickness of 0.010 inches. A 0.040 inch diameter hole was drilled in the center of the insulator to allow for passage of the electrical wire connected to the top surface of the cylinder. The crystal assembly was mounted in a cylindrical stainless steel holder whose diameter is 0.100 inches and whose length is 1.5 inches. A thin coating of neoprene cement was applied to the tip of the crystal holder to seal the crystal in the holder. The crystal holder was welded to a stainless steel rod. This rod has an outside diameter of 3/16 inches, an inside diameter of 1/16 inches, and a length of 12 inches. The two electrical wires which were connected to the crystal pass down through the inside of the crystal holder and rod, and were soldered to a coaxial cable connector which in turn was soldered to the bottom end of the 12 inch rod. A schematic diagram showing the barium titanate crystal mounted in the tip of the crystal holder is shown in Fig 20. Fig 21 is a photograph of the pressure probe together with a coaxial cable which can be connected to an oscilloscope. From Fig 20 it can be seen that the effective diameter of the probe is approximately 0.073 inches which is relatively small compared to the 0.547 inch diameter of the test specimen.

## 2. Calibration of the Pressure Probe

Calibration of the pressure probe was achieved by comparing its voltage output with the output voltage of a calibrated pressure transducer. Fig 22 is a schematic diagram

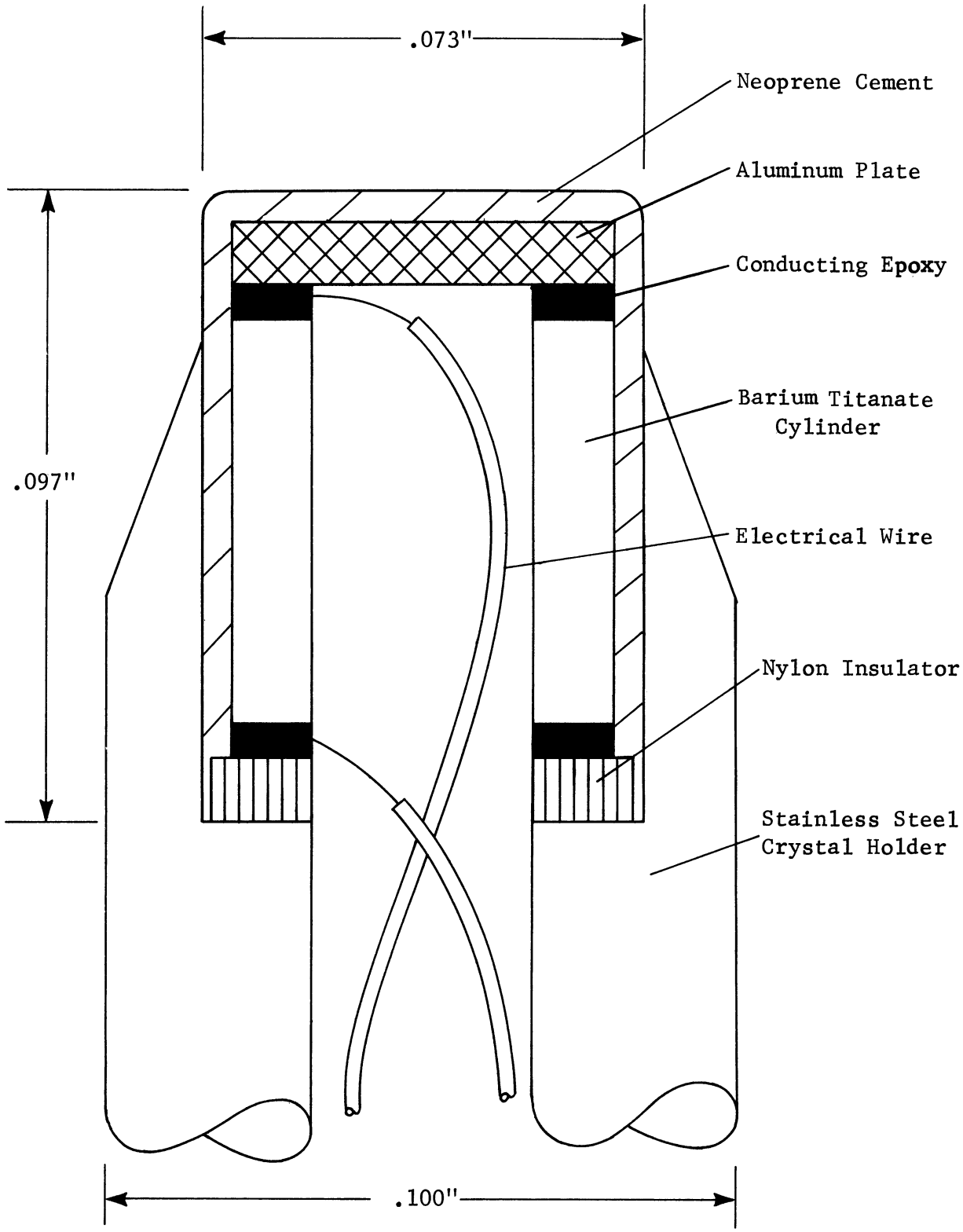


FIGURE 20. CROSS SECTIONAL VIEW OF TIP OF PRESSURE PROBE

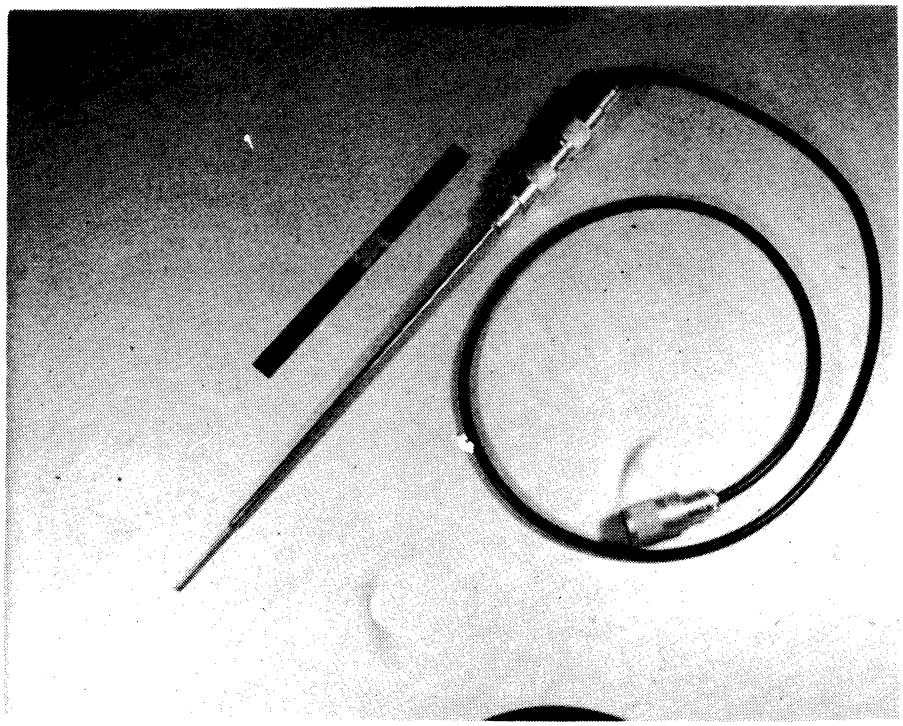

2620

FIGURE 21. PRESSURE PROBE WITH ATTACHED COAXIAL CABLE

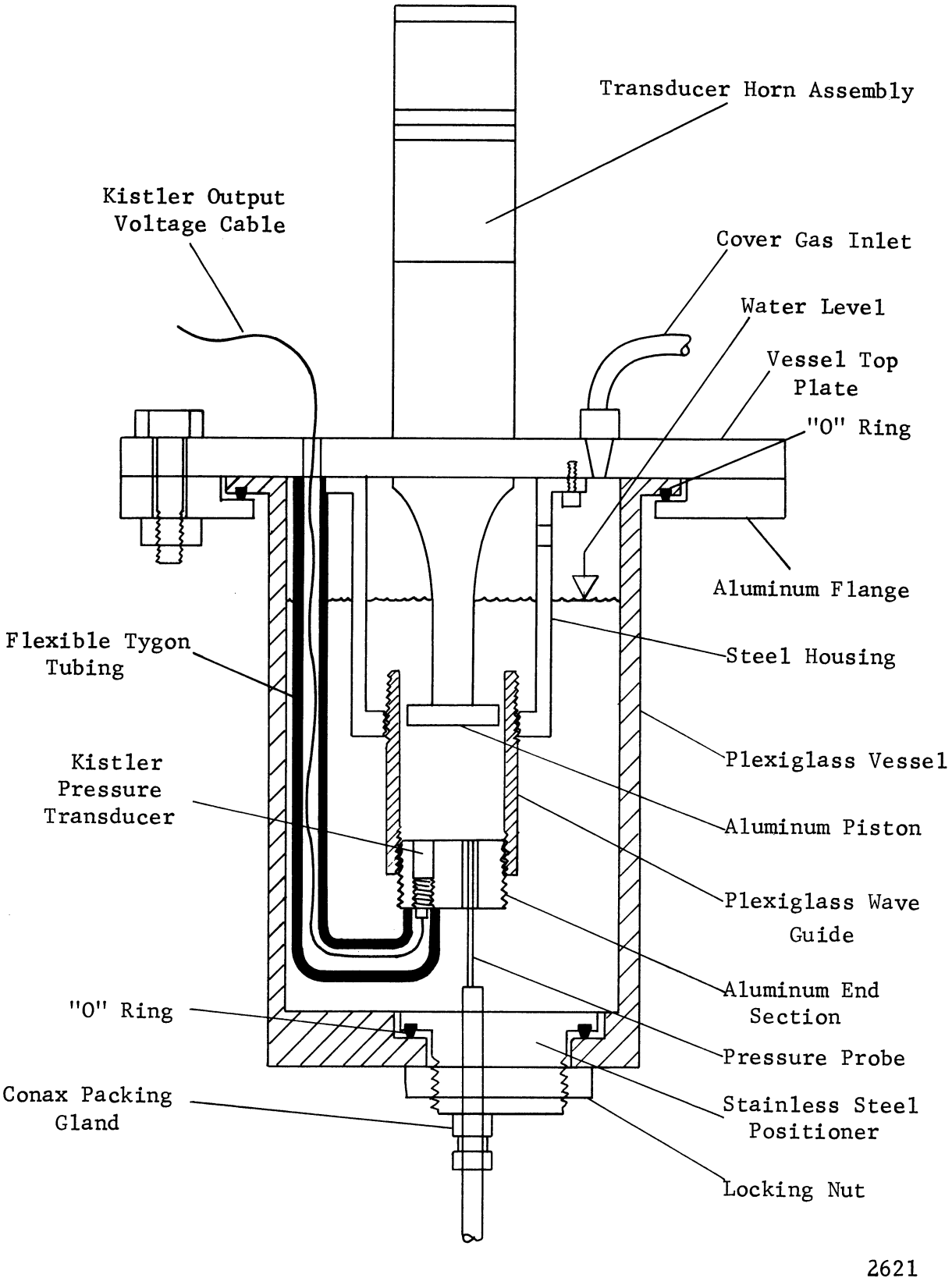


FIGURE 22. EXPERIMENTAL ARRANGEMENT FOR PRESSURE PROBE CALIBRATION

of the arrangement used to calibrate the probe. The calibration technique consists of producing standing waves in a cylindrical plexiglass waveguide. The standing waves are produced by the vibrational motion of an oversize specimen on the horn tip, which serves as the piston source for the standing waves. The standing waves are transmitted down the tube and are incident upon an aluminum end section which houses the pressure transducer and the tip of the pressure probe. The plexiglass wave guide is threaded into a cylindrical steel housing which is bolted to the vessel top plate. The length of the wave guide can be adjusted so that resonant conditions can be achieved. The wave guide and steel housing are enclosed in a plexiglass vessel which is secured to the vessel top plate by means of an aluminum flange which is bolted to the vessel top plate. Located in the bottom of the plexiglass vessel is a stainless steel pressure probe positioner. The vertical axis of the positioner is offset from the vertical axis of the plexiglass vessel. A hole was drilled through the positioner to allow for insertion of the pressure probe. The vertical axis of this hole was offset from the vertical axis of the positioner. It was tapped to allow for a Conax packing gland which was used to secure the pressure probe in the positioner. The positioner assembly is secured to the plexiglass vessel by means of a threaded nut. The pressure transducer cable was enclosed in a flexible tygon tube which provided a watertight seal for the transducer cable. Sealing for the overall arrangement was provided by two "O" rings whose positions are indicated

in Fig 22. A cover gas system was provided to allow for pressurizing the system.

A Kistler quartz pressure transducer Model 601A was used as the standard for the pressure probe calibration. This transducer has a pressure range from 0 to 3000 psi, and has a flat frequency response over the frequency range used in this experiment. Its diameter is 0.250 inches. The output of the transducer was connected to a Kistler charge amplifier Model 566, the output of which was in turn connected to a VTVM and a dual beam oscilloscope. Fig 23 (a) is a photograph of the components of the calibration system and Fig 23 (b) of the assembled calibration system.

Since the pressure fluctuations produced by the piston will not be the same at all points of the top surface of the aluminum end section, some means must be used to compensate for the differences in diameters and positions of the pressure transducer and the pressure probe. The outputs of the transducer and probe will represent an average value for the pressure field acting on their exposed surfaces. Since the exposed surfaces of the transducer and pressure probe are different, the resultant pressures may not be equal. To compensate for the differences in sizes of the transducer and pressure probe three access holes for the pressure probe were drilled in the aluminum end section at different radial positions. Fig 24 is a top view of the aluminum end section indicating the position of the pressure transducer and the three access holes for positioning the pressure probe. The three radii to the

FIGURE 23 (a). COMPONENTS OF THE PRESSURE PROBE CALIBRATION SYSTEM

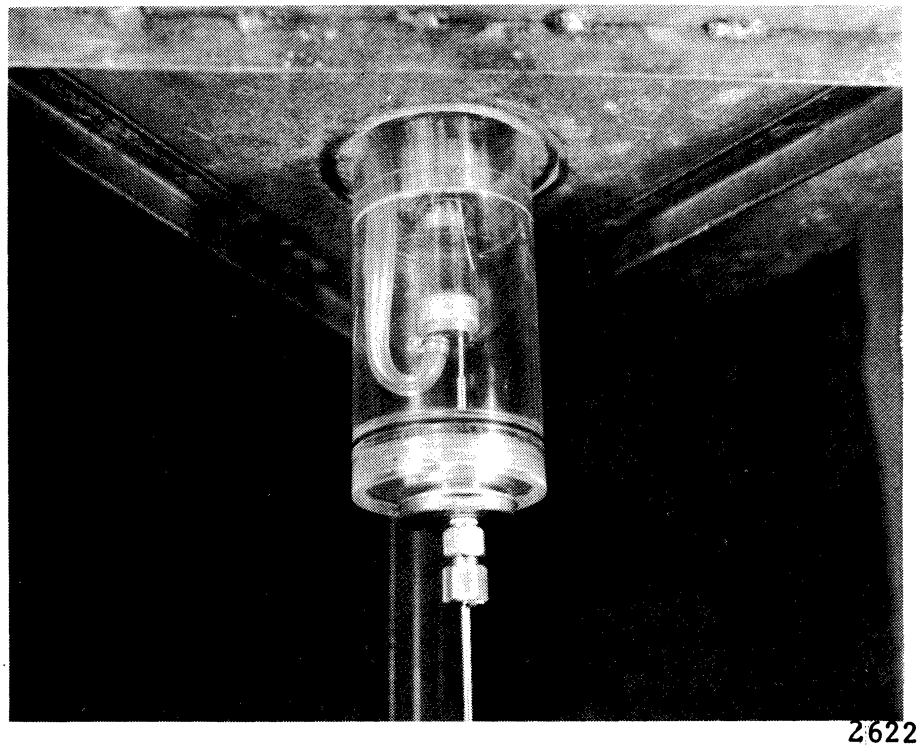

2622

FIGURE 23 (b). ASSEMBLED PRESSURE PROBE CALIBRATION SYSTEM

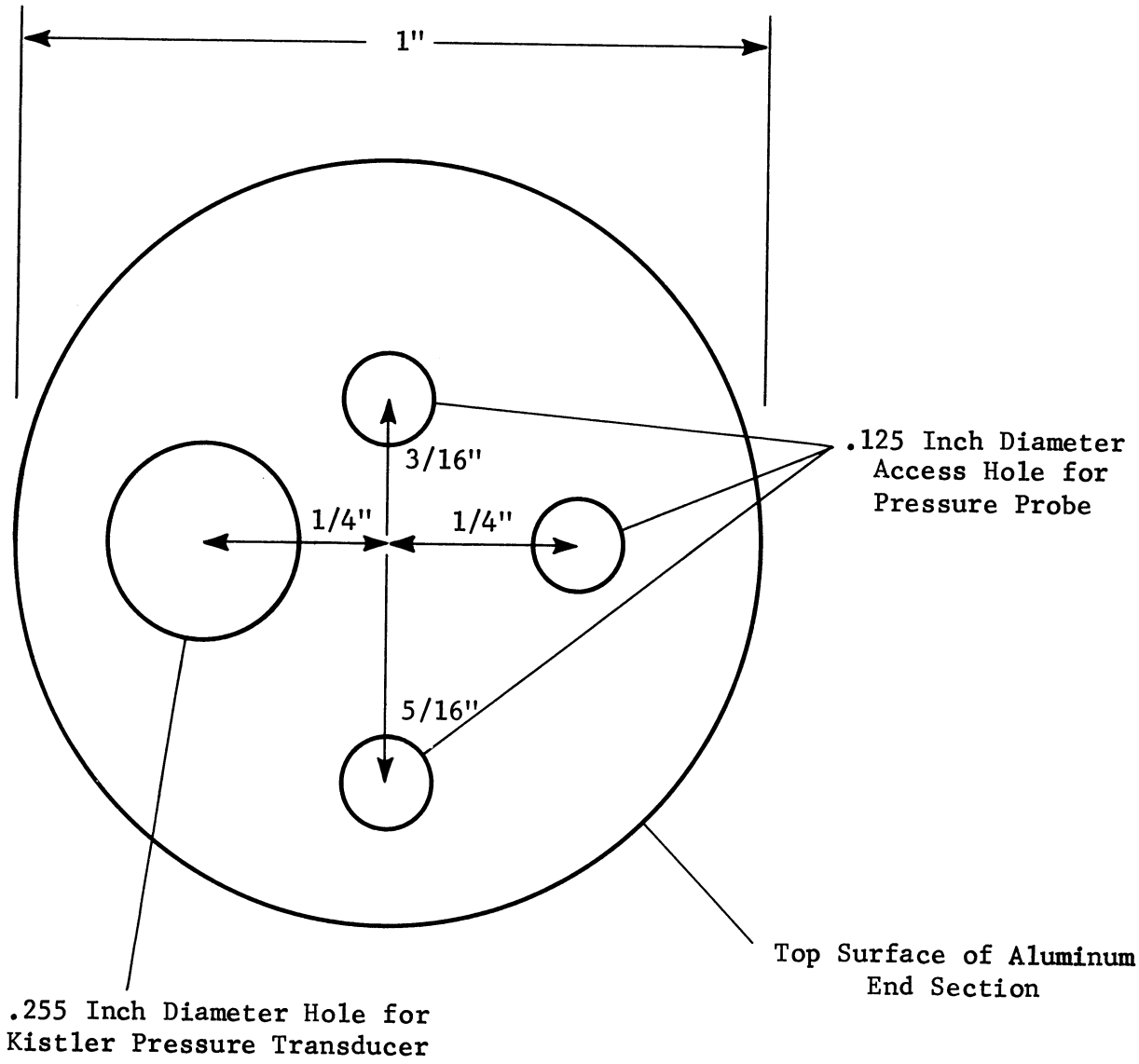


FIGURE 24. TOP VIEW OF ALUMINUM END SECTION

positioning holes for the pressure probe were chosen such that the radial extent covered by the Kistler pressure transducer is also covered by the combination of the three radial positions for the pressure probe.

A cover gas system was employed so that an overpressure could be introduced into the plexiglass vessel. With no overpressure, cavitation will occur in the wave guide for relatively small changes in pressure. In order to obtain a calibration curve for the pressure probe over a relatively large pressure range, an overpressure of 20 psi was applied to the system. This overpressure was sufficient to prevent the formation of cavitation bubbles for the pressure range used in the calibration.

To obtain the calibration curve for the pressure probe, the following experimental procedure was followed. The pressure probe was positioned in one of the three holes in the aluminum end section such that its top surface was flush with the top surface of the aluminum end section. The vertical position of the probe can be adjusted by loosening the Conax packing gland so that the probe can be raised or lowered. The radial position of the probe to be used is made available by rotating the stainless steel positioner. Because the positioner is offset from the center of the plexiglass vessel, and since the pressure probe is offset from the center of the positioner, the three access holes in the aluminum end section are readily assessible to the pressure probe by merely rotating the positioner. The input voltage to

the transducer assembly was held constant at a relatively low level, and the output voltages from the pressure transducer and the pressure probe were recorded. The voltage to the transducer assembly was then increased and the process was repeated. After obtaining several calibration points the pressure probe was relocated in a different access hole in the aluminum end section and the process was then repeated. The calibration procedure was continued until several calibration points were obtained for each of the three access holes. The above data was obtained at two different frequencies by using exponential horns with resonant frequencies of 16.8 and 10.3 kHz. The results of all the calibration runs are plotted in Fig 25. The output voltage from the Kistler pressure transducer was converted to psi using the calibration curve provided by the manufacturer. A least mean square fit was used to obtain the slope of the straight line in Fig 25.[40] From Fig 25 it can be seen that the pressure probe is essentially independent of frequency over the frequency range investigated. The scatter in the calibration data plotted in Fig 25 indicates that the pressure over the surface of the aluminum end section was not uniform. However, the average of these values as represented by the straight line should represent the average pressure incident upon the Kistler pressure transducer. The linear relationship obtained between pressure probe output and applied pressure was to be expected since the barium titanate crystal output is proportional to applied force or applied pressure. Fig 26 is a photograph of a typical set of voltage

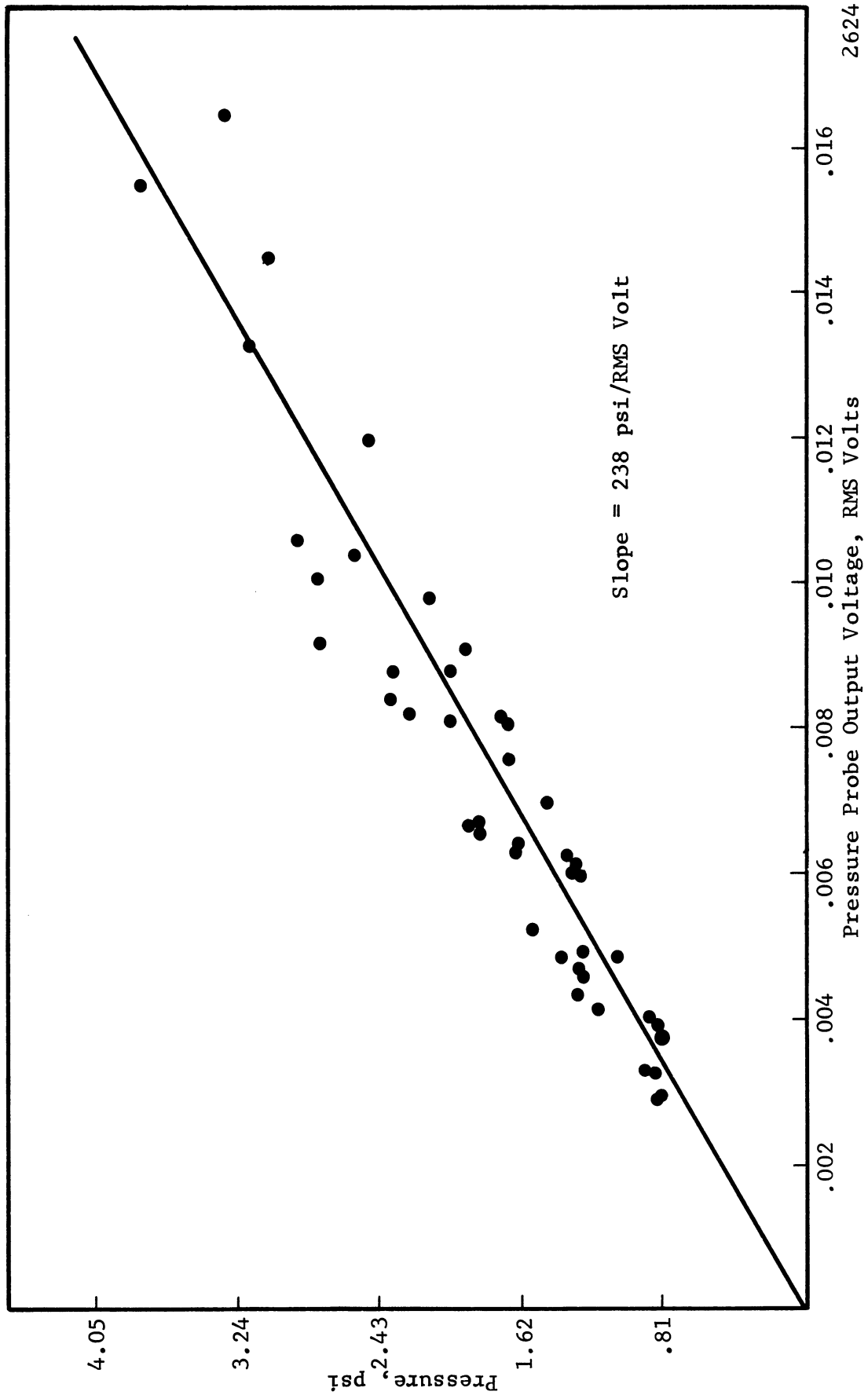


FIGURE 25. CALIBRATION CURVE FOR PRESSURE PROBE

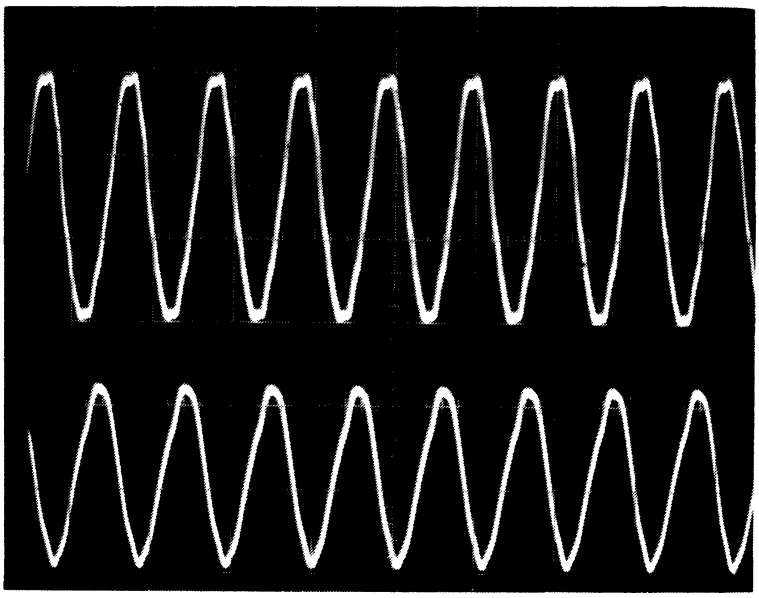


FIGURE 26. PHOTOGRAPH OF TYPICAL VOLTAGE WAVEFORMS OBSERVED DURING PRESSURE PROBE CALIBRATION

waveforms observed during the calibration process.

E. Experimental Measurement of the Pressure Field

To experimentally measure the pressure field in the cavitation vessel the arrangement shown in Fig 27 was used. The solid stainless steel bottom of the vessel was removed and replaced by a modified stainless steel bottom which allowed a stainless steel pressure probe positioner to be installed. The vertical axis of the positioner was offset from the vertical axis of the cavitation vessel by 0.273 inches. The hole which was drilled through the positioner to allow for insertion of the pressure probe was offset from the vertical axis of the positioner by 0.273 inches. This hole was drilled and tapped for a packing gland which was used to secure the pressure probe in the positioner. Because of the two equal offsets it was possible to position the tip of the pressure probe at any desired radial position covering the bottom surface of the horn tip by merely rotating the positioner. With the two offsets lined up, the tip of the probe lay along the horn axis. As the positioner was rotated, the radial distance between the horn axis and the probe increased, and for a rotation of $60^{\circ}$ the tip of the probe was positioned on the edge of the test specimen at a radial distance of 0.273 inches, which is the radius of the test specimen. As indicated in Fig 27 the lower portion of the positioner was scribed in increments of 1/64 of an inch. By using a pointer attached to the bottom of the cavitation vessel, the radial position of the pressure probe can be monitored. The vertical position

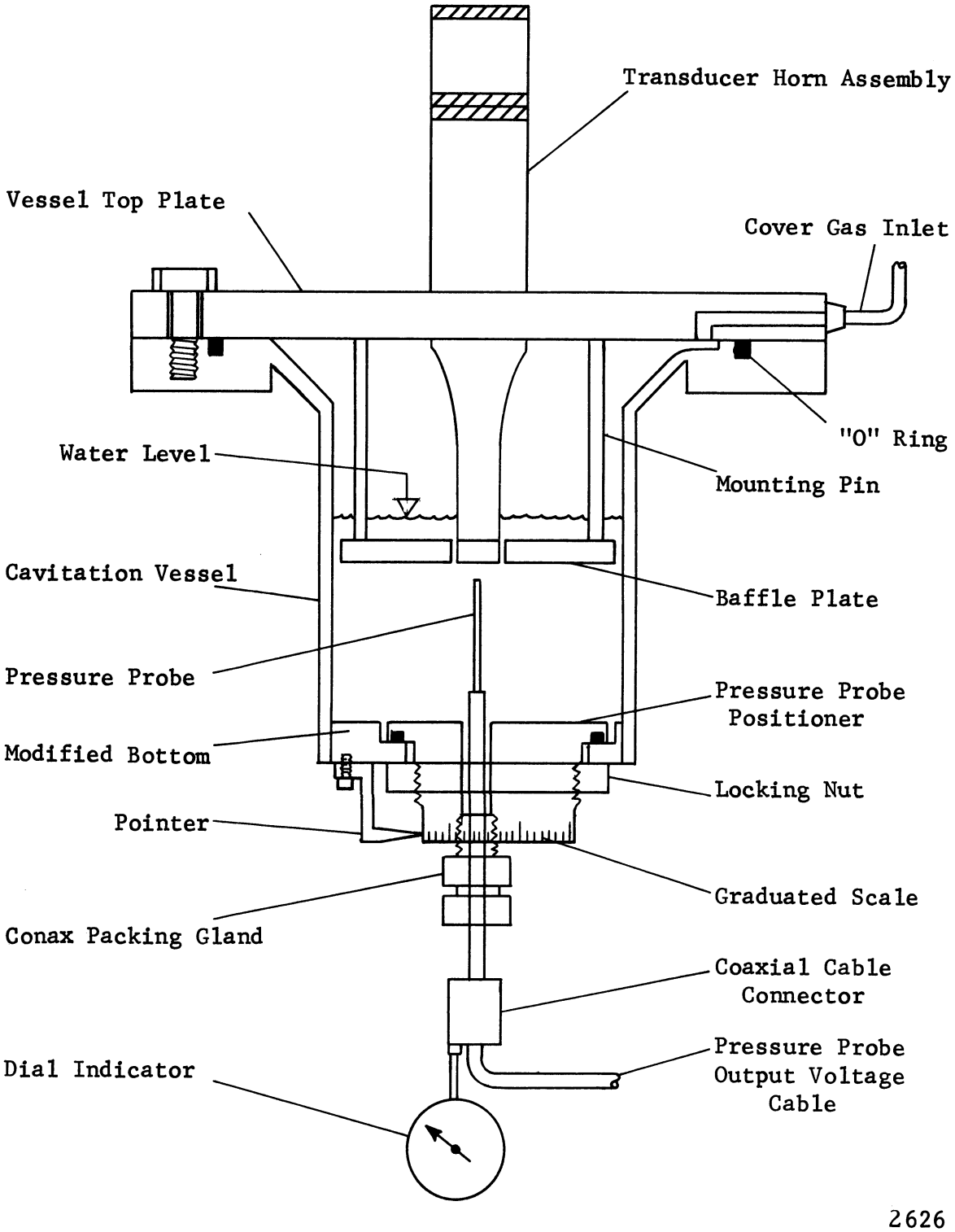


FIGURE 27. EXPERIMENTAL ARRANGEMENT FOR MAPPING PRESSURE FIELD

of the pressure probe was measured by using a dial indicator. The displacement sensing element of the dial indicator was placed against the coaxial cable connector which was welded to the bottom of the pressure probe. By loosening the packing gland the pressure probe can be positioned at any desired vertical location. Fig 28 (a) is a photograph showing the modified vessel bottom and the pressure probe positioner. Fig 28 (b) is a photograph of the assembled cavitation vessel, positioner, pressure probe, and dial indicator.

For the first set of pressure measurements, an exponential horn with a resonant frequency of 18.6 kHz was used. The distance between the bottom surface of the test specimen and the bottom of the cavitation vessel was 2.22 inches. This point is approximately midway between the first two longitudinal resonant modes for the vessel (Fig 14). Therefore, the pressure measurements should not be affected by resonant conditions. The vessel was filled with distilled water to a level just above the baffle plate. The cover gas system utilizing air was adjusted to give an overpressure of 20 psi to prevent the formation of any cavitation bubbles. The pressure probe was initially positioned at the point r = o and z = 0. The dial indicator was then adjusted for a zero reading. The probe was then withdrawn to the point r = 0 and z = 0.030 inches. The input voltage to the transducer assembly was adjusted so that the counterweight crystal voltage was 1.05 volts (RMS), and this value was then held constant for the pressure field measurement. The pressure probe output voltage was recorded

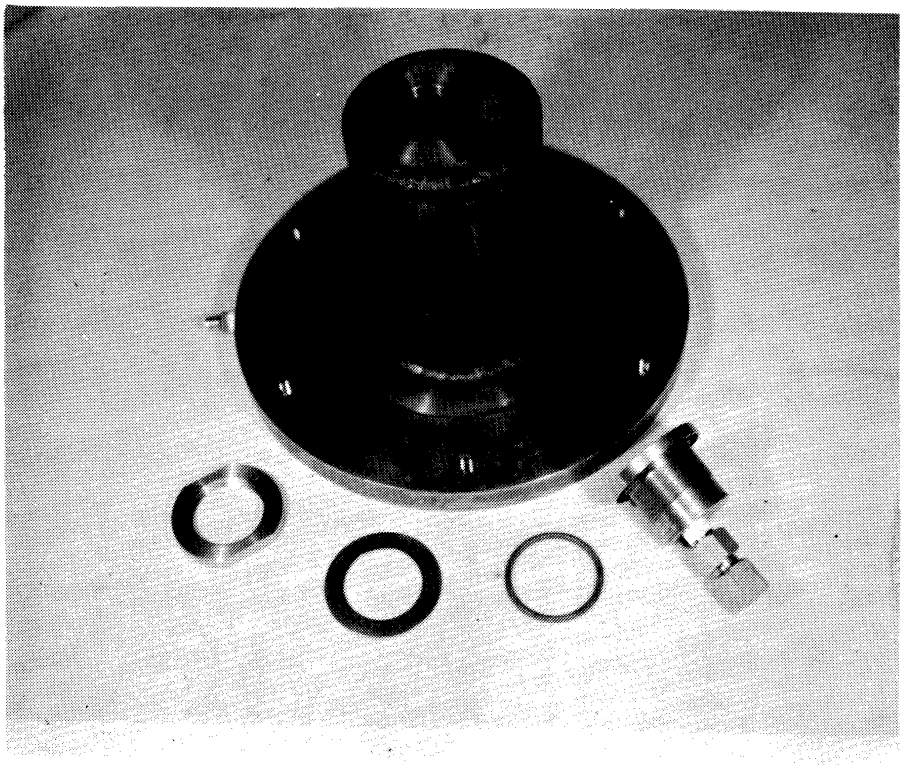

FIGURE 28 (a). CAVITATION VESSEL WITH MODIFIED BOTTOM, POSITIONER, "O" RING, WASHER, AND LOCKING NUT

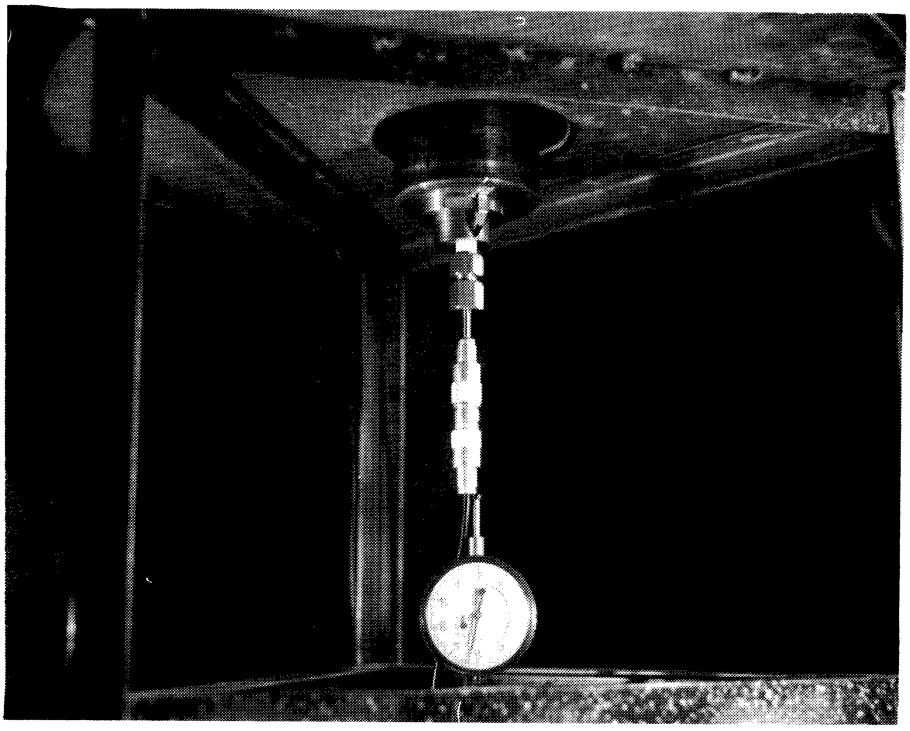

2627

FIGURE 28 (b). ASSEMBLED CAVITATION VESSEL, POSITIONER, PRESSURE PROBE, AND DIAL INDICATOR

using the VTVM. The pressure probe was then withdrawn to a new z value, and the resultant pressure probe voltage recorded. This process was repeated for the entire length of the vessel. The pressure probe was then returned to the position r = 0 and z = 0.030 inches to check for repeatability of the data. The positioner was then rotated to a new r value, and the pressure probe output voltages for various values of z obtained at this new value of r. During these measurements the counterweight crystal output voltage was monitored to insure that the vibrational tip displacement of the test specimen remained constant. Measurements at various z values for five different radial positions were obtained. At the completion of the measurements the probe was again returned to the position r = 0 and z = 0.030 inches to insure repeatability.

A second series of measurements were obtained using an exponential horn with a resonant frequency of 14.5 kHz. With this horn the distance between the bottom surface of the test specimen and the bottom of the cavitation vessel was 0.75 inches. Referring to Fig 14 it is seen that this point is also far removed from any resonant condition for the cavitation vessel. The experimental procedure as outlined above was repeated for this exponential horn. During these measurements the counterweight crystal voltage was maintained at 2.23 volts (RMS). Fig 29 (a) is a photograph of typical waveforms observed during the pressure field measurements using the 18.5 kHz exponential horn, and Fig 29 (b) is a photograph of the waveforms observed using the 14.4 kHz exponential horn.

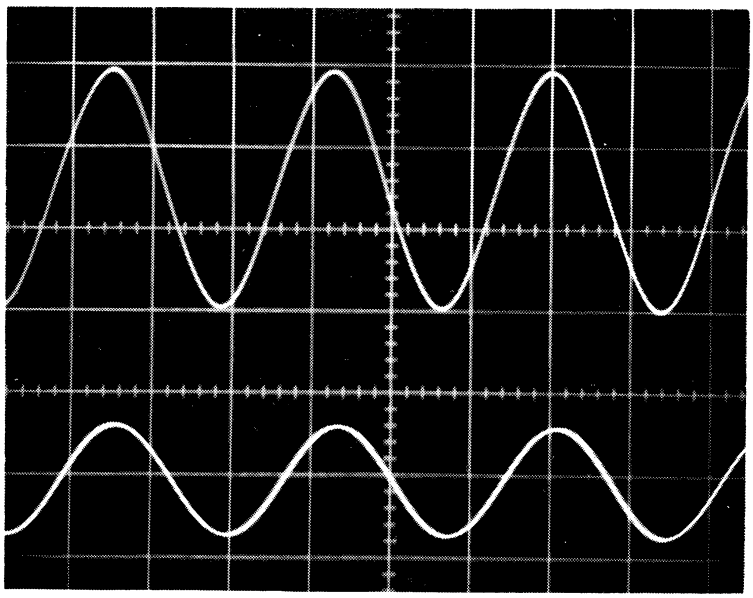


FIGURE 29 (a). WAVEFORMS FOR 18.5 KHZ EXPONENTIAL HORN OBSERVED DURING PRESSURE FIELD MAPPING

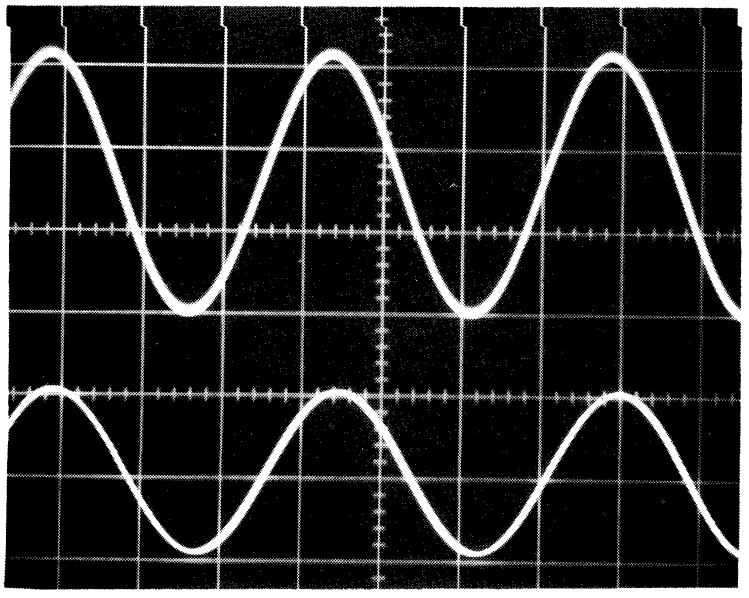


FIGURE 29 (b). WAVEFORMS FOR 14.4 KHZ EXPONENTIAL HORN OBSERVED DURING PRESSURE FIELD MAPPING

For these photographs the pressure probe was at the position $r = 0$ and $z = 0.030$ inches.

## F. Comparison of Experimental Results with Theoretical Results

By referring to the counterweight crystal calibration curves in Fig 17 the test specimen displacements used in the experimental pressure field measurements can be determined. Knowing the test specimen displacements, Eq (3.5) can be evaluated, since all other parameters are known. The theoretical values as computed from Eq (3.5) can then be compared with the experimental values to determine the validity of Eq (3.5).

Eq (3.5) was evaluated using a General Electric 235 digital computer.* In programming Eq (3.5) all Bessel functions were represented by their series approximations so that any number of terms could be considered in the infinite series summation in Eq (3.5). To determine the number of terms that should be considered in the infinite series, an initial check was conducted considering 250 terms. The last term of this series was on the order of $10^{-4}$. 500 terms were then considered and the last term of this series was on the order of $10^{-5}$. It appeared that the infinite series was a slowly converging series. However, it was decided to use 250 terms rather than 500 terms since the last term in this series was small, and since considerable computer time was saved by considering only 250 terms.

---

* The G. E. 235 digital computer was made available on a time share program sponsored by the Ford Motor Company.

The results of the theoretical calculations for the 18.5 kHz and 14.4 kHz exponential horns are plotted as solid curves in Figs 30 and 31, respectively, as well as the corresponding experimental data points. Fig 30 shows that the experimental points are reasonably well predicted by the theoretical curve for z = 0 to z = 0.5 inches. Beyond this point large discrepancies exist between the theorectical curve and the experimental points. However, for this experiment we are only interested in the point of maximum pressure change since nucleation should first occur at this point. According to Figs 30 and 31 this point is at r = 0 and z = 0, i. e., the maximum changes in pressure occur on the surface and at the center of the vibrating test specimen. If the experimental data points in Fig 30 (a), which is for r = 0, are extrapolated to z = 0, it is found that there is approximately a 5.9 per cent error between theory and experiment. The substantial agreement is very heartening, since several experimental errors could have been introduced in the various experimentally determined calibration curves, and in the measurements of the pressure field. Reference to Fig 31 shows that there is good agreement between theory and experiment for the entire range of z. By extrapolating the experimental data points in Fig 32 (a) to z = 0 it is found that there is approximately 8.1 per cent error between theory and experiment for r = 0 and z = 0.

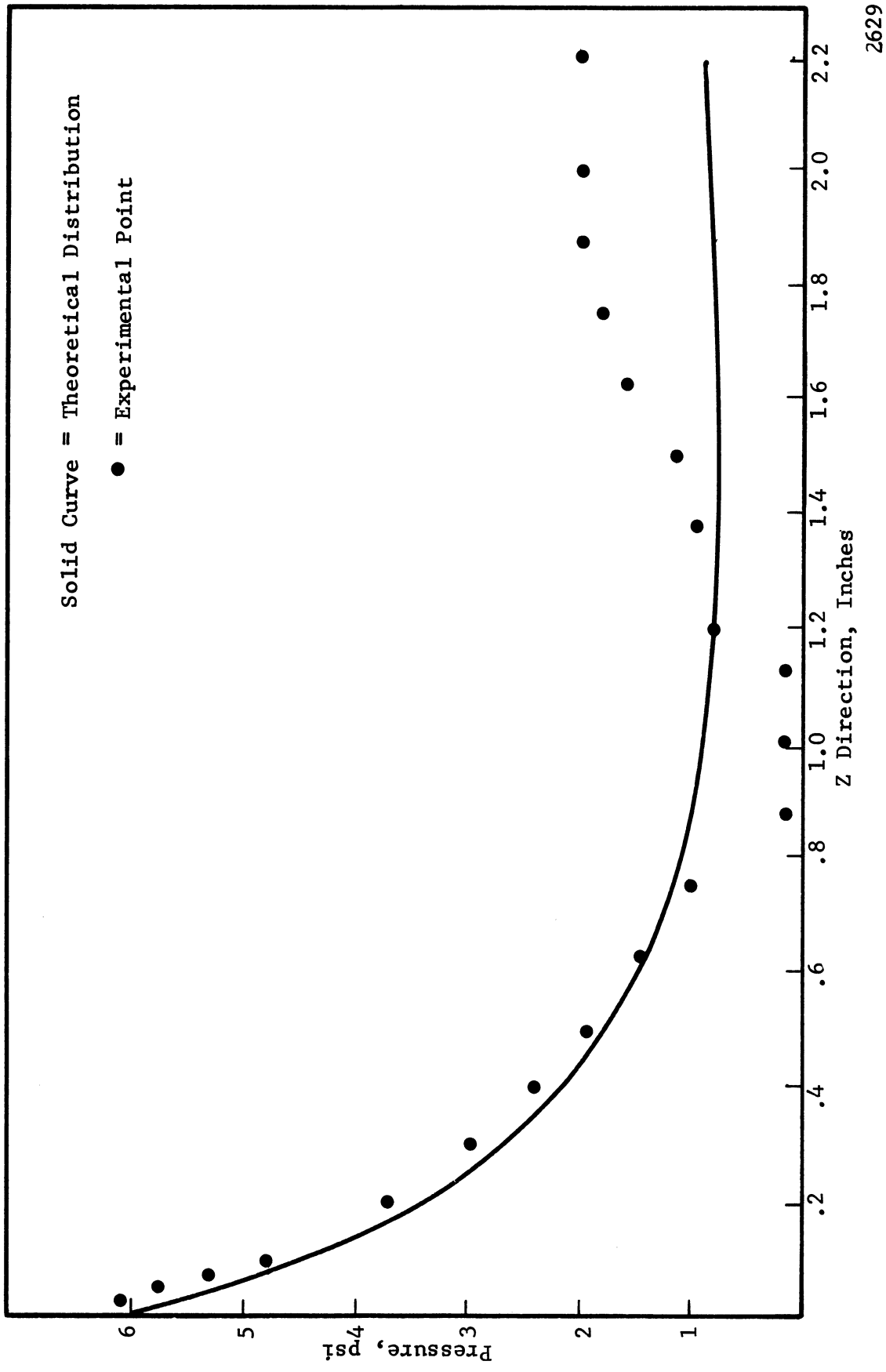


FIGURE 30 (a). PRESSURE DISTRIBUTION IN Z DIRECTION FOR r = 0, $\ell$ = 2.22 INCHES
FREQUENCY = 18560 HZ, AND A = 1.50 x $10^{-6}$ INCHES

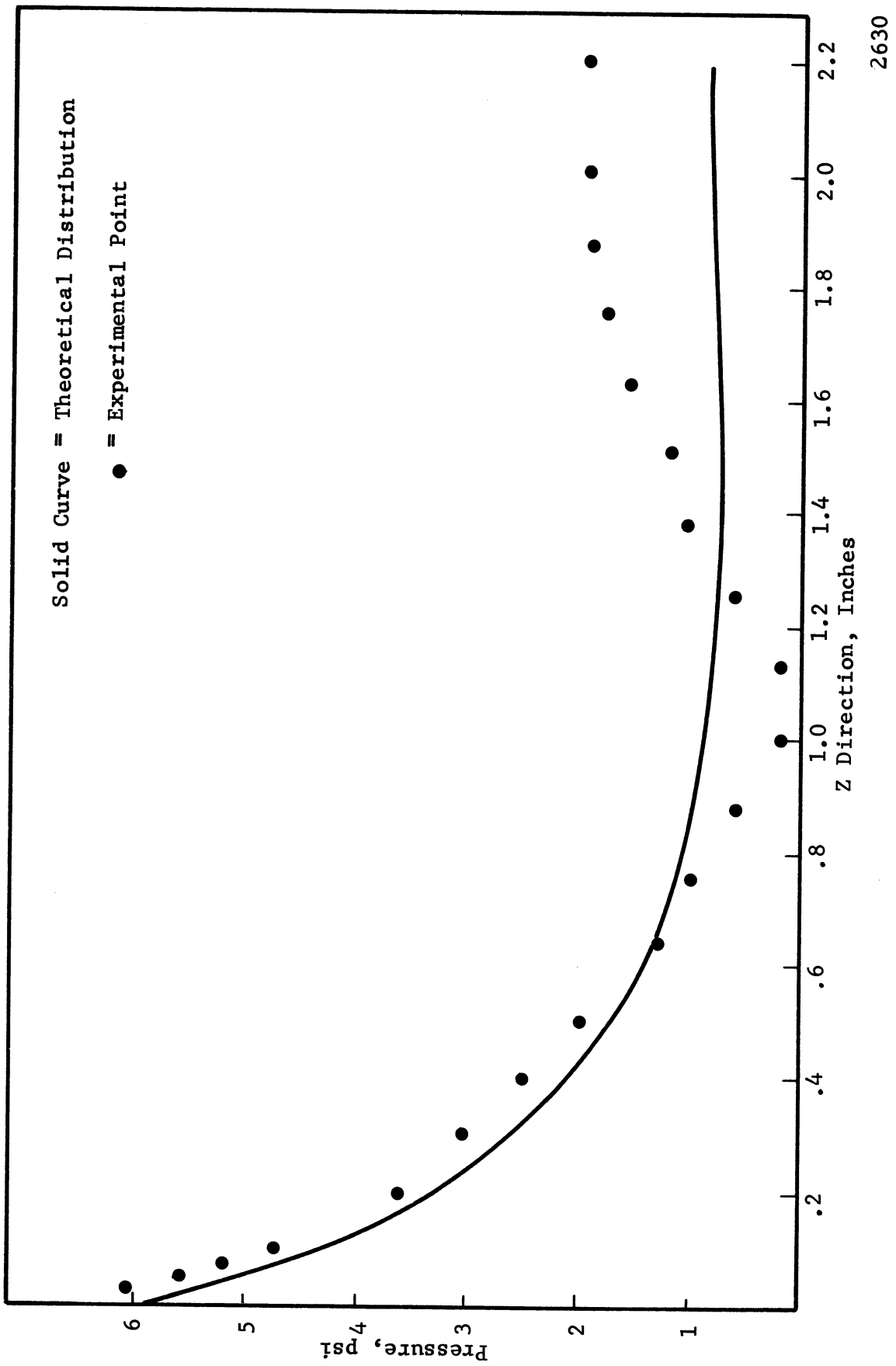


FIGURE 30 (b). PRESSURE DISTRIBUTION IN Z DIRECTION FOR r = .071 INCHES, $\ell$ = 2.22 INCHES, FREQUENCY = 18560 HZ, AND A = 1.50 x $10^{-6}$ INCHES

FIGURE 30 (c). PRESSURE DISTRIBUTION IN Z DIRECTION FOR r = .140 INCHES, $\ell$ = 2.22 INCHES, FREQUENCY = 18560 HZ, AND A = 1.50 x $10^{-6}$ INCHES

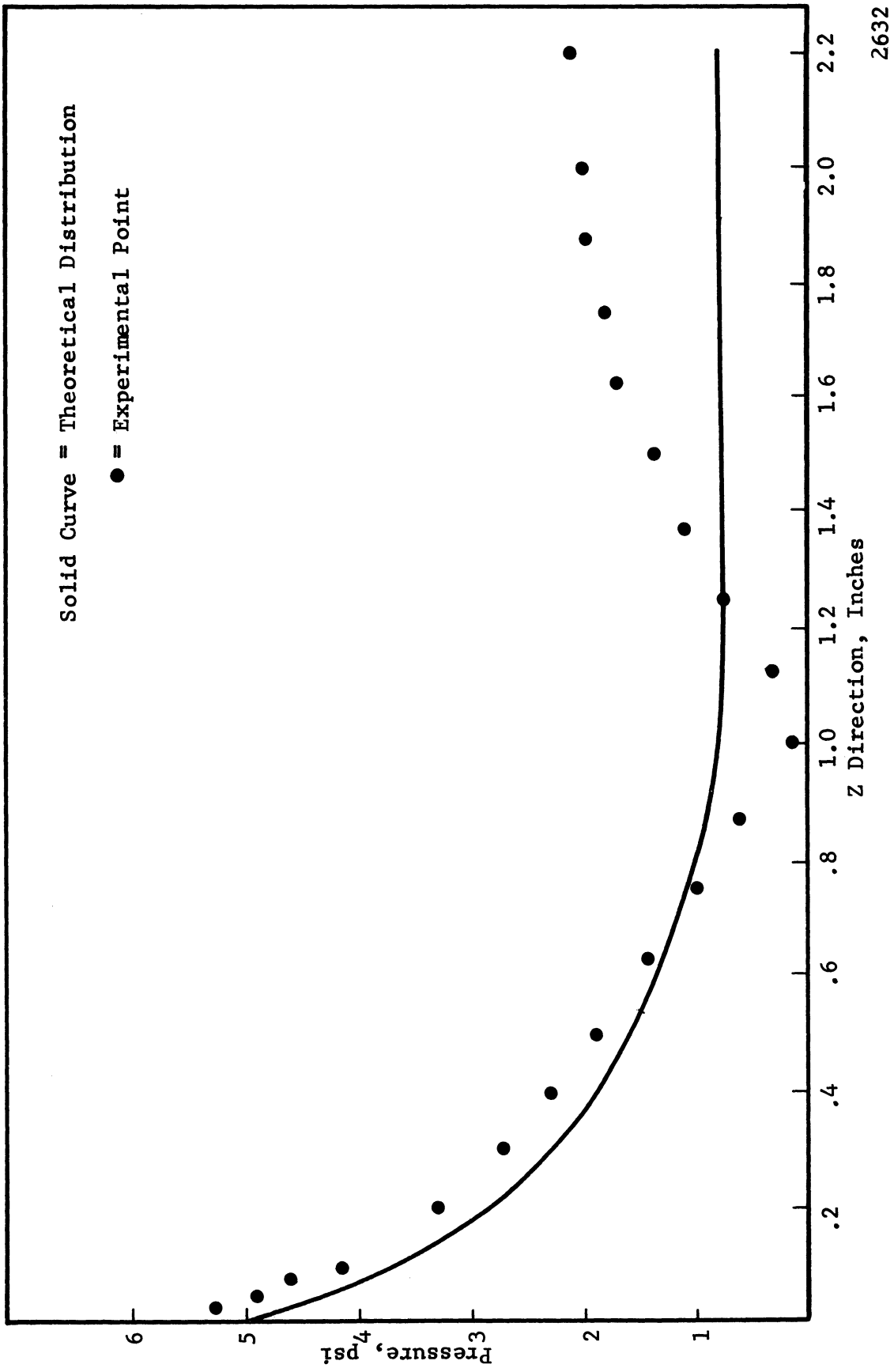


FIGURE 30 (d). PRESSURE DISTRIBUTION IN Z DIRECTION FOR r = .207 INCHES, $\ell$ = 2.22 INCHES, FREQUENCY = 18560 HZ, AND A = 1.50 x $10^{-6}$ INCHES

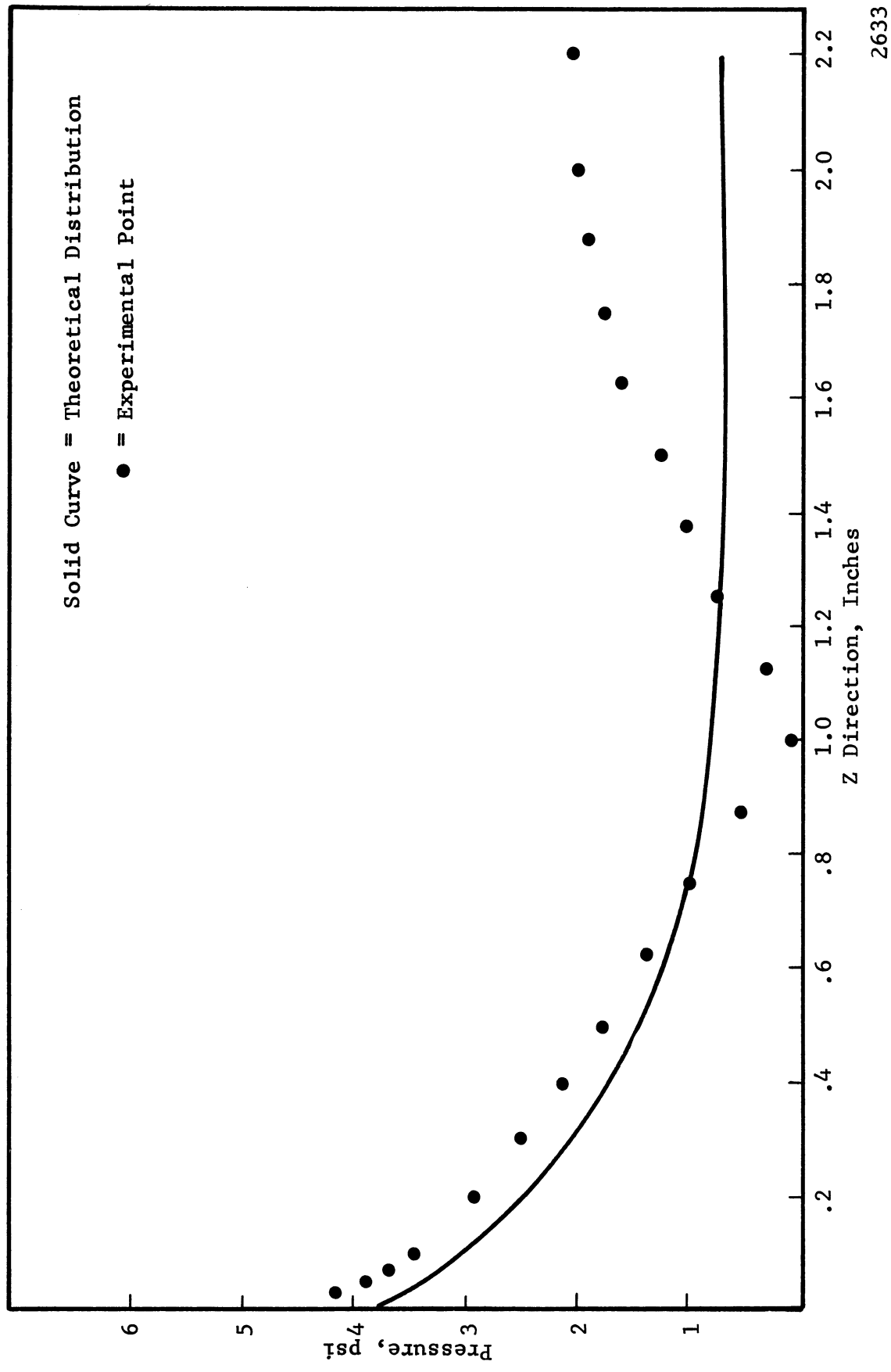


FIGURE 30 (e). PRESSURE DISTRIBUTION IN Z DIRECTION FOR r = .273 INCHES, $\ell$ = 2.22 INCHES, FREQUENCY = 18560 HZ, AND A = 1.50 x $10^{-6}$ INCHES

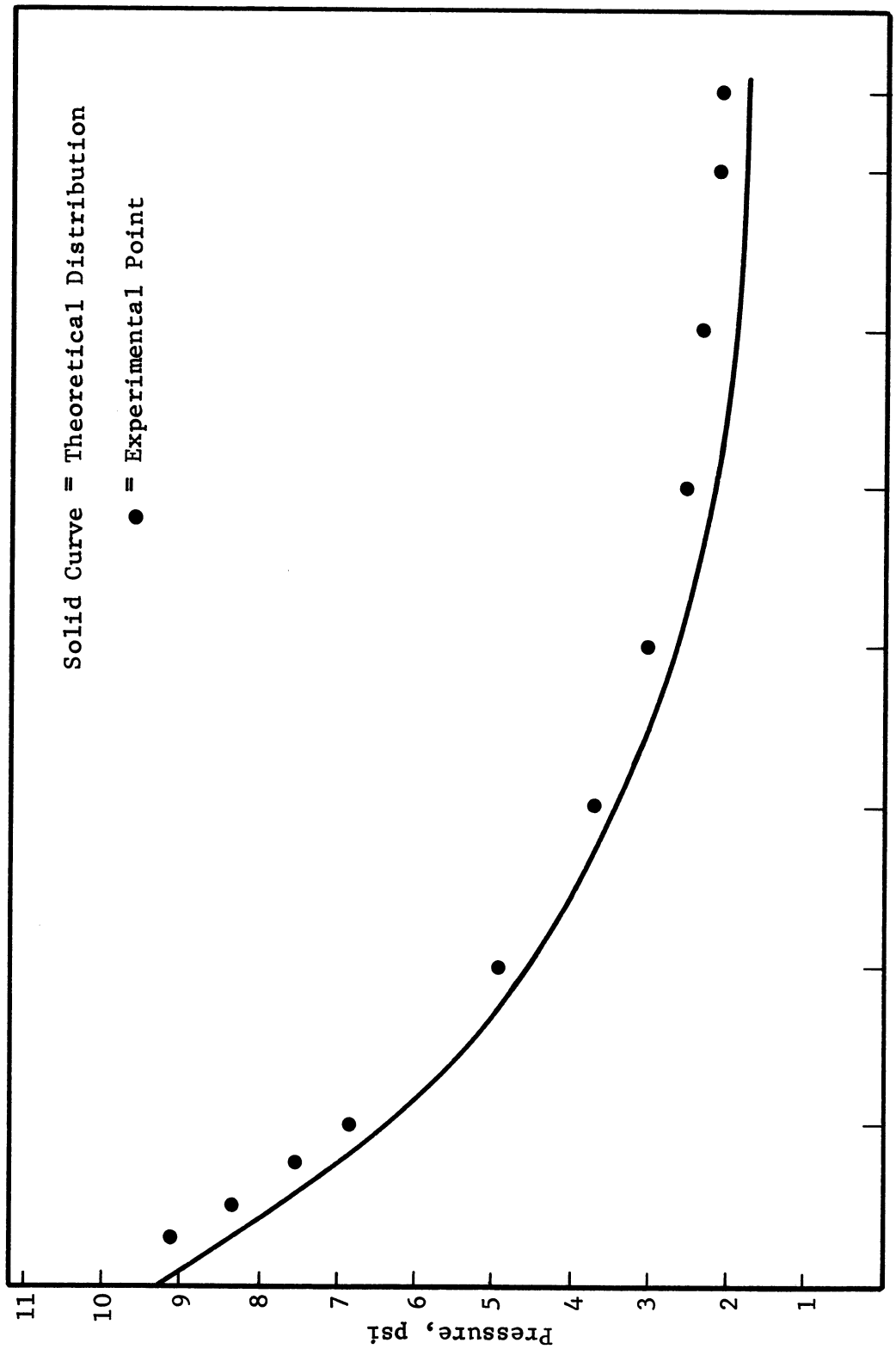


FIGURE 31 (a). PRESSURE DISTRIBUTION IN Z DIRECTION FOR r = 0, $\ell$ = .75 INCHES, FREQUENCY = 14498 HZ, AND A = 4.43 x $10^{-6}$ INCHES

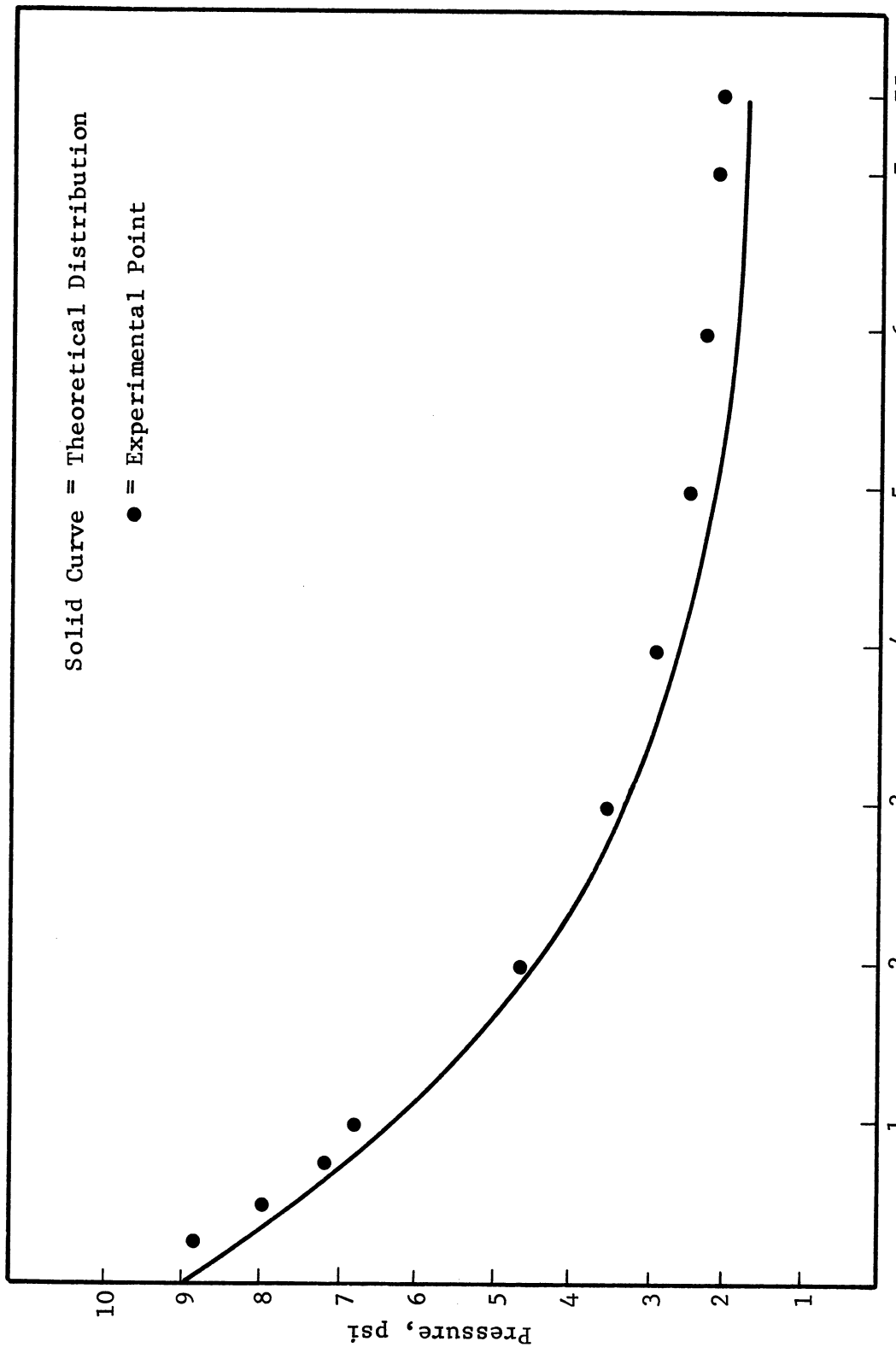


FIGURE 31 (b). PRESSURE DISTRIBUTION IN Z DIRECTION FOR r = .071 INCHES, $\ell$ = .75 INCHES, FREQUENCY = 14498 HZ, AND A = 4.43 x $10^{-6}$ INCHES

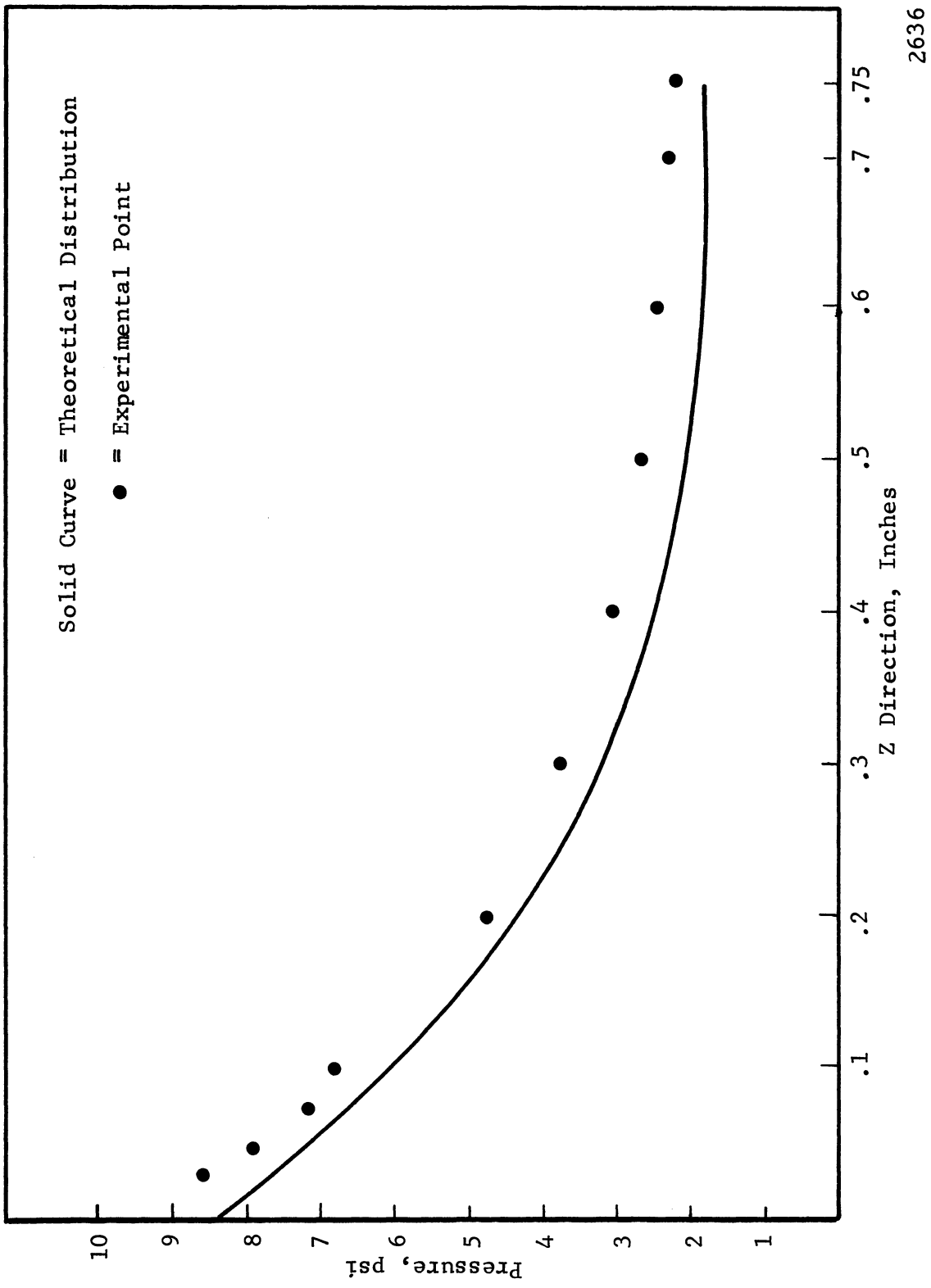


FIGURE 31 (c). PRESSURE DISTRIBUTION IN Z DIRECTION FOR r = .140 INCHES, $\ell$ = .75 INCHES, FREQUENCY = 14498 HZ, AND A = 4.43 x $10^{-6}$ INCHES

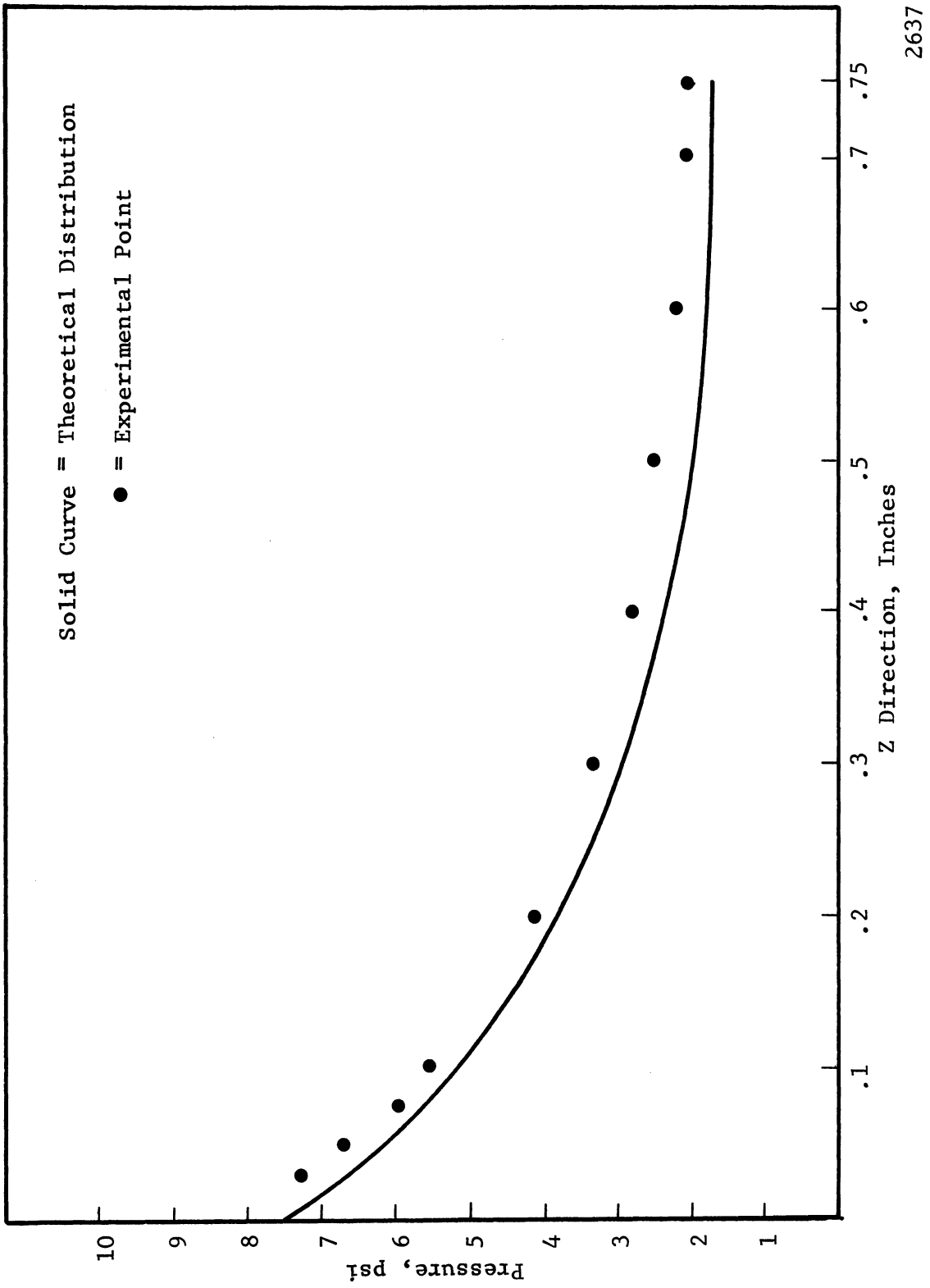


FIGURE 31 (d). PRESSURE DISTRIBUTION IN Z DIRECTION FOR r = .207 INCHES
$\ell$ = .75 INCHES, FREQUENCY = 14498 HZ, AND A = 4.43 x $10^{-6}$ INCHES

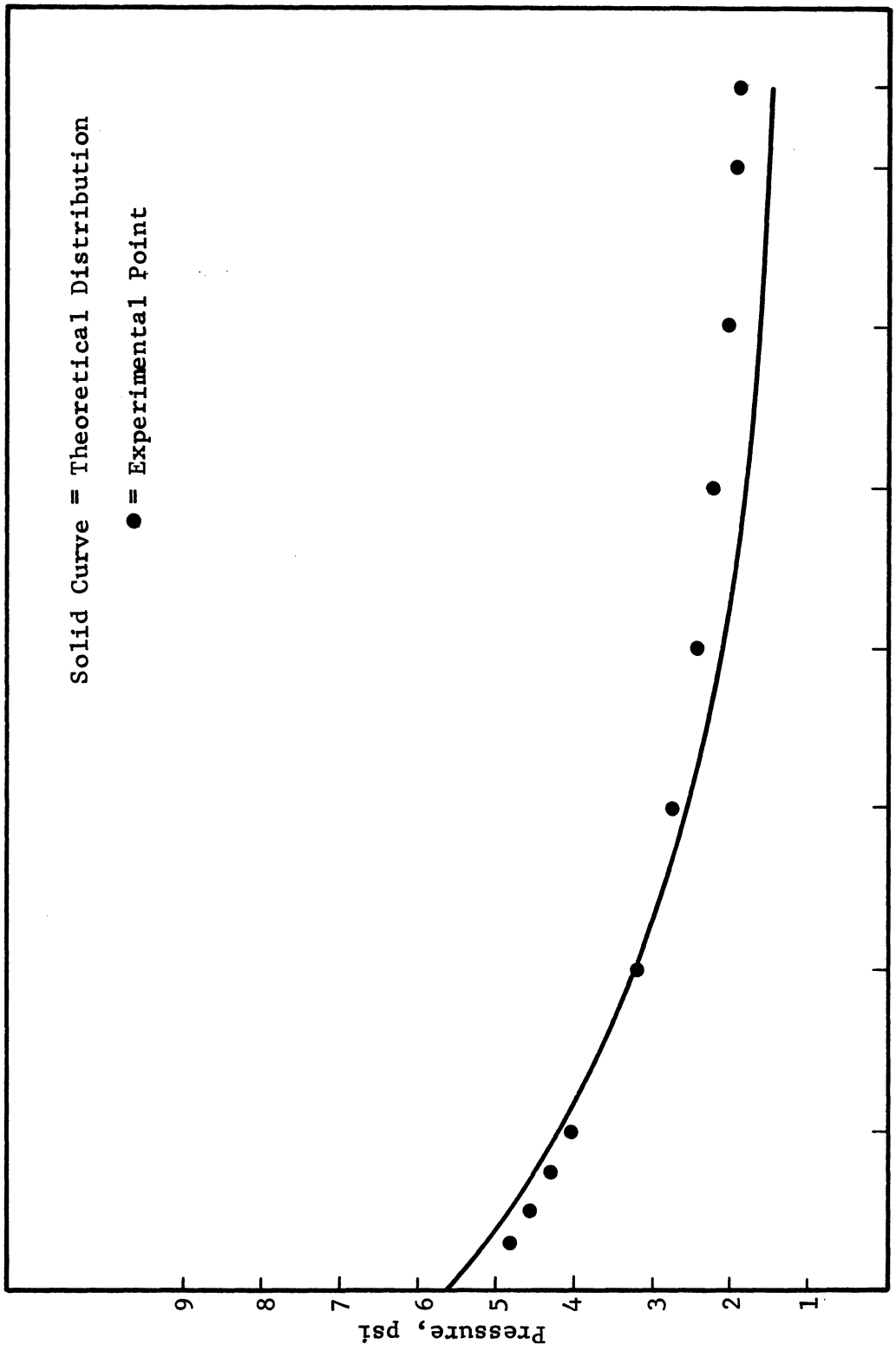


FIGURE 31 (e). PRESSURE DISTRIBUTION IN Z DIRECTION FOR r = .273 INCHES, $\ell$ = .75 INCHES, FREQUENCY = 14498 HZ, AND A = 4.43 x $10^{-6}$ INCHES

G. Conclusion to Chapter III

In order to determine superheat requirements for liquid sodium the maximum changes in pressure produced by the vibrating test specimen must be determined. This maximum change in pressure was found to occur on the surface of the test specimen at the point r = 0 and z = 0. For this point good agreement was obtained between experimentally determined pressure values and theoretically determined values computed using Eq (3.5). For the experimental pressure measurements water was used as the test fluid. In comparing the properties of liquid sodium and water it is found that the densities of the two liquids are approximately the same and that the velocity of sound in liquid sodium is approximately twice the velocity of sound in water.[41]* Since the above two properties are the only test fluid parameters which are included in Eq (3.5), and since the numerical values for the two properties for water and liquid sodium are similar, it seems reasonable that Eq (3.5) can be used to determine pressure changes when using liquid sodium as the test fluid. Also, because zero test fluid viscosity was assumed in the derivation of Eq (3.5) liquid sodium is more appropriate than water as the test fluid since the viscosity of water is approximately three times the viscosity of liquid sodium.[42]*

In view of the above factors it was decided to use Eq (3.5) to determine the maximum changes in pressure produced

---

* Data for liquid sodium was for 500°F.

by the vibrational motion of the test specimen using liquid sodium as the test fluid. Since better overall agreement between theory and experiment was obtained when the length of the vessel was small ( 0.75 inches for the 14.4 kHz horn as compared to 2.22 inches for the 18.5 kHz horn), it was decided that for the measurements using sodium as the test fluid, the length of the cavitation vessel should be relatively short. The determination of the lengths of the cavitation vessel used for the sodium measurements is discussed in Chapter V.

It also appears that because of the good agreement obtained in the pressure field analysis the method of determining test specimen displacement is a reliable one. Therefore, this method was used to determine test specimen displacements for the measurements using liquid sodium as the test fluid.

# CHAPTER IV

## DETERMINATION OF THE ONSET OF CAVITATION

### A. Introduction

In determining the superheat requirements of the test fluid it is necessary to establish the point at which cavitation occurs. It is pointed out in Chapter I that the onset of cavitation can be identified with the onset of nucleate boiling in a liquid. The concepts involved in determining the onset of cavitation in a liquid have been established by many investigators; these concepts are incorporated in the present study and are used in determine the onset of cavitation, or nucleate boiling, in the test fluid.

### B. Selection of Method for Determining Onset of Cavitation

#### 1. Effects Produced by Cavitation

Cavitation in a liquid produces several effects which can be used in the study of cavitation phenomena. Among these effects are erosion of solids, chemical reactions, luminescence, and noise.

Probably the most familiar effect of cavitation is the erosion of solids. The bubble collapse associated with cavitation causes either a shock wave (which is transmitted through the liquid) and/or a high velocity liquid jet which is

produced by the asymmetric bubble collapse. If the bubble collapse occurs sufficiently close to a solid surface the shock wave and/or the liquid jet may have sufficient energy to erode the surface.

Ultrasonically induced cavitation in certain liquids has the effect of promoting chemical reactions within these liquids. One possible source of these chemical reactions may be electrolytic action brought about by the appearance of unequal charge distribution over the bubble surface.[43] Another possible source of chemical reactions may be the extremely high temperatures which may be produced inside a bubble during its collapse phase.[44] One example where above reactions are important is the electrolysis of water. The electrolytic action separates the $H_2O$ molecule into the $H^+$ and $OH^-$ ions. The $OH^-$ ions combine to form $H_2O_2$, and a measure of the amount of $H_2O_2$ produced can then be related to the cavitation activity.

Cavitation may be accompanied by emission of light. One theory, as to the source of this light, is that during the collapse of the bubble the temperature of the vapor or gas within the bubble rises to several thousand degrees which causes it to become incandescent.[45]

Associated with bubbles growing and collapsing in a sound field are pressure pulses produced by the motion of the bubble surfaces. These pressure pulses are transmitted through the liquid as sound waves; the result of these sound waves produced by the motion of many bubbles is referred to as

cavitation noise. The frequency spectrum of this cavitation noise has been studied by many investigators.[46, 47, 48] It has been observed that the noise spectrum produced by ultrasonically induced cavitation in water consists of a continuum of noise pulses with the majority of these pulses occuring between 100 and 300 kHz.

## 2. Methods Used to Determine the Onset of Cavitation

In reviewing the above effects produced by cavitation it appears that the erosion effect and the chemical reactions cannot be used to determine the onset of cavitation since these effects are not generally observed until cavitation has occured for a period of time. On the other hand simple sighting, luminescence, and noise can be used to determine the onset of cavitation, since these effects are produced during the same pressure cycle which produces the cavitation itself.

One of the most widely used methods for determining the onset of cavitation, where a transparent vessel and liquid exist, is to visually observe the formation of cavitation bubbles in a liquid.[49, 50, 51] The onset of cavitation is defined as the point at which bubbles are visibly detected as the power to the driving crystals is increased, and the cessation of cavitation is defined as the point at which bubbles can no longer be visibly detected as the power to the system is decreased.

Another widely used method for determining the onset of cavitation is to detect the noise signal which is associated with cavitation activity.[52, 53, 54] One immediate advantage

of this system is that the container and the fluid need not be transparent. The technique used by Garcia et al[55] in this laboratory consists of using a stainless steel rod as a detector, which transmitts the cavitation noise signal from a stainless steel venturi section in a mercury loop to a piezoelectric crystal which is attached to one end of the steel rod. The output voltage signal from the piezoelectric crystal is observed with an oscilloscope. The onset and cessation of cavitation are associated with the appearance and disappearance of the noise signal produced by the motion of the cavitation bubbles.

There are other less widely used methods for determining the onset of cavitation. For example, Mikhailov and Shutilov[56] used a liquid container with a capillary tube to indicate the level of the liquid. The onset of cavitation was then associated with an increase in the liquid level in the capillary tube. Strasberg[57] determined the onset of cavitation by observing the absorption of sound energy by the cavitation bubbles.

It was mentioned above that luminescence could be used to determine the onset of cavitation. However, no mention was found in the literature that this method has been used to determine the onset of cavitation in the liquid.

### 3. Selection of a System for Determining the Onset of Cavitation

In reviewing the above methods for determining the onset of cavitation it becomes apparent that the method which lends itself most readily to the sodium superheat experiment

is the noise detection system. In working with liquid sodium at high temperatures visual determination of cavitation is not possible and the other methods of determining the onset of cavitation as mentioned above are not practical since they would require extensive modification of the facility.

In utilizing the noise detection system for determining the onset of cavitation in liquid sodium, a stainless steel acoustic probe was developed for detecting the cavitation noise signal. The following section of this chapter discusses the construction and evaluation of the acoustic probe.

## C. Development of the Acoustic Probe

### 1. Construction of the Acoustic Probe

The acoustic probe which was used to detect the cavitation noise signal consists of a solid stainless steel rod whose length was selected to filter the driving frequency of the transducer horn assembly, and to amplify the noise signal being produced by the cavitation bubbles. The resonant frequency of a rod free at both ends is given by[58]

$$f = \frac{nc}{2\ell} \qquad (4.1)$$

where

$c$ = velocity of sound in the rod

$\ell$ = length of the rod

$n$ = 1, 2, 3, . . .

Eq (4.1) defines the frequencies whose signals are amplified while travelling through the rod in the axial direction. It was pointed out earlier in this chapter that the majority

of the noise pulses produced by ultrasonically induced cavitation bubbles occur in a frequency range of 100 to 300 kHz. Selecting a frequency of 200 kHz as the representative noise frequency and using Eq (4.1) to determine an appropriate probe length to amplify the noise signals it is found that

$$\ell\Big|_{f=200\,kHz} = 0.48\,n\text{, INCHES} \qquad (4.2)$$

where c = 16,000 ft/sec was used for stainless steel. As shown in Fig 9 in Chapter II the acoustic probe passes through the vessel top plate and baffle plate so that the tip of the acoustic probe is immersed in the test fluid. The probe is secured to the vessel top plate with a Conax packing gland. Using this method of installing the probe, a suitable working length for the probe appeared to be approximately 12 inches. From Eq (4.2) using n = 25, it is found that

$$\ell\Big|_{f=200\,kHz} = (0.48)(25) = 12 \text{ INCHES}$$

Thus for an acoustic probe length of 12 inches the noise signals with frequencies of approximately 200 kHz will be amplified when transmitted through the probe.

The length of the acoustic probe was also chosen so that the response of the probe to the pressure field produced by the transducer horn assembly would be attenuated. For an exponential horn having a resonant frequency of 18.5 kHz it is found from Eq (4.1) that

$$\ell\Big|_{f=18.5\,kHz} = 5.18\,n\text{, INCHES} \qquad (4.3)$$

From Eq (4.3) it can be seen that a length of 12 inches is approximately midway between the resonant lengths for n = 2 and n = 3. Therefore a length of 12 inches will attenuate the exitation of the probe at a frequency of 18.5 kHz. A diameter of 3/16 inches was selected for the acoustic probe since a small diameter is necessary to minimize the heat transfer through the probe when operating with test fluid temperatures up to 1500°F.

In order to detect the noise signal transmitted through the acoustic probe, a barium titanate piezoelectric crystal was cemented to the top end of the stainless steel rod (Fig 32). The crystal is cylindrical in shape and has a diameter of 0.125 inches, a thickness of 0.051 inches, and a resonant frequency of approximately 2000 kHz. The crystal was polarized in the axial direction and its top and bottom surfaces silver coated to provide for electrical contact. The crystal was cemented to the rod using a conducting epoxy (Eccobond Solder 57C) so that the rod would serve as one electrode (ground) for the crystal. For the other electrode, a copper contactor was spring-loaded against the top surface of the crystal. One end of an electrical wire was soldered to the copper contactor and the other end of this wire was soldered to the center terminal of a coaxial cable connector. The coaxial cable connector was attached to the top of the acoustic probe by means of two set screws. In positioning the coaxial connector on the probe, the spring holding the copper contactor against the crystal is compressed so that electrical

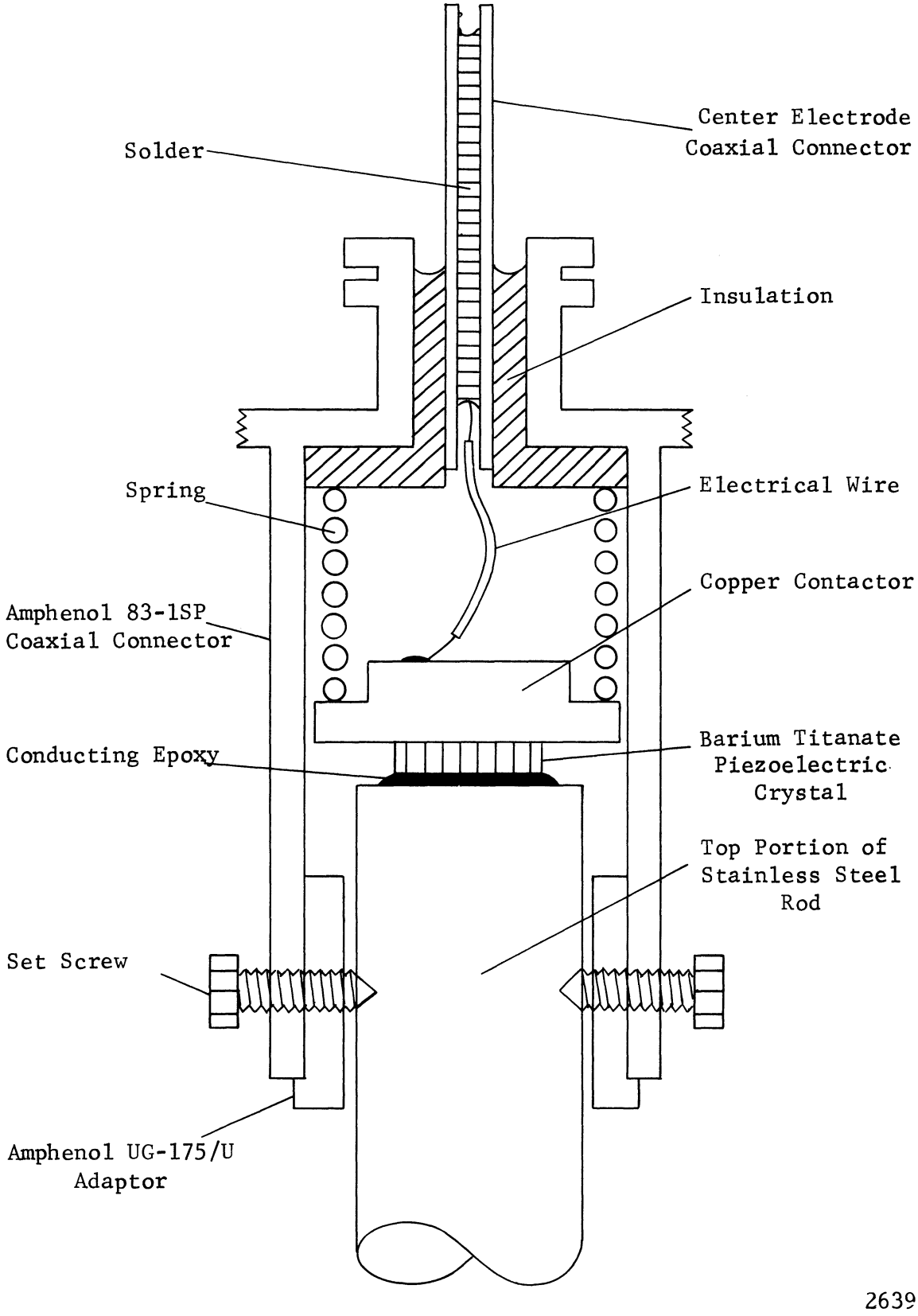


FIGURE 32. SCHEMATIC CROSS SECTIONAL VIEW OF THE CRYSTAL ASSEMBLY FOR THE ACOUSTIC PROBE

contact is guaranteed between the contactor and the top surface of the crystal. Fig 32 is a schematic cross-sectional view of the top of the acoustic probe showing the top of the rod, barium titanate crystal, copper contactor, spring, and coaxial cable connector. It should be noted that the coaxial cable connector not only provides a suitable housing for the spring and contactor but also provides a desirable shield against unwanted noise signals which may be present in the laboratory. A coaxial cable is attached to the acoustic probe and to an oscilloscope so that the output voltage signal from the probe can be visually monitored.

## 2. Experimental Evaluation of the Acoustic Probe

The experimental arrangement shown in Fig 33 was used to determine the effectiveness of the acoustic probe in signalling the onset of nucleate boiling in water. A glass beaker served as the test fluid container so that visual observations of the onset of cavitation could be correlated with the noise signals transmitted through the acoustic probe and displayed on the oscilloscope. The performance tests for the acoustic probe were conducted with the probe secured to the vessel top plate with a Conax packing gland; this arrangement was also used during the measurements in liquid sodium. Any significant damping of the noise signal transmission caused by the packing gland during the measurements in liquid sodium should also occur during the performance tests with water as the test fluid.

The procedure followed for determining the onset of

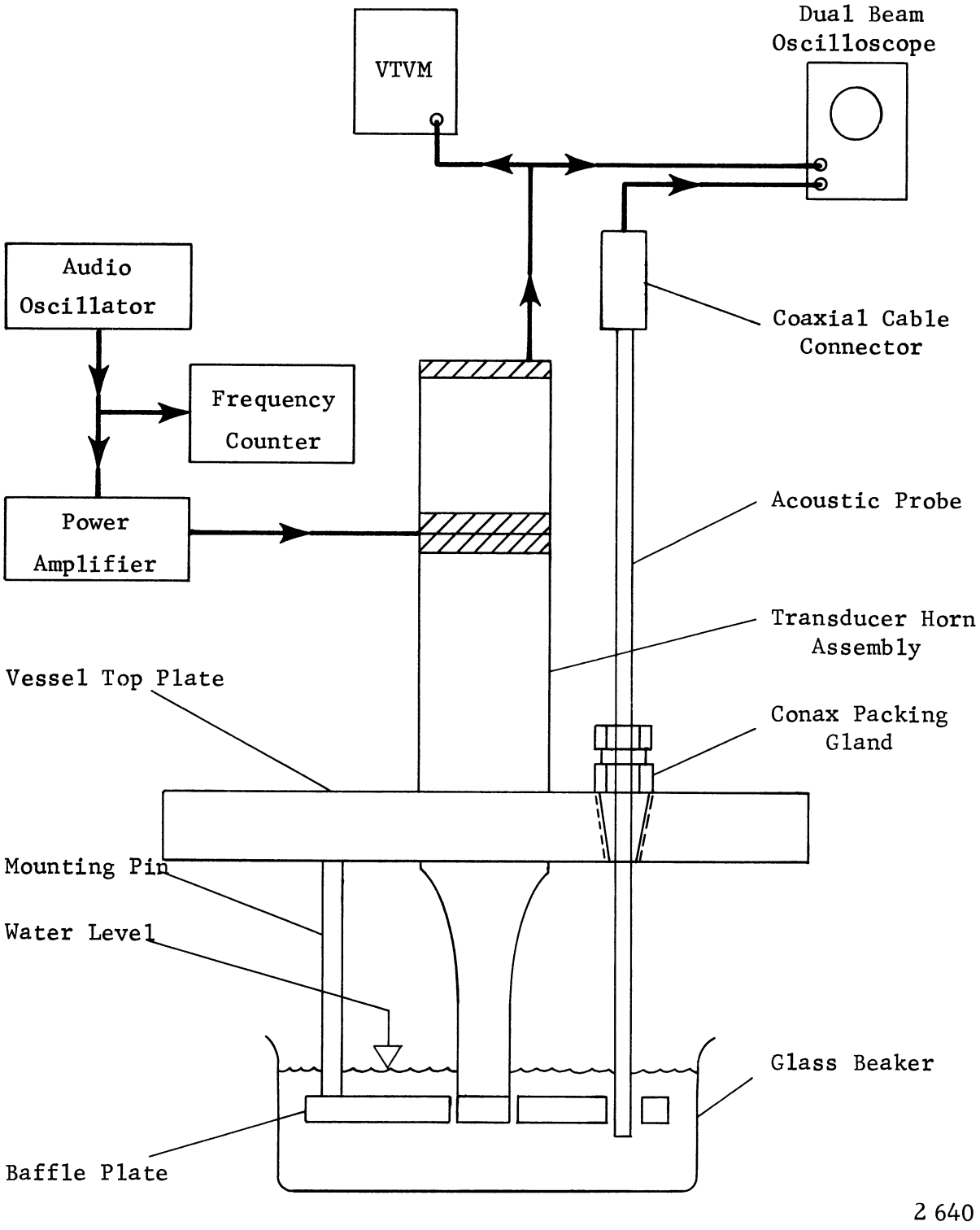


FIGURE 33. EXPERIMENTAL ARRANGEMENT TO DETERMINE PERFORMANCE OF ACOUSTIC PROBE

cavitation in the test fluid was to slowly and continously increase the input power to the transducer horn assembly until the onset of cavitation was reached. After cavitation was established the power to the transducer horn assembly was slowly reduced until cavitation ceased. The power to the transducer horn assembly was then reduced to zero. The onset and cessation of cavitation* were determined in several different ways. The primary method of determining the onset and cessation of cavitation was the noise signal detected by the acoustic probe. Fig 34 (a) is a photograph of the output voltage waveforms from the acoustic probe and the counterweight crystal just prior to the onset of cavitation. Fig 34 (b) is a photograph of the waveforms at the onset of cavitation. From the two photographs it can be seen that there is a marked difference in the two acoustic probe waveforms. The onset of cavitation is characterized by the sudden appearance of a noise signal which is superimposed on a low amplitude voltage signal possessing the same frequency as the counterweight voltage signal. The sudden appearance of this noise signal can be observed in the photographs in Fig 34 by noting that the amplitude of the counterweight crystal voltage is approximately the same in both photographs. In other words it required virtually no change in test specimen displacement to initiate the onset of cavitation in the test fluid. The cessation of cavitation was characterized by the same type of behavior in

---

* Sometimes called "incidence" and "desinence" in cavitation literature.

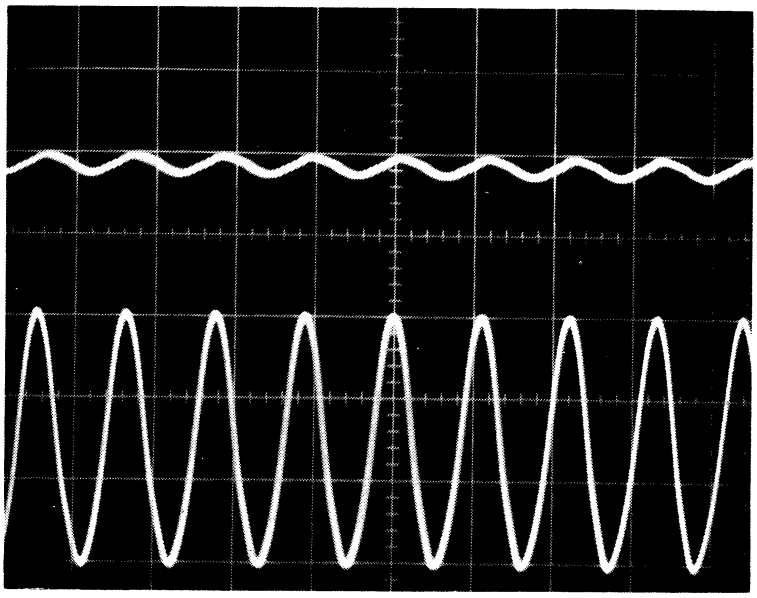

ACOUSTIC PROBE
VOLTAGE WAVEFORM

5 Millivolts/cm
50 Microsec/cm

COUNTERWEIGHT
CRYSTAL VOLTAGE
WAVEFORM

10 Volts/cm
50 Microsec/cm

FIGURE 34 (a). PHOTOGRAPH OF TYPICAL WAVEFORMS OBSERVED JUST PRIOR TO THE ONSET OF CAVITATION

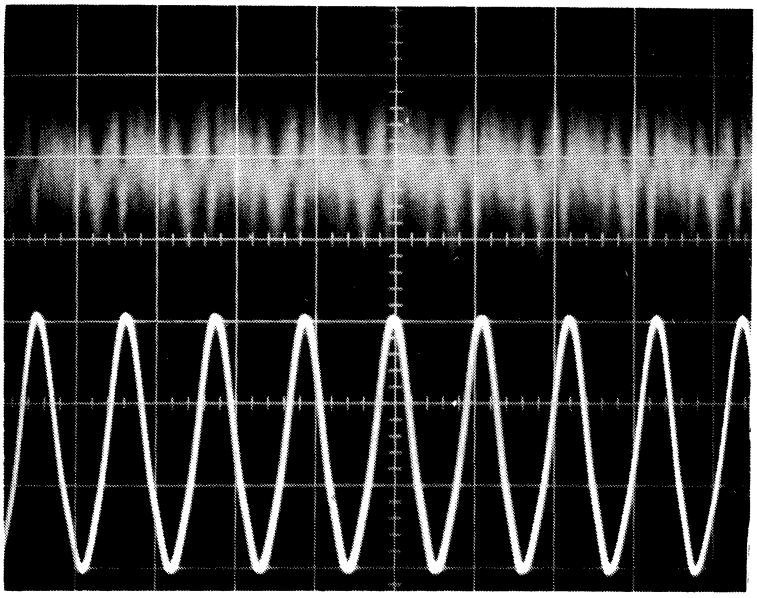

ACOUSTIC PROBE
VOLTAGE WAVEFORM

5 Millivolts/cm
50 Microsec/cm

COUNTERWEIGHT
CRYSTAL VOLTAGE
WAVEFORM

10 Volts/cm
50 Microsec/cm

2641

FIGURE 34 (b). PHOTOGRAPH OF TYPICAL WAVEFORMS OBSERVED AT THE ONSET OF CAVITATION

the acoustic probe output voltage. At the cessation of cavitation there was a sudden disappearance of the noise signal. It was further noted that the onset of cavitation caused a more pronounced signal than that which characterized the cessation of cavitation. However, both the onset and cessation of cavitation were easily noted by the appearance and disappearance of the cavitation noise signal.

When the onset of cavitation is observed visually, a sudden formation of cavitation bubbles on the bottom surface of the test specimen is seen. Generally at the onset of cavitation these bubbles suddenly became visible and covered approximately 30 to 50 per cent of the surface area of the test specimen and were located in the center portion of this surface. As the power to the transducer horn assembly was reduced the surface area covered by the cavitation bubbles decreased, until just prior to the cessation of cavitation a relatively small number of cavitation bubbles could be observed at the center of the bottom surface of the test specimen. The initial appearance of cavitation bubbles at the center of the bottom surface of the test specimen was to be expected since in Chapter III it was determined that maximum changes in pressure occur at the center of the test specimen, and the onset and cessation of cavitation will occur at the point of maximum changes in pressure.

A third phenomenon noted at the onset of cavitation was the audible noise produced by the cavitation bubbles. This noise, characterized as a hissing sound, occured at the

same time that the bubbles were visually observed. However, as the power to the transducer horn assembly was reduced the cavitation bubbles were generally still visible after the audible noise had disappeared.

In reviewing the above performance it appeared that the acoustic probe provides a good indication of the onset and cessation of cavitation in the test fluid. The onset of cavitation as determined by the acoustic probe was verified by visual observation of the cavitation bubbles, and by audible detection of the noise signal. The cessation of cavitation as determined by the acoustic probe was verified by the visual observation of the disappearance of the cavitation bubbles. The audible noise signal was not as sensitive to the cessation of cavitation in that just prior to the cessation of cavitation no audible noise was detected even though a few bubbles still remained at the center of the test specimen. The acoustic probe continued to transmit a noise signal until these bubbles disappeared.

In order to determine the ability of the acoustic probe to consistantly indicate the onset of cavitation at approximately the same test specimen displacement and to indicate the cessation of cavitation at the same test specimen displacement, i. e., to measure the repeatability of this method, several measurements of the onset and cessation of cavitation using the same test fluid were made. A stainless steel test specimen with a smooth bottom surface was attached to the exponential horn. Distilled water was used as the

test fluid. It is pointed out in Chapter I that undissolved gas in the test fluid affects the change in pressure necessary to produce cavitation. Thus if the distilled water contains undissolved gas, the onset and cessation of cavitation will be affected by the amount of gas in the distilled water. Therefore, to reduce the entrained gas to at least a relatively low value, the distilled water sample was degassed by shaking the sample under vacuum for approximately 30 minutes or until all visible gas bubbles disappeared. The sample was then exposed to the atmosphere for 24 hours, at which time, presumably, the rate at which gas being absorbed from the atmosphere by the sample had reached a relatively low level. Thus the amount of gas absorbed during the tests was small so that the gas concentration remained fairly constant during the measurements of the onset and cessation of cavitation. Table 4 lists the counterweight crystal output voltage (RMS volts) at the onset and cessation of cavitation for fifty observations using the acoustic probe to determine the onset and cessation of cavitation. The photographs shown in Fig 34 were taken during these observations. The average value for the onset of cavitation was 13.16 volts with a standard deviation of 2.74 volts (20.8 per cent). The average value for the cessation of cavitation was 5.55 volts with a standard deviation of 0.08 volts (1.4 per cent). It is noted that considerably more power is required to initiate cavitation than to sustain cavitation after it has been established in the fluid. This phenomenon has been observed by other investigators.[50, 59] The mechanisms

TABLE 4

COUNTERWEIGHT CRYSTAL VOLTAGE AT THE ONSET AND CESSATION OF CAVITATION IN PARTIALLY DEGASSED DISTILLED WATER

| Onset of Cavitation(RMS volts) | Cessation of Cavitation(RMS volts) |
|---|---|
| 14.0 | 5.6 |
| 11.5 | 5.6 |
| 10.2 | 5.6 |
| 11.0 | 5.6 |
| 17.0 | 5.6 |
| 10.5 | 5.6 |
| 12.5 | 5.6 |
| 10.5 | 5.7 |
| 15.5 | 5.5 |
| 18.5 | 5.3 |
| 16.5 | 5.6 |
| 15.0 | 5.5 |
| 15.5 | 5.6 |
| 15.5 | 5.5 |
| 17.5 | 5.5 |
| 15.5 | 5.6 |
| 18.0 | 5.5 |
| 10.5 | 5.6 |
| 8.0 | 5.6 |
| 12.5 | 5.5 |
| 12.0 | 5.4 |
| 14.5 | 5.6 |
| 12.0 | 5.5 |
| 9.0 | 5.5 |
| 13.0 | 5.6 |
| 10.5 | 5.6 |
| 15.0 | 5.4 |
| 11.0 | 5.7 |
| 17.0 | 5.6 |
| 11.0 | 5.5 |
| 8.8 | 5.6 |
| 11.0 | 5.6 |
| 14.5 | 5.6 |
| 8.5 | 5.5 |
| 17.0 | 5.6 |
| 14.5 | 5.5 |
| 12.5 | 5.6 |
| 15.0 | 5.6 |
| 16.5 | 5.6 |
| 14.5 | 5.5 |
| 14.0 | 5.6 |
| 14.5 | 5.6 |
| 8.0 | 5.6 |
| 13.5 | 5.6 |
| 11.0 | 5.6 |
| 10.5 | 5.4 |
| 13.0 | 5.5 |
| 14.5 | 5.5 |
| 12.5 | 5.6 |
| 13.0 | 5.5 |

involved in producing this obvious nonlinear fluid system may be due in part to going from a single phase system to a two phase system and then returning to a single phase system; they will not be investigated further in this study. The large per cent standard deviation obtained in the values for the onset of cavitation is consistant with the scatter in the onset of cavitation data reported in the literature.[50, 59] However, from Table 4 it can be seen that the performance of the acoustic probe is reasonably consistant in determining the onset and cessation of cavitation.

Another observation can be made from the data in Table 4. If the cavitation damage produced by the collapsing cavitation bubbles on the bottom surface of the test specimen were sufficient to affect the onset and cessation of cavitation this would be indicated by a continual change in the values for the counterweight crystal voltage at the onset and cessation of cavitation. From Table 4 it can be seen that there is no such trend in the counterweight crystal voltages indicating that after 50 observations the cavitation damage produced on the bottom surface of the test specimen was not sufficient to affect the onset and cessation of cavitation. Visual inspection of the test specimen after the 50 measurements indicated no apparent cavitation damage.

As indicated earlier in this chapter the length of the acoustic probe was chosen to attenuate the response of the probe to the pressure field produced by the transducer horn assembly. It was initially felt that it would be necessary

to provide four probes of different lengths in order to achieve the necessary attenuation when operating with the four different transducer horn assemblies. However, subsequent onset and cessation measurements using water as the test fluid and using the four different transducer horn assemblies with the same 12 inch acoustic probe indicated that there was sufficient attenuation at all frequencies so that the onset and cessation of cavitation was easily determined.

D. Conclusions on Chapter IV

From the above experimental evaluation of the acoustic probe it was decided to use it in order to determine the onset and cessation of cavitation for the measurements using liquid sodium as the test fluid. Because the onset and cessation were not affected by the very slight cavitation damage which was produced on the bottom surface of the test specimen in these tests, it was felt that many observations of the onset and cessation of cavitation could be made at various temperatures in liquid sodium using the same test specimen. It was pointed out in Chapter III that the properties of water and liquid sodium with regard to sound transmission are similar. Thus it was felt that the performance of the acoustic probe in sodium would be similar to its performance in water. Since the attenuation of the response of the probe (to the pressure field produced by the four different transducer horn assemblies) was sufficient to easily determine the onset and cessation at the four different frequencies, the same 12 inch acoustic probe was used for all measurements in liquid sodium.

# CHAPTER V

# EXPERIMENTAL INVESTIGATIONS IN LIQUID SODIUM

## A. Introduction

The present chapter discusses the experimental investigations using liquid sodium as the test fluid. The onset and cessation of cavitation were obtained in liquid sodium at temperatures up to 1500°F in a frequency range of approximately 14 to 25 kHz. The following sections of this chapter discuss the experimental procedures used and the results obtained in determining the onset and cessation of cavitation in liquid sodium.

## B. Experimental Equipment

The high temperature ultrasonic vibratory facility as described in Chapter II was utilized in determining the onset and cessation of cavitation in liquid sodium. However, one additional modification was incorporated into the facility. It is pointed out in Chapter III that the theoretical expression describing the pressure field produced by the vibrational motion of the tip of the transducer horn assembly is valid only at conditions far removed from any resonant condition inside the cavitation vessel. In order to determine the proper length of the cavitation vessel the curves of frequency versus

its effective length (distance between the bottom surface of the test specimen and the bottom of the cavitation vessel), $\ell$, for the various resonant modes using liquid sodium as the test fluid are plotted in Fig 35. The shaded area of each curve takes into account the changes in the velocity of sound in liquid sodium for changes in temperature ranging from 500 to 1500°F. It was determined in Chapter III that good agreement between theoretical and experimental values for the pressure field was obtained for a small value of $\ell$. The distance between the vessel top plate and the bottom of the cavitation is 5.25 inches. Table 3 of Chapter II lists the dimensions of the four exponential horns. It can be determined from this and the vessel dimensions, that with a test specimen of thickness 0.25 inches attached to the exponential horn, $\ell$ is equal to 0.75 inches for the 14 kHz exponential horn. From Fig 35 it can be seen that this point is far removed from any resonant condition. However, for the 20 kHz exponential horn $\ell$ becomes 2.23 inches and reference to Fig 35 indicates that this point will be affected by the $f_{001}$ resonant mode which is the first longitudinal mode. In order to reduce $\ell$ for the 20 kHz exponential horn to a relatively small value, a solid stainless steel spacer was placed in the bottom of the cavitation vessel. The spacer is cylindrical in shape with a 3.38 inch diameter and a thickness of 1.50 inches. The spacer was secured to the bottom of the vessel by means of three bolts which pass through the spacer and are threaded into the vessel bottom. The head of each bolt is countersunk

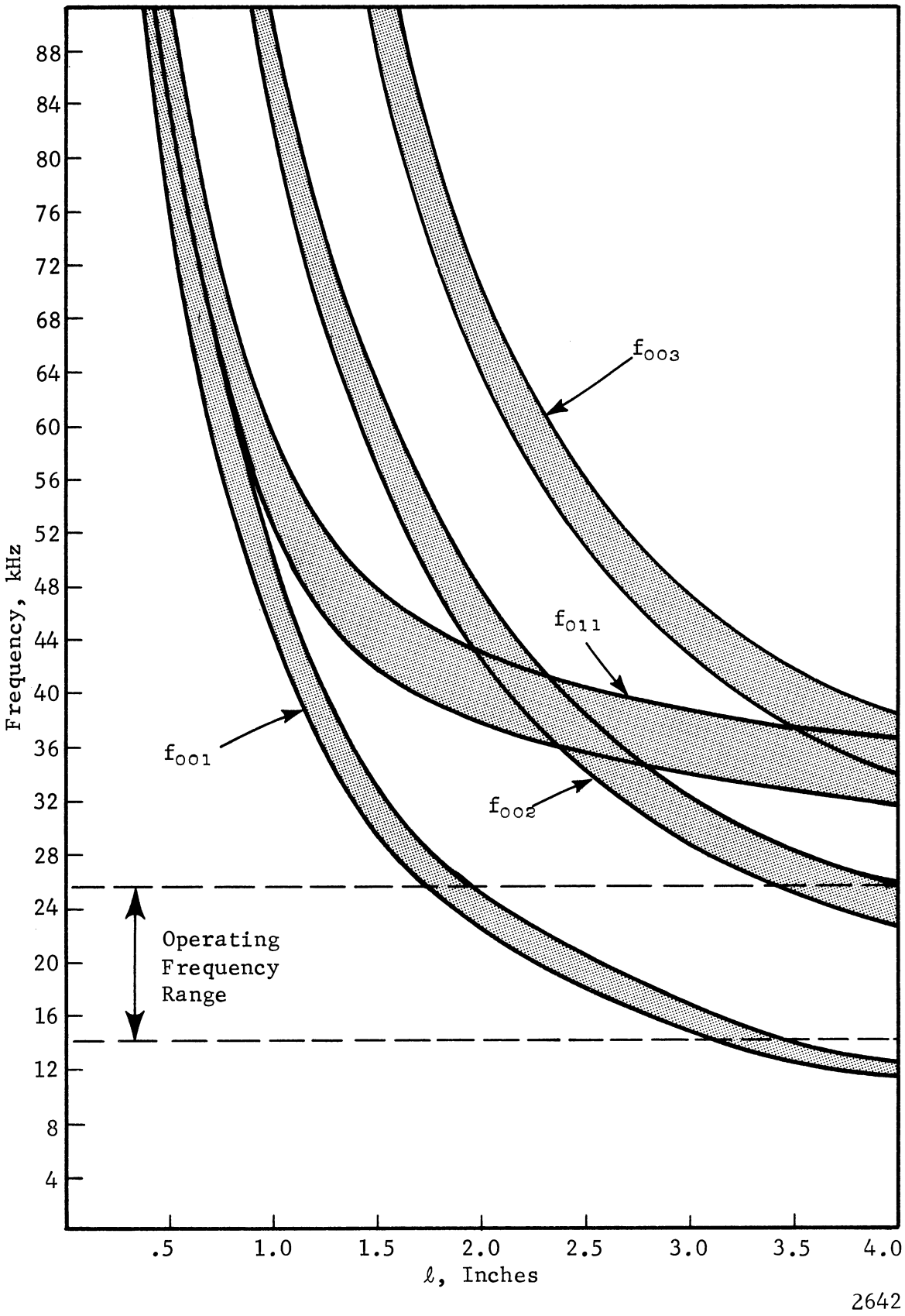


FIGURE 35. CURVES OF RESONANT FREQUENCY FOR VARIOUS MODES OF VIBRATION USING LIQUID SODIUM AS TEST FLUID

so that the top surface of the spacer is smooth. With the spacer in place $\ell$ for the 20 kHz horn becomes 0.73 inches which is far removed from any resonant mode. For the 22 kHz exponential horn a second stainless steel spacer with a thickness of 0.50 inches was bolted to the first spacer which resulted in a value for $\ell$ of 0.62 inches. Reference to Fig 35 indicates that this point is not affected by the resonant modes of the vessel. A third spacer of thickness 0.38 inches was added to the first two spacers to provide an $\ell$ value of 0.56 inches for the 25 kHz exponential horn. The combined thickness of the three spacers was 2.75 inches.

The use of spacers to change the effective length of the cavitation vessel provided a simple means of maintaining a small value of $\ell$ for the four exponential horns. The addition of the spacers did not affect the boundary conditions used in Chapter III since these spacers provided the same rigid boundary to the incident sound waves as the steel bottom. It is pointed out in Chapter III that for a water-steel interface, the velocity transfer to the steel is only 6 per cent of the incident wave velocity. For the sodium-steel interface approximately 12 per cent of the incident wave velocity is transferred to the steel. It is felt that because of the relatively small velocity transfer to the steel, the sodium-steel interface using the stainless steel spacers can be treated as a rigid boundary.

## C. Description of Test Specimens Used in Liquid Sodium

The test specimens as shown in Fig 8 of Chapter II

used for the measurements in liquid sodium were fabricated from 304 stainless steel. The bottom surfaces of these specimens were machined in a lathe to a smooth finish. Using a General Electric surface roughness gauge, it was estimated that the average roughness (average deviation from a centerline on a profile contour of the surface) of the bottom surface was 32 microinches. This roughness is comparable to that of drawn tubing which has an average surface roughness of 32-63 microinches.[60] Thus the bottom surfaces of the test specimens used in this investigation are comparable to the smooth sodium containment surfaces found in nuclear reactors. However, it is pointed out in Chapter I that the condition of the surface in contact with the sodium will affect the onset of cavitation and it is recommended in Chapter VII that a continuation of this study should include the effect of changing the bottom surface conditions of the test specimen on the onset and cessation of cavitation in liquid sodium.

## D. Sodium Handling Technique

Sodium is a soft, ductile metal with a lustrous, silvery appearance. At one atmosphere sodium has a melting point of 208°F and a boiling point of 1618°F.[61] Sodium has a high chemical reactivity, and, as a solid, sodium rapidly oxidizes in air to a dull, gray color. If molten sodium exposed to air is heated above 248°F (ignition temperature), it will burn rapidly and produce considerable sodium oxide

smoke and heat.[62] Sodium also reacts vigorously with water, forming sodium hydroxide and hydrogen. If air is present during the reaction with water the heat of reaction can ignite the hydrogen-oxygen mixture and cause an explosion.[63] In reviewing the above properties it becomes readily apparent that special care must be employed in the handling of sodium.

The metallic sodium used in this experiment was obtained from the U. S. Industrial Chemicals Company. The sodium was in the form of single one pound ingots which were individually hermetically sealed in cylindrical cans. The sodium ingot was cylindrical in shape with a diameter of 2 1/4 inches and a length of 7 7/8 inches. The impurities in the sodium were listed by volume at 50 ppm (parts per million) chlorides and 400 ppm calcium. After the experiments were completed a sample of the sodium was analyzed for oxygen, hydrogen, and carbon concentrations. This analysis will be discussed later in this chapter.

The charging of the sodium into the cavitation vessel was accomplished in a glove box. Initially the cavitation vessel, vessel top plate, and one can of metallic sodium were placed in the glove box. The transducer horn assembly, baffle plate, thermocouple probe, and acoustic probe were attached to the vessel top plate as shown in Fig 12 of Chapter II prior to placing the top plate in the glove box. The cavitation vessel and top plate assembly were cleaned with acetone before being placed in the glove box, which was then sealed. A vacuum pump attached to the glove box produced a partial

vacuum inside the glove box of approximately 15 inches of Hg which was the structural limit of the box. The glove box was then filled with argon gas and maintained at a pressure of approximately 2 psig. Argon was used as cover gas since it is inert to sodium.[64] Access into the glove box was provided by rubber gloves which were attached to its two access ports. The metallic sodium was removed from the can and approximately 1/3 of the sodium was cut from the ingot using a standard stainless steel kitchen knife. The 1/3 portion of the ingot was then placed in the cavitation vessel, which was then heated by an electric hot plate until the sodium inside the vessel melted. With the sodium in the molten form, the vessel top plate assembly was bolted to the cavitation vessel. With the top plate in position the level of the liquid sodium inside the vessel was approximately 1/4 inches above the baffle plate. The cavitation vessel assembly was then removed from the glove box and placed in the furnace.

Upon completion of the observations of the onset and cessation of cavitation in liquid sodium at various temperatures the sodium was cooled below its melting point. The cavitation vessel assembly was removed from the furnace and returned to the glove box. Prior to placing the vessel inside the glove box the water cooling coil which is soldered to the vessel top plate was flushed with argon gas to insure that no water would be brought into the glove box. The glove box was sealed, evacuated to a vacuum of 15 inches of Hg and then pressurized

with argon gas. The cavitation vessel assembly was heated on the electric hot plate until the sodium melted. The vessel top plate was then removed and the molten sodium was poured into a stainless steel receptacle and allowed to solidify. The cavitation vessel and vessel top plate assembly were removed from the glove box and the residual sodium was cleaned from these components by using a mixture of propyl alcohol and kerosene.[65] After cleaning with alcohol and kerosene, the vessel and vessel top plate were flushed with water. The sodium in the stainless steel receptacle plus the unused portion of the sodium ingot were removed to an outdoor location and burned by using kerosene-soaked rags.[66]

Several recommended safety precautions were observed during all experimental phases involving sodium handling. All personnel involved in the handling of sodium wore suitable chrome-leather protective clothing. A dry powder fire extinguishing material especially designed for liquid metal fires was available in case of a sodium fire. A steel spill pan was located directly beneath the furnace to contain any possible sodium leakage resulting from a failure in the cavitation vessel.

The sodium handling technique as described above proved satisfactory in that loading, unloading, and disposal of the sodium was carried out more than 20 times without incident.

## E. Experimental Procedure

### 1. Calibration of Counterweight Crystal

Prior to conducting the measurements using liquid sodium as the test fluid the counterweight crystal was calibrated for each of the four exponential horns. The calibration curves of counterweight crystal voltage versus zero to peak test specimen displacement were obtained using the KD-38 fotonic sensor and the procedure outlined in Chapter III. After all experimental measurements of the onset and cessation of cavitation in liquid sodium were completed the calibration procedure was repeated to insure that the performance of the counterweight crystal did not change during the test runs. The counterweight crystal calibration curves using the four transducer horn assemblies are shown in Fig 36. The curves were established using the calibration data obtained before and after the experiment. It can be seen from Fig 36 that there is no appreciable scatter in the calibration data. This lack of scatter indicates that the performance of the counterweight crystal did not change during the measurements using liquid sodium as the test fluid.

### 2. Determination of the Onset and Cessation of Cavitation

After initially charging the cavitation vessel with liquid sodium in the glove box (in preparation for each succeeding run) the vessel was placed in the furnace. In order to remove any remaining impurities still present on the surfaces in contact with the sodium, it was recommended[67]

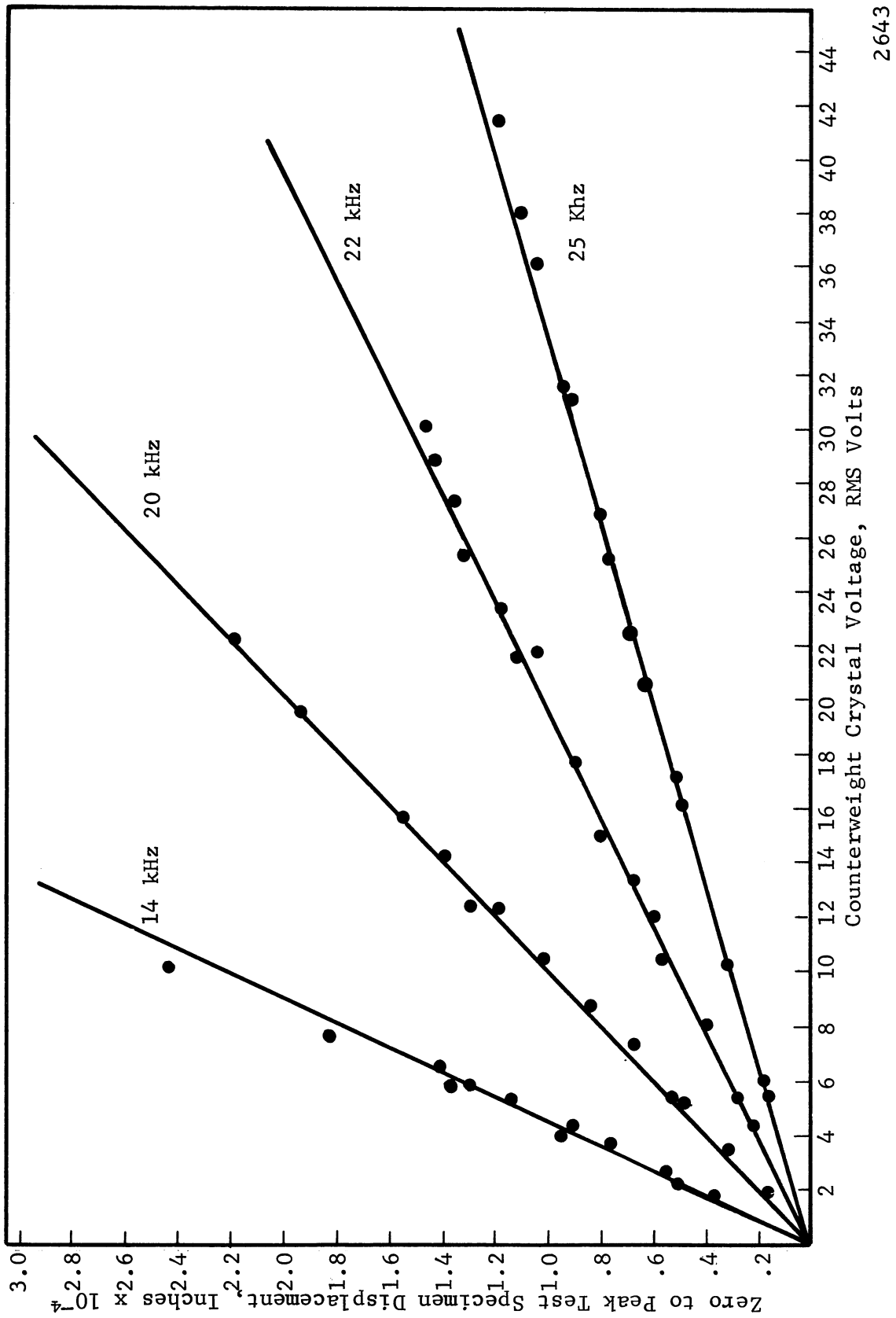


FIGURE 36. COUNTERWEIGHT CRYSTAL CALIBRATION CURVES FOR THE 14, 20, 22, AND 25 KHZ TRANSDUCER-HORN ASSEMBLIES

that the temperature of the sodium be raised to 1500°F and held at that temperature for several hours to allow the sodium to react with these impurities. The above procedure was followed, after which the sodium was cooled to below its melting point. The vessel was removed from the furnace and placed in the glove box where the contaminated sodium was removed and a new charge of sodium was placed in the vessel for the actual test. The vessel was then again placed in the furnace.

The system was connected as shown in Fig 4 of Chapter II. The output of the thermocouple measuring the liquid sodium temperature was connected to a Brown potentiometer pyrometer for visual monitoring of the sodium temperature. The acoustic probe was connected to a VTVM and a dual beam oscilloscope. The argon used as cover gas was maintained at a pressure of 15.0 psia, providing a slight overpressure to prevent air leakage into the cavitation vessel.

The temperature of the liquid sodium was then raised to 500°F. With the temperature held constant at 500°F the input power to the transducer horn assembly was slowly and continuously increased until the onset of cavitation was observed. The onset of cavitation was determined by observing on the oscilloscope the appearance of the cavitation noise signal transmitted by the acoustic probe. The power to the transducer horn assembly was then decreased until the cessation of cavitation was reached which was determined by the disappearance of the cavitation noise signal. The power to the transducer

horn assembly was then reduced to zero. The counterweight crystal output voltage was observed by using a VTVM for the onset and cessation of cavitation. This process was repeated ten times while maintaining the temperature constant at 500°F. The resulting ten values for the counterweight crystal voltage at the onset of cavitation were averaged to obtain one data point for the onset of cavitation at 500°F. Similarly, the resulting ten values of counterweight crystal voltage at the cessation of cavitation were averaged to obtain one data point for the cessation of cavitation at 500°F. The temperature was then increased to 750°F and the onset and cessation of cavitation were again determined for a total of 10 times each, and these values averaged to obtain two data points for the onset and cessation of cavitation at 750°F. This process was repeated at approximately 1000, 1250, and 1500°F. The sodium was then allowed to cool with additional data points taken at approximately 1250, 1000, 750, and 500°F. To determine repeatability in the data the above procedure was repeated using the same charge of sodium and the same transducer horn assembly. Upon completion of the two data runs the cavitation vessel was removed from the furnace and placed in the glove box.

The entire process as described above was repeated for each of the four exponential horns using a new 304 stainless steel test specimen and a fresh charge of sodium for each exponential horn. The only difference in the procedures used for each of the four exponential horns was the addition of the stainless steel spacers which were described earlier in this

chapter.

After completing the above described experimental runs an additional check run was conducted for each of the four exponential horns to further check the repeatability of the data. A fresh charge of sodium and a new test specimen were used for each of the four check runs.

The data listed in Table 5 represents a typical set of ten values for the counterweight crystal output voltage at the onset and cessation of cavitation which were averaged to obtain one data point for the onset of cavitation and one data point for the cessation of cavitation. This data was obtained at a frequency of 18534 Hz and a sodium temperature of 1465°F. The scatter in the onset and cessation of cavitation data as shown in Table 5 is approximately equal since the standard deviations for the onset and cessation data are 0.12 and 0.13 volts, respectively. Fig 37 are photographs of the voltage waveforms for the counterweight crystal and acoustic probe taken just prior to the onset of cavitation and at the onset of cavitation at a frequency of 18534 Hz and a liquid sodium temperature of 1465°F. It is noted that in comparing the photographs of Fig 37 with the photographs of Fig 34 of Chapter IV the performance of the acoustic probe using liquid sodium as the test fluid was similar to its performance in water.

## F. Sodium Analysis

Upon completion of the last data run using liquid sodium as the test fluid, the cavitation vessel was removed

TABLE 5

COUNTERWEIGHT CRYSTAL VOLTAGE AT THE ONSET AND CESSATION OF CAVITATION IN LIQUID SODIUM AT 18534 HZ AND 1465°F

| Onset of Cavitation | Cessation of Cavitation |
|---|---|
| 3.8 volts (RMS) | 2.9 volts (RMS) |
| 3.9 | 3.0 |
| 4.0 | 3.2 |
| 3.8 | 3.1 |
| 3.8 | 3.3 |
| 3.8 | 3.2 |
| 3.6 | 3.3 |
| 3.7 | 3.2 |
| 3.6 | 3.1 |
| 3.8 | 3.1 |
| 3.78[a] | 3.14[a] |
| 0.12[b] | 0.13[b] |

[a] Average Value

[b] Standard Deviation

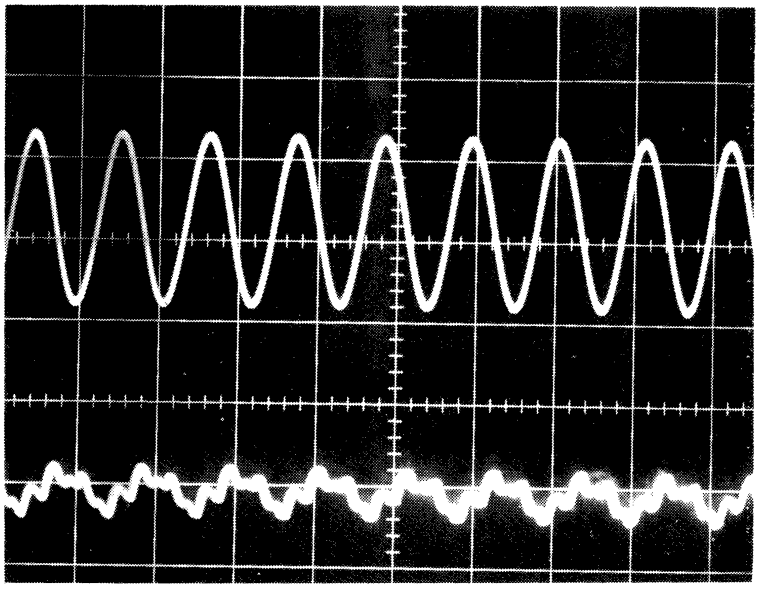

COUNTERWEIGHT
CRYSTAL VOLTAGE
WAVEFORM

10 Volts/cm
50 Microsec/cm

ACOUSTIC PROBE
VOLTAGE WAVEFORM

0.1 Volts/cm
50 Microsec/cm

FIGURE 37 (a). PHOTOGRAPH OF TYPICAL WAVEFORMS OBSERVED JUST PRIOR TO THE ONSET OF CAVITATION IN LIQUID SODIUM

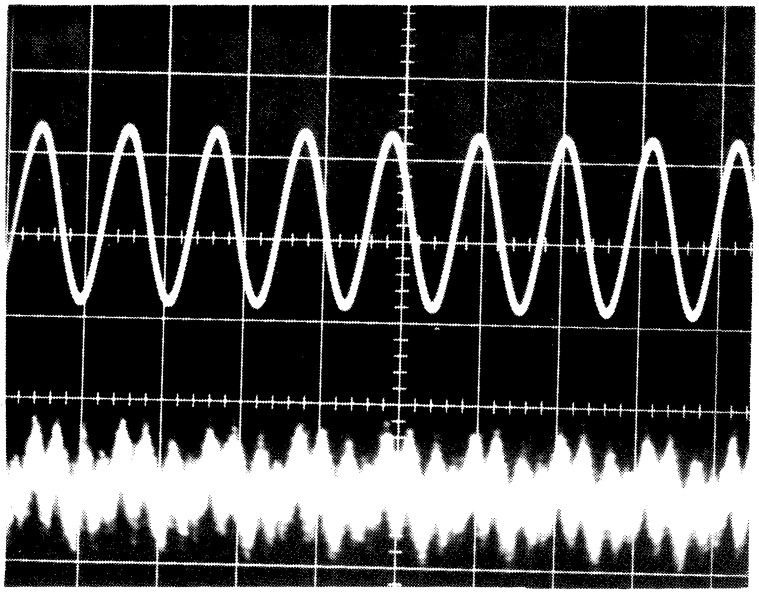

COUNTERWEIGHT
CRYSTAL VOLTAGE
WAVEFORM

10 Volts/cm
50 Microsec/cm

ACOUSTIC PROBE
VOLTAGE WAVEFORM

0.1 Volts/cm
50 Microsec/cm

2644

FIGURE 37 (b). PHOTOGRAPH OF TYPICAL WAVEFORMS OBSERVED AT THE ONSET OF CAVITATION IN LIQUID SODIUM

from the furnace and delivered to Atomic Power Development Associates, Inc., Detroit, Michigan for analysis of the sodium. Table 6 lists the oxygen, hydrogen, and carbon content of the sodium used in the last data run which can be considered a typical data run since the procedures followed for all runs were identical. For comparative purposes Table 6 also lists the range of concentrations of oxygen, hydrogen, and carbon impurities found in sodium samples taken from the Enrico Fermi sodium cooled fast reactor. From Table 6 it can be seen that although the concentration of impurities is toward the high end of the concentration range of impurities found in the Enrico Fermi reactor for oxygen (and low for carbon), the impurity level for this experiment is low enough so that the sodium can be considered reactor grade and the results obtained in this experiment can thus be realistically related to the behavior of sodium used in nuclear reactors.

## G. Discussion of Experimental Results

### 1. Experimental Results

The experimental results obtained for the onset of cavitation and the cessation of cavitation using liquid sodium as the test fluid are indicated in Figs 38 and 39, respectively. Shown in Figs 38(a), 38(b), 38(c), and 38(d) are the data points obtained for the onset of cavitation using the 14, 20, 22, and 25 kHz exponential horns, respectively, while 39(a), 39(b), 39(c), and 39(d) show the corresponding data points for the cessation of cavitation. As pointed out earlier in

TABLE 6

ANALYSIS OF SODIUM USED IN THIS EXPERIMENT AND ANALYSIS OF SODIUM USED IN THE ENRICO FERMI NUCLEAR REACTOR

| Impurity | Concentration Found In Sodium Used In Experiment | Concentration Found In Sodium Used In Fermi Reactor |
|---|---|---|
| Oxygen | 22-25 ppm | 5-25 ppm |
| Total Hydrogen Content | 3.6 ppm | 1-5 ppm |
| Total Carbon Content | 33-50 ppm | 20-200 ppm |

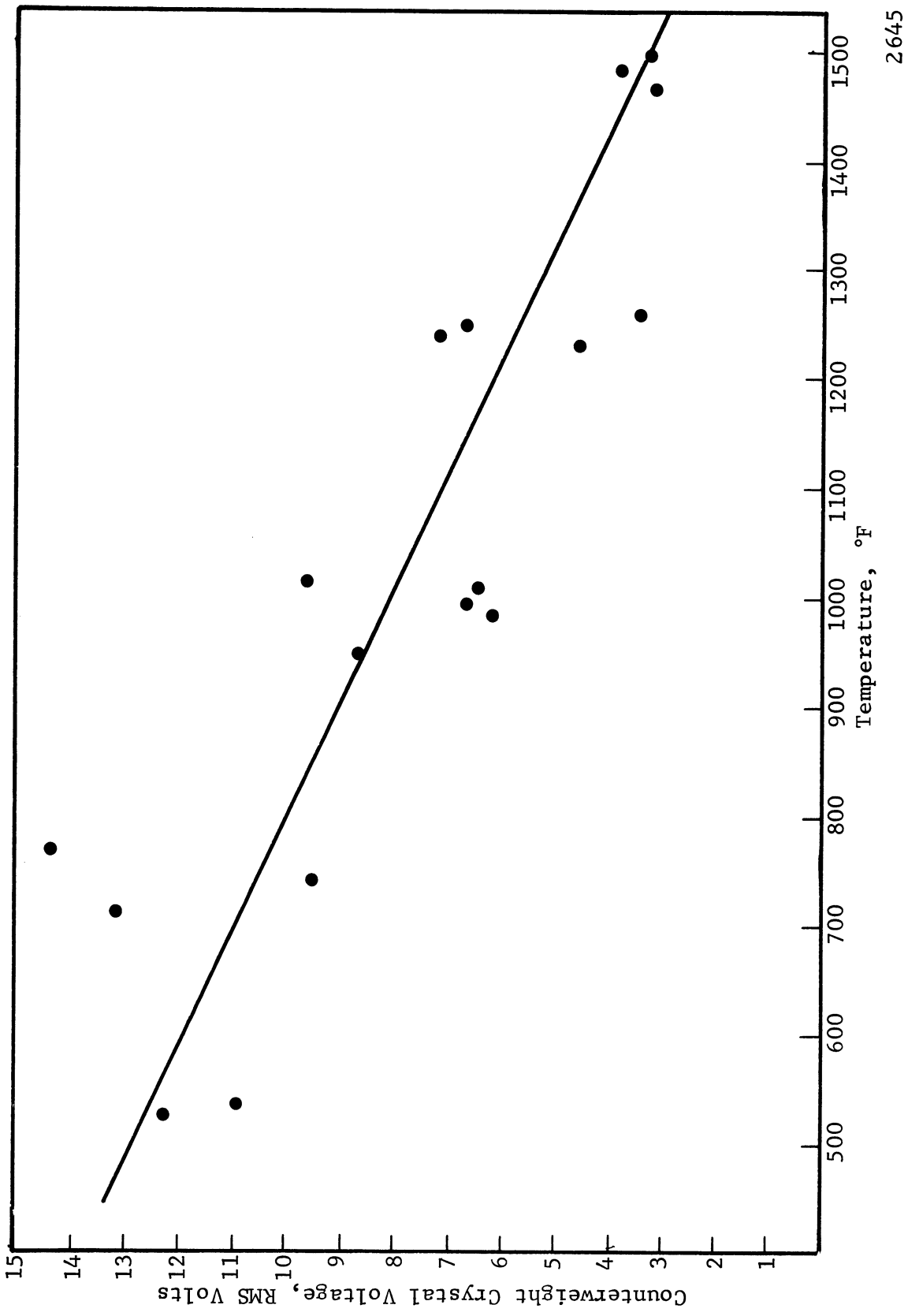


FIGURE 38 (a). COUNTERWEIGHT CRYSTAL VOLTAGE AT ONSET OF CAVITATION IN LIQUID SODIUM USING 14 KHZ TRANSDUCER HORN ASSEMBLY

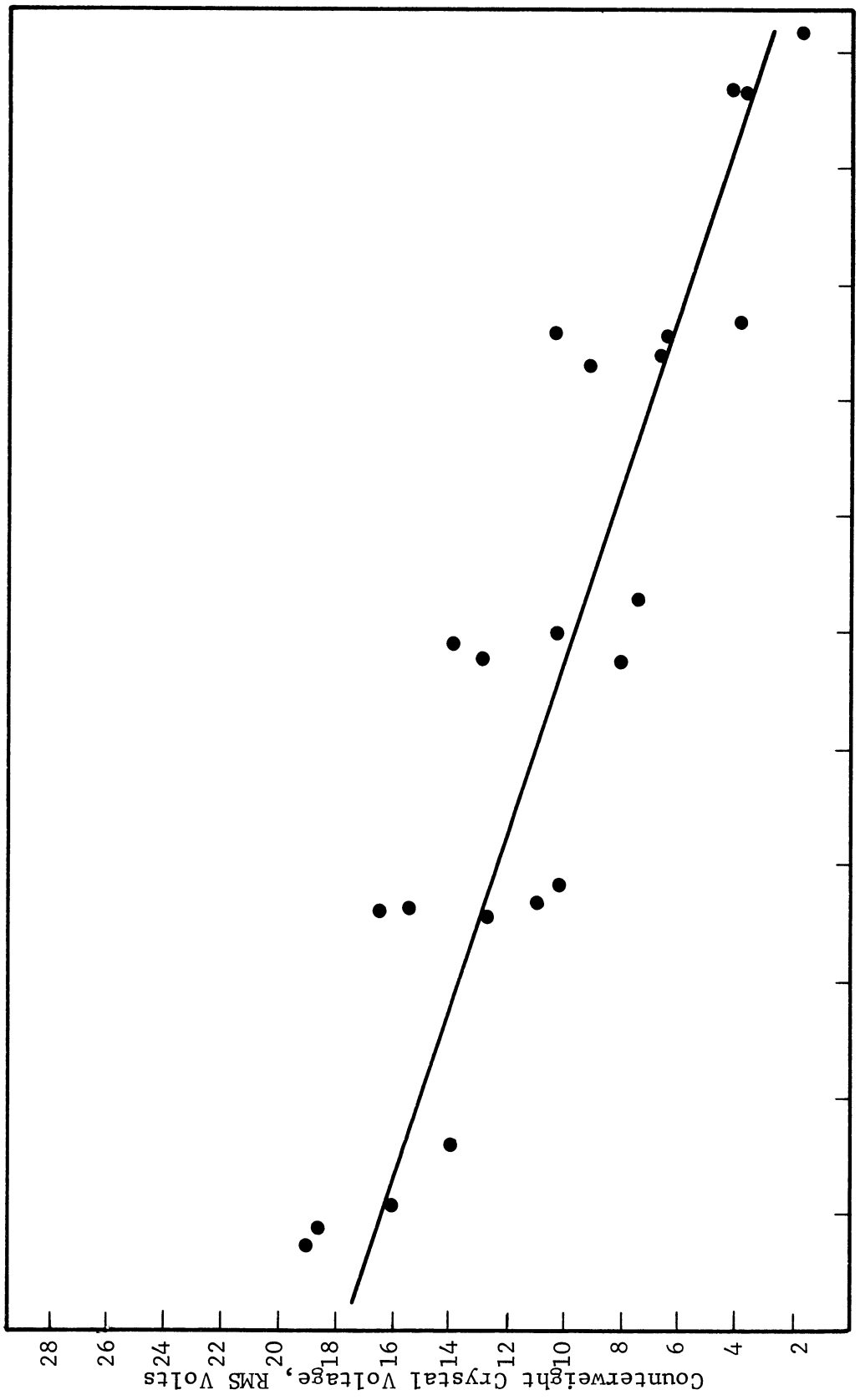


FIGURE 38 (b). COUNTERWEIGHT CRYSTAL VOLTAGE AT ONSET OF CAVITATION IN LIQUID SODIUM USING 20 KHZ TRANSDUCER HORN ASSEMBLY

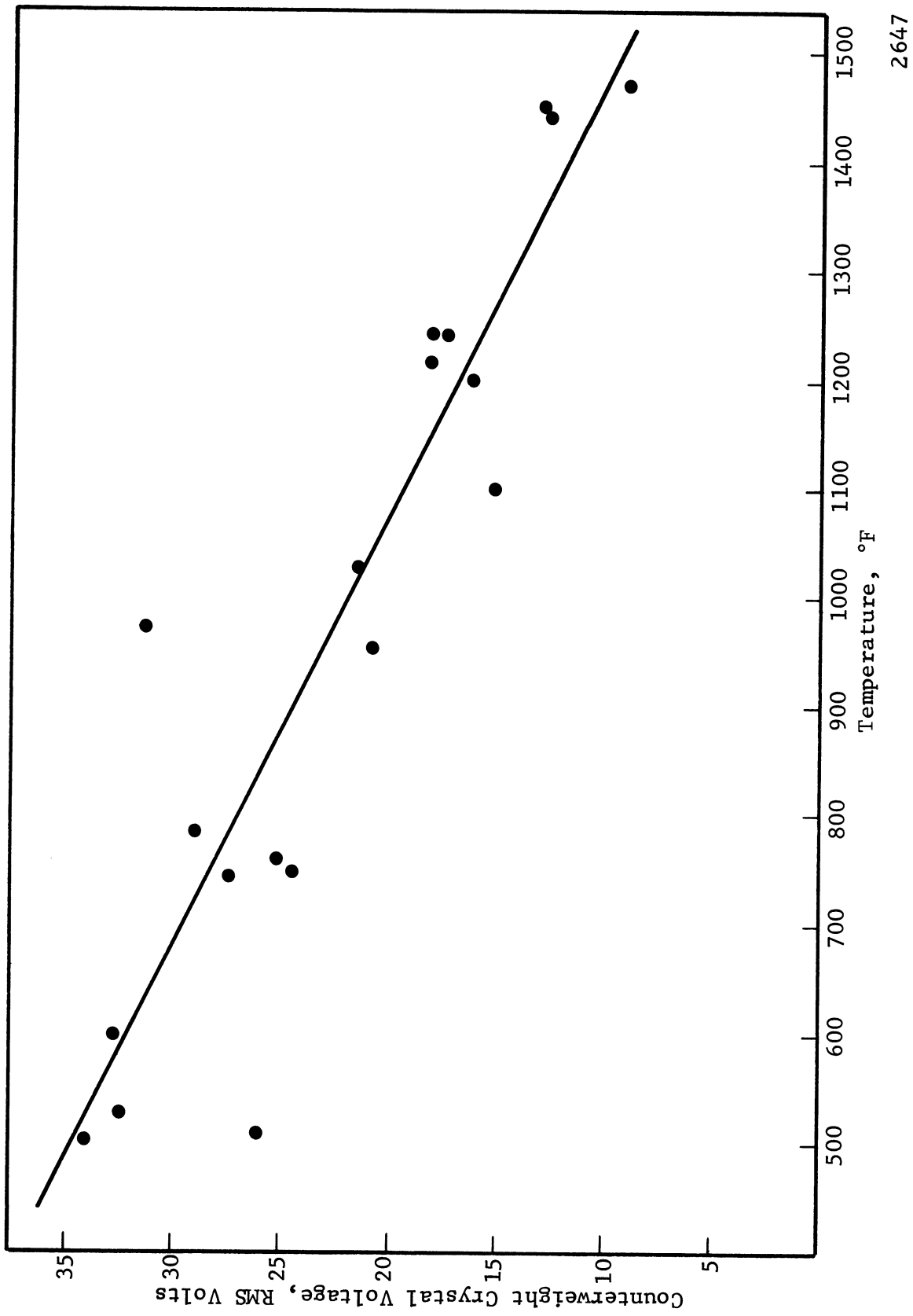


FIGURE 38 (c). COUNTERWEIGHT CRYSTAL VOLTAGE AT ONSET OF CAVITATION IN LIQUID SODIUM USING 22 KHZ TRANSDUCER HORN ASSEMBLY

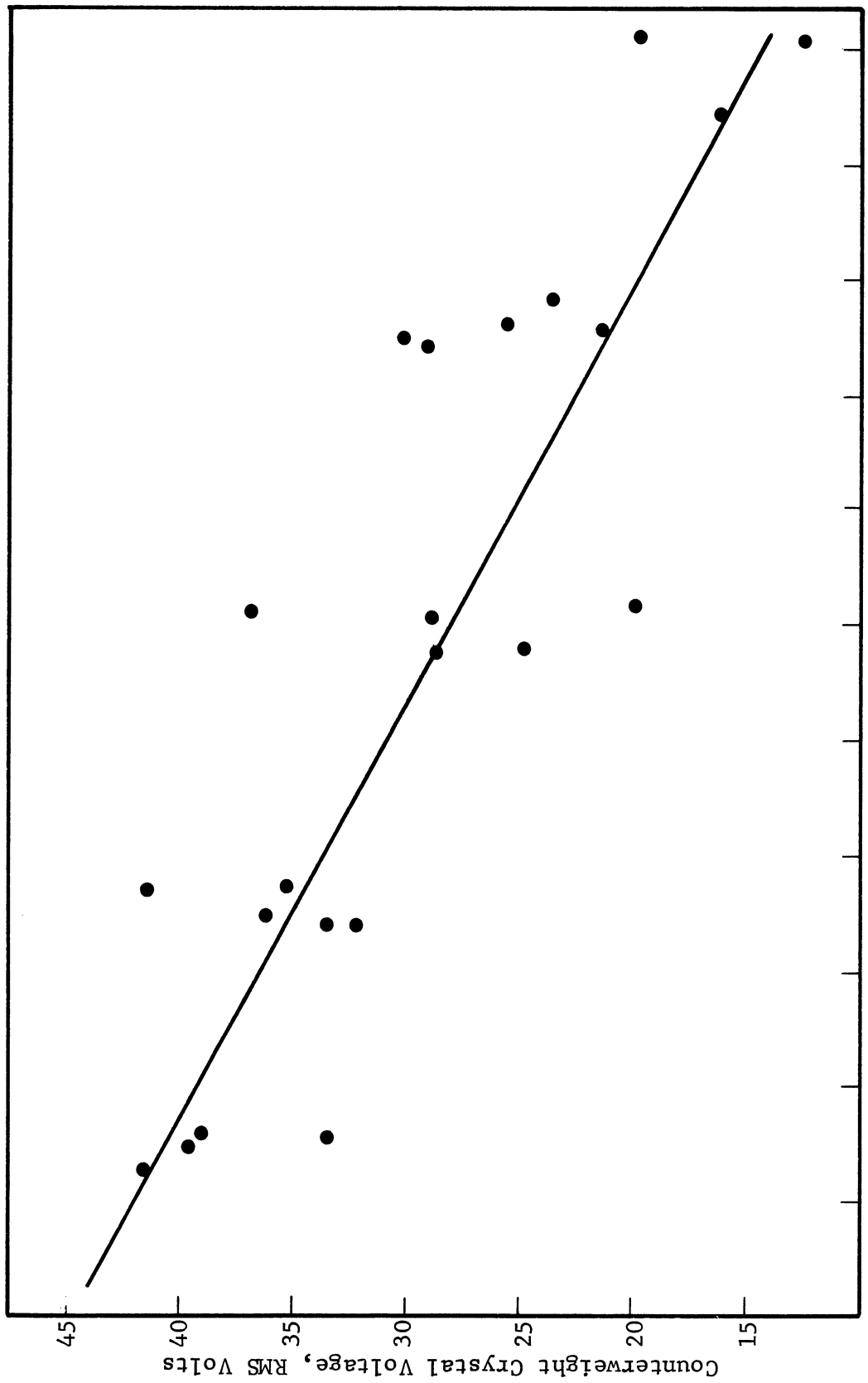


FIGURE 38 (d). COUNTERWEIGHT CRYSTAL VOLTAGE AT ONSET OF CAVITATION IN LIQUID SODIUM USING 25 KHZ TRANSDUCER HORN ASSEMBLY

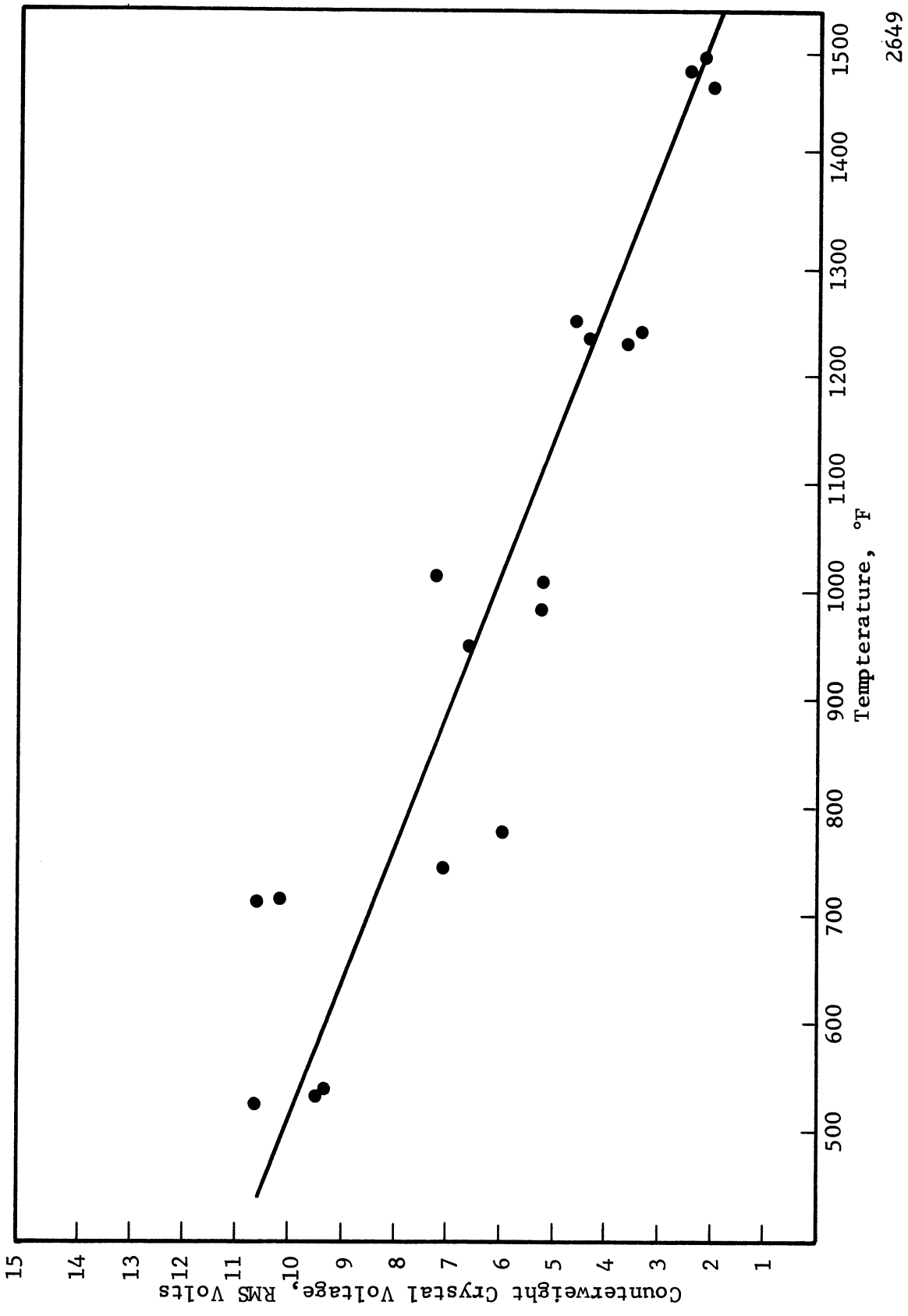


FIGURE 39 (a). COUNTERWEIGHT CRYSTAL VOLTAGE AT CESSATION OF CAVITATION IN LIQUID SODIUM USING 14 KHZ TRANSDUCER HORN ASSEMBLY

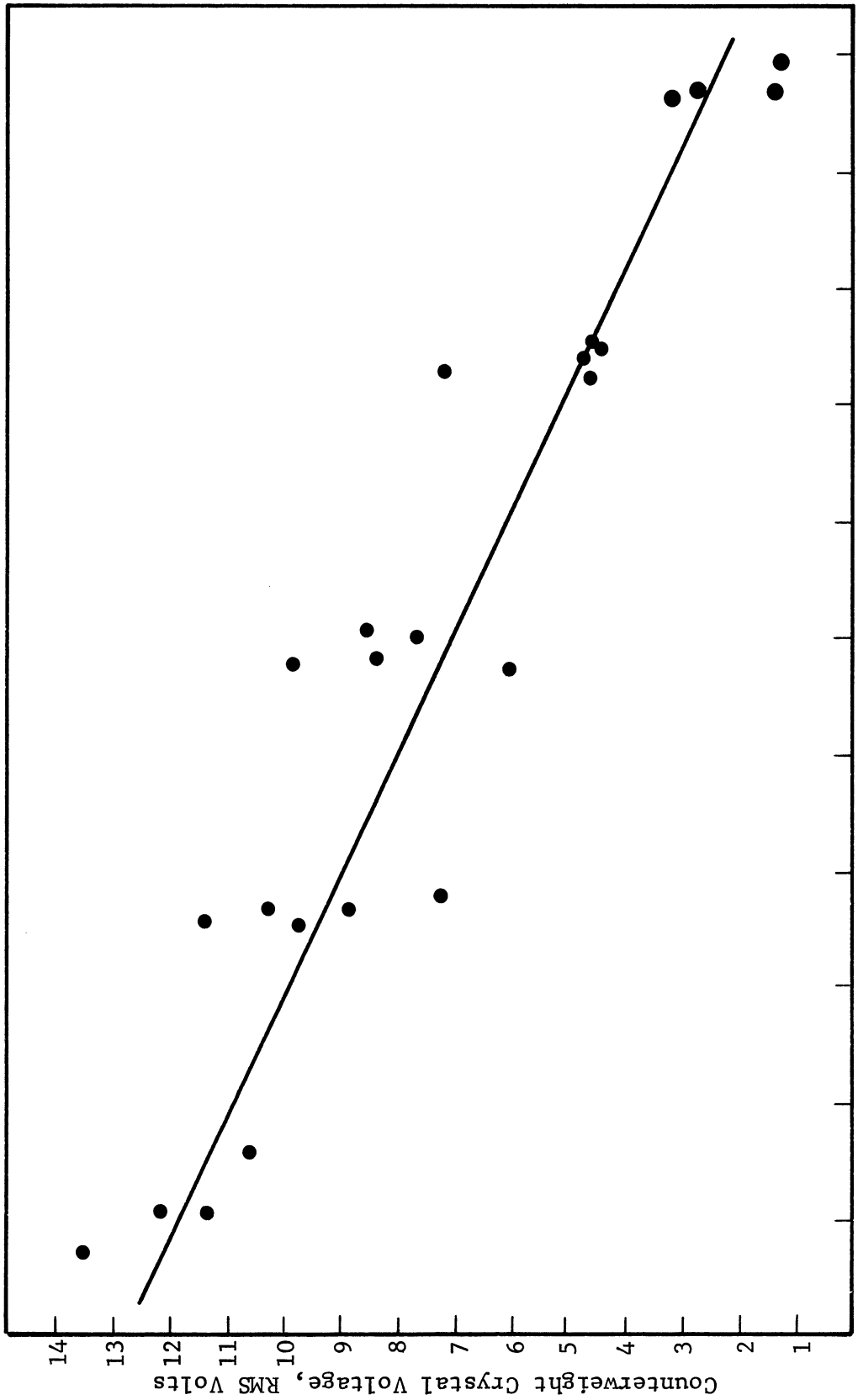


FIGURE 39 (b). COUNTERWEIGHT CRYSTAL VOLTAGE AT CESSATION OF CAVITATION IN LIQUID SODIUM USING 20 KHZ TRANSDUCER HORN ASSEMBLY

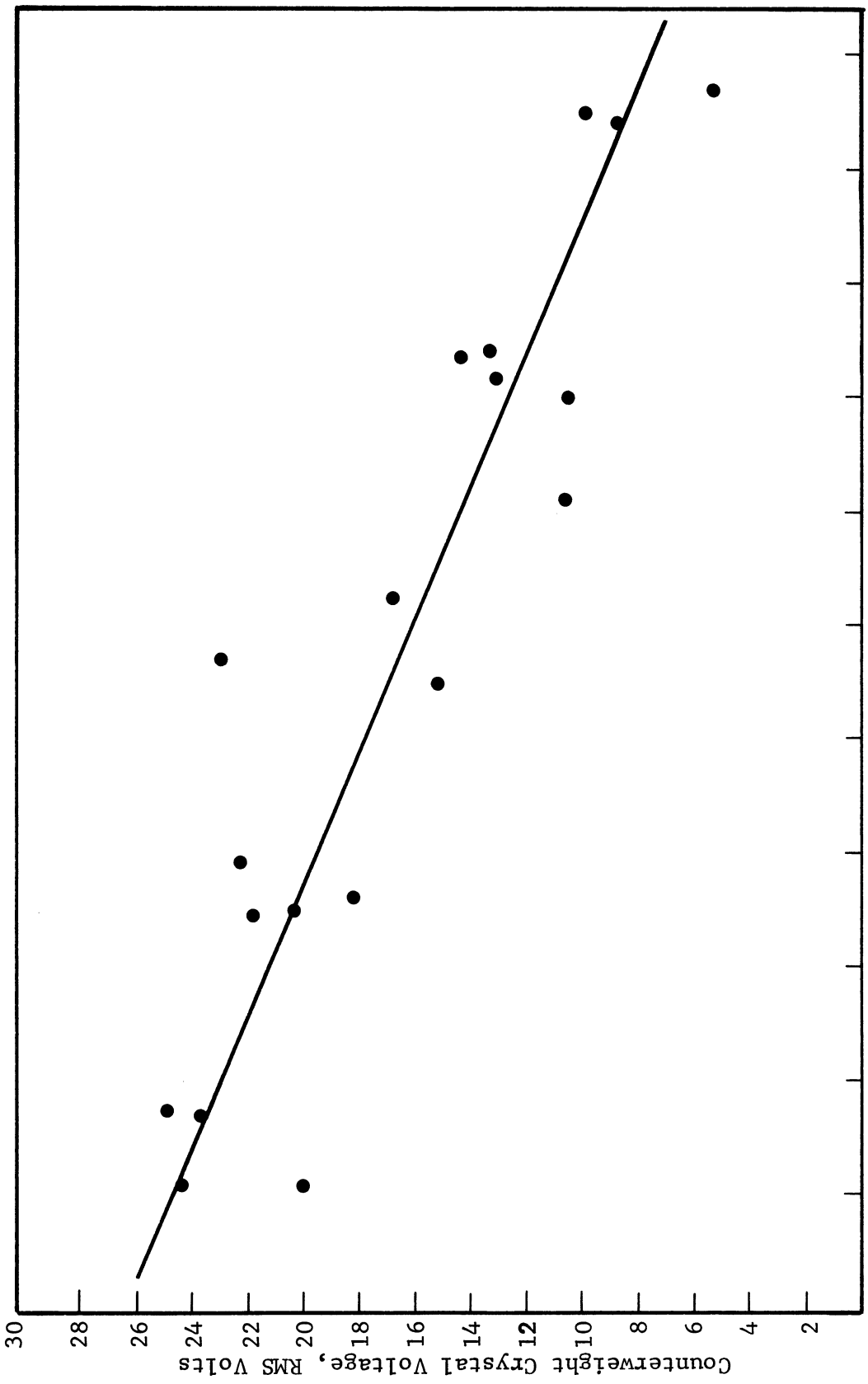


FIGURE 39 (c). COUNTERWEIGHT CRYSTAL VOLTAGE AT CESSATION OF CAVITATION IN LIQUID SODIUM USING 22 KHZ TRANSDUCER HORN ASSEMBLY

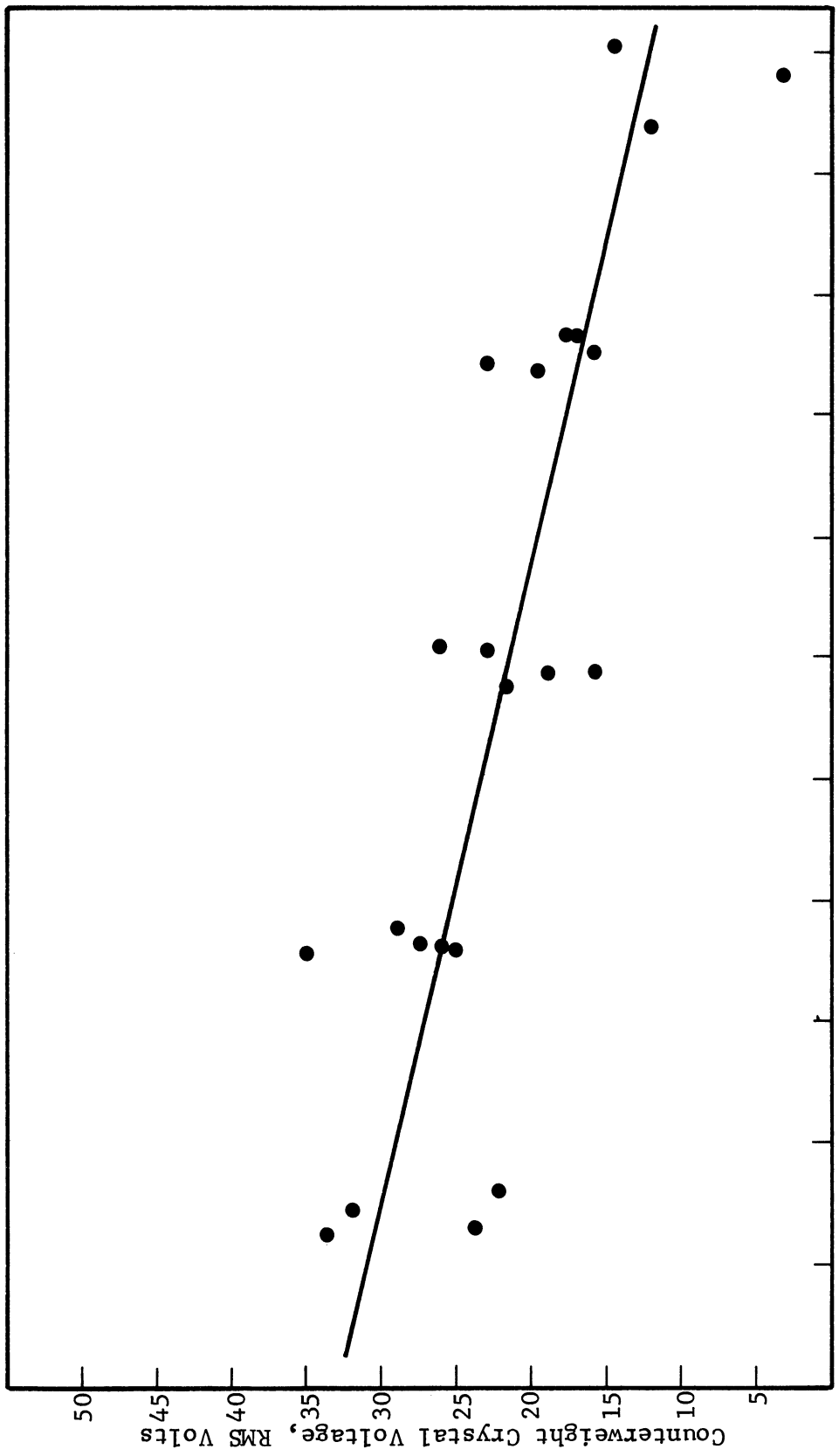


FIGURE 39 (d). COUNTERWEIGHT CRYSTAL VOLTAGE AT CESSATION OF CAVITATION IN LIQUID SODIUM USING 25 KHZ TRANSDUCER HORN ASSEMBLY

this chapter each data point represents the average of ten experimental observations of the onset or cessation of cavitation at that particular temperature. A straight line was used to establish a relationship between the counterweight crystal voltage at the onset or cessation of cavitation and the temperature of the liquid sodium. A least mean square analysis was used to fit the straight line to the data.[40] Similar linear relationships between the onset of cavitation and the temperature of the test fluid have been reported in the literature where water was used as the test fluid.[9, 49]

In reviewing the experimental data several observations can be made. These concern data scatter, fluid nonlinearity, frequency dependence, and temperature dependence.

2. Data Scatter

From Figs 38 and 39 it can be seen that appreciable scatter exists in the data. This scatter was present in each individual data run. In other words, the data scatter obtained on the two additional check runs for each frequency was essentially the same as obtained on the first data run for that particular frequency. The average scatter in the values for the onset of cavitation at each particular temperature is approximately ± 25 per cent. Comparable scatter also appears in the cessation of cavitation data. A similar scatter in data was reported by Blake[9] in determining cavitation thresholds using water as the test fluid. Reference to Figs 2 and 3 of Chapter I indicates that the data for nucleate boiling in sodium and potassium obtained by Edwards and Hoffman[19]

contains similar scatter. The mechanisms involved in producing this scatter aside from experimental error are not fully understood although several theories have been developed. One possible explanation was presented by Messino et al.[68] Messino presented the possibility that cavitation nuclei exist in a spatial distribution within the cavitation vessel and because of the motion of the fluid produced by the sound field nuclei of various sizes are brought into the region of high pressure fluctuations. The result is that the cavitation threshold will vary depending on the size of the nuclei which are present in this region at a particular time.

3. Fluid Nonlinearity (Hysteresis)

A second observation which can be made from the data is the nonlinearity* of the fluid in going from a single phase to a two phase regime and then back to a single phase fluid. Using the 14 kHz exponential horn data the reduction in counterweight crystal voltage (which is proportional to the magnitude of the pressure field produced by the transducer horn assembly) in going from the onset of cavitation to the cessation of cavitation is approximately 27 per cent. For the 20 kHz data this reduction is approximately 35 per cent. The 22 and 25 kHz data show reductions of 28 and 22 per cent, respectively. The average reduction is approximately 28 per cent. From the data reported by Connolly and Fox[50] it is noted that the

* Sometimes referred to as "hysteresis" in the cavitation literature.

reduction in threshold values going from the onset to the cessation of cavitation in water is approximately 31 per cent. Since water and sodium (over the temperature ranges involved) have certain similar fluid properties (density, velocity of sound, viscosity, surface tension) it was expected that the reduction in threshold values in going from the onset to the cessation of cavitation for the two fluids should be similar.

As discussed in Chapter VI the superheat requirements for liquid sodium are determined from the onset of cavitation data; the cessation of cavitation data does not enter into the superheat calculation. However, the cessation of cavitation data was recorded for two reasons. First, this data provides a quantitative measure of the nonlinearity of liquid sodium. Second, it serves as a check on the onset of cavitation data. In other words, if at a particular temperature both the onset and cessation of cavitation are recorded, and if the reduction in threshold in going from the onset to the cessation of cavitation is consistent, then an additional check on the validity of the onset data is obtained.

4. Frequency Dependence

In order to determine the effect of frequency on the onset of cavitation, the data was replotted in Fig 40 as curves of counterweight crystal voltage at the onset of cavitation versus frequency. For example, three data points from Fig 38(a) for the temperatures 500 1000, and 1500°F were plotted in Fig 40 at a frequency of approximately 14 kHz. The exact frequencies used in this plotting are measured points.

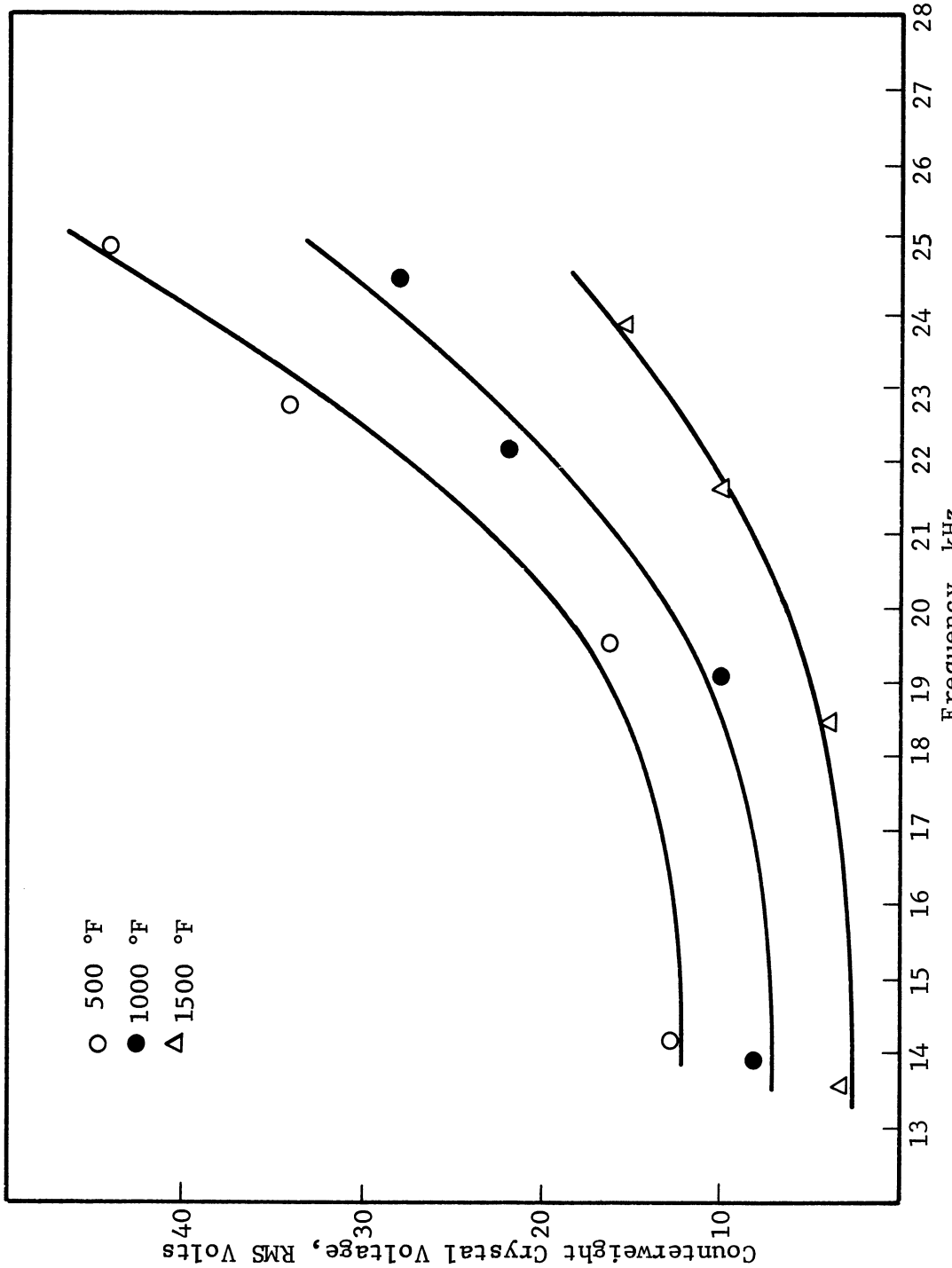


FIGURE 40. COUNTERWEIGHT CRYSTAL VOLTAGE AT ONSET OF CAVITATION VERSUS FREQUENCY FOR LIQUID SODIUM TEMPERATURES 500, 1000, AND 1500 °F

It is noted that as the temperature is increased the frequency decreases slightly due to the thermal expansion of the 14 kHz exponential horn. The plotting process was repeated using the data points at 500, 1000, and 1500°F from Figs 38(b), 38(c), and 38(d). Three curves were then drawn connecting the data points taken at the same temperature.

In comparing the cavitation threshold data obtained at the four different frequencies it is noted that there is a definite frequency dependence. From Fig 40 it can be seen from the three curves for the three liquid sodium temperatures that as the frequency of the applied pressure field is increased the observed cavitation thresholds increase. It appears that the slopes of the curves begin to increase more rapidly for frequencies above approximately 20 kHz. In other words, there appears to be relatively little frequency dependence on the cavitation thresholds for frequencies below 20 kHz. For frequencies above 20 kHz the cavitation thresholds begin tc increase sharply.

Boguslavskii and Korets[69] provide the most comprehensive theoretical investigation of the effect of frequency on the cavitation threshold. They considered the influence of the inertial and viscous forces on the motion of vapor cavities in an incompressible liquid under the action of an alternating pressure field. In order to discuss the frequency dependence a partial review of their analysis will be given here.

Starting with the Noltingk-Neppiras equation[70, 71] describing the growth of a vapor cavity, we have

$$\rho\left(R\ddot{R}+\frac{3}{2}\dot{R}^2\right)+\frac{2\sigma}{R}+4\eta\frac{\dot{R}}{R}=P_0\sin\omega t+P_s-P_a \qquad (5.1)$$

where

$\rho$ = density of fluid

$R$ = radius of vapor bubble

$\sigma$ = surface tension

$\eta$ = dynamic viscosity

$P_0 \sin \omega t$ = applied pressure field

$P_s$ = saturation vapor pressure

$P_a$ = atmospheric pressure

$\omega = 2\pi f$

$f$ = frequency of applied field.

Boguslavskii and Korets approximated the sinusoidal pressure field by a square wave variation, with the dilation and compression pulses possessing an amplitude $\tau$ for a time $\tau = T/2$ where $T = 2\pi/\omega$. If Eq (5.1) is written for the dilation pulse we have with the square wave approximation

$$\rho\left(R\ddot{R}+\frac{3}{2}\dot{R}^2\right)+\frac{2\sigma}{R}+4\eta\frac{\dot{R}}{R}=Z_0 \qquad (5.2)$$

where

$$Z_0 = P_0 + P_s - P_a$$

is the tension applied to the liquid during the dilation pulse. The first term of Eq (5.2) is the inertial term and has an order of magnitude $\rho\bar{R}^2/\tau^2$ where $\bar{R}$ represents the radius of the bubble at the end of the dilation period $\tau$. The second term is the surface tension term. The third

term of Eq (5.2) represents the effects of viscosity, and has an order of magnitude $4\eta/\bar{R}$. Boguslaskii defines the onset of cavitation as the point at which the incipient nuclei with radius of approximately $10^{-4}$ cm grow to a radius of the order $\bar{R} = 5\times10^{-2}$ cm during the time $\tau$. This choise of $\bar{R}$ is consistant with the calculations conducted by Noltingk and Neppiras.[70, 71]

Using an initial radius of $10^{-4}$ cm it is found for water ($\sigma$ = 72 dynes/cm) that the surface tension term is approximately 1.5 atmospheres. The inertial term reaches the same order of magnitude when the frequency is increased to approximately 12 kHz. The viscous term ($\eta = 10^{-2}$ poise) remains small compared to the inertial and surface tension terms for the frequencies of interest. The viscous term does not reach 1.5 atmospheres until the frequency is raised to approximately $10^7$ Hz. Thus for water the cavitation threshold is essentially independent of frequency until the frequency reaches approximately 10-15 kHz. At these frequencies the inertial term becomes appreciable and increases significantly the tension requirements necessary to produce cavitation in the liquid. The experimental work conducted by Esche[46] is in good agreement with the analysis by Boguslavskii and Korets. Esche experimentally determined for water that the cavitation threshold is essentially independent of frequency up to approximately 10 kHz. At higher frequencies the cavitation threshold increases sharply with increasing frequency.

Using liquid sodium as the test fluid it is found

that the surface tension term is approximately 3 atmospheres where $\sigma$ = 148 dynes/cm which is an average value for the temperature range of 500 to 1500°F. The inertial term reaches 3 atmospheres when the frequency is increased to approximately 17.5 kHz. The viscous term ( $\eta = 0.41 \times 10^{-2}$ poise) does not reach 3 atmospheres until the frequency reaches approximately $10^8$ Hz and therefore remains relatively negligible for the present investigation. Therefore, using the above analysis and assuming an initial radius of $10^{-4}$ cm it appears that the cavitation threshold for liquid sodium is essentially independent of frequency until the frequency reaches approximately 15-20 kHz. The cavitation threshold then becomes frequency dependent and increases significantly for increases in frequency above 15-20 kHz. Comparing these results with Fig 40 it appears that there is reasonably good agreement in that the curves in Fig 40 begin to increase more sharply above frequencies of 20 kHz. It should be pointed out that the choice of an initial bubble size with liquid sodium as the test fluid is somewhat arbitrary. However, it is discussed in Chapter VI that by assuming that spherical vapor bubbles serve as nucleation sites for the onset of cavitation, the radii of these bubbles is calculated to be on the order of $10^{-4}$ cm.

Summarizing the above discussion, assuming an incompressible liquid with vapor bubbles of initial radii of $10^{-4}$ cm it was determined that for low frequencies the inertial and viscous terms are small compared to the surface tension term, which is independent of frequency. As the

frequency is increased to approximately 15-20 kHz for liquid sodium the inertial term becomes comparable to the surface tension term and above 15-20 kHz the cavitation threshold increases with increasing frequency. The viscosity term remains relatively small for the entire frequency range of this experiment.

5. Temperature Dependence

In determining the onset of cavitation in liquid sodium at various temperatures it was noted that the counter-weight crystal voltage at the onset of cavitation decreased linearly with temperature. This decrease in cavitation threshold for an increase in temperature has been observed by several investigators using water as the test fluid.[9, 49, 50] Generally this temperature dependence can be better understood by considering the effects of a change in temperature on the physical properties of the fluid, namely vapor pressure, surface tension, viscosity, and gas content.

As discussed in Chapter I, in order to achieve nucleation and bubble growth in a liquid Eq (1.2) of Chapter I must first be satisfied. For convience this equation is restated here.

$$P_v + P_g - P_L = \frac{2\sigma}{R} \qquad (1.2)$$

The vapor pressure, $P_v$, for the test fluid increases as the temperature of the test fluid is increased. From Eq (1.2) it can be seen that if $P_v$ is increased the required change in the local liquid pressure, $P_L$, necessary to produce

bubble growth is reduced. In other words, as the temperature of the fluid is increased the vapor pressure of the liquid is increased and the pressure change required to produce cavitation in the test fluid is reduced. For liquid sodium $P_v = 5.15 \times 10^{-4}$ psi at 500°F and $P_v = 7.88$ psi at 1500°F.[72] Thus the change in $P_v$ over the experimental temperature range is approximately 8 psi and although this total change is relatively small it nevertheless contributes to the observed temperature dependence.

The surface tension for liquid sodium decreases linearly from 176 dynes/cm at 500°F to 120 dynes/cm at 1500°F.[73] From Eq (1.2) it can be seen that this decrease in surface tension results in reducing the change in pressure requirements necessary to produce cavitation. As was pointed out in the previous section of this chapter the surface tension term is dominant over the viscous term and the inertial term in the Noltingk-Neppiras equation for frequencies up to approximately 15-20 kHz. At higher frequencies, the inertial term becomes the controlling term. It thus appears that for the present experimental frequency range the surface tension property significantly influenced the temperature dependence of the cavitation threshold.

It was pointed out in the previous section that the viscosity effect on bubble behavior was small compared to inertial and surface tension effects for frequencies of interest. Briggs et al[74] compared the cavitation threshold strengths of liquids with varying values of viscosity and

found that the cavitation threshold decreased slightly with a decrease in viscosity. The viscosity of liquid sodium decreases from $0.41 \times 10^{-2}$ poise at 500°F to $0.17 \times 10^{-2}$ poise at 1500°F.[75] Thus the reduction in viscosity contributes to the decrease in cavitation threshold for an increase in temperature. However, this effect is probably relatively small.

Cavitation thresholds are also affected by the test fluid gas content. From Eq (1.2) it can be seen that an increase in the partial pressure, $P_g$, due to the gas present in the bubble reduces the required changes in $P_L$ which are necessary to produce cavitation in the test fluid. Galloway[49] observed cavitation thresholds for water and benzine while varying the per cent air concentrations. He reported a linear increase in the cavitation threshold as the air concentration was decreased from 100 per cent to approximately 5 per cent. Below 5 per cent the cavitation threshold reached a limiting value, and was essentially independent of air concentration. Friedland[76] reports the solubility of argon in liquid sodium at 1 atmosphere to be approximately 92 ppm at 500°F and increases linearly to approximately 127 ppm at 1050°F. Extrapolating this curve to 1500°F it is found that the solubility at 1500°F would be approximately 160 ppm. Thus for an increase in temperature from 500°F to 1500°F, the solubility of argon in liquid sodium increases from 92 to 160 ppm and this increase in solubility reduces the cavitation threshold requirements.

In summarizing the temperature effect on the cavitation

threshold, it appears that changes in vapor pressure, surface tension, viscosity, and gas content all contribute to the observed decrease in cavitation threshold as the temperature of the liquid sodium is increased. In comparing the magnitude of the effects of these liquid properties it appears that the surface tension effect was significant in that surface tension is reduced from 176 to 120 dynes/cm for a temperature increase from 500 to 1500°F. For the same temperature increase the solubility of argon in sodium increases from 92 to 160 ppm and this may appreciably affect the cavitation threshold. The effects of vapor pressure also affect the cavitation threshold. Even though the total change in the vapor pressure is only approximately 8 psi, the vapor pressure for liquid sodium at 1500°F is approximately $1.5 \times 10^4$ times the vapor pressure at 500°F. Thus this relative change in the vapor pressure may significantly affect the cavitation threshold. The viscosity decreases for increasing temperature; however, it is felt that this affect is relatively small.

## H. Conclusion to Chapter V

The onset and cessation of cavitation were obtained in liquid sodium in a temperature range of 500 to 1500°F and in a frequency range from 14 to 25 kHz. The scatter in the data, fluid nonlinearity, frequency dependence, and temperature dependence were investigated, and it was found that the behavior of these characteristics compared well with similar data reported in the literature for water. The frequency and temperature dependence found in the onset and

cessation data were related to surface tension, viscosity, inertial effects, gas content, and vapor pressure, and to the changes in these properties for changes in temperature.

The bottom surfaces of the test specimens used in the experiment were smooth surfaces and are similar to the type of surfaces found in a sodium cooled nuclear reactor. Analysis of a sodium sample used in the experiment indicated the impurity level was within the range of impurity concentrations found in a sodium cooled reactor. It is therefore felt that the data obtained in this experiment can be realistically related to the sodium behavior in a sodium cooled nuclear reactor where it may be subjected to a pulsing pressure or temperature field for a variety of causes (pump performance, reactivity changes, etc.).

# CHAPTER VI

## CONVERSION OF THE ONSET OF CAVITATION DATA TO SODIUM SUPERHEAT REQUIREMENTS

### A. Introduction

The primary objective of this investigation was to determine the superheat requirements necessary to produce nucleate boiling in liquid sodium. The superheat requirements were to be determined as a function of the temperature of the liquid sodium and as a function of the heating rate (rate of increase in temperature per unit time). As outlined in Chapter I the superheat requirements were to be determined ultrasonically by investigating the conditions at the onset of cavitation in liquid sodium. Knowing the changes in liquid pressure necessary to produce cavitation the superheat requirements can be established by converting the changes in pressure to changes in temperature necessary to produce nucleate boiling in liquid sodium. As discussed in Chapter V the onset of cavitation was established in liquid sodium both as a function of the liquid sodium temperature and as a function of the frequency of the applied pressure field. The following sections of this chapter discuss the conversion of the onset of cavitation data to changes in liquid pressure required to produce cavitation in liquid sodium. From these values of liquid pressure the superheat requirements necessary to

produce nucleate boiling are determined as a function of temperature and as a function of heating rate.

## B. Calculation of Changes in Pressure Required at the Onset of Cavitation

As discussed in Chapter V the onset of cavitation in liquid sodium was determined both as a function of the liquid sodium temperature and as a function of the frequency of the applied pressure field. The onset of cavitation data obtained using the four different transducer horn assemblies is shown in Fig 38 of Chapter V in which the counterweight crystal voltage at the onset of cavitation is plotted as a function of the sodium temperature. As pointed out in Chapter III the counterweight crystal output voltage is an indirect measurement of the vibrational displacement of the tip of the horn. By referring to the counterweight crystal calibration curves shown in Fig 36 of Chapter V obtained for each of the four transducer horn assemblies, the displacement of the tip of the transducer horn assembly at the onset of cavitation can be determined. It is shown in Chapter III that Eq (3.4) represents the pressure field produced by the vibrational motion of the tip of the horn assembly inside the cavitation vessel. The onset of cavitation occurs at the point of maximum changes in pressure and it was determined in Chapter III that this point is located at the center of the bottom surface of the test specimen, i. e., at the point $\bar{r} = 0$ and $\bar{z} = 0$. With $\bar{r} = 0$ and $\bar{z} = 0$, Eq (3.4) becomes

$$P'(0,0) = \bar{\ell}\bar{k}\rho_0 U_0 C \left\{ \frac{\lambda^2 \cos(\bar{\ell}\bar{k})}{\bar{\ell}\bar{k}\,\sin(\bar{\ell}\bar{k})} + 2\lambda \sum_{j=1}^{\infty} \frac{\cos(\bar{\ell}\bar{k})\, J_1(\alpha_j \lambda)}{\alpha_j \bar{H}_j J_0^2(\alpha_j)} \right\} \sin \omega t \qquad (6.1)$$

All parameters necessary to evaluate Eq (6.1) are known. The density, $\rho_0$, and the velocity of sound in liquid sodium, $C$, which are functions of temperature are known quantities and can be found in the literature.[41, 77] The angular velocity, $\omega = 2\pi f$, was measured at the onset of cavitation using an electronic frequency counter. The tip displacement, A, was determined by observing the counterweight crystal output voltage and by using the appropriate calibration curve. The geometry of the system was determined from the experimental apparatus. As shown in Chapter III the pressure field produced by the transducer horn assembly has a sinusoidal time dependence. However, for the present study we are primarily interested in maximum changes in pressure which are produced by the transducer horn assembly. By considering the peak values of the sinusoidal pressure field and by considering the point $\bar{r} = 0$ and $\bar{z} = 0$ in the pressure field the resulting pressure calculations provide the maximum changes in pressure imposed on the liquid sodium at the onset of cavitation. The selection of the peak value of the pressure field is discussed further in Section C of this chapter.

Using the onset of cavitation data shown in Fig 38 Eq (6.1) was evaluated using the General Electric 235 digital computer. A total number of 250 terms of the infinite series

were considered since as shown in Chapter III additional terms of the series provided a negligible effect on the final sum. Plotted in Fig 41 are the resulting peak values of the pressure field produced by the vibrational motion of the tip of the transducer horn assembly as a function of the sodium temperature for the four different transducer horn assemblies used in the experiment. Fig 41 illustrates the linear temperature dependence on the onset of cavitation which is discussed in detail in Chapter V. To better indicate the frequency dependence on the peak pressures of the pressure field at the onset of cavitation the data in Fig 41 were replotted in Fig 42 as curves of peak pressure versus frequency for the various liquid sodium temperatures. This frequency dependence is discussed in Chapter V.

Although the primary purpose of this investigation was to obtain superheat requirements for liquid sodium the data obtained on changes in liquid pressure required to produce cavitation as a function of frequency is desirable in predicting the behavior of sodium cooled nuclear reactors under operating conditions in which pressure fluctuations may exist in the sodium. As discussed in Chapter I the primary reason for investigating conditions leading to boiling is that boiling changes the sodium void coefficient which in turn affects the nuclear reactivity of the reactor. In a similar manner cavitation bubbles within the reactor may also affect reactivity in addition to producing erosive damage to sodium containment surfaces as discussed in Chapter IV.

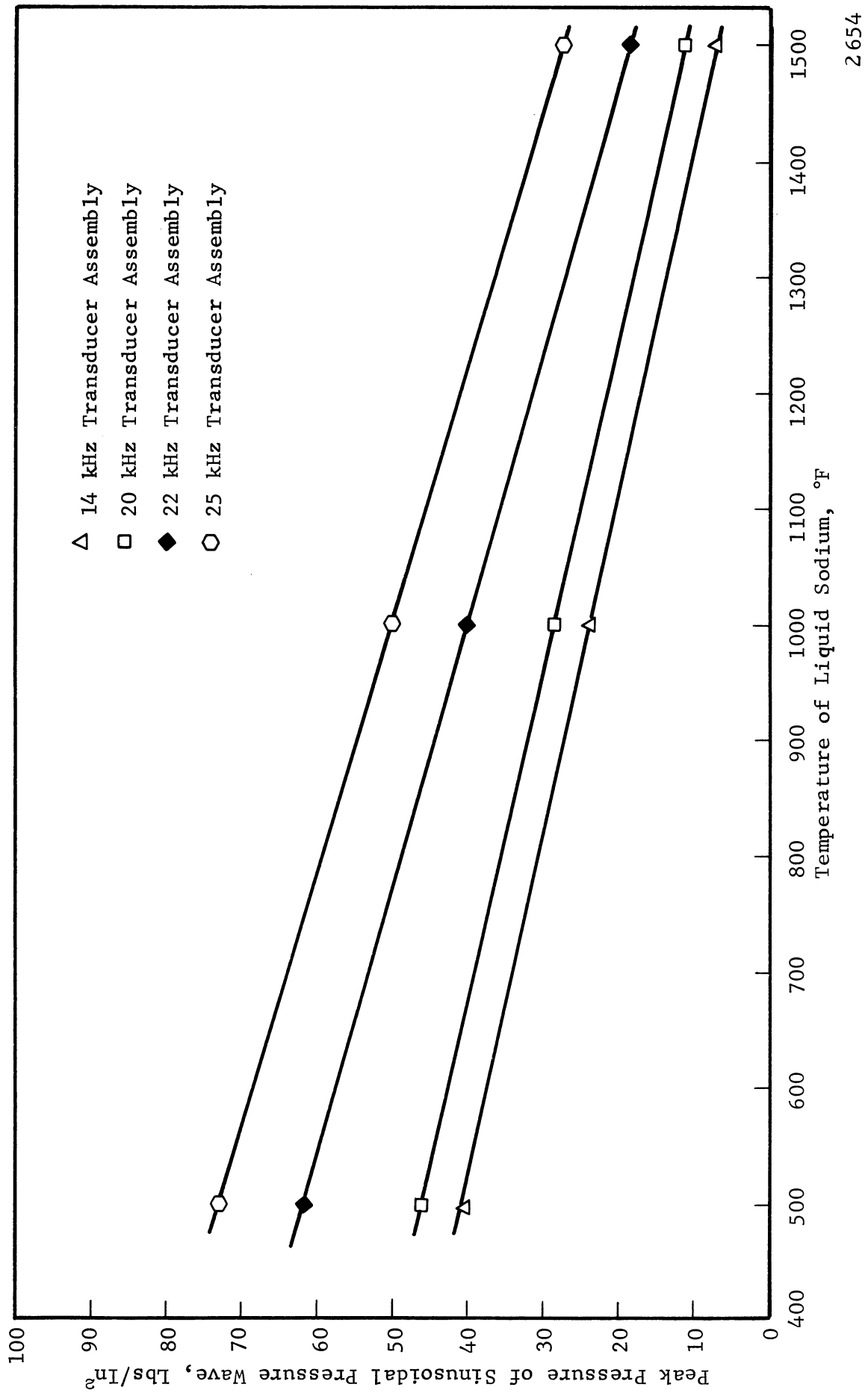


FIGURE 41. PEAK PRESSURE OF SINUSOIDAL PRESSURE WAVE AT ONSET OF CAVITATION VERSUS LIQUID SODIUM TEMPERATURE USING THE 14, 20, 22, AND 25 KHZ TRANSDUCER HORN ASSEMBLIES

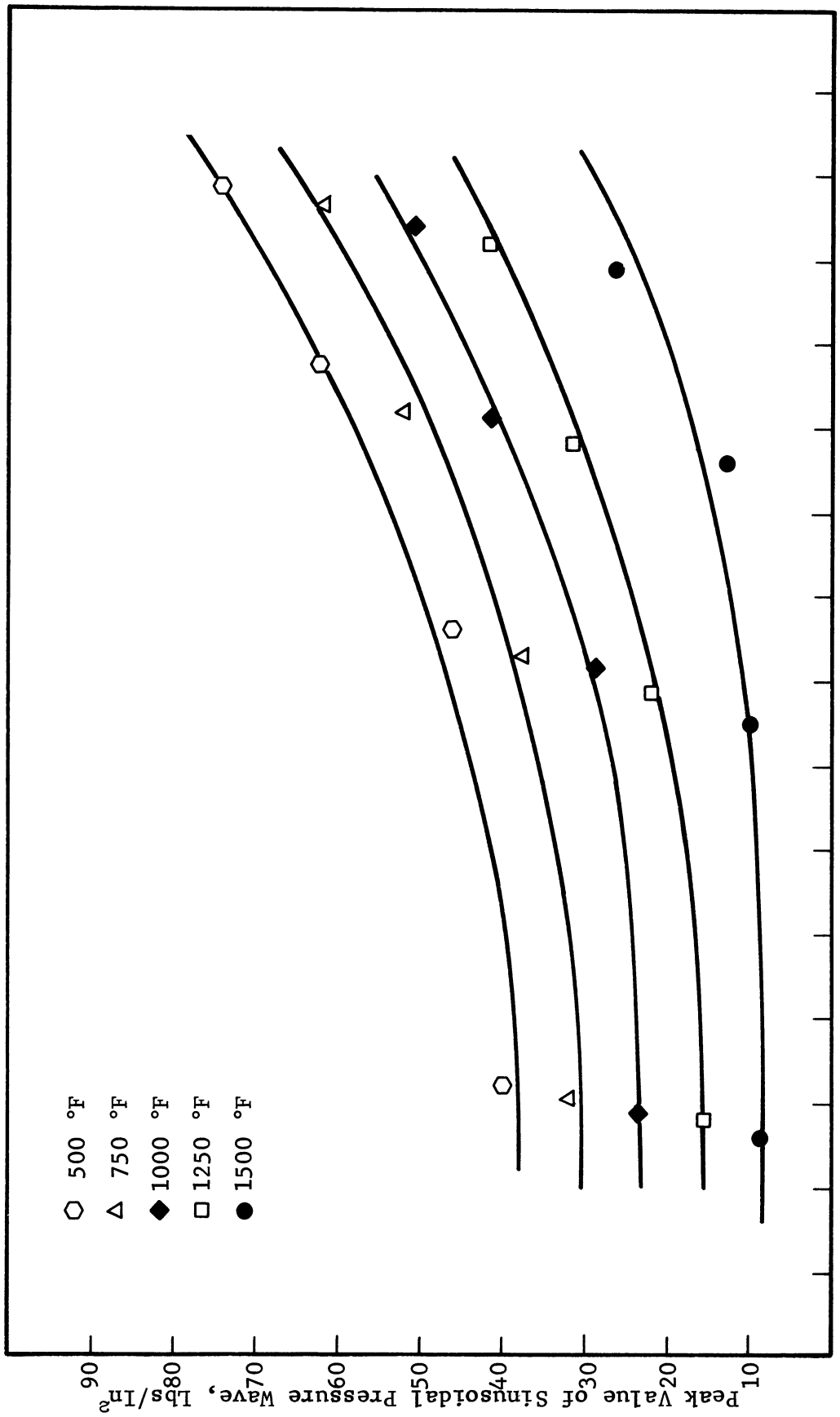


FIGURE 42. PEAK VALUE OF SINUSOIDAL PRESSURE WAVE AT ONSET OF CAVITATION VERSUS FREQUENCY FOR LIQUID SODIUM TEMPERATURES 500, 750, 1000, 1250, AND 1500 °F

A possible source of pressure fluctuations which may produce cavitation in a reactor was suggested by Lotz and Raabe.[78] They investigated the blade oscillations in one-stage axial turbomachinery and determined that pressure fluctuations may be produced with magnitudes ranging up to approximately 20 per cent of total output pressure. Coolant pumps which circulate the sodium through the reactor may then be sources of large pressure fluctuations which may conceivably produce cavitation within the reactor even though the time mean pressure is everywhere well above the vapor pressure.

## C. Review of the Cavitation Process

Before discussing the conversion of the onset of cavitation data to superheat requirements it is necessary to first review the process involved in initiating cavitation in a liquid.

Cavitation is produced in a liquid generally by a pressure change in the liquid (conceivably caused by a variety of possible mechanisms) such that the local liquid pressure becomes less than the vapor pressure of the liquid. In order for nucleation and bubble growth to occur in the liquid when the liquid pressure is reduced, nucleation sites must exist in the liquid. As pointed out in Chapter I, these sites may consist of nonwetted cracks or crevices in the surface of the fluid container or these sites may be small spherical bubbles containing vapor and/or gas which are stabilized in the liquid.

For this investigation it is assumed that the nucleation sites consist of small spherical vapor bubbles of radius R.

For liquid sodium with an argon cover gas it is assumed that the gas content is zero since it is pointed out in Chapter V that the solubility of argon in sodium is very low. For a spherical bubble with zero gas content in the liquid, the amount that the liquid pressure must be reduced below the vapor pressure is given by Eq (1.1) of Chapter I which is restated here for purposes of discussion.

$$P_V - P_L = 2\sigma/R \qquad (1.1)$$

Therefore, to initiate cavitation in liquid sodium, a pressure change must be applied to the liquid sodium which contains spherical vapor bubbles of radius R. If this change in the liquid pressure is sufficient to overcome the surface tension force, such that Eq (1.1) is satisfied, bubble growth or cavitation will be initiated.

If an ultrasonic facility is used to produce cavitation in a liquid the changes in liquid pressure are produced by applying a sinusoidally varying pressure field to the liquid. Fig 43 illustrates the relationships among the vapor pressure, $P_V$, the argon cover gas pressure, $P_a$, and the applied pressure field, $P_o \sin \omega t$. The hydrostatic pressure due to the submergence of the tip of the horn in the liquid sodium is small and may be neglected. The applied sinusoidal pressure field then alternates about the applied gas pressure which for the present experiment was maintained at 15.0 psia. With the application of the alternating pressure field the liquid pressure, $P_L$, becomes

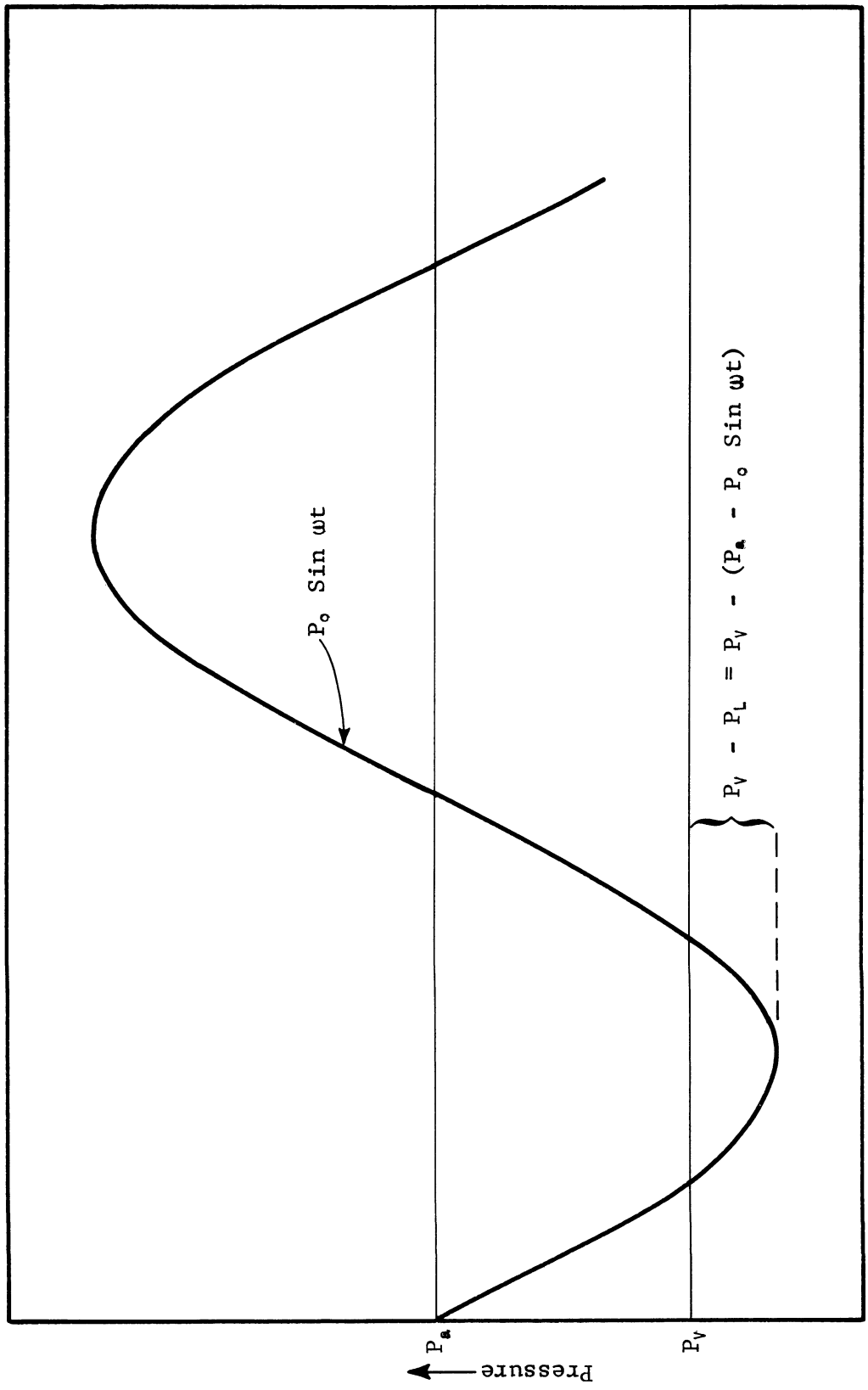


FIGURE 43. RELATIONSHIPS AMONG ATMOSPHERIC PRESSURE, $P_a$, VAPOR PRESSURE, $P_v$, AND APPLIED SINUSOIDAL PRESSURE FIELD, $P_o$ Sin ωt

$$P_L = P_a - P_o \sin \omega t \qquad (6.2)$$

As shown in Fig 43 the liquid pressure must be reduced to some value below the vapor pressure to satisfy Eq (1.1) and to initiate cavitation in the liquid. Substituting Eq (6.2) into Eq (1.1) we obtain

$$P_v - (P_a - P_o \sin \omega t) = 2\sigma/R$$

or

$$P_o \sin \omega t + P_v - P_a = 2\sigma/R. \qquad (6.3)$$

A question now arises as to the response of the liquid sodium to the alternating pressure field. In other words, is it an acceptable approximation to assume that cavitation is produced in the liquid when the peak value, $P_o$, of the alternating pressure field satisfies Eq (6.3) such that

$$P_o + P_v - P_a = 2\sigma/R$$

or must it be assumed that cavitation is produced when some average value of the alternating pressure field, $\bar{P}$, satisfies Eq (6.3) such that

$$\bar{P} + P_v - P_a = 2\sigma/R \quad ?$$

A second question must also be considered. How does the amplitude of a sinusoidal varying pressure field compare with the amplitude of a single pressure pulse if the amplitudes

in either case are just sufficient to produce cavitation? In other words, will the response of the liquid to a sinusoidal pressure signal be essentially the same as the liquid response to a single pressure pulse whose amplitude and application time are equal to that of a single sine wave oscillation.

Results have been reported by Flynn[79, 80] in which the response of the liquid to a sinusoidal varying pressure signal was compared to the response of the liquid to a single pressure pulse. Flynn calculated that the behavior of a cavity in a liquid under a pulse or sinusoidal excitation is practically the same for a given initial radius. In an example cited by Flynn, he found that a single negative pressure pulse with a width of 10 microsec and an amplitude of 5 bars was equivalent to a continuous sinusoidal pressure wave with a period of 68 microsec and an amplitude of 4 bars. In this example the application time of the negative pressure pulse of the sine wave was 34 microsec and its mean pulse width was 19 microsec. From this example it is noted that the amplitudes of the two pressure signals are similar and the mean pulse widths differ only by a factor of two. There is considerable detail and difficulty involved in converting a sinusoidal pressure wave to an equivalent single pressure pulse, and therefore this conversion has been assumed to be outside of the particular scope of this study. Because of the similarities in amplitudes and application times between a single pressure pulse and a sine wave pressure signal it has been assumed for this study that the response of the fluid

to the sinusoidal pressure wave can be considered to be at least approximately the same as the response of the fluid to a single pressure pulse. It is realized that this assumption is not exact; however, it is felt the results will provide an initial understanding of sodium superheat requirements and the time dependence of these superheat requirements, as well as providing exact data for response to a sinusoidal pressure or temperature variation, either of which may be important in sodium cooled fast reactors. Also it may be possible to construct the response to other types of pressure and temperature variations by Fourier analysis techniques using the measured response to the sinusoidal case. It is recommended in Chapter VII that a continuation of this study include the conversion of the sinusoidal pressure waves to single pressure pulse so that a more exact interpretation of the superheat requirements and their time dependence can be made.

In view of our assumption that the liquid responds to the peak value of the sinusoidal pressure field at the onset of cavitation, Eq (6.3) becomes

$$P_o + P_v - P_a = 2\sigma/R \qquad (6.4)$$

As shown in the previous section of this chapter $P_o$ is determined from the data recorded at the onset of cavitation. $P_v$ and $\sigma$ which are functions of temperature are known quantities. $P_a$ was held constant at 15.0 psia. Thus the radius of the vapor bubble which serves as the nucleation site becomes the only unknown quantity and this quantity can be determined

from Eq (6.4). In other words, for frequencies below 20 kHz by determining the change in liquid pressure required to produce cavitation the radius of the vapor bubble existing in the liquid which serves as a nucleation site can be determined. For frequencies above 20 kHz it was mentioned in Chapter V that inertial effects begin to affect the onset of cavitation appreciably with the result that changes in liquid pressure at the onset of cavitation are affected not only by the value of R but also by inertial effects. Recognizing this effect at higher frequencies an effective bubble radius, R', can be utilized such that the equation

$$P_o + P_v - P_a = 2\sigma/R' \qquad (6.5)$$

can be used for all frequencies. For frequencies below 20 kHz the effective radius R' is equal to the radius of the bubble serving as the nucleation site. For frequencies above 20 kHz R' represents a bubble of reduced radius with the reduction in radius taking into account inertial effects and possibly viscous effects. Thus by utilizing the onset of cavitation data in Eq (6.5) the resulting effective radii not only define the radii of the bubbles serving as nucleation sites but also reflect the frequency dependence of the onset of cavitation requirements.

D. Conversion to Superheat Requirements

It is pointed out in Chapter I that in order to produce nucleate boiling or cavitation in a liquid, Eq (1.1) of Chapter I must first be satisfied. Eq (1.1) is restated here for

discussion purposes.

$$P_V - P_L = 2\sigma/R \qquad (1.1)$$

In the cavitation case, Eq (1.1) is satisfied by maintaining the temperature of the liquid constant and by lowering the liquid pressure, $P_L$, until bubble growth occurs. In the heat transfer case, the liquid pressure is held constant and the liquid temperature is increased until the vapor pressure, $P_V$, associated with this increase in temperature satisfies Eq (1.1). If it is assumed that thermal equilibrium exists at the bubble wall, then the temperature of the liquid is equal to the temperature of the vapor inside the bubble.[19, 81] Therefore, in order to satisfy Eq (1.1) the increased liquid temperature becomes equal to the saturation temperature corresponding to the vapor pressure, $P_V$.

As defined in Chapter I, superheat is the amount that the temperature of the liquid must be increased above its "boiling point," i. e., above the saturation temperature corresponding to the pressure of the liquid, in order to produce nucleate boiling in the liquid. In satisfying Eq (1.1) the required superheat becomes

$$\text{superheat} = T_V - T_{sat}$$

where the saturation temperature corresponding to $P_V$ is generally referred to as $T_V$ and the saturation temperature corresponding to the liquid pressure $P_L$ is referred to as $T_{sat}$.[19, 81]

Generally in the heat transfer case, the pressure of the liquid, $P_L$, and hence $T_{sat}$ are known and the temperature of the liquid is increased until boiling occurs. The temperature at which nucleate boiling occurs becomes $T_v$ and the difference $T_v - T_{sat}$ becomes the measured superheat for the liquid. By determining the saturation pressure corresponding to $T_v$ and by using Eq (1.1) the quantity $2\sigma/R$ can be determined. The quantity $2\tau/R$ which is temperature dependent is associated with the temperature $T_v$ since the liquid is at this temperature at the time nucleate boiling occurs.

In using cavitation techniques to determine superheat requirements, the process is reversed. By measuring the change in pressure required at the onset of cavitation, the quantity $2\sigma/R$ can be determined. The quantity $2\sigma/R$ is a function of the liquid temperature at the onset of cavitation and hence the temperature of the liquid which is held constant during the cavitation process is identified as $T_v$. The difference between the saturation pressure corresponding to the liquid temperature and the quantity $2\sigma/R$ is then equal to the saturation pressure corresponding to $T_{sat}$. The required superheat becomes $T_v - T_{sat}$ which is the same difference as in the heat transfer case.

Summarizing, we have the following steps in converting the onset of cavitation data to superheat requirements.

1. From the onset of cavitation data determine the corresponding quantity $2\sigma/R'$ using Eq (6.5). As discussed in the previous section Eq (6.5) is derived from Eq (1.1) in

which $P_L$ is replaced by $P_a - P_o$ and the bubble radius R is replaced by an effective bubble radius R' to account for the frequency dependence of the cavitation data.

2. Identify the temperature of the liquid at the onset of cavitation as the temperature $T_v$.

3. For a particular value of $T_v$ determine the difference between the saturation pressure corresponding to $T_v$ and the value of $2\sigma/R'$ determined from the cavitation data for the chosen value of $T_v$. This difference becomes the saturation pressure corresponding to $T_{sat}$.

4. From the curve of saturation pressure versus saturation temperature for liquid sodium determine $T_{sat}$. The temperature difference $T_v - T_{sat}$ is then the required superheat. The interpretation of this superheat requirement is that liquid sodium with a boiling point of $T_{sat}$ must be heated to $T_v$ before nucleate boiling occurs in the liquid.

Following the above outlined steps the onset of cavitation data shown in Fig 42 were converted to sodium superheat requirements. Shown in Fig 44 are curves of $2\sigma/R'$ versus $T_v$ for 14.0. 17.5, 21.0, and 24.5 kHz. These frequencies were selected from the onset of cavitation data since they divided the frequency range used in this study into four equal segments. The curves of $2\sigma/R'$ were determined using the data in Fig 42 and Eq (6.5). Listed in Table 7 are the numerical values used in the calculation of the sodium superheat. It was necessary to extrapolate the $2\sigma/R'$ curves for the 21.0 and 24.5 kHz frequencies since at relatively low temperatures the

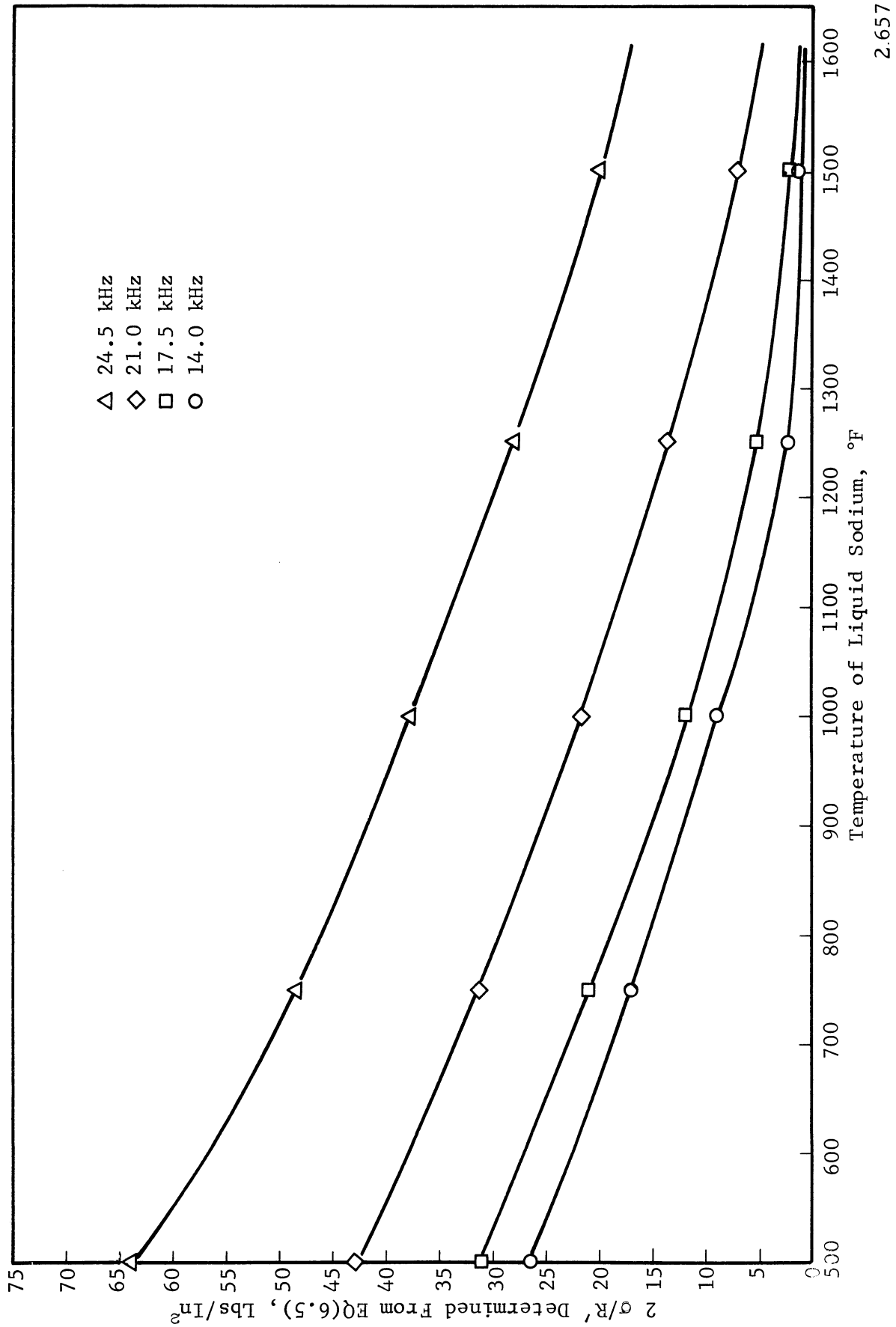


2.657

FIGURE 44. 2 σ/R′ VERSUS TEMPERATURE OF LIQUID SODIUM AT THE ONSET OF CAVITATION FOR 14, 17.5, 21, AND 24.5 kHz

TABLE 7

NUMERICAL VALUES USED IN THE CALCULATION OF SODIUM SUPERHEAT

| Freq kHz | $T_v$ °F | $P_v$* psi | $2\sigma/R'$** psi | $P_L$ psi | $T_{sat}$* °F | $T_v - T_{sat}$ °F |
|---|---|---|---|---|---|---|
| 14.0 | 1500 | 7.88 | 1.10 | 6.78 | 1473 | 27 |
| 14.0 | 1400 | 4.28 | 1.15 | 3.13 | 1353 | 47 |
| 14.0 | 1350 | 3.06 | 1.30 | 1.76 | 1271 | 79 |
| 14.0 | 1300 | 2.12 | 1.55 | 0.57 | 1120 | 180 |
| 14.0 | 1275 | 1.80 | 1.78 | 0.02 | 821 | 454 |
| 17.5 | 1500 | 7.88 | 1.70 | 6.18 | 1458 | 42 |
| 17.5 | 1450 | 5.85 | 2.15 | 3.70 | 1376 | 74 |
| 17.5 | 1400 | 4.27 | 2.75 | 1.52 | 1252 | 148 |
| 17.5 | 1370 | 3.54 | 3.10 | 0.44 | 1105 | 265 |
| 17.5 | 1361 | 3.32 | 3.30 | 0.02 | 821 | 540 |
| 21.0 | 1600 | 13.28 | 4.70 | 8.58 | 1515 | 85 |
| 21.0 | 1550 | 10.18 | 5.60 | 4.58 | 1410 | 140 |
| 21.0 | 1500 | 7.88 | 6.80 | 1.08 | 1207 | 293 |
| 21.0 | 1485 | 7.27 | 7.20 | 0.07 | 925 | 560 |
| 21.0 | 1484 | 7.22 | 7.21 | 0.01 | 775 | 709 |
| 24.5 | 1750 | 27.82 | 14.10 | 13.72 | 1608 | 142 |
| 24.5 | 1700 | 22.00 | 15.20 | 6.80 | 1476 | 224 |
| 24.5 | 1675 | 19.56 | 15.70 | 3.86 | 1383 | 292 |
| 24.5 | 1650 | 17.12 | 16.30 | 0.82 | 1173 | 477 |
| 24.5 | 1642 | 16.51 | 16.50 | 0.01 | 775 | 867 |

* Obtained from reference (72)

** Obtained from Fig 44

resulting difference between the saturation pressure corresponding to $T_v$ and the quantity $2\sigma/R'$ becomes negative and cannot be used as a saturation pressure for $T_{sat}$. Plotted in Fig 45 are the resulting curves of superheat versus liquid sodium saturation temperature for 14.0. 17.5, 21.0, and 24.5 kHz. To indicate the frequency dependence the data in Fig 45 were replotted in Fig 46 as curves of superheat requirements versus frequency for the saturation temperatures of 500. 750. 1000, 1250, and 1500°F.

It is pointed out in Chapter I that Eq (1.3) is used to determine superheat requirements for nucleate boiling in a liquid. Thus it would be of interest to compare the results using Eq (1.3) with the results shown in Fig 45. Eq (1.3) which is derived in Appendix A is restated here for discussion purposes.

$$T_v - T_{SAT} = \frac{G T_v T_{SAT}}{h} \ln\left(1 + \frac{2\sigma}{R P_e}\right) \qquad (1.3)$$

As shown in Appendix A Eq (1.3) is obtained by integrating the Clausius-Clapeyron equation from the saturated conditions to the superheated conditions in the liquid. The Clausius-Clapeyron equation relates changes in pressure to changes in temperature along the saturation line.[82] In the integration it is assumed that the vapor in a spherical vapor bubble is an ideal gas, the latent heat, $h$, is a constant, and that the specific volume of liquid is much smaller than the specific volume of vapor and can be neglected. It is pointed out by Edwards and Hoffman[19] that the Clausius-Clapeyron equation

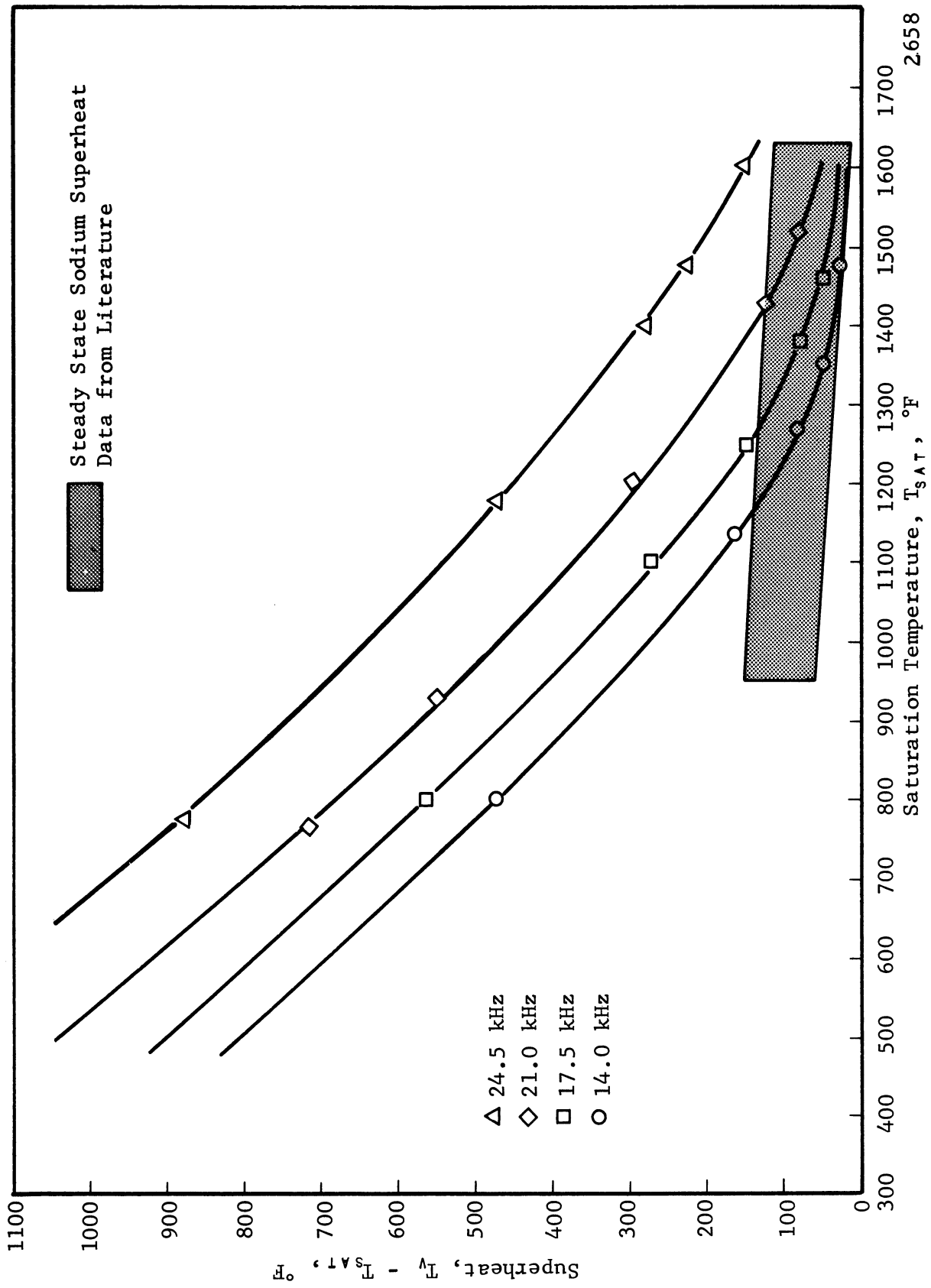


FIGURE 45. LIQUID SODIUM SUPERHEAT VERSUS SATURATION TEMPERATURE FOR 14.0, 17.5, 21.0, AND 24.5 kHz

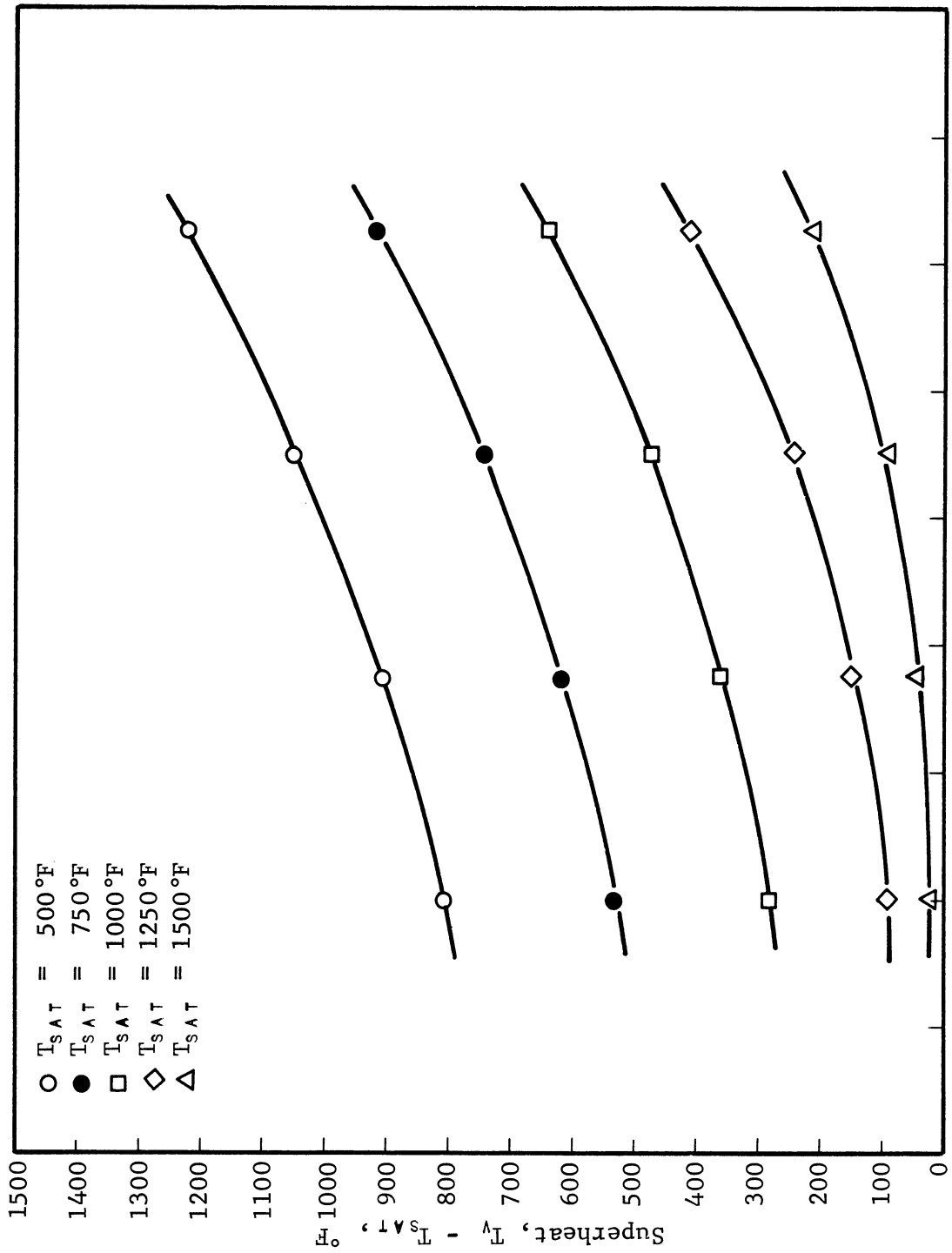


FIGURE 46. LIQUID SODIUM SUPERHEAT VERSUS FREQUENCY FOR SATURATION TEMPERATURES 500, 750, 1000, 1250, AND 1500 °F

applies only along the saturation line where $P_V$ is equal to $P_L$ and in the superheating process $P_V$ is not equal to $P_L$. However, the Clausius-Clapeyron equation is used in the derivation of Eq (1.3) to provide an approximation for the superheat requirement.

Listed in Table 8 are the sodium superheat results obtained using Eq (1.3). For a particular value of $T_V$, the corresponding value of $T_{sat}$ was obtained from Fig 45. Values of $G$ and $h$ for $T_V$ were obtained from reference (72) and $P_L$ corresponding to the temperature $T_{sat}$ was also obtained from reference (70). The value of $2\sigma/R'$ corresponding to $T_V$ was obtained from Fig 44. The resulting value of $T_V - T_{sat}$ was calculated using Eq (1.3). In this calculation the temperatures were converted to degrees Rankine since the thermodynamic relationships used in the derivation of Eq (1.3) are defined in terms of absolute temperatures.

Also listed in Table 8 are the corresponding values of sodium superheat taken from Fig 45. In comparing the superheat results from Fig 45 and the results obtained using the superheat equation, Eq (1.3), it can be seen that the results are essentially identical. Thus the approximations used in the derivation of Eq (1.3) appear to be reasonable approximations at least over the temperature range used in Table 8.

## E. Discussion of Superheat Results

From the curves of $2\sigma/R'$ versus temperature of liquid sodium the effective bubble radius, $R'$, can be determined. As

TABLE 8

NUMERICAL VALUES USED IN THE COMPARISON OF SODIUM SUPERHEAT RESULTS USING EQ (1.3) WITH RESULTS SHOWN IN FIG 45

| Freq kHz | $T_v$ °F | $T_{sat}$ °F | $P_L$ [a] psi | G [a] ft/°R | h [a] BTU/lb | $2\sigma/R'$ [b] psi | $T_v - T_{sat}$ [c] °F | $T_v - T_{sat}$ [d] °F |
|---|---|---|---|---|---|---|---|---|
| 14.0 | 1500 | 1473 | 6.78 | 57.8 | 1654 | 1.10 | 25 | 25 |
| 14.0 | 1400 | 1353 | 3.13 | 58.8 | 1678 | 1.15 | 48 | 50 |
| 14.0 | 1350 | 1271 | 1.76 | 59.2 | 1693 | 1.30 | 78 | 80 |
| 14.0 | 1300 | 1120 | 0.57 | 59.7 | 1707 | 1.55 | 164 | 165 |
| 14.0 | 1275 | 821 | 0.02 | 59.9 | 1700 | 1.78 | 453 | 475 |
| 17.5 | 1500 | 1458 | 6.18 | 57.8 | 1654 | 1.70 | 41 | 40 |
| 17.5 | 1450 | 1376 | 3.70 | 58.2 | 1665 | 2.15 | 72 | 75 |
| 17.5 | 1400 | 1252 | 1.52 | 58.8 | 1678 | 2.75 | 149 | 150 |
| 17.5 | 1370 | 1105 | 0.44 | 59.0 | 1688 | 3.10 | 269 | 275 |
| 17.5 | 1361 | 821 | 0.02 | 59.1 | 1690 | 3.30 | 538 | 565 |
| 21.0 | 1600 | 1515 | 8.58 | 57.4 | 1631 | 4.70 | 81 | 85 |
| 21.0 | 1550 | 1410 | 4.58 | 57.6 | 1642 | 5.60 | 136 | 140 |
| 21.0 | 1500 | 1207 | 1.08 | 57.8 | 1654 | 6.80 | 292 | 293 |
| 21.0 | 1485 | 925 | 0.07 | 58.0 | 1658 | 7.20 | 562 | 560 |
| 21.0 | 1484 | 775 | 0.01 | 58.1 | 1659 | 7.21 | 713 | 709 |
| 24.5 | 1750 | 1608 | 13.72 | 56.4 | 1594 | 14.10 | 147 | 142 |
| 24.5 | 1700 | 1476 | 6.80 | 56.6 | 1606 | 15.20 | 223 | 224 |
| 24.5 | 1675 | 1383 | 3.86 | 56.9 | 1612 | 15.70 | 290 | 292 |
| 24.5 | 1650 | 1173 | 0.82 | 57.2 | 1618 | 16.30 | 476 | 477 |
| 24.5 | 1642 | 775 | 0.01 | 57.3 | 1621 | 16.50 | 875 | 867 |

[a] Obtained from reference (72)
[b] Obtained from Fig 44
[c] Calculated using Eq (1.3)
[d] Obtained from Fig 45

pointed out in Chapter V, the surface tension of liquid sodium decreases linearly from 176 dynes/cm at 500°F to 120 dynes/cm at 1500°F.[73] Knowing the values of surface tension as a function of temperature the effective radius R' was calculated and varies from $0.80 \times 10^{-4}$ cm at 500°F and 24.5 kHz to $31.7 \times 10^{-4}$ cm at 1500°F and 14 kHz. For constant frequency the effective bubble radius R' increases for increasing temperature. For example, at 14 kHz the effective bubble radius increases from $1.93 \times 10^{-4}$ cm at 500°F to $31.7 \times 10^{-4}$ cm at 1500°F. In other words, as the temperature at which boiling occurs in the liquid is increased the effective radius of the bubble serving as the nucleation site is increased. Physically this appears reasonable for several reasons. As the temperature is increased the surface tension is reduced and this would tend to increase the radius of the bubble stabilized in the liquid. The vapor pressure, $P_v$, increases with temperature with the possible result that the radius of the bubble would be increased. The solubility of argon in liquid sodium increases with temperature and this solubility may contribute to a larger radius for the bubble stabilized in the fluid. However, it should be emphasized that the mechanisms involved in the stabilization of these spherical bubbles are not known and the exact effect of the changes in the above mentioned variables cannot be determined although the effects as outlined above appear reasonable in accounting for the increase in R' for an increase in temperature.

It is noted that for a constant liquid sodium temperature

the effective radius R' decreases for increasing frequency. As discussed in the previous section this decrease in R' provides for the frequency dependence of the onset of cavitation data, and is presumably primarily a result of inertial resistance to bubble growth in the liquid.

In reviewing the numerical values calculated for the effective bubble radius it is observed that for temperatures below 1000°F, the values of R' are on the order of $10^{-4}$ cm which was the value assumed for the radius in the discussion on frequency dependence in Chapter V. Since there is good agreement between the theoretical frequency dependence using a bubble radius of $10^{-4}$ cm and the experimentally determined frequency dependence, the above calculated values of R' appear to be reasonable values.

The curves of superheat required to initiate nucleate boiling in liquid sodium versus saturation temperature shown in Fig 45 indicate that as the saturation temperature is increased the required superheat decreases. This behavior is primarily due to two effects. First, the superheat requirement is proportional to the quantity $2\sigma/R'$ and it can be seen from Fig 44 that $2\sigma/R'$ decreases for increasing sodium temperature. Second, in converting changes in pressure to changes in temperature using the saturation line for liquid sodium it is noted that for a constant change in pressure the corresponding changes in saturation temperature decreases for higher liquid temperatures.[70] In other words, because of the nonlinearity of the saturation line for liquid sodium a change in pressure

required to produce cavitation would result in a much larger superheat requirement for a relatively low value of temperature compared to the same change in pressure at a relatively high value of temperature. Therefore, the combination of the reduction in the measured $2\sigma/R'$ for increasing liquid sodium temperature and the nonlinearity of the saturation line for liquid sodium results in a decrease in superheat for an increase in saturation temperature.

The decrease in superheat requirements for increasing $T_{sat}$ can also be explained by reviewing the superheat equation, Eq (1.3). From Eq (1.3) it can be seen that the superheat is proportional to the term $T_v T_{sat}$. An increase in $T_{sat}$ increases the term $T_v T_{sat}$ which would tend to increase the superheat requirements. For example, with $T_{sat} = 821^{\circ}F$ and with a frequency of 14 kHz, the required $T_v$ is $1275^{\circ}F$. Converting to degrees Rankine, the product becomes $2.20 \times 10^6$. For $T_{sat} = 1473^{\circ}F$ the required $T_v$ is $1500^{\circ}F$ and this product becomes $3.80 \times 10^6$. Thus by increasing $T_{sat}$ from 821 to $1473^{\circ}F$ the term $T_v T_{sat}$ increases by a factor of 1.73. However, from Eq (1.3) it can be seen that the required superheat is also proportional to the term $\ln(1 + 2\sigma/R'P_L)$. At $T_{sat} = 821^{\circ}F$ and for a frequency of 14 kHz $2\sigma/R'$ is 1.75 psi and $P_L$ is 0.02 psi. At $T_{sat} = 1473^{\circ}F$, $2\sigma/R'$ becomes 1.10 psi and $P_L = 6.78$ psi. Thus by increasing the saturation temperature from 821 to $1473^{\circ}F$ the term $\ln(1 + 2\sigma/R'P_L)$ decreases by a factor of 30 and thus dominates the small increase in the term $T_v T_{sat}$. The remaining term in the superheat equation,

$G/h$, remains essentially constant over the range of $T_v$ used in the calculations.

The frequency dependence on the superheat requirements is shown in Fig 46. It is noted that the superheat requirements increase slowly as the frequency is increased from 14 to approximately 18 kHz. For frequencies above 18 kHz the superheat requirements increase more rapidly. This frequency dependence was expected in the superheat requirements since as discussed in the previous section an effective bubble radius R' was utilized in transforming the onset of cavitation data to superheat requirements. This effective radius provided essentially identical frequency dependence in the superheat requirements as was determined for the onset of cavitation data.

As discussed above the superheat requirements for frequencies from 14 to approximately 18 kHz are essentially independent of frequency and as such should be comparable to superheat requirements determined from steady state heat transfer experiments. The majority of the sodium superheat requirements reported in the literature were determined from essentially steady state heat transfer experiments in which the increase in temperature necessary to produce boiling in the liquid sodium was applied over relatively long periods of time compared to application times utilized in this study. Holtz and Singer[83] presented a comparison of currently available data on sodium superheating taken from seven different sources. The majority of the superheat reported by Holtz and Singer

lies within the shaded area shown in Fig 45. In comparing the results of this investigation with the data represented by the shaded area in Fig 45 it is noted that the curves of superheat requirements for the frequencies 14 and 17.5 kHz are within this shaded area for saturation temperatures from approximately 1150 to 1600°F. In other words, there appears to be reasonably good agreement between the frequency independent data of this study and the data reported in the literature for comparable values of $T_{sat}$. It would be difficult to obtain a more exact comparison because of the many variables that can affect superheat behavior of liquid sodium. As discussed by Fauske[84] these variables include heat flux, heating surface, fluid velocity, pressure, pressure-temperature history, aging, purity, radiation, and heating method. However, it is encouraging to note that the sodium superheat data obtained using cavitation techniques does fall within the range of superheat data obtained using heat transfer techniques.

## F. Calculation of Heating Rate

It is pointed out in Section C of this chapter that the response of the liquid to a sinusoidal pressure wave is similar to the response of the liquid to a single pulse whose amplitude is equal to the peak amplitude of the sine wave and whose length is equal to half the period of the sine wave. It was thus assumed for this study that in the onset of cavitation the liquid is responding to a single negative pulse of the sine wave and the effect of continually reapplying this negative pulse to the liquid is neglected.

In the previous section the onset of cavitation data was converted to superheat requirements which are a function of frequency. In order to relate this data to non-periodic transient heating in a sodium cooled nuclear reactor, one approach is to convert the frequency dependence to a heating rate, i. e., to an increase in temperature per unit time. Knowing the superheat requirements as a function of heating rate the transient changes in temperature in a sodium cooled reactor can be more accurately assessed as to their nucleate boiling capabilities.

The application of a sinusoidal temperature change of frequency f to liquid sodium initially at its saturation temperature is shown in Fig 47. The magnitude of this sinusoidal temperature variation of frequency f is $T_v - T_{sat}$ and represents the superheat necessary to produce nucleate boiling. If it is assumed that the response of the liquid to a sinusoidal temperature change can be represented by a single positive pulse of this sine wave and if it is assumed that the liquid responds to the peak value of this single pulse, then the heating rate becomes the slope of the sine curve as the superheat is increased from zero to $T_v - T_{sat}$. If an average value of this slope is utilized then the heating rate can be represented by the slope of the straight line as indicated in Fig 47. The heating rate becomes

$$\text{heating rate} = \frac{T_v - T_{sat}}{1/4f}$$

Rearranging, the heating rate becomes

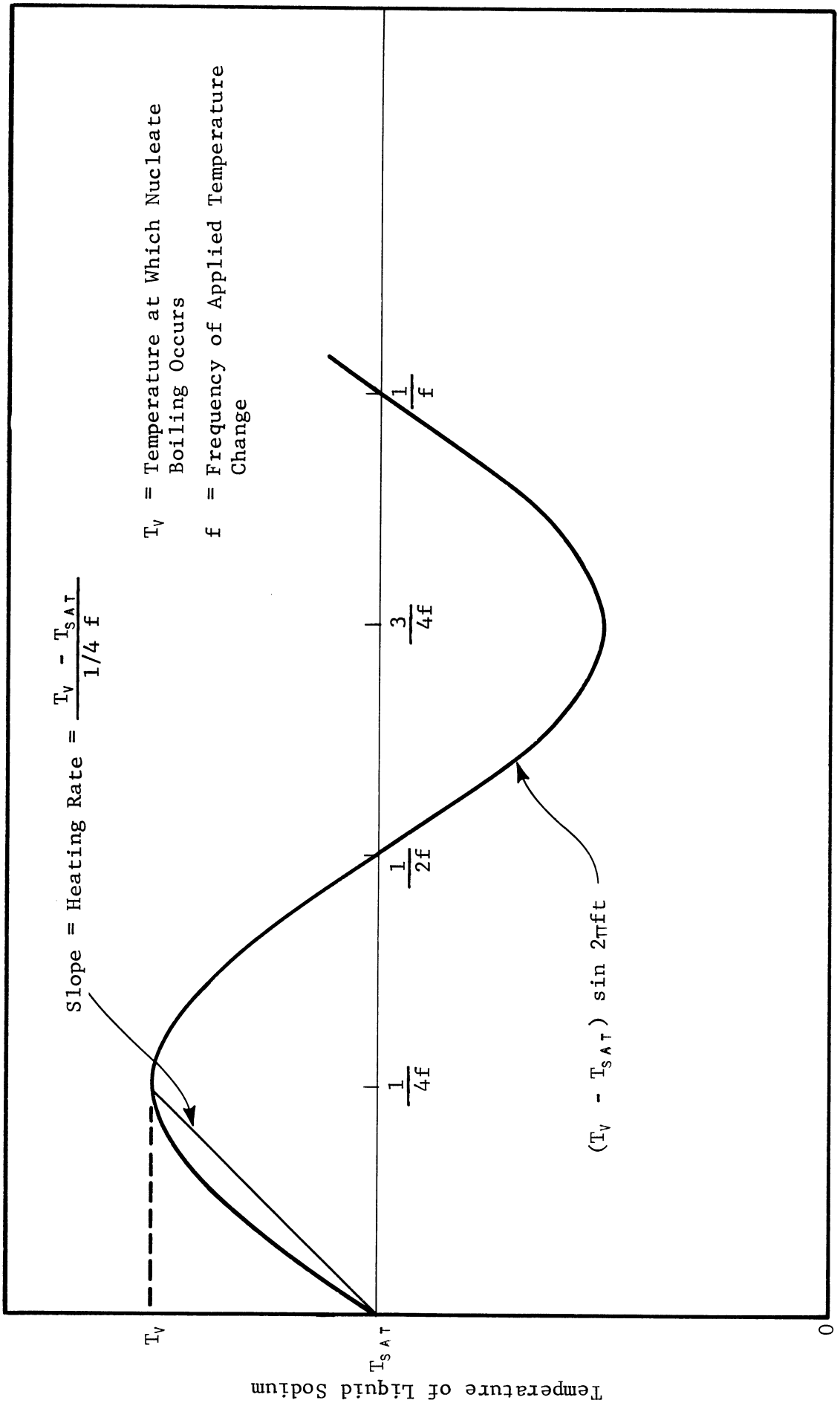


FIGURE 47. APPLICATION OF A SINUSOIDAL TEMPERATURE CHANGE OF FREQUENCY f TO LIQUID SODIUM INITIALLY AT ITS SATURATION TEMPERATURE, $T_{SAT}$

$$\text{heating rate} = 4f(T_v - T_{sat}) \qquad (6.7)$$

Summarizing, Eq (6.7) represents the rate at which the temperature of liquid sodium is increased above its saturation temperature $T_{sat}$ to the temperature $T_v$ at which nucleate boiling occurs in the liquid sodium. In deriving Eq (6.7) it was assumed that the sinusoidal temperature change can be represented by a single positive pulse and that the liquid responds to the peak value of this positive pulse. Eq (6.7) represents the average slope of this positive pulse as the superheat is increased from zero to $T_v - T_{sat}$.

Using the curves of superheat versus frequency in Fig 46 and using the heating rate equation, Eq (6.7), curves of superheat required for nucleate boiling versus heating rate were calculated and are plotted in Fig 48 for various saturation temperatures. From these curves in Fig 48 it appears that for heating rates up to approximately $10^6$ $^oF$/sec the superheat required to produce nucleate boiling in liquid sodium is independent of the heating rate. As the heating rate is increased above approximately $10^6$ $^oF$/sec the superheat requirements increase with increasing heating rate.

## G. Summary to Chapter VI

In converting the onset of cavitation data to changes in pressure required to produce cavitation it was determined that peak pressures of the applied pressure field ranged from approximately 7 to 72 psi for sodium temperatures from 500 to 1500$^o$F using a frequency range of 14 to 25 kHz. Using the changes in pressure required at the onset of cavitation,

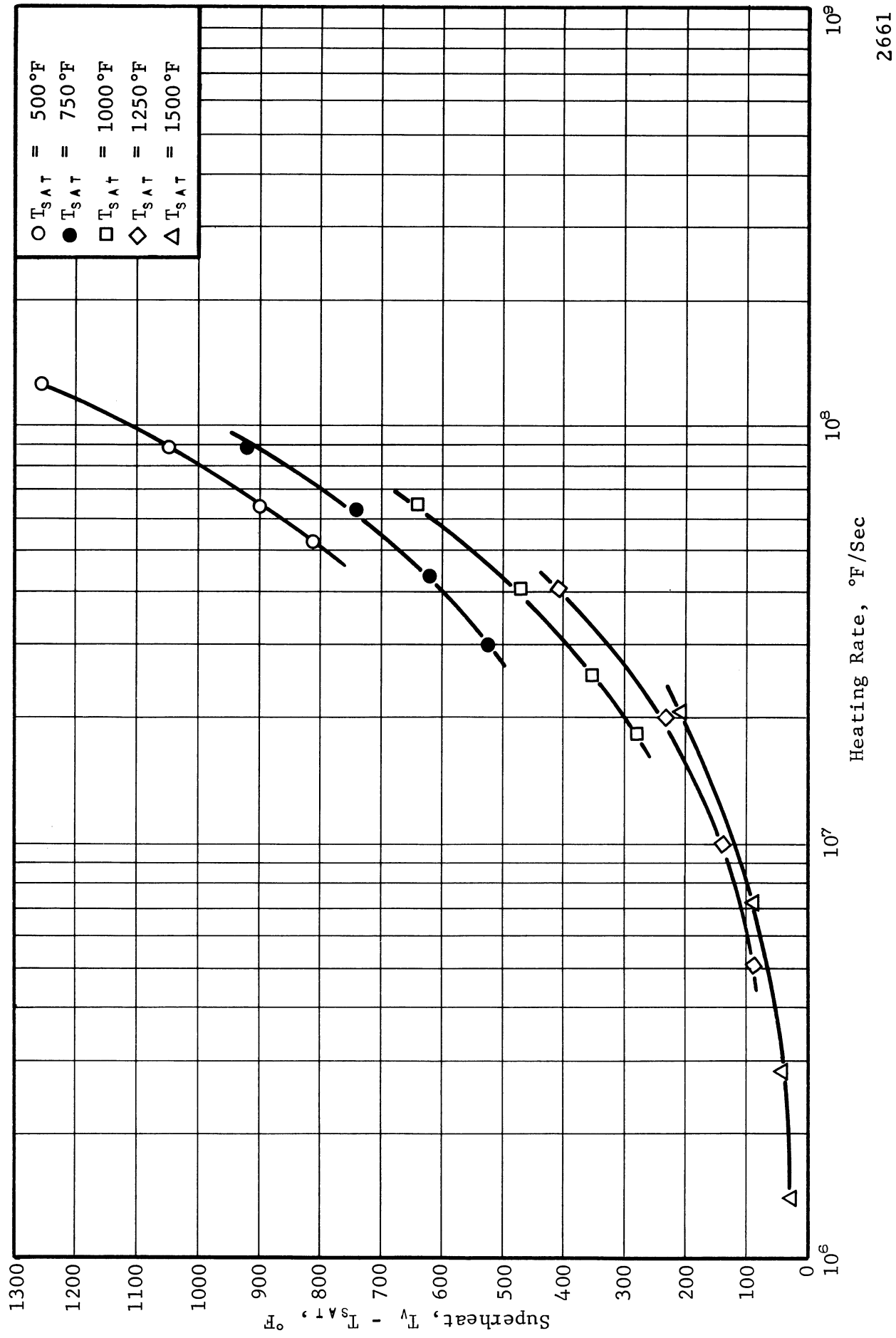


FIGURE 48. HEATING RATE VERSUS LIQUID SODIUM SUPERHEAT FOR SATURATION TEMPERATURES 500, 750, 1000, 1250, AND 1500 °F

effective radii of spherical bubbles which served as nucleation sites were determined and from this information superheat requirements for the liquid sodium were determined. The superheat requirements were obtained as functions of saturation temperature, frequency, and heating rate. As the saturation temperature is increased the superheat required to produce nucleate boiling decreases. The superheat requirements are essentially independent of frequency up to approximately 18 kHz and for higher frequencies the superheat requirements begin to increase rapidly. For heating rates up to approximately $10^6$ $^{o}$F/sec the superheat requirements are independent of the heating rate and for heating rates above $10^6$ $^{o}$F/sec the superheat requirements increase with increasing heating rate.

# CHAPTER VII

## SUMMARY, CONCLUSIONS, AND SUGGESTIONS FOR FURTHER STUDY

### A. Summary

Utilizing the University of Michigan high temperature ultrasonic vibratory cavitation facility the onset of cavitation was observed in liquid sodium both as a function of the liquid sodium temperature and as a function of the frequency of the applied sinusoidal pressure field.

It was determined that the cavitation threshold decreases approximately linearly as the temperature of the liquid sodium is increased from 500 to 1500°F. This decrease in cavitation threshold resulting from an increase in temperature was best explained in terms of the effects of temperature on vapor pressure, surface tension, viscosity, and gas solubility.

The cavitation threshold in liquid sodium is essentially independent of frequency for frequencies up to approximately 20 kHz. For frequencies above 20 kHz the pressure wave amplitude required to initiate cavitation begins to increase sharply. The frequency dependence of the cavitation threshold was theoretically investigated by utilizing the Noltingk-Neppiras[70, 71] equation which describes the growth of a vapor cavity in a sinusoidal pressure field. For frequencies

below 20 kHz the surface tension term which is independent of frequency is the controlling factor in the behavior of bubbles in a sinusoidal pressure field, and hence the cavitation threshold is essentially independent of frequency. The inertial term in the equation of motion for the spherical bubble is a function of frequency and becomes comparable in magnitude to the surface tension term for frequencies of approximately 20 kHz. For still higher frequencies the inertial effects become dominant with the result that the changes in liquid pressure required at the onset of cavitation begin to increase with increasing frequency. The viscosity term remains relatively small for the entire range of frequencies used in this investigation.

From the cavitation threshold data the peak values of the applied sinusoidal pressure field required to produce cavitation in the liquid sodium were calculated using a theoretical expression for the pressure field. The validity of this expression had been verified earlier in this study. The peak values of the sinusoidal pressure field ranged from approximately 73 psi for a sodium temperature of 500°F and a frequency of 25 kHz to 7 psi at 1500°F and at a frequency of 14 kHz.

Knowing the pressure wave amplitude required to produce cavitation and assuming that spherical vapor bubbles in the liquid sodium served as nucleation sites for the cavitation process, the effective radii of these bubbles were calculated. The effective radii were defined and calculated so as

to include the frequency dependence of the onset of cavitation. For frequencies below 20 kHz these effective radii are equal to the actual radii of the spherical bubbles which served as sites for the cavitation process, and ranged from $1.93 \times 10^{-4}$ cm for a liquid temperature of 500°F to $31.7 \times 10^{-4}$ cm for a liquid temperature of 1500°F at a frequency of 14 kHz. For frequencies above 20 kHz the effective radii are reduced because of the frequency dependence.

Utilizing the effective radii of the spherical bubbles which served as nucleation sites for the onset of cavitation, the superheat requirements for liquid sodium were determined. In determining the superheat requirements it was assumed that the spherical vapor bubbles which served as nucleation sites for the onset of cavitation would also serve as the nucleation sites for nucleate boiling for a heat transfer mode. By using the effective radii the frequency dependence of the onset of cavitation data was used to compute the liquid sodium superheat requirements. The superheat requirements were calculated for various saturation temperatures as a function of frequency. It was calculated that as the saturation temperature is increased the resulting superheat requirements decreased. The calculated superheat ranged from approximately 1250°F at a saturation temperature of 500°F and a frequency of 24.5 kHz to a superheat of approximately 20°F at a saturation temperature of 1500°F and a frequency of 14 kHz.

The frequency dependence of the superheat requirements was utilized to calculate an equivalent heating rate. The

heating rate is here defined as the increase in temperature above the saturation temperature per unit time which is required to produce nucleate boiling in liquid sodium. Using the frequency dependence data it was determined that for heating rates below approximately $10^6$ °F/sec the required superheat is essentially independent of heating rate. For heating rates above $10^6$ °F/sec the superheat required to produce nucleate boiling in liquid sodium begins to increase rapidly.

B. Conclusions

1) The results obtained in this study can be related to conditions which may arise in a sodium cooled nuclear reactor. The purity of the sodium used in this study was comparable to the purity of liquid sodium used in fast breeder nuclear reactors. The bottom surfaces of the test specimens used in this study were machined in a lathe to a commercially smooth condition (approximate roughness of 32 microinches) and may be compared to the sodium containment surfaces found in nuclear reactors.

2) In the investigation of the behavior of a sodium cooled reactor for changes in the sodium void fraction the effect of the formation of cavitation bubbles in the liquid sodium must be considered. From the data obtained in Chapter VI the change in liquid pressure required to produce cavitation bubbles in liquid sodium can be determined. As pointed out in Chapter VI a possible source of these liquid pressure

changes are pressure fluctuations which may be produced by the sodium circulation pump.

3) In determining conditions in a sodium cooled reactor which affect the sodium void formation the primary concern is an increase in temperature which leads to nucleate boiling within the core of the reactor. In particular, for rapid changes in temperature it is desirable to know the time dependence of the superheat required to produce nucleate boiling in the reactor. If the rate of increase in the sodium temperature in the reactor can be established then the superheat requirement necessary to produce nucleate boiling in the reactor can be determined from the data in Chapter VI. From the data obtained in Chapter VI it appears that unless the heating rates are extremely rapid, i. e., greater than $10^6$ $^{o}F/sec$, the required superheat is independent of the heating rate.

## C. Suggestions for Further Study

It is felt that in order to acquire additional understanding of the problems related to sodium superheat and its effect on reactor behavior the present study should be continued in several areas.

1) As indicated in Chapter I, superheat requirements are a function of the liquid purity. In order to determine the extent of the effect of the liquid purity it is necessary to determine the onset of cavitation for various levels of sodium purity and from this data calculate the superheat requirements as a function of liquid purity.

2) It is also discussed in Chapter I that superheat required to produce nucleate boiling on a heated surface is a function of the roughness of that surface. It would be desirable to obtain onset of cavitation data in liquid sodium using test specimens having bottom surfaces of various degrees of roughness. This data could then be converted to superheat requirements versus surface roughness and knowing the exact roughness of sodium containment surfaces in nuclear reactors a more exact prediction of superheat requirements for the reactor could be obtained.

3) In Chapter VI it was assumed that the response of the liquid to the negative pulse of the sinusoidal pressure wave was identical to the response of the liquid to a single pulse of equal amplitude and equal time duration. It is pointed out that although the response of the liquid to the two different signals is similar it is not exactly the same. Therefore, in order to obtain more accurate superheat data the single pulse equivalent of the sine wave signal should be determined and from this equivalent single pulse more precise superheat information can be obtained.

## APPENDIX A

## DERIVATION OF THE SUPERHEAT EQUATION, EQ (1.3)

The superheat equation, Eq (1.3), which was first intoduced by Ellion,[15] is derived using the Clausius-Clapeyron equation. The Clausius-Clapeyron equation is a basic thermodynamic relationship which relates changes in temperature to changes in pressure along the saturation line and is given by[82]

$$\frac{dP}{dT} = \frac{h}{T(v_g - v_\ell)} \qquad (1)$$

where

$P$ = pressure

$T$ = temperature

$h$ = latent heat of vaporization

$v_g$ = specific volume of vapor

$v_\ell$ = specific volume of liquid.

As pointed out by Edwards and Hoffman[19] Eq (1) is valid only for equilibrium conditions in which the vapor pressure $P_v$ is equal to the liquid pressure $P_L$. In the derivation of Eq (1.3) it is assumed that the Clasius-Clapeyron equation can be used to describe superheating in a liquid even though during the superheating process the vapor pressure $P_v$ becomes greater than $P_L$.

If it is assumed that the specific volume of vapor is much larger than the specific volume of liquid then Eq (1) becomes

$$\frac{dP}{dT} = \frac{h}{T v_g} \tag{2}$$

From the ideal gas law we have

$$P v_g = G T$$

and rewriting, we obtain

$$v_g = \frac{G T}{P} \tag{3}$$

where $G$ is the ideal gas constant. Substituting Eq (3) into Eq (2) we obtain

$$\frac{dP}{dT} = \frac{h P}{G T^2}$$

Rearranging, we obtain

$$\frac{dP}{P} = \frac{h\, dT}{G T^2} \tag{4}$$

Eq (4) can now be integrated. In the integration we are concerned in the change in temperature in going from saturated conditions to superheated conditions in the liquid. Eq (4) is thus integrated from $T_{sat}$ and its corresponding pressure $P_L$ to the superheat temperature $T_v$ and its corresponding pressure $P_v$. Assuming that $h$ is a constant, Eq (4) becomes

$$\int_{P_L}^{P_v} \frac{dP}{P} = \frac{h}{G} \int_{T_{SAT}}^{T_v} \frac{dT}{T^2}$$

Integrating, we obtain

$$\ln \frac{P_v}{P_\ell} = \frac{h}{G}\left[\frac{1}{T_{SAT}} - \frac{1}{T_v}\right] \tag{5}$$

For a spherical vapor bubble of radius R, we have at the onset of nucleate boiling

$$P_v - P_\ell = \frac{2\sigma}{R}$$

and rewriting, we obtain

$$\frac{P_v}{P_\ell} = 1 + \frac{2\sigma}{R P_\ell} \tag{6}$$

where $\sigma$ is the surface tension.

Substituting Eq (6) into Eq (5), we obtain

$$\ln\left(1+\frac{2\sigma}{R P_\ell}\right) = \frac{h}{G}\left[\frac{1}{T_{SAT}} - \frac{1}{T_v}\right]$$

Rearranging, we obtain

$$T_v - T_{SAT} = \frac{G T_v T_{SAT}}{h} \ln\left(1+\frac{2\sigma}{R P_\ell}\right) \tag{7}$$

which is the superheat equation and is denoted as Eq (1.3) in Chapter I.

## REFERENCES


1. Trocki, T., Bruagerman, W. H., and Crever, F. E., "Sodium and Sodium-Potassium Alloy for Reactor Cooling and Steam Generation," Progress in Nuclear Energy, Series IV, R. Hurst, and M. Lain, Editors, McGraw Hill Book Co, New York, 1956, p. 146.

2. Friedland, A. J., "Coolant Properties, Heat Transfer, and Fluid Flow of Liquid Metals," Fast Reactor Technology: Plant Design, J. G. Yevick, Editor, M.I.T. Press, Cambridge, Mass, 1966, pp. 18-19.

3. Lamarsh, J. R., Introduction to Nuclear Reactor Theory, Addison-Wesley Publishing Co, Reading, Mass, 1966, p. 420.

4. Wensch, G. W., "Introduction to Fast Reactors," Fast Reactor Technology: Plant Design, J. G. Yevick, Editor, M.I.T. Press, Cambridge, Mass, 1966, p. 9.

5. Nims, J. B., and Zweifel, P. F., "Sodium Temperature Coefficients in Fast Reactors," Trans American Nuclear Society, Vol. 2, No. 2, November, 1959, pp. 172-173.

6. Brooks, H., "Introduction Remarks," Proc of the 1957 Fast Reactor Information Meeting, G. W. Wench, Editor, held at Chicago, Ill, November 20-21, 1957, p. 65.

7. Nukiyama, S., "Maximum and Minimum Values of Heat Transmitted from Metal to Boiling Water under Atmospheric Pressure," Journal Society Mechanical Engineers of Japan, Vol. 37, No. 206, 1934, p. 267.

8. Ibelle, W., Modern Developments in Heat Transfer, Academic Press, New York, 1963, p. 96.

9. Blake, F. G., Jr., "The onset of Cavitation in Liquids," Technical Memo No. 12, Acoustics Research Laboratory, Harvard University, Cambridge, Mass, 1949.

10. Harvey, E. N., McElroy, W. D., and Whitely, A. H., "On Cavity Formation in Water," Journal Applied Physics, Vol. 18, 1947, pp. 162-167.

11. Ibelle, op. cit., p. 103.

12. Bennett, C. O., and Myers, J. E., Momentum, Heat, and Mass Transfer, McGraw Hill Book Co., New York, 1962, p. 355.

13. Grober, H., Erk, S., and Grigull, U., Fundamentals of Heat Transfer, McGraw Hill Book Co, New York, 1961, p. 361.

14. Keenan, J. H., and Keyes, F. G., Thermodynamic Properties of Steam, John Wiley & Sons, Inc., New York, 1936.

15. Ellion, M., "Study of Mechanism of Boiling Heat Transfer," Jet Propulsion Laboratory Memorandum 20-28, California Institute of Technology, March, 1954.

16. Griffith, P., and Wallis, J. D., "The Role of Surface Conditions in Nucleate Boiling," Chem Eng Sym Series, Vol. 56, No. 30, 1960, pp. 49-63.

17. Berenson, P., "Transition Boiling Heat Transfer from a Horizontal Surface," MIT Tech Report No. 17, Heat Transfer Laboratory, Mass Institute of Technology, Cambridge, Mass, March, 1960.

18. Farber, E. A., and Scorah, R. L., "Heat Transfer to Water Boiling Under Pressure," Trans ASME, Vol. 70, No. 4, May, 1948, pp. 369-384.

19. Edwards, J. A., and Hoffman, H. W., "Superheat with Boiling Alkali Metals," Proc of the Conf on Application of High Temp Inst to Liquid Metal Experiments, ANL-Report 7100, Sept, 1965, pp. 515-534.

20. Marto, P. J., and Rohsenow, W. M., "Effects of Surface Conditions on Nucleate Pool Boiling of Sodium," A.S.M.E.-A.I.Ch.E. Heat Transfer Conf, Paper No. 65-HT-51, Los Angeles, Calif, August, 1965.

21. Krakoviak, A. I., "Superheat Requirements with Boiling Liquid Metals," Proc of 1963 High-Temperature Liquid-Metal Heat Transfer Technology Meeting, Vol. I, USAEC Report ORNL-3605, Oak Ridge National Laboratory, November, 1964, pp. 310-322.

22. Dwyer, O. E., "Recent Developments in Liquid Metal Heat Transfer," Atomic Energy Review, Vol. 4, No. 1, 1966, pp. 3-92.

23. Hall, W. B., and Harrison, W. C., "Transient Boiling of Water at Atmospheric Pressure," Proc Third International Heat Transfer Conference, American Institute of Chem Eng, New York, 1966, pp. 186-192.

24. Johnson, H. A., et al, "Transient Boiling Heat Transfer and Void Volume Production in Channel Flow," SAN-1007, March, 1963.

25. MacFarlane, D. R., "An Analytic Study of the Transient Boiling of Sodium in Reactor Coolant Channels," ANL-7222, Argonne National Laboratory, June, 1966.

26. Holtz, R. E., and Singer, R. M., "Sodium Superheat Experiment," Trans ANS, Vol. 10, No. 1, June, 1967, p. 336.

27. Hooper, F. C., and Abdelmessih, A. H., "The Flashing of Liquids at Higher Superheats," Proc Third International Heat Transfer Conference, American Institute of Chem Eng, Vol. IV, New York, 1966, pp. 44-50.

28. Garcia, R., "Comprehensive Cavitation Damage Data for Water and Various Liquid Metals Including Correlations with Material and Fluid Properties," Ph.D. Thesis and ORA Technical Report No. 05031-6-T, Department of Nuclear Engineering, The University of Michigan, August, 1966.

29. Blitz, J., Fundamentals of Ultrasonics, Butterworth & Co., Ltd, London, 1963, p. 45.

30. Hueter, T. F., and Bolt, R. H., Sonics, John Wiley & Sons, Inc., New York, 1955, p. 275.

31. Blitz, op. cit., p. 25.

32. Blitz, op. cit., p. 49.

33. Blitz, op. cit., p. 24.

34. Lansing, D. L., Watkins, C. E., and Kantarges, G. T., "Oscillating Pressures within a Cylindrical Chamber That Has a Circular Piston in One End Wall," Journal of the Acoustical Society of America, Vol. 36, No. 11, November, 1964, pp. 2222-2232.

35. Lord Rayleigh, Theory of Sound, Vol. 2, Chapter 11, Dover Publications, Inc., New York, 1945.

36. Morse, P. M., Vibration and Sound, 2nd ed., McGraw Hill Book Co., New York, 1948, pp. 398-399.

37. Wilson, W. D., "Speed of Sound in Distilled Water as a Function of Temperature and Pressure," Journal of the Acoustical Society of America, Vol. 31, No. 8, August, 1959, pp. 1067-1072.

38. Blitz, op. cit., p. 41.

39. Hueter, and Bolt, op. cit., p. 119.

40. Geffner, J., Treatment of Experimental Data, John Wiley & sons, Inc., New York, November, 1947, p. 240.

41. Ying, S., and Scott, C. C., "Attenuation Measurements of Sound and Performance of Ultrasonic Transducers in 600 F Liquid Sodium," APDA-180, Atomic Power Development Associates, Inc., December, 1965, p. 19.

42. Dunning, E. L., "The Thermodynamic and Transport Properties of Sodium and Sodium Vapor," ANL-6246, Argonne National Laboratory, October, 1960, p. 27.

43. Blitz, op. cit., p. 208.

44. Mason, W. P., Physical Acoustics, Vol. 1, Part B, Acedemic Press, New York, 1964, p. 140.

45. Jarman, P., "Sonoluminescence: a Discussion," Journal of the Acoustical Society of America, Vol. 32, No. 2, 1960, pp. 1459-1461.

46. Esche, V. R., "Untersuchung der Schwingungskavitation in Flussigkeiten," Akusticke Beihefte, Vol. 2, 1952, pp. 208-218.

47. Numachi, F., "An Experimental Study of Accelerated Cavitation Induced by Ultrasonics," ASME Paper No. 65-FE-2, 1965.

48. Mellen, R. H. "An Experimental Study of the Collapse of a Spherical Cavity in Water," Journal of the Acoustical Society of America, Vol. 28, No. 3, May, 1956, pp. 447-454.

49. Galloway, W. J., "An Experimental Study of Acoustically Induced Cavitation in Liquids," Journal of the Acoustical Society of America, Vol. 26, No. 5, September, 1954, pp. 849-857.

50. Connolly, W., and Fox, F. E., "Ultrasonic Cavitation Thresholds in Water," Journal of the Acoustical Society of America, Vol 26, No. 5, September, 1954, pp. 843-848.

51. Sirotyuk, M. G., "Experimental Investigation of the Growth of Ultrasonic Cavitation at 500 kHz," Soviet Physics-Acoustics, Vol. 8, No. 2, Oct-Dec, 1962, pp. 165-169.

52. Lange, Th., "Methoden zur Untersuchung der Schwingungskavitation in Flussigkeiten mit Ultraschall," Akusticke Beihefte, Vol. 2, 1952, pp. 75-82.

53. Akuluchev, V. A., and Il'ichev, V. I., "Spectral Indication of the Origin of Ultrasonic Cavitation in Water," Soviet Physics-Acoustics, Vol. 9, No. 2, Oct-Dec, 1963, pp. 128-130.

54. "Ultrasonic Instrumentation for Nuclear Applications," Bimonthly Progress Report No. 31, NYO-3622-6, Aeroprojects Inc., AEC Contract AT (30-1)-3622, December, 1966, pp. 5-14.

55. Garcia, R., Hammitt, F. G., and Robinson, M. J., "Acoustic Noise from a Cavitating Venturi," ORA Technical Report No. 06110-1-T, Department of Nuclear Engineering, The University of Michigan, June, 1964.

56. Mikhailov, I. G., and Shutilov, V. A., "A Simple Method for Observing Cavitation in Liquids," Soviet Physics-Acoustics, Vol. 5, No. 3, July-Sept, 1959, pp. 385-387.

57. Strasberg, M., "Onset of Ultrasonic Cavitation in Tap Water," Journal of the Acoustical Society of America, Vol. 31, No. 2, February, 1950, pp. 163-176.

58. McLachlan, N. W., Theory of Vibrations, Dover Publications Inc., New York, 1951, p. 96.

59. Holl, J. W., and Treaster, A. L., "Cavitation Hysteresis," Journal of Basic Engineering, Trans. ASME, Vol. 88, Series D, No. 1, March, 1966, pp. 199-212.

60. Mechanical Design and Systems Handbook, H. A. Rothbart, Editor-in-Chief, McGraw-Hill Book Co., New York, 1964, p. 19-23.

61. Liquid Metals Handbook, Sodium-NaK Supplement, C. B. Jackson, Editor, U. S. Government Printing Office, Washington, D. C., July, 1955.

62. Sittig, M., Sodium, Its Manufacture, Properties, and Uses, Reinhold Publishing Co., New York, 1956.

63. Handling Metallic Sodium on a Plant Scale, U. S. Industrial Chemicals Co., Division of National Distillers and Chemical Corporation, New York, 1959, p. 12.

64. Du Pont Sodium Handling and Properties, E. I. duPont de Nemours & Co., Electrochemicals Division, Wilmington, Delaware, 1962, p. 12.

65. Ibid., p. 16.

66. Handling Metallic Sodium on a Plant Scale, U. S. Industrial Chemicals Co., Division of National Dsitillers and Chemical Corporation, New York, 1959, p. 41.

67. Private communication with Eugene Hill, Atomic Power Development Associates, Inc., Detroit, Michigan, 1968.

68. Messino, D., Sette, D., and Wanderlingh, F., "Statistical Approach to Ultrasonic Cavitation," Journal of the Acoustical Society of America, Vol. 35, No. 10, October, 1963, pp. 1575-1583.

69. Boguslavskii, Yu., and Korets, V. L., "Cavitation Threshold and its Frequency Dependence," Soviet Physics-Acoustics, Vol. 12, No. 4, April-June, 1967, pp. 364-368.

70. Noltingk, B. E., and Neppiras, E. A., "Cavitation Produced by Ultrasonics," Proc. Phy. Soc. (London), Vol. B63, 1950, pp. 674-685.

71. Neppiras, E. A., and Noltingk, B. E., "Cavitation Produced by Ultrasonics: Theoretical Condition for the Onset of Cavitation," Proc. Phy. Soc. (London), Vol. B64, 1951, pp. 1032-1038.

72. Dunning, op. cit., p. 20.

73. Dunning, op. cit., p. 28.

74. Briggs, H. B., Johnson, J. B., and Mason, W. P., "Properties of Liquids at High Sound Pressures," Journal of the Acoustical Society of America, Vol. 19, No. 4, 1947, pp. 664-677.

75. Dunning, op. cit., p. 27.

76. Friedland, op. cit., p. 40.

77. Dunning, op. cit., p. 26.

78. Lotz, M., and Raabe, J., "Blade Oscillations in One-Stage Axial Turbomachinery," ASME Paper No. 68-FE-7, 1968.

79. Flynn, H. G., "Physics of Acoustic Cavitation in Liquids," Physical Acoustics, Vol. 1, Part B, W. P. Mason, Editor, Academic Press, New York, 1964, p. 91.

80. Flynn, H. G., "Cavitation Dynamics: 1. A Mathematical Formulation," Technical Memorandum No. 50, Office of Naval Research Contract Nonr-1866(24), Acoustics Research Laboratory, Harvard University, Cambridge, Mass., January, 1966.

81. Holtz, R. E., "A Study of the Initiation of Nucleate Boiling in the Liquid Metals," ANL-6980, Argonne National Laboratory, Argonne, Illinois, December, 1964.

82. Lee, J. F., and Sears, F. W., Thermodynamics, Addison-Wesley Publishing Co., Inc., Reading, Mass., 1963, p. 165.

83. Holtz, R. E., and Singer, R. M., "On the Superheating of Sodium at Low Heat Fluxes," ANL-7383, Argonne National Laboratory, Argonne, Illinois, November, 1967.

84. Fauske, H. K., "Liquid Metal Boiling in Relation to LMFBR Safety Design," Presented at the Tenth National Heat Transfer Conference A.I.Ch.E.-A.S.M.E., Philadelphia, Pennsylvania, August 11-14, 1968.